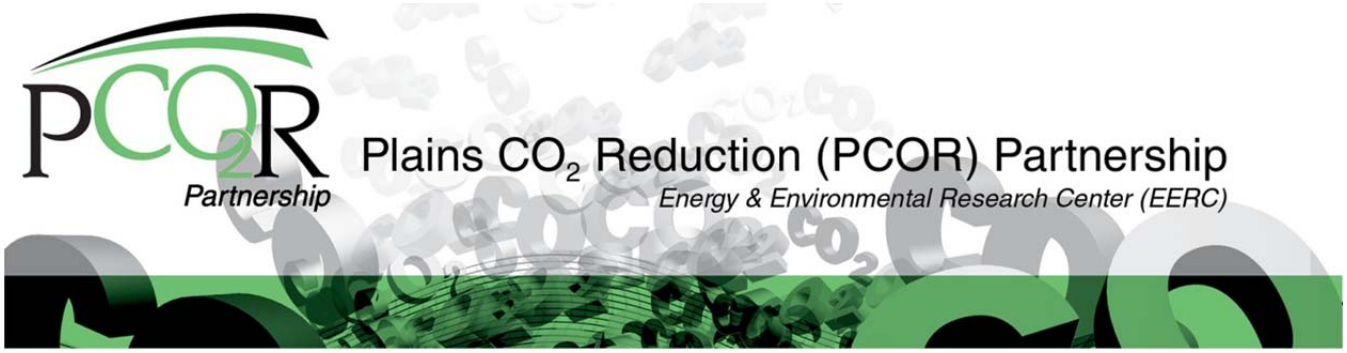

BELL CREEK TEST SITE – SIMULATION REPORT

Plains CO_2 Reduction (PCOR) Partnership Phase III
Task 9 – Deliverable D66

Prepared for:

Andrea T. McNemar

National Energy Technology Laboratory
U.S. Department of Energy
3610 Collins Ferry Road
PO Box 880
Morgantown, WV 26507-0880

DOE Cooperative Agreement No. DE-FC26-05NT42592

Prepared by:

Dayanand Saini
Jason R. Braunberger
Hui Pu
Terry P. Bailey
Jun Ge
Chad M. Crotty
Guoxiang Liu
John A. Hamling
Charles D. Gorecki
Edward N. Steadman
John A. Harju

Energy & Environmental Research Center
University of North Dakota
15 North 23rd Street, Stop 9018
Grand Forks, ND 58202-9018

August 2012
Approved

2013-EERC-01-12

EERC DISCLAIMER

LEGAL NOTICE This research report was prepared by the Energy & Environmental Research Center (EERC), an agency of the University of North Dakota, as an account of work sponsored by the U.S. Department of Energy. Because of the research nature of the work performed, neither the EERC nor any of its employees makes any warranty, express or implied, or assumes any legal liability or responsibility for the accuracy, completeness, or usefulness of any information, apparatus, product, or process disclosed or represents that its use would not infringe privately owned rights. Reference herein to any specific commercial product, process, or service by trade name, trademark, manufacturer, or otherwise does not necessarily constitute or imply its endorsement or recommendation by the EERC.

ACKNOWLEDGMENTS

This work was performed under the U.S. Department of Energy (DOE) Cooperative Agreement No. DE-FC26-05NT42592. The EERC would like to thank Denbury Onshore LLC (Denbury) for providing necessary data to perform this work. Special thanks go to the members of Denbury's Bell Creek team for their valuable input and fruitful discussions. The authors acknowledge the members of the EERC's Editing and Graphics staff and especially Kim M. Dickman and Raymond J. Pikarski who assisted in the review of this document. The help of Neil Dotzenrod and Megan M. Grove with the creation of several new figures for this report is gratefully acknowledged. Many thanks go to Katherine K. Anagnost, Janelle R. Ensrud, Nola F. Pithey, Heather L. Altepeter, and Sue Kimber for their assistance during the preparation of this report.

DOE DISCLAIMER

This report was prepared as an account of work sponsored by an agency of the United States Government. Neither the United States Government, nor any agency thereof, nor any of their employees, makes any warranty, express or implied, or assumes any legal liability or responsibility for the accuracy, completeness, or usefulness of any information, apparatus, product, or process disclosed, or represents that its use would not infringe privately owned rights. Reference herein to any specific commercial product, process, or service by trade name, trademark, manufacturer, or otherwise does not necessarily constitute or imply its endorsement, recommendation, or favoring by the United States Government or any agency thereof. The views and opinions of authors expressed herein do not necessarily state or reflect those of the United States Government or any agency thereof.

NDIC DISCLAIMER

This report was prepared by the EERC pursuant to an agreement partially funded by the Industrial Commission of North Dakota, and neither the EERC nor any of its subcontractors nor the North Dakota Industrial Commission nor any person acting on behalf of either:

(A) Makes any warranty or representation, express or implied, with respect to the accuracy, completeness, or usefulness of the information contained in this report or that the use of any information, apparatus, method, or process disclosed in this report may not infringe privately owned rights; or

(B) Assumes any liabilities with respect to the use of, or for damages resulting from the use of, any information, apparatus, method, or process disclosed in this report.

Reference herein to any specific commercial product, process, or service by trade name, trademark, manufacturer, or otherwise does not necessarily constitute or imply its endorsement, recommendation, or favoring by the North Dakota Industrial Commission. The views and opinions of authors expressed herein do not necessarily state or reflect those of the North Dakota Industrial Commission.

TABLE OF CONTENTS

LIST OF FIGURES iii

LIST OF TABLES iv

EXECUTIVE SUMMARY v

INTRODUCTION 1

PURPOSE 6

SCOPE OF WORK 7

GEOLOGIC HISTORY 8
- Local Depositional Environments 8

PHASE 1 3-D GEOLOGIC MODELING 12
- Stratigraphic Framework 14
- Structural and Property Model 14
- Limitations 17

PVT AND SLIM-TUBE EXPERIMENT MODELING 17
- PVT Study 17
- EOS Model-Based Predictions of Minimum Miscibility Pressure 19
- 1-D Compositional Simulation of the Slim-Tube Test 21

PHASE 1 RESERVOIR SIMULATION 23
- Numerical Tuning and History Matching 23
- Phase 1 Areawide History-Matching Results 24
  - Individual Well History-Matching Results 26
- Predictive Fluid Flow Simulations 27
  - Quarter Five-Spot Pattern Model 28
  - Five-Spot Pattern Model 30
  - Full Phase 1 Area Model 32
  - Summary of CO_2 Breakthrough Times 39
- Limitations 39

MVA UPDATE 42
- Monitoring Well (0506 OW) 42
- Geophysical Data 42

Continued . . .

TABLE OF CONTENTS (continued)

FIELDWIDE 3-D GEOLOGIC MODELING 42
Stratigraphic Framework 42
Structural Model 45
Petrophysical Interpretation 45

GEOMECHANICAL MODELING 47

FUTURE WORK 48
Fieldwide 3-D Geologic Model 48
Reservoir Simulation 49
3-D Geomechanical Model 50

SUMMARY 50

REFERENCES 51

PHASE 1 3-D GEOLOGIC MODELING ..... Appendix A

PVT AND SLIM-TUBE EXPERIMENT MODELING ..... Appendix B

RESERVOIR SIMULATION ..... Appendix C

LIST OF FIGURES

1 Map depicting the location of the Bell Creek oil field in relation to the Powder River Basin and the planned pipeline route to the site from the Lost Cabin gas plant 2

2 Late Cretaceous to Quaternary stratigraphic column of the Powder River Basin 3

3 Static geologic and dynamic reservoir model boundaries for the Phase 1 (Unit D) area..... 4

4 Study area for the fieldwide 3-D geologic model, showing all wells and cores available.... 5

5 Project elements of the Bell Creek CO_2 capture and sequestration project 6

6 Stratigraphic column of the Lower Cretaceous period..... 9

7 Maximum transgression of the Early Cretaceous seaway, depositing the Skull Creek shale..... 10

8 Regression of the Early Cretaceous seaway, depositing the Muddy sandstone..... 10

9 Transgression of the Early Cretaceous seaway, depositing the Mowry shale 11

10 Map showing the geologic model boundary (black), the dynamic model boundary (red), and their relation to the planned Bell Creek project development phases 13

11 Type log including the seven picked stratigraphic tops..... 15

12 Map views of the BC10, BC20, and BC30 zones with labeled thickness contours..... 16

13 Map of the Bell Creek oil field, showing development phases and the three wells with available PVT analysis within the field..... 18

14 Composition of recombined live crude oil..... 19

15 Graph illustrating the calculated effects on MMP as the GOR is increased..... 21

16 Comparison of simulated MMP and experimental MMP at 108°F with CO_2 22

17 3-D view of the dynamic simulation model..... 24

18 History-matching result of field oil rate..... 25

19 History-matching result of field water cut 25

Continued…

LIST OF FIGURES (continued)

20 History-matching result of field gas rate 26

21 Average reservoir pressure 27

22 Well locations and porosity distribution in the quarter five-spot pattern model 28

23 The five-spot pattern model 31

24 2-D view of the full Phase 1 model 34

25 Areal extent of the CO_2 plume at the end of the injection period (Case 9) 35

26 Areal extent of the CO_2 plume at the end of the injection period (Case 10) 37

27 Areal extent of the CO_2 plume at the end of the injection period (Case 11) 38

28 Areal extent of the CO_2 plume at the end of the injection period (Case 12) 40

29 Map illustrating the monitoring well location in relation to the Bell Creek oil field 43

30 West-to-east cross section through wells nearest to and including the observation well ... 44

31 Outcrop photo of the Bell Creek sand conformably lying on top of the Rozet siltstone 45

32 Map of the Bell Creek oil field and flanking edges when the P10 structural surface is subtracted from the P90 46

33 Bell Creek 1-D MEM of 0506 OW, with wireline logs, rock mechanical properties, and in situ stresses shown 49

LIST OF TABLES

1 Model Layering of the Geologic Model 16

2 Comparison of Experimental MMP Values and Calculated Simulation Results 20

3 MMP for Reservoir Fluid and Stock Tank Oil 20

4 Slim-Tube Model Data 22

5 CO_2 Breakthrough Times 41

6 Layers and Associated Thicknesses of Stratigraphy in the Fieldwide Geologic Model 47

BELL CREEK TEST SITE – SIMULATION REPORT

EXECUTIVE SUMMARY

The Plains CO_2 Reduction (PCOR) Partnership is working with Denbury Onshore LLC (Denbury) to evaluate the effectiveness of large-scale injection of carbon dioxide (CO_2) into the Bell Creek oil field for simultaneous CO_2 enhanced oil recovery (EOR) and long-term CO_2 storage. Discovered in 1967, the Bell Creek oil field in southeastern Montana has undergone primary production (solution gas drive), waterflooding, and two micellar–polymer pilot tests. About 37.7% of the estimated 353 million barrels (MMbbl) of original oil in place (OOIP) has been produced to date. This leaves behind an estimated 220 MMbbl of oil in the reservoir. It is anticipated that 30 to 50 MMbbl of additional oil could be produced through CO_2 flooding in this field.

With the goal of providing a comprehensive assessment of CO_2 storage behavior and potential while supporting Denbury's EOR efforts, members of the PCOR Partnership have initiated a preliminary modeling and numerical simulation program to 1) characterize and model the study area using advanced geologic modeling, 2) develop a robust pressure, volume, and temperature (PVT) model to predict miscibility behavior of the CO_2–Bell Creek crude system and to aid in compositional simulation, and 3) history-match the constructed dynamic reservoir model and utilize predictive simulations to aid in the development of effective strategies for monitoring long-term behavior of injected CO_2 during the implementation of an integrated CO_2 EOR and long-term CO_2 storage project in this initially sub-normally pressured reservoir.

To construct a detailed three-dimensional (3-D) static geologic model of the Phase 1 area (Version 1 model), fieldwide data reconnaissance activities were performed to acquire pertinent reservoir characterization data for the entire Bell Creek oil field in general and the Phase 1 area in particular. Available data were analyzed, interpreted, and incorporated into the 3-D static geologic and dynamic reservoir models to represent geologic and reservoir properties in order to provide a solid groundwork for simulation activities.

A seven-component Peng–Robinson (PR) equation of state (EOS) model was developed and tuned based on the available experimental PVT data. To ensure the robustness of the developed EOS model, one-dimensional (1-D) compositional simulation of the experimental slim-tube tests was performed. The minimum miscibility pressure estimated from slim-tube simulation is lower than what was determined from the slim-tube experiment. The constructed geologic model was validated through history matching and was used for various predictive simulation scenarios. A good agreement between the field history and simulation results (oil rate, water cut, and gas–oil ratio) for the Phase 1 area model was observed.

In the case of continuous CO_2 injection, a total of 4.09 to 5.34 million tons of CO_2 can be stored by the end of 1 hydrocarbon pore volume (HCPV) period and 2 HCPV injection periods, respectively. For WAG injection scenarios, the amounts of stored CO_2 varied from 2.48 million tons (1 HCPV injection) to 3.00 million tons (2 HCPV injection). It is worth mentioning here that these storage amounts are based on simulations performed so far, which did not consider the effects of relative permeability hysteresis if any, and CO_2 solubility in the aqueous phase. The effects of these variables on CO_2 storage capacity are being evaluated further. Based on the current predictive simulation results, the CO_2 plume is not expected to cross the Phase 1 area boundary. However, injected CO_2 appears to move into the adjacent downdip aquifer region in all of the predictive simulation scenarios evaluated so far. Further predictive simulations are being performed to evaluate multiple likely CO_2 EOR and storage schemes; the migration pathway, long-term (50–100 years postinjection period) plume behavior, and reservoir storage efficiency of the injected CO_2; CO_2 breakthrough timing, monitoring, verification, and accounting for geophysical deployment periods; and CO_2 storage volumetrics.

Dynamic reservoir simulation results suggest that alternately injecting slugs of CO_2 and water during the CO_2 injection program would be more effective than continuously injecting a single CO_2 slug. In the case of continuous CO_2 injection, earliest CO_2 breakthrough at production wells is expected to be in 6 months after commencement of CO_2 injection. The CO_2 breakthrough at the monitoring well is expected to be in 5.5 years. Overall, WAG injection slows down gas breakthrough and yields a better sweep efficiency, although the earliest CO_2 breakthrough at production wells occurs in 3 months. In the WAG process, injected CO_2 is expected to reach the monitoring well after 6 years of injection. These long breakthrough times for CO_2 to reach the monitoring well could be due to geologic uncertainty and/or the fact that the monitoring well is downdip from the nearest injector and was kept in shut-in condition while various predictive simulation scenarios were being evaluated.

A new fieldwide 3-D geologic model (Version 2) is being constructed. The log and core data acquired from the newly drilled monitoring well and lidar (light detection and ranging) survey are expected to greatly improve this new model. Upon completion of the uncertainty and sensitivity analysis, numerical tuning and history matching will be performed for the Version 2 model. The base case, P10, P50, and P90 realizations and historical production and injection data will be used for history matching and future predictive simulations. The dynamic modeling workflow developed at the EERC will be used to perform this simulation work.

The fieldwide 3-D geomechnical model is being constructed to identify, anticipate, and evaluate the potential risk for out-of-zone fluid migration caused by a possible breach of reservoir integrity. This model will then be used for the predictive geomechanical simulation during and after the injection process in order to guide the monitoring program.

BELL CREEK TEST SITE – SIMULATION REPORT

INTRODUCTION

The Plains CO_2 Reduction (PCOR) Partnership, led by the Energy & Environmental Research Center (EERC), is working with Denbury Onshore LLC (Denbury) to determine the effect of a large-scale injection of carbon dioxide (CO_2) into a deep clastic reservoir for the purpose of simultaneous CO_2 enhanced oil recovery (EOR) and CO_2 storage at the Bell Creek oil field, which is owned and operated by Denbury. A technical team that includes Denbury, the EERC, and others will conduct a variety of activities to determine the baseline reservoir characteristics including predictive simulations of the CO_2 injection. This will facilitate assessment of various potential injection schemes, guide monitoring strategies, and determine the ultimate fate of injected CO_2. Denbury will carry out the injection and production operations, while the EERC will provide support for the site characterization, modeling and simulation, and integrated risk assessment and will aid in the development of the monitoring, verification, and accounting (MVA) plan to address key technical subsurface risks.

The Bell Creek CO_2 EOR and CO_2 storage project provides a unique opportunity to develop a characterization and predictive modeling workflow for a complex, large-scale (>1 million tons per year) combined CO_2 EOR and CO_2 storage operation in an active oil field. To facilitate these activities, a detailed static geologic model (Version 1 model) of the Phase 1 (Unit D) area and its surrounding area was built. During the reporting period, history matching and predictive simulations were performed to aid in the ongoing planning of various pre- and postinjection monitoring activities in the Phase 1 area.

A new fieldwide static geologic model (Version 2 model) is being constructed using the fieldwide geologic and reservoir data. The history matching and predictive simulation results obtained with the Version 1 static geologic model have provided valuable insights about the geological and reservoir characteristics of the Phase 1 area. These are being incorporated in the ongoing fieldwide (Version 2 model) geologic model to refine the overall quality of ongoing geologic and reservoir modeling efforts at the EERC. The baseline geologic characterization and simulation work that will be conducted over the course of this project will also provide valuable data to support the design and implementation of an injection/production scheme for this large-scale CO_2 EOR and storage project.

The EERC's geologic, geomechanical, numerical, and predictive simulation modeling of the subsurface will aid in understanding the behavior of injected CO_2 and reservoir fluids over

the injection and postinjection project periods. The ongoing modeling and simulation activities zone fluid migrations. This type of assessment is an essential input to the integrated risk assessment and MVA plans, which in turn helps to ensure that the maximum benefit to the EOR process is achieved in a safe and efficient manner.

The Bell Creek oil field in southeastern Montana is a sub-normally pressured reservoir with significant hydrocarbon accumulation that lies near the northeastern corner of the Powder River Basin (Figure 1). Exploration and production activities for mineral and energy resources in the area over the last 55 years have yielded a significant amount of information about the geology of southeastern Montana and the northern Powder River Basin. Over the course of decades, oil and gas production through primary and secondary recovery (waterflood and polymer flood pilot tests) has resulted in reservoir decline and has now led to the planned implementation of a CO_2 injection-based tertiary oil recovery project for simultaneous EOR and CO_2 storage purposes. CO_2 will be delivered to the site via pipeline from the Lost Cabin gas plant, where it is separated from the process stream during refinement of natural gas. The plant is located in Fremont County, Wyoming (Figure 1). It currently generates around 50 million cubic feet of CO_2 per day.

CO_2 will be injected into the oil-bearing sandstone reservoir in the Lower Cretaceous Muddy (Newcastle) Formation at a depth of approximately 4500 feet (1372 meters). CO_2 injection will occur in a staged approach (nine planned CO_2 development phases, designated as Phases 1 to 9) across the field. It is expected that the reservoir will be suitable for miscible

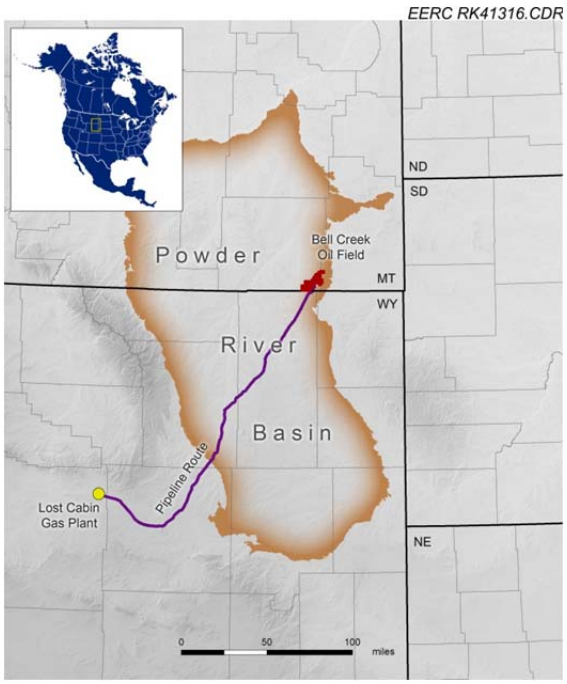

Figure 1. Map depicting the location of the Bell Creek oil field in relation to the Powder River Basin and the planned pipeline route to the site from the Lost Cabin gas plant.

flooding conditions with an incremental oil production target ranging from 30 to 50 million barrels. The activities at the Bell Creek oil field will inject an estimated 1.1 million tons of CO_2 annually, much of which will be permanently stored at the end of the EOR project.

Within the Bell Creek oil field, the Muddy Formation is dominated by high-porosity (25%–35%), high-permeability (150–1175 millidarcy) sandstones deposited in a near-shore marine environment (Encore Acquisition Company, 2009). The initial reservoir pressure was 1200 psi, which is significantly lower than the regional hydrostatic pressure regime (2100 psi at 4500 ft). The oil field is located structurally on a shallow monocline with a 1–2° dip to the northwest and with an axis trending southwest to northeast for a distance of approximately 20 miles. Stratigraphically, the Muddy Formation in the Bell Creek oil field features an updip facies change from sand to shale that serves as a trap. The barrier bar sand bodies of the Muddy Formation strike southwest to northeast and are overlain by a deltaic siltstone that strikes perpendicularly to the Muddy Formation and finally is partially dissected and somewhat compartmentalized by intersecting shale-filled incisive erosional channels.

The overlying Upper Cretaceous Mowry Formation shale will provide the primary seal, preventing fluid migration to overlying aquifers and to the surface. On top of the Mowry Formation are several thousand feet of low-permeability shale formations, including the Belle Fourche, Greenhorn, Niobrara, and Pierre shales, which will provide redundant layers of protection in the unlikely event that the primary seal fails to prevent upward fluid migrations fieldwide (Figure 2).

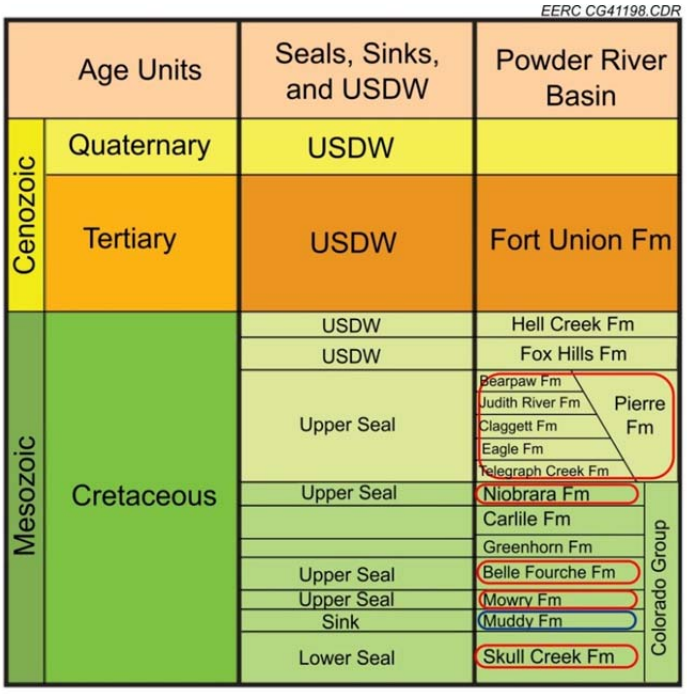

Figure 2. Late Cretaceous to Quaternary stratigraphic column of the Powder River Basin. Sealing formations are circled in red, and the primary oil-producing and sink formation is circled in blue. Formations bearing underground sources of drinking water (USDW) are also identified.

To meet project and simulation modeling goals, a detailed 3-D geologic model of the first CO_2 development phase (Phase 1) area and its surrounding area (Figure 3) was constructed, with pertinent geological and reservoir attributes. These attributes were collected and assigned based on a literature review of geologic reports; special core analysis, fluid analysis, and pressure, volume, and temperature (PVT) studies; and well logs. These data enabled the development of a detailed static geologic and dynamic flow model for Phase 1, to assess the impact of various operating conditions on miscibility, flow dynamics, and other reservoir properties. The constructed dynamic reservoir model was validated by history matching of gas, oil, and water production and water injection volumes for the period from 1967 to 2012. The history-matched reservoir model was then used to run predictive fluid flow simulations for three CO_2 injection scenarios with four cases per scenario. This culminated in 12 cases with results from the predictive simulations. Predictive fluid flow simulations were then run on three scenarios with four cases per scenario, which are discussed in detail later in the report.

To further understand the reservoir, a fieldwide 3-D geologic model (Version 2 model) is being constructed. It has properties similar to those of the Phase 1 model but will continue across the entire study area (Figure 4). Once the construction of this fieldwide geologic model is completed, a computer-assisted history-matching process using the available production and injection data will be applied to validate the model. Upon completion of successful history matching, predictive fluid flow simulations will commence with multiple CO_2 injection scenarios and cases based on the proposed injection plan.

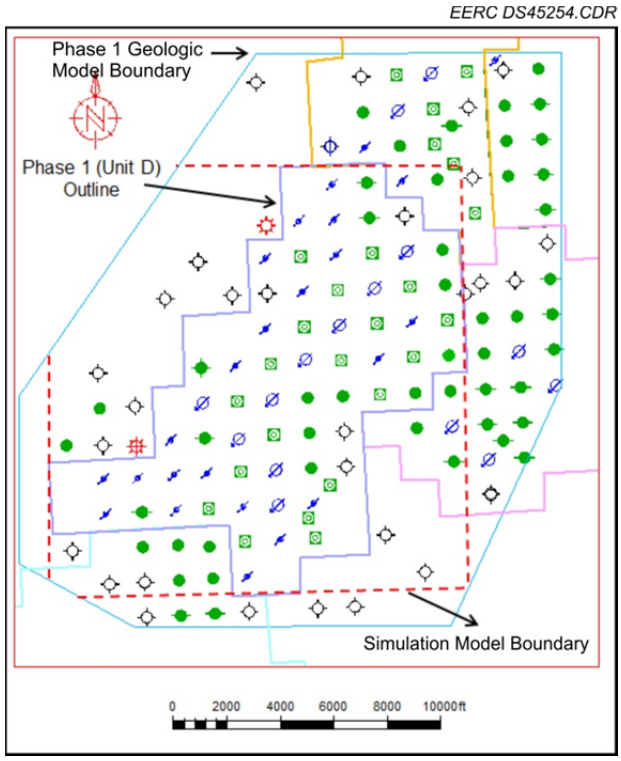

Figure 3. Static geologic and dynamic reservoir model boundaries for the Phase 1 (Unit D) area.

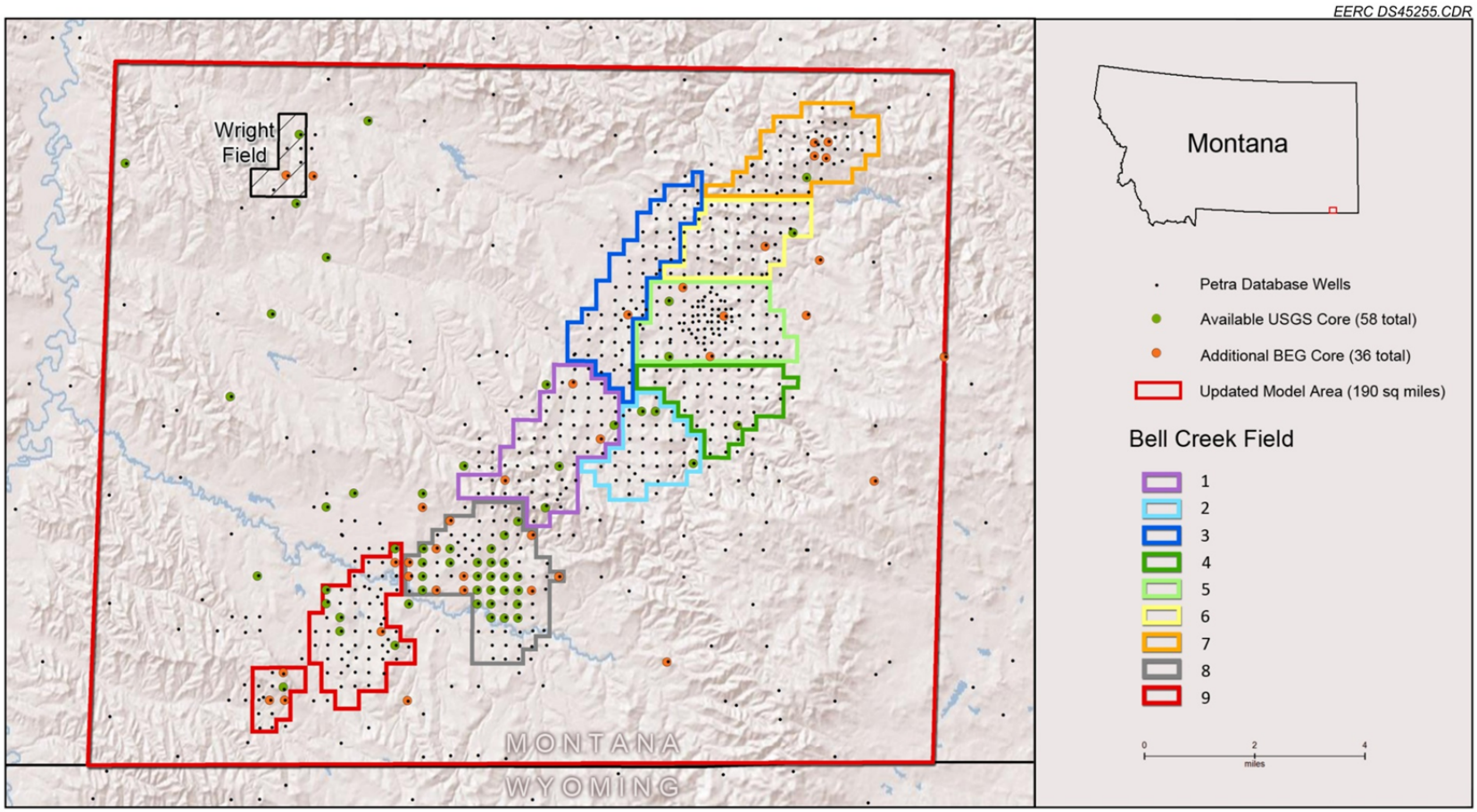

Figure 4. Study area for the fieldwide 3-D geologic model, showing all wells and cores available. (USGS stands for United States Geological Survey, and BEG stands for Bureau of Economic Geology at the University of Texas Austin, Houston Research Center.)

To assist in the overall MVA plan, a 3-D geomechanical model has been planned as a way to assess the potential for CO_2 leakage during and after injection. The foundation of a 3-D geomechanical model is a mechanical earth model (MEM) that has been built based on data received from the monitor well that was drilled in December 2011. The 1-D MEM has been constructed to assess the state of stress and rock properties for one individual well in the field. This analysis will be input directly into the 3-D structural model that will be the base for both the future 3-D geologic and geomechanical models.

PURPOSE

The PCOR Partnership is developing a philosophy that integrates site characterization, modeling, simulation, risk identification, and MVA strategies into an iterative process to produce meaningful results for large-scale CO_2 storage projects (Figure 5). Elements of any of these activities play a crucial role in the understanding and development of the others. The modeling and simulation activities described in this report were developed to 1) identify areas where more site characterization data is needed, 2) aid in the identification of potential subsurface risks such as out-of-zone fluid migration, and 3) help in the development of effective monitoring strategies. This integrated process will be iterated and refined through each incremental stage of the project, from initial planning to injection and through postclosure.

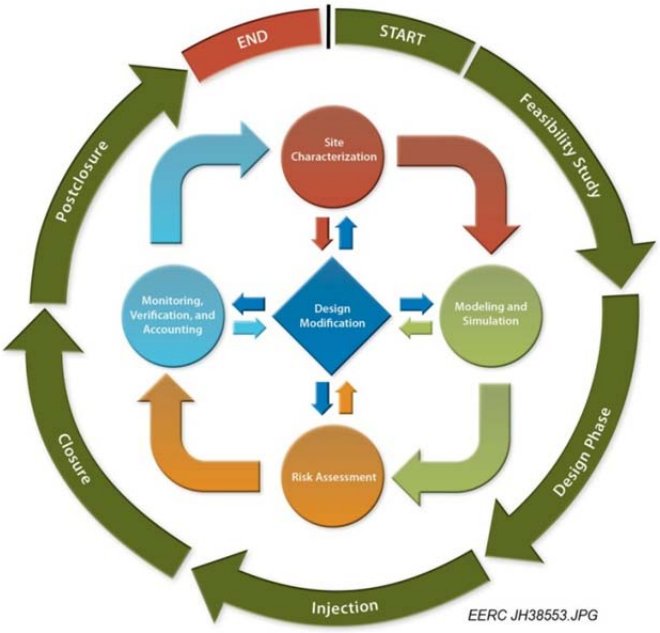

Figure 5. Project elements of the Bell Creek CO_2 capture and sequestration project. Each of these elements feeds into another, iteratively improving results and efficiency of evaluation.

The EERC's geologic and geomechanical modeling of the subsurface assists in understanding and predicting the behavior of the injected CO_2 and reservoir fluids over the injection and postinjection period. To aid in the validation of the reservoir model, history matching is performed on a numerically tuned dynamic reservoir model that is constructed using a completed 3-D static geologic model. This is followed by simulation work, which is a valuable tool for assessing scenarios of fluid migration within the reservoir and the potential for out-of-zone fluid migration. Additionally, simulation activities provide a means to evaluate the efficiency and applicability of various injection strategies and parameters related to both CO_2 storage and CO_2 EOR.

This type of assessment is an essential input for risk identification and to guide MVA strategies, as it lays the foundation for a project-specific, risk-based, goal-oriented MVA plan. The goal of the MVA plan is to effectively monitor the behavior of the CO_2 in the subsurface, the reservoir, and reservoir fluids to help ensure that the maximum benefit to the EOR process is achieved in a safe and efficient manner. Accurate simulations allow for targeted deployment of MVA data acquisitions at optimal geographic locations and time intervals to maximize the knowledge gained. The results and experience gained at the Bell Creek oil field will provide insight and knowledge that can be directly and readily applied to similar projects within the PCOR Partnership region and throughout the world.

SCOPE OF WORK

In order to evaluate the efficiency of large-scale CO_2 injection for simultaneous CO_2 EOR and CO_2 storage in the Muddy Formation of the Bell Creek oil field, several iterations of a 3-D geologic model coupled with dynamic simulation work are under way. The first static geologic model of the Phase 1 area (the Version 1 model) has been completed along with subsequent history matching and a few predictive simulation scenarios. Further predictive fluid flow simulations are being conducted to more accurately model CO_2 propagation in the subsurface. This allows for targeted monitoring activities and a means of theoretically evaluating various injection scenarios for oil recovery and CO_2 storage. Based on the insights gained from the Version 1 model, a second iteration representing the entire field—that is, the Version 2 model—is currently being built.

Extensive data reconnaissance was performed to fully evaluate both current and anticipated reservoir behavior, original oil in place (OOIP), incremental production assessments, and the ultimate fate of injected CO_2 through geologic modeling and dynamic simulations. Available data were analyzed, interpreted, and incorporated into the 3-D static geologic and dynamic reservoir models to represent geologic and reservoir properties in order to provide a solid groundwork for simulation activities. Furthermore, what was learned from construction and simulation of the Phase 1 geologic model was carried over into the fieldwide geologic model, which is more robust and less uncertain in several areas because of the incorporation of new and refined knowledge.

GEOLOGIC HISTORY

The Muddy Formation within the boundaries of the Bell Creek oil field comprises a near-shore marine barrier bar sequence that was deposited in the Albian age of the Cretaceous period (Figure 6), approximately 99 million years ago. Several transgressive and regressive sequences occurred over the Early and Middle Cretaceous periods, depositing the entire system seen within the Muddy Formation. At the base of the Muddy Formation lies the Skull Creek Shale which was deposited in an offshore marine environment where copious amounts of clay material could accumulate over an extensive time period. The Skull Creek was the direct result of sea rise southward across the Western Interior during the Early Albian age (Figure 6). This southward transgression continued and eventually joined the northward-transgressing Gulf Sea. At its maximum transgression, the Early Cretaceous seaway covered most of Montana, North Dakota, South Dakota, Wyoming, and Colorado and much of eastern Nebraska (Figure 7) (Vuke, 1984; Young, 1970).

The sea began a major regression northward during the Middle Albian (Figure 8). This regression exposed the Skull Creek to subaerial erosion and caused the formation of large deltas and major drainage systems that cut deep channels into the Skull Creek shale. These regressive deltaic and fluvial deposits make up much of the lower part of the Newcastle and Muddy sandstones (Wulf, 1962). The Newcastle sandstone and the Muddy sandstone are Lower Cretaceous Albian-age rocks, deposited in western North Dakota and southwestern Montana, respectively (Figure 6). Weimer et al. (1982) interpret variations in thickness and lithology within the Muddy/Newcastle Formation as being caused by recurrent movement on basement fault blocks, influencing the location and pattern of the incised valleys. Evidence of the regressing shoreline can be found as far north as southern Montana (Vuke, 1984). This major regression and maximum lowstand of the sea combined with the subsequent and future transgression allowed deltaic sediments to be reworked into beaches, offshore bars, and barrier bars.

The sea began to transgress south again during the Late Albian (Figure 9). This transgression eroded and reworked the previous deltaic sands, forming a major unconformity termed the Coastal Plain Member within the Muddy and Newcastle sandstones. Valleys incised into the Coastal Plain were also filled with marine sands and muds. As the sea deepened during another dominant transgressive stage, it began to deposit the thick marine shales of the Mowry Formation on top of the Muddy and Newcastle Formations.

Local Depositional Environments

The Muddy Formation comprises, in descending order, the Coastal Plain Member, the Bell Creek Sandstone Member, and the Rozet Member (Figure 6). The Muddy Formation is stratigraphically positioned between the thick marine shale sequences of the Skull Creek and Mowry Formations. Within the field, the Muddy Formation has an average depth of 4500 ft and dips to the northwest at about 1–2°. The nomenclature for the sequences within the Muddy Formation has changed over time and is regionally variable.

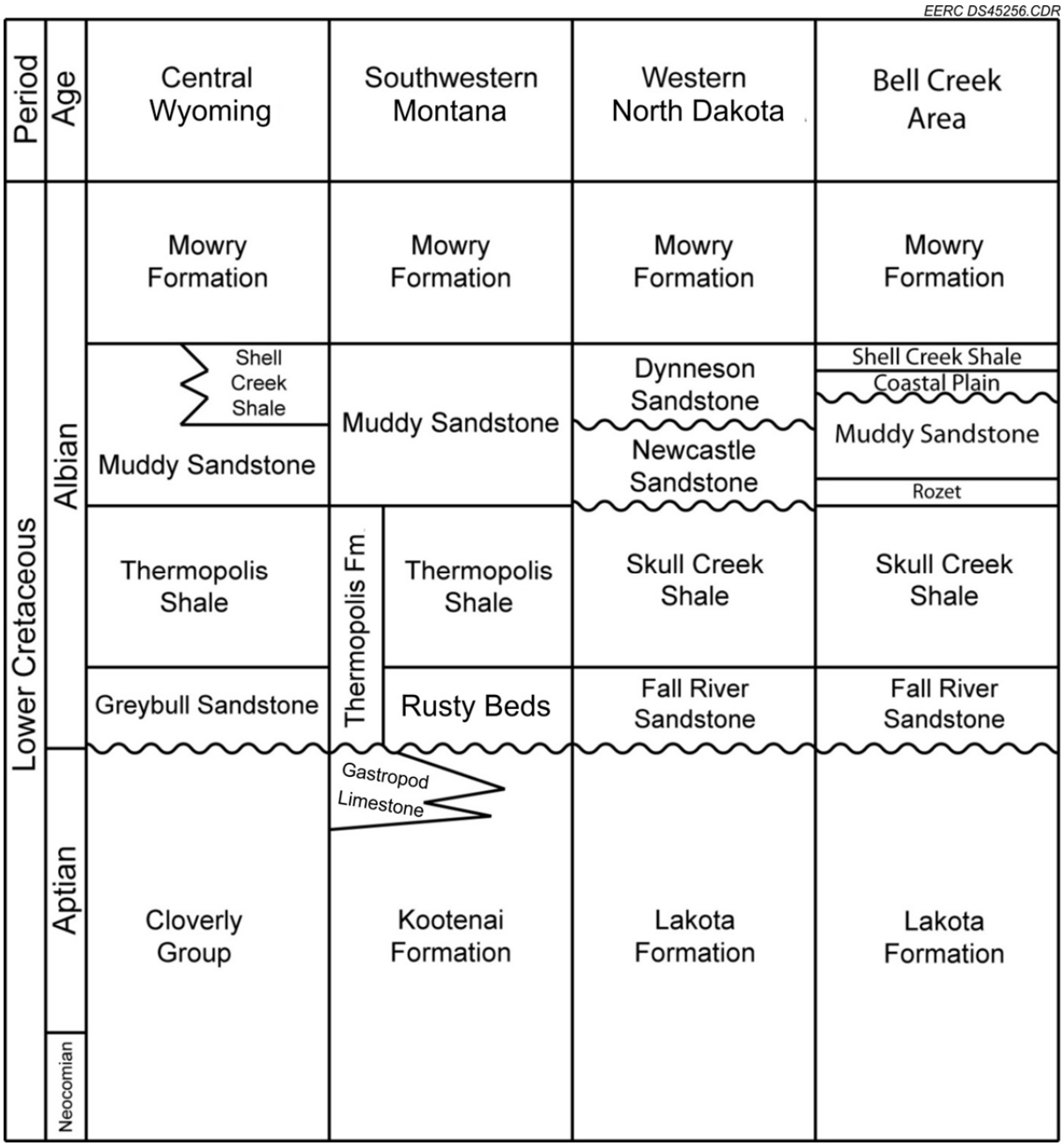

Figure 6. Stratigraphic column of the Lower Cretaceous period. The Bell Creek Area column contains the nomenclature used in this report (modified from Vuke, 1984).

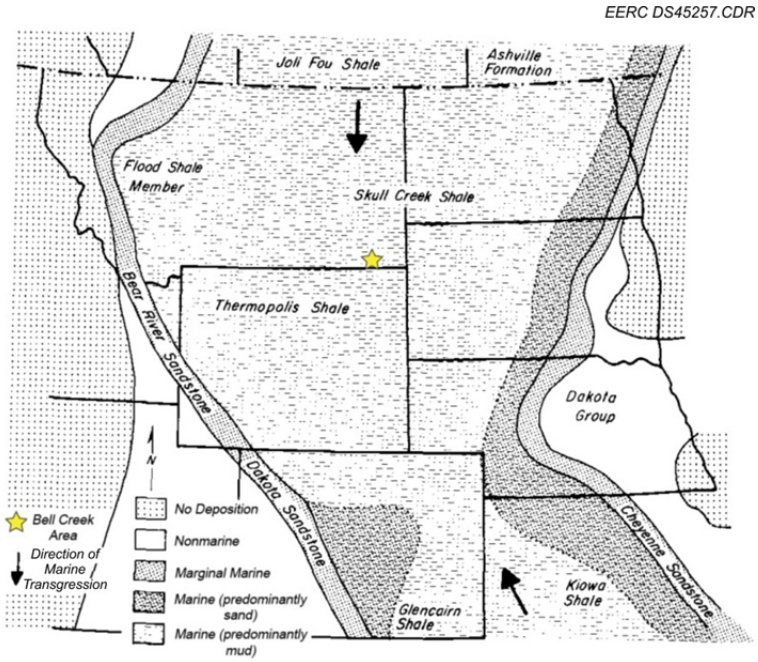

Figure 7. Maximum transgression of the Early Cretaceous seaway, depositing the Skull Creek shale. (Modified from Vuke, 1984.)

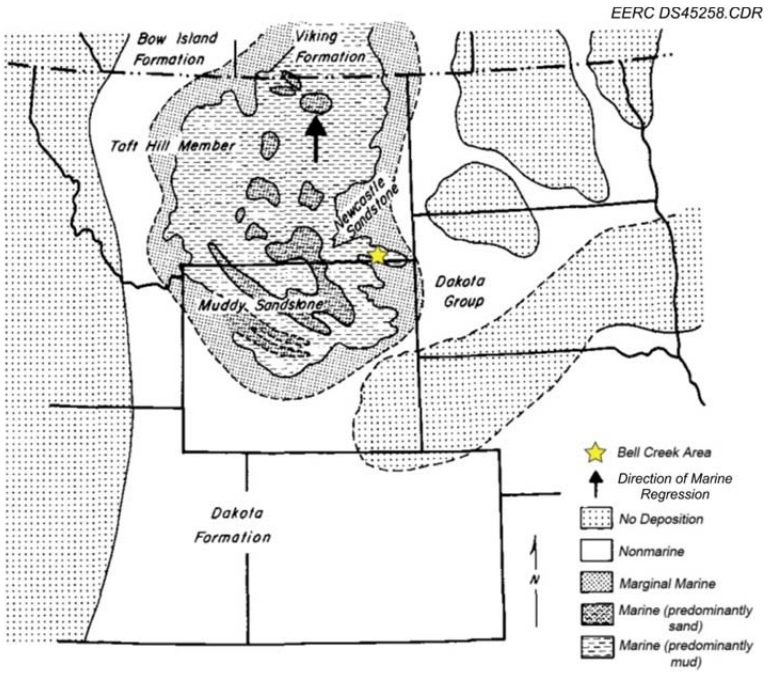

Figure 8. Regression of the Early Cretaceous seaway, depositing the Muddy sandstone. (Modified from Vuke, 1984.)

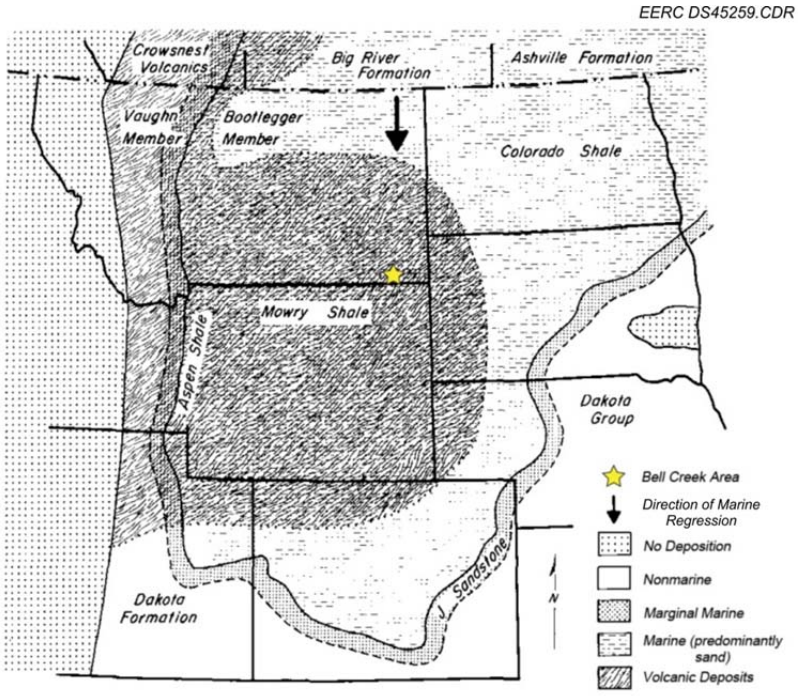

Figure 9. Transgression of the Early Cretaceous seaway, depositing the Mowry shale. (Modified from Vuke, 1984.)

The Rozet Member directly overlies the Skull Creek shale and is marked by a thin (0.5–3 ft) hummocky cross-stratified sandstone bed, which is conformably overlain by a dark gray mudstone (Molnar and Porter, 1990). This sequence was deposited in an offshore marine environment and marks a basinward shift in facies, correlating to the first major regression of the Western Interior Seaway that deposited the Skull Creek shale, as described above. After a minor rise in sea level, corresponding to the dark gray mudstone at the top of the Rozet Member, sea level began to fall again (regression).

As sea level continued to fall, large deltas and drainage systems began to form and cut channels into the Skull Creek shale. The Bell Creek Member is composed of stacked barrier-bar sediments that were reworked and transported by longshore drift from these drainage systems (Molnar and Porter, 1990). The barrier-bar sands of the Bell Creek Member make up the best reservoir rock within the field. These sediments intertongue with marine shales to the west-northwest and lagoonal sediments to the east-southeast, representing minor changes in sea level during deposition. This facies change up-dip to the east and southeast provides the trapping mechanism to allow pooling of hydrocarbons in the barrier-bar sandstones.

The Coastal Plain Member lies unconformably on the Bell Creek Member. It was deposited when another drop in sea level caused the incision of fluvial channels into the Bell Creek Member, some of which cut down to the Skull Creek shale. These channels, oriented mainly east-west, were filled with fluvial sandstone, floodplain shale, coal, and marginal marine deposits during the subsequent rise in sea level (Molnar and Porter, 1990). This sea level rise

corresponds to the early stages of the major transgression that led to the deposition of the Mowry shale.

PHASE 1 3-D GEOLOGIC MODELING

The 3-D geologic modeling efforts completed so far were focused on Unit D or the Phase 1 area and its vicinity because the first CO_2 development phase is planned in Unit D. To construct a detailed 3-D static geologic model of the Phase 1 area (Version 1 model), fieldwide data reconnaissance activities were performed to acquire pertinent reservoir characterization data for the entire Bell Creek oil field in general and the Phase 1 area in particular. Because of the historical oil and gas activity within the field, an abundance of vintage geologic data exists in the form of geophysical well logs, lithology descriptions from well files, geologic maps, core data analysis, and cross sections. These data aided the selection of stratigraphic tops across the study area. In order to create a structural framework, stratigraphic tops must be picked for each zone of interest. This is primarily accomplished by analyzing geophysical well logs and incorporating other applicable geologic data, ultimately assigning a depth value to each top.

Advanced 3-D geologic modeling utilizing Schlumberger's Petrel® software was conducted in order to characterize the geologic framework of the Muddy Formation within the geologic model boundary that is underlain by Skull Creek shale and overlain by Mowry shale. The study area encompasses the Phase 1 area and portions of the Phase 2, 3, and 8 areas so as to engage surrounding data and eliminate extrapolation edge effects (Figure 10). The 3-D geologic model was constructed to incorporate a distribution of geological and geophysical properties, commonly referred to as petrophysical properties. These properties were geostatistically assigned throughout the model and include the following:

- Total porosity
- Shale volume
- Effective porosity
- Net-to-gross ratio
- Absolute permeability
- Water saturation
- Formation pressure
- Formation temperature

The geologic framework and assigned properties contained within the geologic model are necessary components for performing dynamic flow simulations that aid in estimating CO_2 storage and EOR efficiencies; estimating CO_2 breakthrough time at various production wells; studying the long-term CO_2 plume and pressure behaviors and ultimate fate of injected CO_2; and estimating OOIP and incremental oil recoveries. Various predictive simulation scenarios also provide necessary inputs for preparing and enhancing a monitoring program to track CO_2 movement in the reservoir through targeted monitoring equipment deployments.

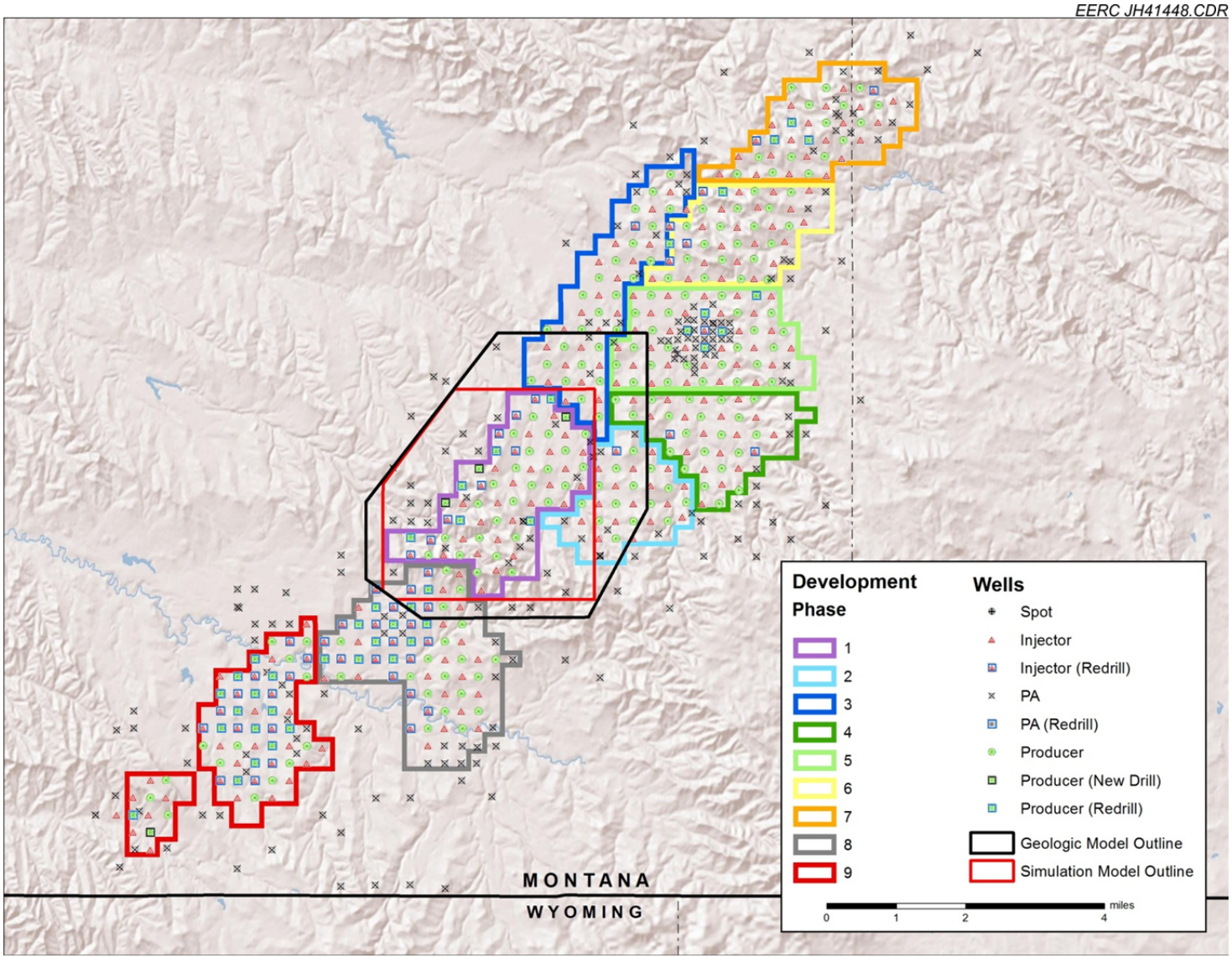

Figure 10. Map showing the geologic model boundary (black), the dynamic model boundary (red), and their relation to the planned Bell Creek project development phases. (PA means plugged and abandoned.)

Stratigraphic Framework

The Muddy Formation in the area of the Bell Creek oil field consists of four distinct lithofacies, which were assigned structure and variability according to observed properties and trends in available data. In ascending order, these depositional sequences are designated as the Rozet, the Bell Creek sand, Coastal Plain, and the Springen Ranch shale. For the geologic model, the Bell Creek sequence was further subdivided into three separate but connected producing zones: BC10, BC20, and BC30, corresponding to three previously identified barrier-bar sequences in the field. The Bell Creek subdivisions were implemented in order to model and assess compartmentalization in the reservoir caused by short-scale transgressive/regressive events, which led to deposition of thin layers of low-permeability rock in some areas. Subdivision also enables finer-scale property prediction based on more focused and geostatistically applicable rock.

Following data preparation and analysis, over 1000 formation subunit tops were picked from analysis on 154 wells within the model boundary. The stratigraphic tops were used to generate surfaces representing intervals of interest containing geologically similar reservoir properties. A total of seven surfaces were produced for the 3-D geologic model: Springen Ranch, Coastal Plain, Bell Creek 10 (BC10), BC20, BC30, Rozet, and a basal surface corresponding to the Skull Creek (Figure 11). The Springen Ranch and basal surfaces were assigned arbitrary thicknesses so as not to incorporate several hundred feet of nonrelevant tight cap rock.

Areas exist within the geologic model where pressure compartmentalization and sparse available well log data show that the Bell Creek sand has been completely eroded away, resulting in a network of deep incised valleys, which were later filled with tight marine sediments (Figure 12). Definition of these barriers will be imperative to the design of the injection process and the analysis of long-term reservoir flow effects. History-matching practices will aid in defining the impact of the incised valley network present in the Bell Creek oil field.

Structural and Property Model

Grid thickness was assigned to each zone to refine reservoir properties and model resolution. In total, 34 layers were assigned to the structural model within the six zones (Table 1), based on optimal grid size analysis that resulted in cell sizes of 100 ft × 100 ft and maximum thicknesses of 3–5 ft. The model contains a total of 1,462,884 grid cells, with 202, 213, and 34 cells in the i, j, and k directions, respectively.

The structural model was then populated with petrophysical properties obtained through data reconnaissance. These properties include total porosity, shale volume, effective porosity, net-to-gross ratio (NTG or N/G), horizontal permeability (K_{xy}), water saturation (S_w), formation pressure, and formation temperature. The distributions of these properties within the 3-D geologic model are provided in Appendix A. The example distributions of various properties in the 3-D geologic model are shown in Figures A-2 to A-13 of Appendix A.

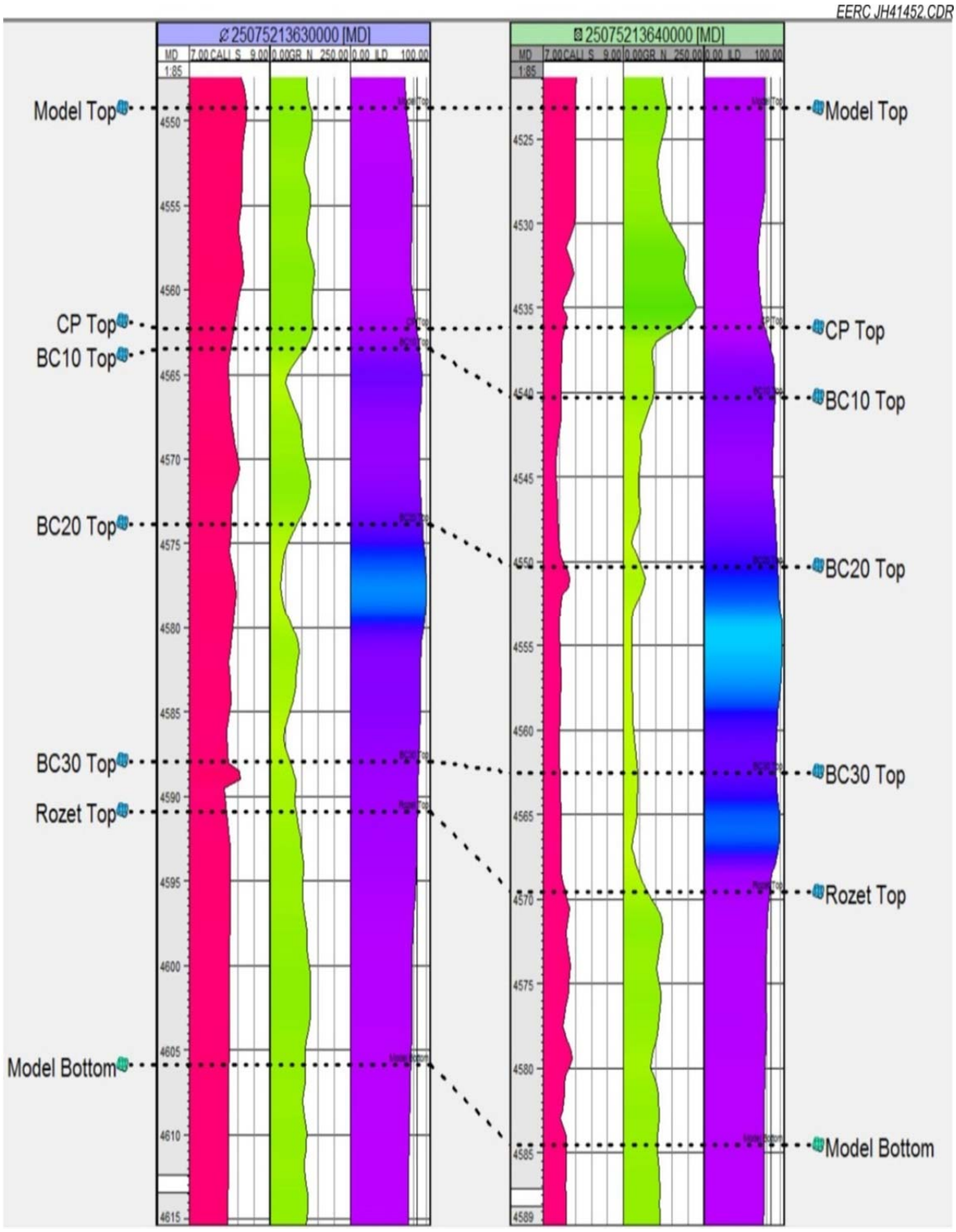

Figure 11. Type log including the seven picked stratigraphic tops. (CP designates Coastal Plain.) The first column from left to right is caliper, followed by gamma ray and resistivity.

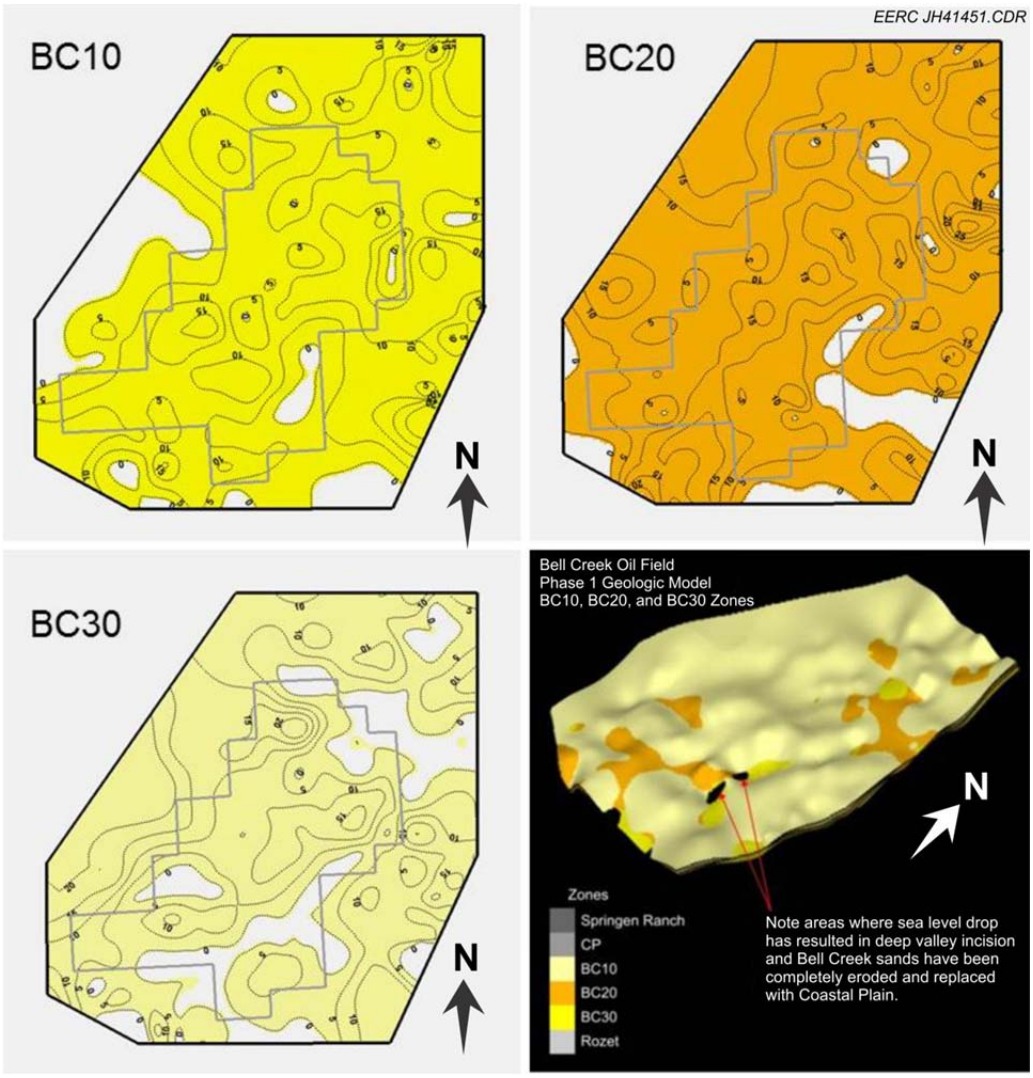

Figure 12. Map views of the BC10, BC20, and BC30 zones with labeled thickness contours. The Phase 1 development area outline is in gray.

Table 1. Model Layering of the Geologic Model

			Cell Thickness, ft	
Zone	Layers	Layer Numbers	Range	Average
Springen Ranch	3	1–3	4.33	4.33
Coastal Plain	5	4–8	0–4.5	0.94
BC10	8	9–16	0–3.0	1.03
BC20	8	17–24	0–3.4	1.08
BC30	7	25–31	0–3.1	1.05
Rozet	3	32–34	5	5.00

Limitations

The Phase 1 3-D geologic model (Version 1 model) has several areas of uncertainty due to limited availability, or nonavailability, of certain geologic and reservoir data. The use of preprocessed data from an historical database also seems to be a major contributing factor for such uncertainties. The lidar (light detection and ranging) data have since been acquired across the entire field to help quality assurance and quality control (QA/QC) of actual well locations and the associated ground elevations. This QA/QC workflow moved some well locations by up to 200 feet in the x and y directions and up to 100 feet in the z direction. The z-direction shifts (elevation shifts) require recalculations to be made for stratigraphic tops, perforation intervals, and property distribution among the geophysical logs. Furthermore, this model was built prior to drilling of the monitoring well in December 2011. The newly drilled monitoring well (0506 OW) has provided an extensive suite of log and core data. These newly acquired data will be used in future modeling construction, including the fieldwide 3-D geologic and geomechanical models and the 1-D MEM.

PVT AND SLIM-TUBE EXPERIMENT MODELING

PVT Study

The successful compositional simulation of various oil recovery stages (primary depletion, secondary waterflood, and tertiary CO_2 EOR) relies greatly on the accuracy of the equation of state (EOS) model used in the compositional simulation. A robust EOS model is needed to accurately define various thermodynamic properties and phase behavior of reservoir oil and injected solvents (water or CO_2) at varying reservoir conditions.

A seven-component Peng–Robinson (PR) EOS model was developed and tuned based on the available experimental PVT data using WinProp™, a phase property program developed by the Computer Modelling Group Ltd. (CMG). The available experimental PVT data for three Bell Creek crude oil samples from Wells 2605, 2608, and 0511 (Figure 13) were used to develop this EOS model, used in the dynamic simulation work described in this report. These data include constant composition expansion (CCE), differential liberation (DL) analysis, separator, swelling test, and compositional analysis of recombined live crude oil. The composition of a recombined live crude oil sample (Well 0511) expressed in terms of the carbon number of hydrocarbon constituents is shown in Figure 14.

Simulations of PVT experiments on the three available samples were conducted. Because of the tight range of resulting data, only the results from Well 0511 are discussed, as the data set and location of this well are most applicable to the model area. PVT data from Well 0511 were tested in regard to simulated results of DL, CCE, and swelling tests and showed less than a 2% variance between experimental data and simulated results obtained from the tuned EOS model. Comparative results between the simulation results and the PVT experimental data are shown in Figures B-1 through B-3 of Appendix B.

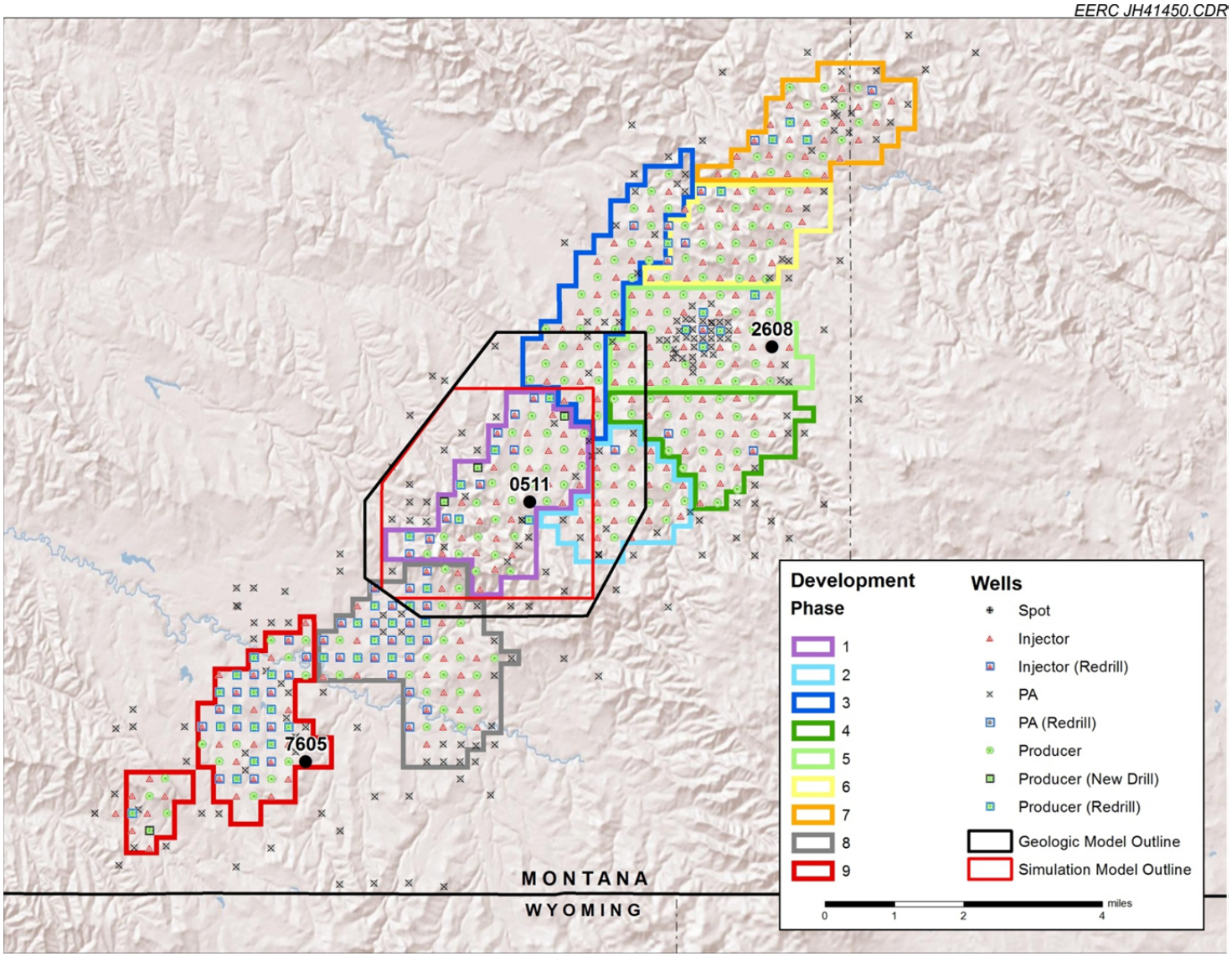

Figure 13. Map of the Bell Creek oil field, showing development phases and the three wells with available PVT analysis within the field.

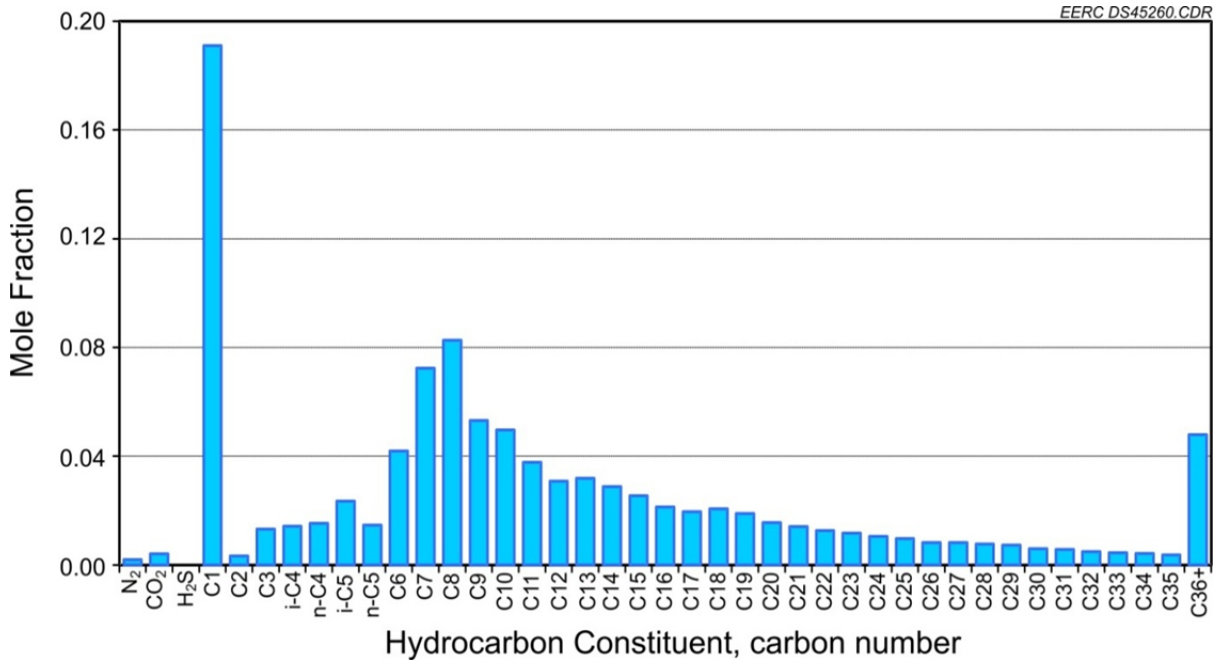

Figure 14. Composition of recombined live crude oil (Well 511).

EOS Model-Based Predictions of Minimum Miscibility Pressure

Injected CO_2 interacts with reservoir fluids to lower interfacial tension between different phases and reduce the oil viscosity. The fashion and efficiency of this system are highly dependent on reservoir conditions (pressure [miscible or immiscible] and temperature) but are also a function of gas and oil composition. For instance, high-molecular-weight oil and oils already containing dissolved gas such as methane and nitrogen tend to have higher minimum miscibility pressures (MMPs). Therefore, it is necessary that the EOS model developed to perform phase equilibrium and property calculations also be able to reasonably predict the MMP for better representation of compositional changes occurring in the reservoir during a CO_2 injection displacement process.

Compositional analyses of Bell Creek crude oil from Wells 2608 and 0511 show that the reservoir produces sweet black crude oil with a mole fraction of liquid hydrocarbons (carbon number greater than C_7 [i.e., C_{7+}]) greater than 25% for all samples. Results show that the crude oil samples from Wells 2608 and 0511 are of similar composition. The same were utilized in conjunction with appropriate reservoir conditions in order to predict MMP. Table 2 provides a comparison of experimental values of MMP (obtained from slim-tube tests performed with initial reservoir oil and pure CO_2) and calculated simulation results.

On the basis of collected experimental data, the solution gas-to-oil ratio (GOR, expressed in standard cubic feet [scf] per stock tank barrel [stb] of oil) as a function of pressure, was determined from the DL experiment, as shown in Table 3. After the regression of PVT tests, the predicted CO_2 MMP for oil with a GOR of 227.8 scf/stb is 2875 psia. It should be noted,

Table 2. Comparison of Experimental MMP Values and Calculated Simulation Results

	Oil from Well 0511		
Experimental	3181		
	C_{6+} Fraction	C_{36+} Fraction	Component Lumping
Calculated	2825	2750	2725

Table 3. MMP for Reservoir Fluid and Stock Tank Oil (Well 2608)

Bubble-Point Pressure, psia	GOR, scf/stb	MMP, psia
1208	227.80	2875
915	175.64	2665
615	126.71	2470
215	54.32	2140
15	0	1915

however, that the PVT tests for oil samples with GORs other than 227.8 scf/stb were not performed. With the exception of the MMP prediction of 2875 psia, the other MMP predictions were made without regression of PVT tests. It has been shown that GOR has a strong impact on MMP, with higher light fractions raising miscibility pressures and low gas contents lowering miscibility pressures. These results suggest that current MMP could be in range from 1900 to 2100 psia.

Light fractions in Bell Creek crude oil consist primarily of methane (C_1). The mole fractions of the methane were varied to have different GORs in the reservoir fluid, and then a simulation was run to predict the MMP (Table 3). The predicted value for MMP dropped 33%, from 2875 psia for Bell Creek recombined live crude oil to 1915 psia for the stock tank oil, which is considered to be completely degassed (Figure 15). CO_2 MMP for the reservoir fluid as the solution gas is released decreases monotonically with the GOR of the oil, assuming the primary gas contribution is methane. The results show that the effect of GOR (solution gas) present in the oil can be significant. While GOR and the required reservoir pressure are complicated in terms of reservoir heterogeneity and past and future management, this value should be a target to reach, exceed, and maintain to maximize production. In the event that compartmentalized blocks have been shown to produce low gas or dead oil, miscibility may be significantly lower, as predicted above, and may be reasonably managed as such if lower pressures are determined to be practical.

In order to test the suitability of the tuned EOS model for reliable modeling of compositional changes occurring in the reservoir during the displacement of reservoir oil by CO_2 injection, 1-D compositional simulations of the experimental slim-tube test were also performed. The results are summarized next.

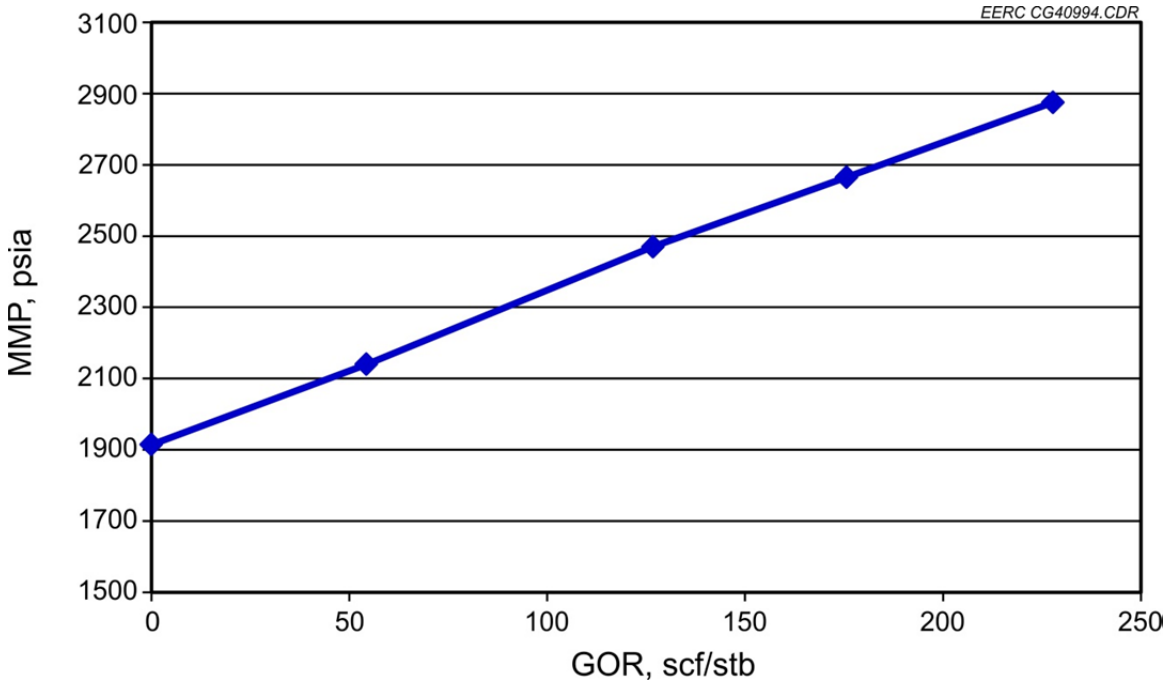

Figure 15. Graph illustrating the calculated effects on MMP as the GOR is increased.

1-D Compositional Simulation of the Slim-Tube Test

The slim-tube test is one of the most widely used experimental methods to determine or estimate MMP. Slim-tube MMP in this project (data provided by Denbury) was determined by performing displacement experiments in a 60-ft slim tube with an inside diameter of 0.25 in., producing 1-D displacement with a very low level of mixing. The slim tube has an average pore volume of 151 cm^3. The packing material was 160–200 mesh quartz sand.

The slim-tube test begins with a sand pack saturated with oil at a constant temperature. CO_2 is introduced at a given pressure (controlled by a back pressure regulator), and oil displacement is measured as is oil recovery. No water is involved. In the experimental study, a number of slim-tube displacements were conducted at the pressures of 1215, 3015, 3515, and 4515 psi at the reservoir temperature (108°F) to determine the MMP of Bell Creek crude oil. An oil recovery factor of at least 90% at 1.2 hydrocarbon pore volumes (HCPV) of CO_2 injected is used to define the MMP of the system.

1-D compositional simulations of the experimental slim-tube test were performed using CMG's GEM, a generalized EOS model compositional reservoir simulator. GEM can simulate compositional effects of reservoir fluid during primary and enhanced oil recovery processes (Computer Modelling Group Ltd., 2011).

In these simulations, the slim tube was represented by a one-dimensional linear model using 480 grid blocks. The cross section of the slim tube was 0.25 in. × 0.25 in. CO_2 was injected at a low constant rate of 0.1667 cc/min into the simulation model. One injector and one producer

were incorporated at the ends of the model. Selected properties of slim-tube model data are summarized in Table 4.

The experimental slim-tube displacements conducted at different operating pressures (1215, 3015, 3515, and 4515 psi) were simulated. The detailed simulation results are provided in Appendix B (Figures B-4–B-8). The gas injection duration for all of the slim-tube experiments was about 18 hours, and the cumulative injected CO_2 was about 1.2 HCPV for each slim-tube test. The experimental MMP was determined by calculating the intersection point between the line of high recovery and the line of low recovery after 1.2 pore volumes (PV) of gas injection to be 3181 psi (Figure 16). Percentage of oil recovery at 1.2 HCPV of CO_2 injected from simulation

Table 4. Slim-Tube Model Data

Length, ft	60
Porosity, fraction	0.2607
Permeability, md	4900
Pore Volume, cm^3	151
Number of Grid Cells	480
Grid Size in the k Direction, ft	0.125
Grid Size in the i and j Directions, ft	0.01846

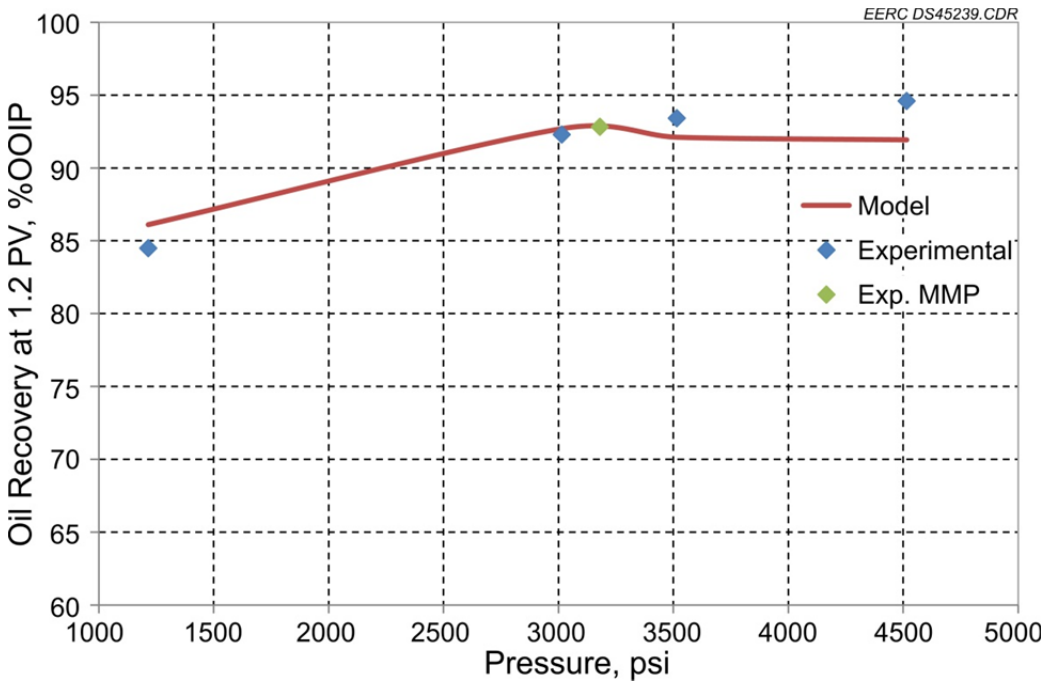

Figure 16. Comparison of simulated MMP and experimental MMP at 108°F with CO_2.

was plotted against slim-tube operating pressures to determine the MMP of the system. As shown in Figure 16, simulated MMP of the system is estimated to be 2750 psi at 108°F. Figure 16 also shows the comparison of simulated MMP and experimental MMP for the initial reservoir oil–pure CO_2 system at 108°F. As showed in Figure 16, a good agreement between the simulated and experimental recoveries at different pressure steps indicates the robustness of the developed EOS model.

PHASE 1 RESERVOIR SIMULATION

While the geologic model provides a framework for dynamic simulation activities, the dynamic reservoir model incorporates a variety of additional reservoir data to accurately simulate the reservoir's pressure and fluid mobilization response to injection or production processes. Much of the geologic and structural reservoir properties were directly incorporated through the integration of the 3-D geologic model. Several realizations of the static geologic model were generated using Petrel, which is a geologic modeling software product developed by Schlumberger. One of the static geologic model realizations having mean OOIP value was exported to the CMG Builder software to construct a reservoir model. The PVT data, relative permeability data, well production history, and so on were brought into CMG Builder to begin the process of building the dynamic reservoir model.

Fluid flow simulation was performed on the dynamic reservoir model using CMG's GEM. These flow simulation studies allowed the validation of the geologic model and the fine tuning of model parameters to match reservoir production, pressure, and injection responses through history matching. After a history match was done, the predictive simulations of CO_2 injection and CO_2 water alternating gas (WAG) injection were run. The results of history matching and predictive simulations are provided in Appendix C.

The dynamic reservoir model used for history matching and predictive simulations covers the Phase 1 area and a small portion of the surrounding areas. Of the 104 wells involved, 68 are production wells, and 36 are injection wells (32 converted injectors and 4 injectors). All of the wells are vertical wells. The grid was 158 × 162 × 34 with 870,264 total cells in the dynamic model. The grid block size was 100 ft in length and 100 ft in width. The thickness of each grid varied, with the average grid cell thickness being 1 ft. Figure 17 shows a 3-D view of the structural top of the dynamic simulation model. The depths shown in Figure 17 correspond to subsurface true vertical depth (SSTVD).

Numerical Tuning and History Matching

Different numerical settings were attempted to optimize and tune the simulation model for increasing the speed of the simulation runs by optimization criteria balance error, central processing unit (CPU) time, and solver failure percent. History matching is a method of adjusting reservoir characteristics (variables) of a simulation model to match historical field data (production or injection data) through an iterative trial-and-error process. This trial-and-error process varies parameters and properties within accepted and realistic engineering and geologic

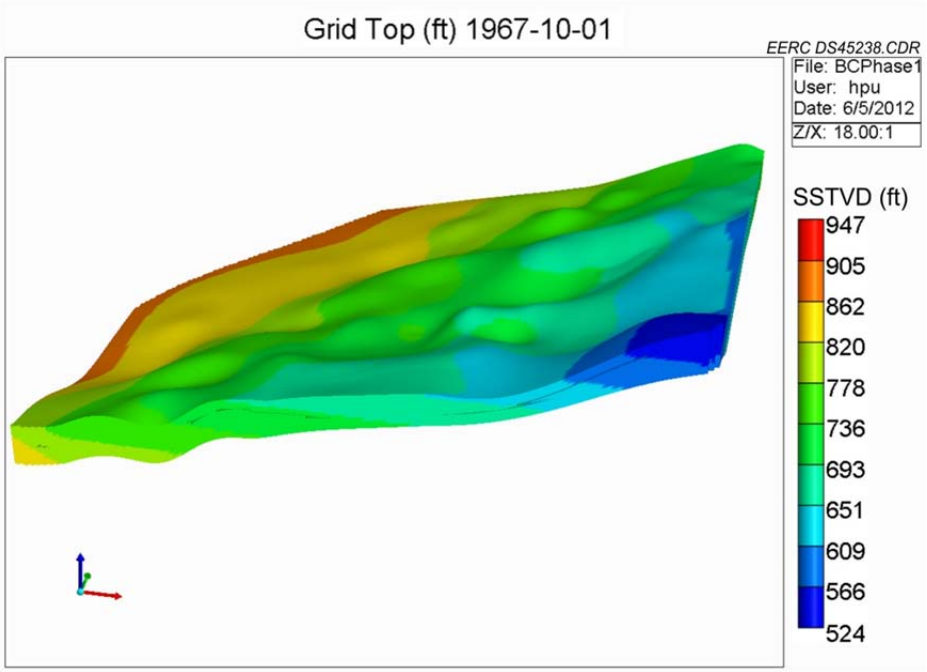

Figure 17. 3-D view of the dynamic simulation model.

limits. In this way, the resulting properties and parameters still accurately reflect the original hard data. History matching reduces the geologic uncertainties, which will allow for more accurate prediction of future reservoir performance during and after injection. Simulation runs to match the reservoir's oil and water production during primary depletion and waterflooding were run using the dynamic reservoir model described above. The history match was performed utilizing production and injection rates from the field dates spanning from 1967 to 2012. The reason behind simulating the full history was to provide an estimate of fluid saturation and reservoir pressure before the CO_2 flood and to provide an accurate representation of the current reservoir conditions. During the history match period, oil production rates were used as primary constraints, and bottomhole pressures were used as the secondary constraints. Historical oil production and water rates and water cut of each well were used to compare with the simulation adjusted. After a number of simulation runs, which included modifications of the relative permeability curve, permeability, and well productivity indices, a reasonable good match of the production history was obtained, as shown in detailed simulation results presented in Appendix C.

Phase 1 Areawide History-Matching Results

The detailed history-matching results of the Phase 1 areawide dynamic reservoir model are provided in Appendix C (Figures C-1–C-9) and are briefly discussed here. The resultant oil production rate and actual production rate are plotted versus time in Figure 18. The simulated and actual water cut of the field are shown in Figure 19, where the symbols represent the field data while the curves represent the simulation results. A good match between the actual water cut

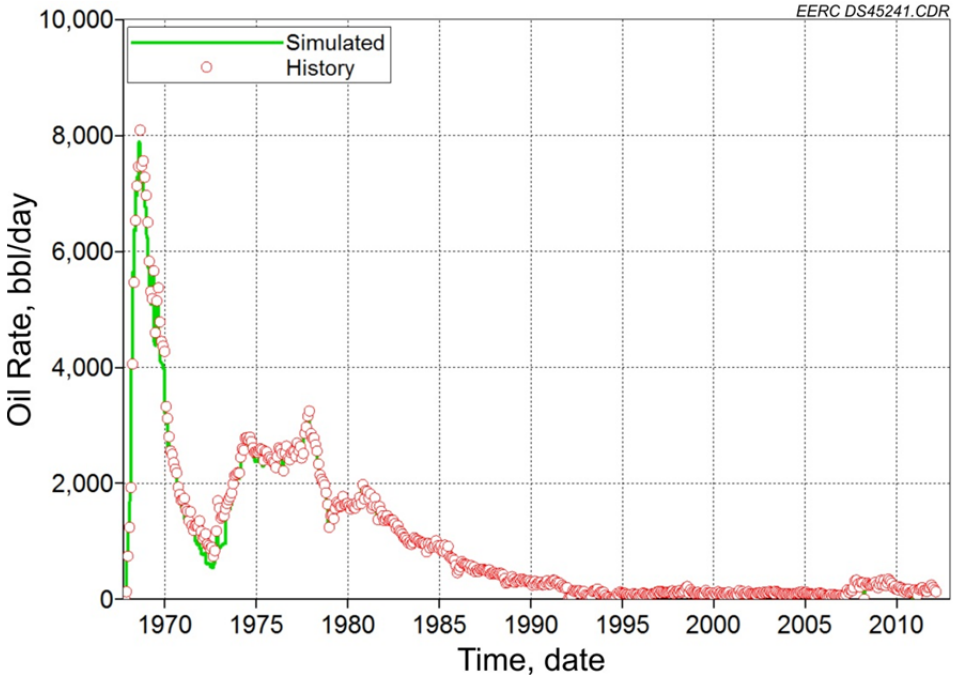

Figure 18. History-matching result of field oil rate.

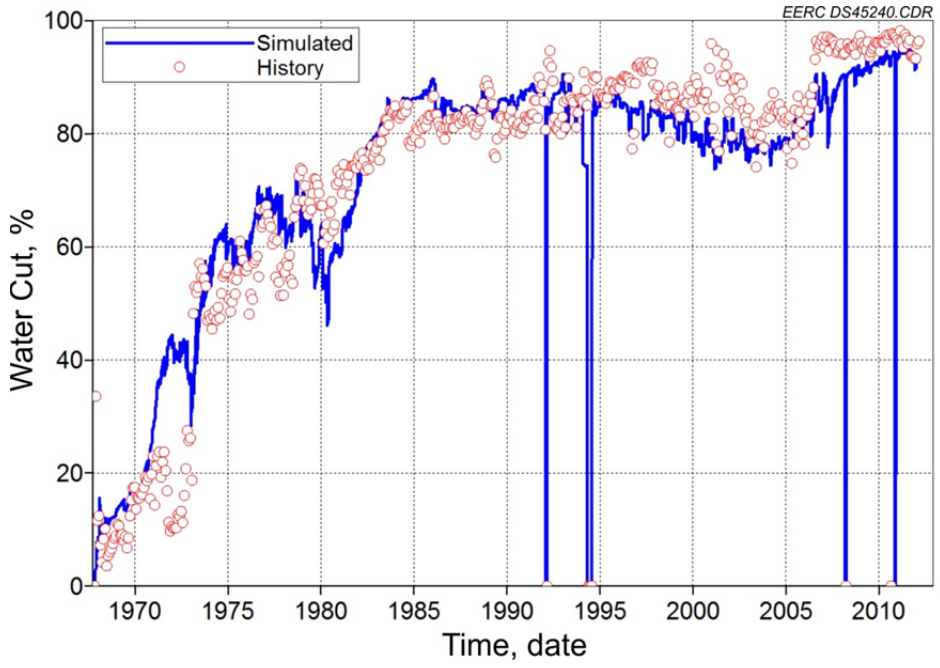

Figure 19. History-matching result of field water cut.

and the simulated water cut was observed (Figure 19). The figure shows a very good match between the actual production rate and the simulated production rate because the oil production rate is specified as input based on the actual production record. Figure 20 shows the history matching result of gas rate. The simulated gas production rate fits with the historical data. Initial hydrocarbon production at the Bell Creek oil field was solution gas drive, so the gas rate increased rapidly and then dropped during the primary depletion.

Figure 21 shows the average reservoir pressure based on the model calculation. The actual reservoir pressure history, except for a few initial reservoir pressure data (1100–1200 psi at an average depth of 4500 ft) obtained in drill stem tests (DST), is unavailable; hence, the simulated reservoir pressure response could not be verified. The history-matching results show that reservoir model was able to inject the specified water rate throughout the history. The examples of remaining oil saturation of top layers of Coastal Plain (CP) and BC10, BC20, and BC30 are shown in Figure C-7 of Appendix C.

Individual Well History-Matching Results

In order to verify the primary history-matching model, individual wells were also history-matched. The detailed results are provided in Appendix C (Figures C-8 and C-9). These results show the water-cut behavior observed in primary and secondary recovery for twelve individual wells. As can be seen in these figures (C-8 and C-9), the actual and simulated water cut data for individual wells are in good agreement. The model was able to produce the specified oil rates throughout the history. As a result, oil rates of individual wells are not shown in the history-matching plots.

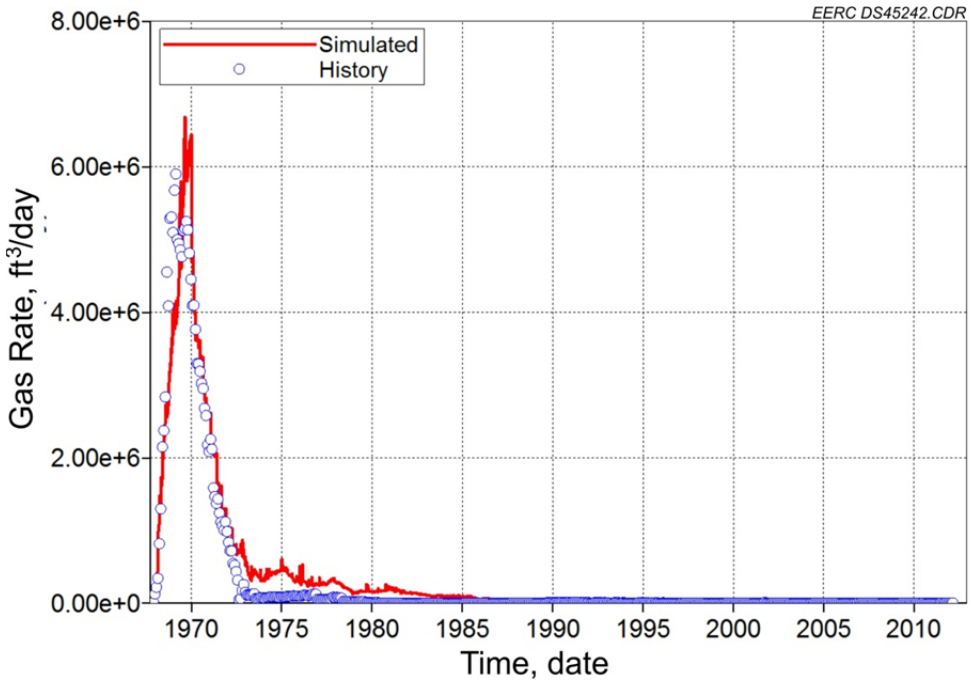

Figure 20. History-matching result of field gas rate.

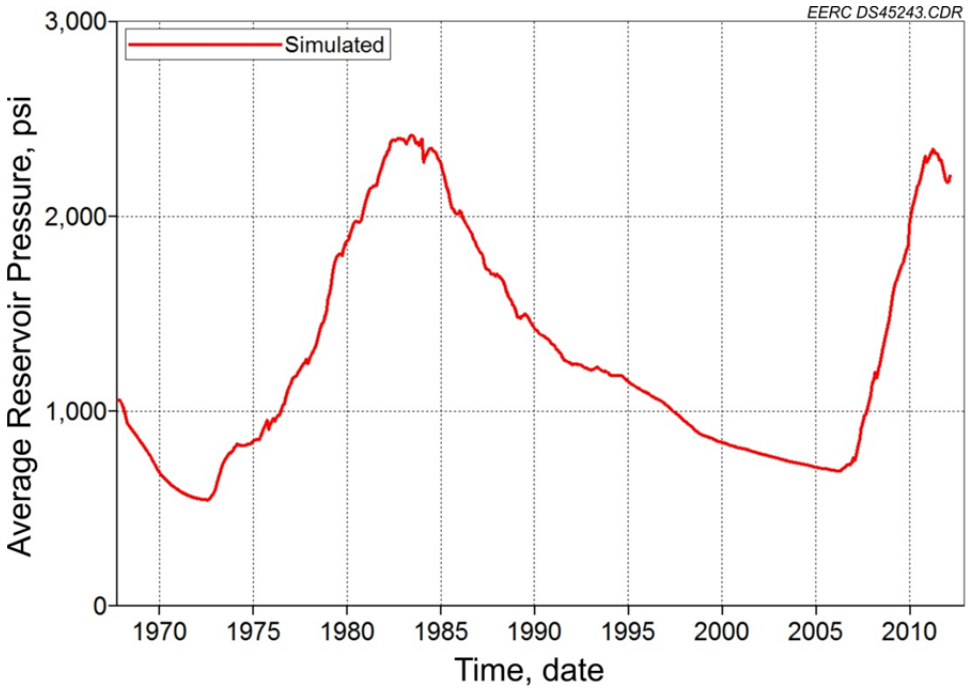

Figure 21. Average reservoir pressure (simulated).

In conjunction with history matching, a sensitivity analysis has been utilized to identify parameters having the greatest effect on simulation results. These key parameters can be targeted for fine tuning, thereby greatly reducing the time and resources required for the history-matching process. The identified key parameters can be targeted for enhanced evaluation during the drilling and completion of the monitoring well to further minimize uncertainties in the model.

Predictive Fluid Flow Simulations

Once a satisfactory history match was obtained, predictive simulations were performed to evaluate the effects of various CO_2 injection schemes on incremental oil recovery and movement of injected CO_2 in the reservoir over time. Although the performance of the waterflooding program in the Bell Creek oil field had been successful (37.7% primary + secondary recovery), it still left a tremendous volume of oil (around 221 million barrels) behind in the reservoir. This has prompted engineering studies to investigate means of economically recovering additional amounts of this oil. Continuous miscible CO_2 flooding and CO_2 WAG were chosen as tertiary EOR processes, and both were used to evaluate various future production and injection scenarios in the predictive simulations reported here.

Predictive simulations were repeated under different operating scenarios to evaluate the reservoir performance. In order to provide the comparison of the performance of the miscible recovery process, CO_2 movement, and long-term fate, predictive simulations were performed using the quarter five-spot pattern model, single five-spot pattern model, and full Phase 1 model, as described above. The quarter five-spot pattern model and single five-spot pattern model (around the monitoring well 0506 OW) were clipped from the full Phase 1 model, and all the

reservoir properties after adjustment for the history matching were kept intact in the quarter five-spot and five-spot pattern models. During the prediction stage, the matched parameters are used to evaluate the movement of CO_2 and oil and CO_2 breakthrough times at monitoring and production wells.

According to the CO_2 injection plan, a total of 32 active injection wells and 34 production wells are included in the predictive simulation model. The CO_2 injection rate is specified to be 50 MMscf/day. In all cases, bottomhole flowing pressure is specified for the production wells as the operating constraint. The CO_2 injection well was controlled by CO_2 injection rates and maximum bottomhole pressure constraint.

Quarter Five-Spot Pattern Model

The quarter five-spot pattern model, which included one production and one injection well along with a newly drilled monitoring well, was clipped from the Phase 1 area model. As shown in Figure 22, there are three wells in the model: the production well 25075215020000 (BCUD 0506), the CO_2 injection well 25075215030000 (BCUD 0507) and the monitoring well (0506 OW), near the center of the square pattern. Figure 22 also shows the distribution of porosity in the quarter five-spot pattern area. The quarter five-spot model only simulated Bell Creek sand (BC10, BC20, and BC30), and the wells were completed in all of the 23 layers. The grid was 16 × 17 × 23 with 6256 total cells in the model. The grid size was 100 × 100 ft. A compositional fluid model was used to represent the miscible process of enhanced oil recovery in the Muddy Formation. To investigate the effect of CO_2 injection on the enhanced oil recovery process, four cases were run:

- Case 1: 1 HCPV continuous CO_2 injection
- Case 2: 2 HCPV continuous CO_2 injection
- Case 3: 1 HCPV WAG process (0.5 HCPV CO_2 slug and 0.5 HCPV water slug)

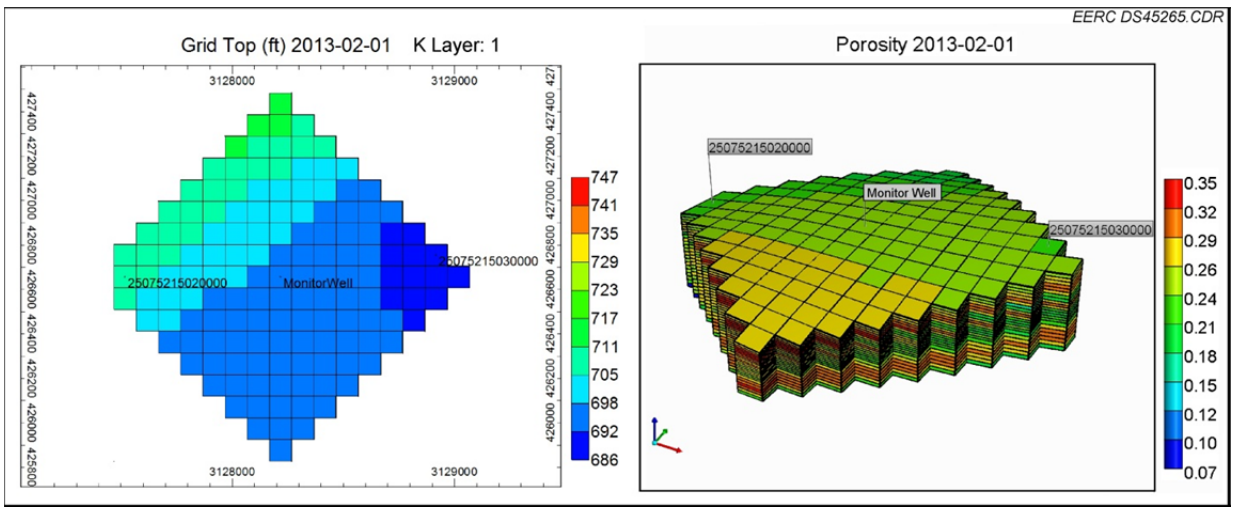

Figure 22. Well locations and porosity distribution in the quarter five-spot pattern model.

- Case 4: 2 HCPV WAG process (1 HCPV CO_2 slug and 1 HCPV water slug)

The simulation results for the quarter five-spot pattern model are provided in Appendix C (Figures C-10–C-26) and are summarized below.

Case 1: 1 HCPV Continuous CO_2 Injection

The results for Case 1 are presented in Figures C-10–C-17 of Appendix C. In this case, a CO_2 injection rate at surface condition of 436.334 Mscfd (thousand standard cubic feet per day) of CO_2 was used. Figure C-11 shows the CO_2 injection profile for the well 2507521503 (BCUD 0507) in the quarter five-spot pattern model. No injectivity problem was observed at the injection rates used. It took 21 years to inject 1 HCPV of CO_2. The average reservoir pressure varied from 2592 to 2841 psi during the process of continuous CO_2 injection (Figure C-12).

An example comparison of the oil saturation profile (K Layer 21) before and after CO_2 injection is shown in Figure C-13. It shows a significant reduction in the remaining oil saturation after the injection of 1 HCPV CO_2. The example of variation in global mole fraction of CO_2 (K Layer 21) with time is shown in Figure C-14. Global mole fraction of CO_2 is used as a variable to track the movement of CO_2 in the field. The first map in the figure (at date 2013-02-01) is the initial condition of the model. After this, the CO_2 injection starts, and CO_2 flows toward the monitoring well and sweeps the oil that it contacts on the way. As the CO_2 injection continues, the CO_2 front moves toward the production well, which is located in the low-potential regions in the model; CO_2 sweeps the oil in the region, and also the global mole fraction of CO_2 has increased. In this case, CO_2 breakthrough at the production well and the monitoring well occurs in 2.7 years and 6 months, respectively. Figure C-15 shows an example of the cross-sectional view of CO_2 saturation (J Layer 9) during the injection of CO_2. The flow of CO_2 in each perforated layer is clearly demonstrated. As expected, the flow of CO_2 in some high-permeability layers is much faster than flow in low-permeability layers.

Case 2: 2 HCPV Continuous CO_2 Injection

Compared to Case 1, the only difference presented by Case 2 is the longer CO_2 injection duration due to a one-fold increase in injection volume. The results for Case 2 are presented in Figures C-16–C-18 of Appendix C. In order to inject 2 HCPV of CO_2, the injection duration was extended to 42 years from the previous 21 years for Case 1 (Figure C-11). The average reservoir pressure profile is shown in Figure C-12. The comparison of oil saturation profile in Layer 21 before and after CO_2 injection is shown in Figure C-16. Figure C-17 shows the variation of global mole fraction of CO_2 in K Layer 21 with time. Figure C-18 shows the cross-sectional view of CO_2 saturation during the injection of CO_2.

Case 3: 1 HCPV WAG Process

The WAG process (1:1 ratio) was also simulated for the quarter five -spot pattern model. The results for this case are shown in Figures C-19–C-22 of Appendix C. The CO_2 injection rate was 436 Mscfd, which was same as those of Cases 1 and 2, and the water injection rate was 160 stb/day (Figure C-19). From the beginning to the end of the simulation period (21 years),

CO_2 and water were injected in cycles of three months of CO_2 injection followed by three months of water injection. The average reservoir pressure increased from the initial pressure of 2257 psi and plateaued at 2843 psi shortly after the injection (Figure C-12). The CO_2 breakthrough times were 3.6 years and 1.7 years for production and monitoring wells, respectively.

Figure C-20 shows the comparison of oil saturation profile before and after the WAG process. Figure C-21 shows the changes of global mole fraction of CO_2 in K Layer 21 during the WAG process. Figure C-22 shows the cross-sectional view of CO_2 saturation during the injection of CO_2.

Case 4: 2 HCPV WAG Process

For Case 4, the injection duration was extended to 42 years in order to inject 2 HCPV of CO_2. The results for Case 4 are presented in Figures C-23–C-26 of Appendix C. The CO_2 and water injection is shown in Figure C-23. The average reservoir pressure profile is shown in Figure C-12.

The comparison of oil saturation in K Layer 21 before and after the WAG process is shown in Figure C-24. Figure C-25 shows the changes of global mole fraction of CO_2 in Layer 21 during the WAG process. Figure C-26 shows the cross-sectional view of CO_2 saturation during the injection of CO_2.

Five-Spot Pattern Model

The quarter five-spot pattern model mentioned above was enlarged to a single five-spot pattern model, as shown in Figure 23. A total of six wells are in the five-spot pattern model. Four of the water injection wells (Wells 25075213630000 [BCUD 0503], 25075213650000 [BCUD 0505], 25075215660000 [BCUD 0511], and 25075215030000 [BCUD 0507]), located at the corners of model, were selected as the CO_2 injection wells. Well 25075215020000 (BCUD 0506), located in the center of the model, was selected as the production well. The newly drilled monitoring well (0506 OW) is located midway between the production well and Well 25075215030000. The distribution of porosity in the five-spot model is also shown in Figure B-29. The five-spot model also included only Bell Creek sand (BC10, BC20, BC30), and the wells were completed in all of the 23 layers. The grid was 31 × 32 × 23 with 22,816 total cells in the model. The grid size was 100 × 100 ft. A compositional fluid model was used to represent the miscible process of enhanced oil recovery in the Muddy Formation. To investigate the effect of CO_2 injection, four cases were run:

- Case 5: 1 HCPV continuous CO_2 injection
- Case 6: 2 HCPV continuous CO_2 injection
- Case 7: 1 HCPV WAG process (0.5 HCPV CO_2 slug and 0.5 HCPV water slug)
- Case 8: 2 HCPV WAG process

The simulation results for the five-spot pattern model are provided in Appendix C (Figures C-27–C-43) and are summarized below.

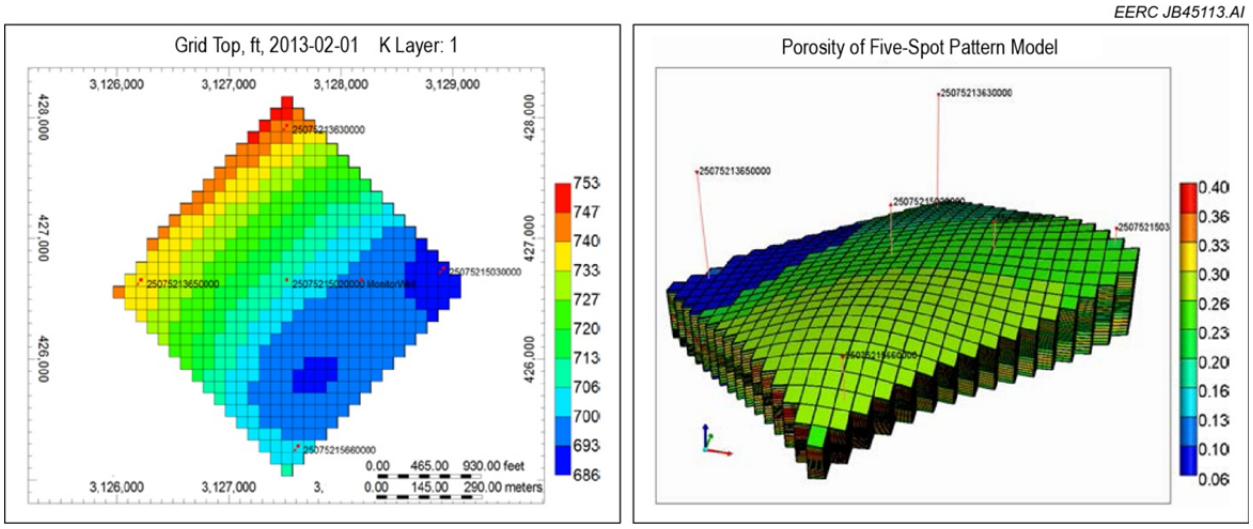

Figure 23. The five-spot pattern model.

Case 5: 1 HCPV Continuous CO_2 Injection

The results for Case 5 are presented in Figures C-27–C-32 of Appendix C. In this case, a CO_2 injection rate of 1.77 MMscfd was used. Given the goal of injecting 1 HCPV of CO_2, the injection duration would be 16 years. The CO_2 injection process was smooth. As shown in Figure C-28, almost all of the specified amount of CO_2 was injectable into the five-spot model.

Figure C-29 shows the pressure profile during CO_2 injection. The average reservoir pressure increased initially to 2862 psi and then decreased and became stable at 2644 psi. The earliest CO_2 breakthrough at the production well was observed after 2.7 years of injection. The breakthrough at the monitoring well occurred in 6 months.

An example comparison of oil saturation profile (K Layer 21) before and after CO_2 injection is shown in Figure C-29. After the sweeping of CO_2, the remaining oil saturation was significantly reduced after the injection of 1 HCPV CO_2. Figure C-31 shows an example of the variation of global mole fraction of CO_2 (K Layer 21) with time. Due to the heterogeneity of the layers in the model, the areas swept by the injected CO_2 are different for four corner injectors, even though the same amount of CO_2 is injected through all of the four injection wells. The example cross-sectional view of CO_2 saturation (J Layer 17) is shown in Figure C-32.

Case 6: 2 HCPV Continuous CO_2 Injection

For Case 6, the total injected pore volume of CO_2 was increased to 2 HCPV from 1 HCPV of Case 5 (Figure C-28). The injection duration was 32 years for this scenario. The results for Case 6 are presented in Figures C-33–C-35 of Appendix C. The average reservoir pressure of Case 6 is similar to that of Case 5 (Figure C-29). The average reservoir pressure rises above the initial reservoir pressure at the early stage of injection and declines slightly to remain below that during the rest of the injection period.

The oil saturation comparison for before and after carbon dioxide flooding is demonstrated in Figure C-33. The remaining oil saturation was significantly reduced after the sweeping of CO_2. Figure C-34 shows the variation of global mole fraction of CO_2 in K Layer 21 with time. The cross-sectional view of CO_2 saturation is shown in Figure C-35.

Case 7: 1 HCPV WAG Process

The CO_2 injection rate was 1.77 MMscfd of CO_2, which was same as for Cases 5 and 6, and the water injection rate was 640 stb/day (Figure C-36). From the beginning to the end of the simulation period (16 years), alternating 3-month injection cycles of CO_2 and water were specified. The results for Case 7 are presented in Figures C-36–C-39 of Appendix C.

The average reservoir pressure increased from the initial pressure of 2281 psi and plateaued at 2862 psi shortly after the injection (Figure C-29). In Case 7, the earliest CO_2 breakthrough at the production well occurred in 3.7 years; for the monitoring well, the breakthrough time was 7 months.

Figure C-37 shows the comparison of oil saturation profile before and after the WAG process. Compared to Cases 5 and 6, the reduction in the remaining oil saturation is higher, and Case 7 also shows a better areal sweeping. Figure C-38 shows the changes of global mole fraction of CO_2 in K Layer 21 during the WAG process. The cross-sectional view of CO_2 saturation is shown in Figure C-39.

Case 8: 2 HCPV WAG Process

The results for Case 8 are presented in Figures C-40–C-43 of Appendix C. For Case 8, the injection duration was extended to 32 years in order to inject 2 HCPV of CO_2. The CO_2 and water injection is shown in Figure C-40. The average reservoir pressure profile is shown in Figure C-29.

The comparison of oil saturation in Layer 21 before and after the WAG process is shown in Figure C-41. Figure C-42 shows the changes of global mole fraction of CO_2 in K Layer 21 during the WAG process. Figure C-43 shows the cross-sectional view of CO_2 saturation during the injection of CO_2.

Full Phase 1 Area Model

With the knowledge gained from slim-tube simulations and with the results of two model studies (quarter five-spot pattern model and five-spot pattern model), continuous CO_2 injection and WAG (1:1 injection ratio) processes were simulated for the full Phase 1 model to evaluate their effect on CO_2 EOR efficiencies, CO_2 breakthrough time at various production wells, and long-term CO_2 plume and pressure behaviors. As with the quarter five-spot and five-spot models, all of the history-matched properties were used to provide an input to a full Phase 1 predictive simulation model for the CO_2 flood. In other words, the history match discussed in the previous section was used as the initial condition for the predictive simulation model to develop the reservoir management strategies.

In the full Phase 1 area model, there are 32 injection wells and 34 production wells (Figure 24). The x–y–z grid used is 158 × 162 × 34, which includes all the wells in the Phase 1 area, resulting in a total number of cells used of 870,264 grid blocks. The grid size is 100 × 100 ft with average grid thickness of 1 ft. A compositional fluid model was used to represent the miscible process of enhanced oil recovery in the Muddy Formation. To investigate the effect of CO_2 injection on the EOR process, four cases were run:

- Case 9: 1 HCPV continuous CO_2 injection
- Case 10: 2 HCPV continuous CO_2 injection
- Case 11: 1 HCPV WAG process (0.5 HCPV CO_2 slug and 0.5 HCPV water slug)
- Case 12: 2 HCPV WAG process

The simulation results for the Phase 1 area model are provided in Appendix C (Figures C-44–C-72) and are summarized below.

Case 9: 1 HCPV Continuous CO_2 Injection

The results for Case 9 are presented in Figures C-45–C-56 of Appendix C. The daily CO_2 injection rate was 50 MMscfd (Figure C-45). This CO_2 injection volume was distributed to 32 injection wells based on the wells' injectivity during the waterflooding. In predictive simulations, CO_2 injection starts in February 2013 and ends in February 2026. It took 13 years to inject 1 HCPV of CO_2 into the Phase 1 area model (Figure C-46). The average reservoir pressure is shown in Figure C-47. The initial reservoir pressure before CO_2 injection was 2213 psi. The reservoir was first pressurized after the CO_2 injection started; the pressure increased to 2667 psi and then gradually became flat at 2592 psi.

Figure C-48 shows the gas and cumulative gas rates. The gas rate is very small during the first seven months of CO_2 injection, but after the gas breakthrough, the produced gas increased significantly, as expected. The earliest CO_2 breakthrough time at production wells was 6 months. In the case of the monitoring well, CO_2 showed up at the wellbore after 5.5 years. The latest CO_2 breakthrough time at a production well was 9.2 years. The cumulative produced gas reached 1.57×10^{11} ft^3, which accounts for 66% of total injected CO_2 volume. The calculated amount of net (injected-produced) CO_2 stored in the reservoir was found to be 4.09 million tons.

The GOR results are shown in Figure C-49. The GOR shows a linear increase during the CO_2 injection. The daily and cumulative water rates of Case 1 are shown in Figure C-50. The prediction result of water cut is shown in Figure C-51. The water cut declined during the first four years of CO_2 injection and then became flat after that.

An example of gas per unit area (K Layer 1) is shown in Figure C-52. The areal extent of the CO_2 plume for the injection period is limited to the Phase I area (Figure 25). As can be seen in Figure 25, at the end of injection period, some of the CO_2 injected at the down-structure wells has moved to adjacent aquifer region. The change in CO_2 mole fraction over time is shown in Figure C-53. The gas saturation in K Layer 24 (BC20) is shown in Figure C-54. The example cross-sectional view of gas saturation (J Layer 91) is shown in Figure C-55. The average reservoir pressure of K Layer 24 is shown in Figure C-56.

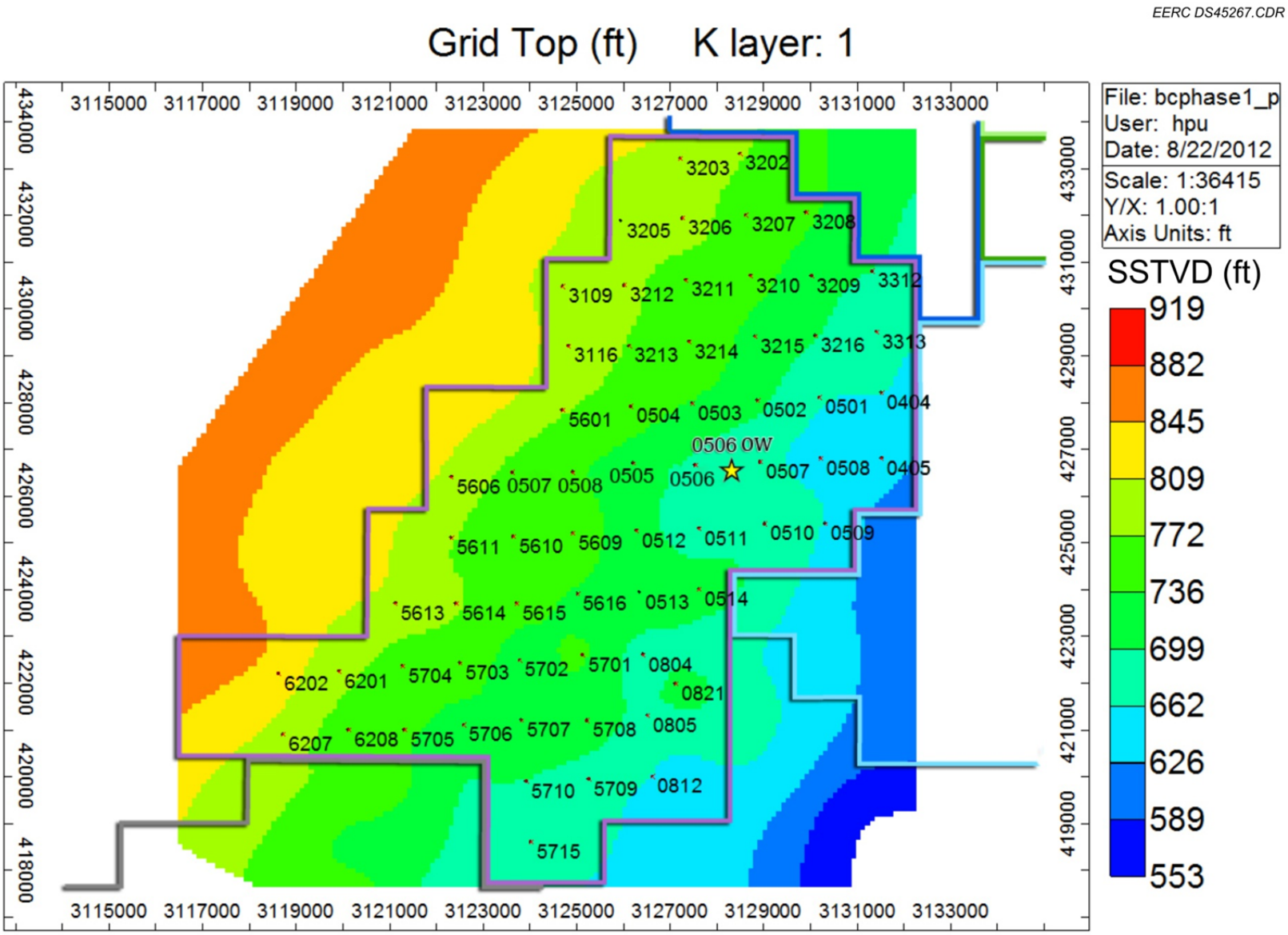

Figure 24. 2-D view of the full Phase 1 model.

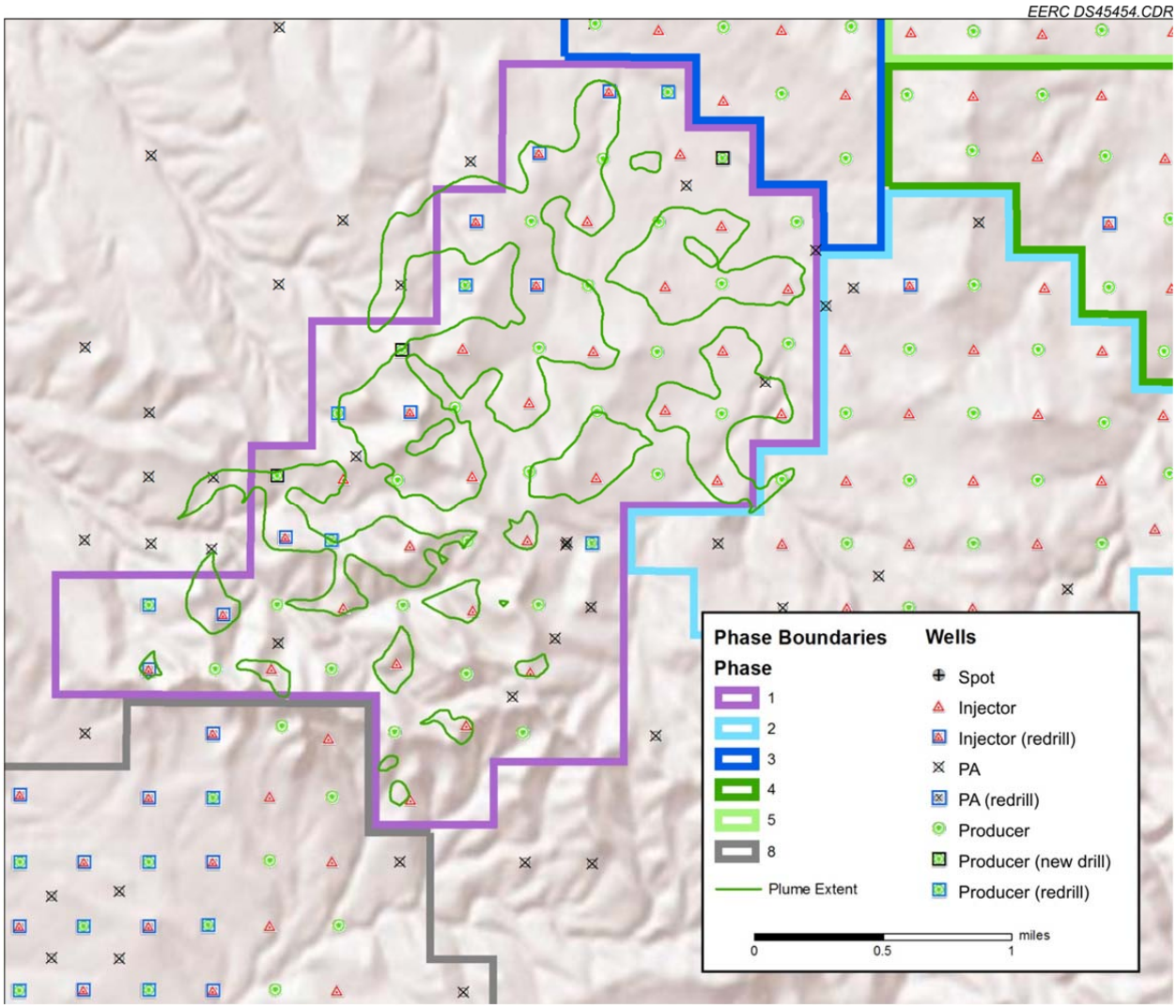

Figure 25. Areal extent of the CO_2 plume at the end of the injection period (Case 9).

Case 10: 2 HCPV Continuous CO_2 Injection

The total injected CO_2 was increased to 2 HCPV compared to Case 9. Subsequently, the injection duration for Case 10 was increased to 26 years (Figures C-45 and C-46). The average reservoir pressure profile is similar to that of Case 9 (Figure C-47). Figure C-48 shows the daily and cumulative gas rates. The GOR result is demonstrated in Figure C-49. The daily and cumulative water rates for Case 9 are shown in Figure C-50. The prediction result of water cut is shown in Figure C-51. In this case, the calculated amount of stored CO_2 in the reservoir was 5.34 million tons. The CO_2 breakthrough times were the same as in Case 9.

The gas per unit area is shown in Figure C-57. The areal extent of CO_2 plume at the end of injection period is shown in Figure 26. More CO_2 spread into the adjacent aquifer can be seen in Figure 26. An example of change in CO_2 mole fraction over time is shown in Figure C-58. The gas saturation in K Layer 24 (BC20) is shown in Figure C-59. The cross-sectional view of gas saturation is shown in Figure C-61. The average reservoir pressure of Layer 24 is shown in Figure C-62.

Case 11: 1 HCPV WAG Process

The WAG (1:1 injection ratio) process was simulated to evaluate the reservoir response to the WAG. The total injected fluid is 1 HCPV, including 0.5 HCPV of CO_2 and 0.5 HCPV of water, with a half-cycle injection 3 months in duration. CO_2 injection starts in February 2013 for half of the injection wells (16), and water is injected simultaneously into the other half of the injection wells (16). Water and CO_2 are injected alternately into wells. The daily CO_2 injection rate was 50 MMscfd, and the daily water injection rate was 20,135 bbl (Figure C-45). The specified CO_2 injection rate of 50 MMscfd led to injectivity problems, and some of the wells were not able to inject the specified water rate, resulting in the injection of 59% of the total specified water rate (Figure C-46). The average reservoir pressure shown in Figure C-47 is slight higher than for Cases 9 and 10. Figure C-48 shows the daily and cumulative gas rates of Case 11.

The gas-to-oil ratio of Case 11 is also shown in Figure C-49. The GOR is much lower than those of Cases 9 and 10 because of the smaller volume of injected CO_2 for Case 11. The daily and cumulative water rates of Case 11 are shown in Figure C-50. The prediction result of water cut is shown in Figure C-51. Due to the water injection in the WAG process, the water cut of Case 11 is much higher than the water cut of Cases 9 and 10. The stored CO_2 amount in this case was 2.48 million tons, which is significantly lower (54%) compared to Case 9. In this case, the earliest and latest CO_2 breakthrough times at a production well were found to be 3 months and 5 years, respectively. The injected CO_2 showed up at the monitoring well after 6 years of injection.

The gas per unit area is shown in Figure C-63. The areal extent of the CO_2 plume at the end of the injection period is shown in Figure 27. The CO_2 mole fraction over time is shown in Figure C-64. The gas saturation in K Layer 24 (BC20) is shown in Figure C-65. The cross-sectional view of gas saturation is shown in Figure C-66. The average reservoir pressure of K Layer 24 is shown in Figure C-67.

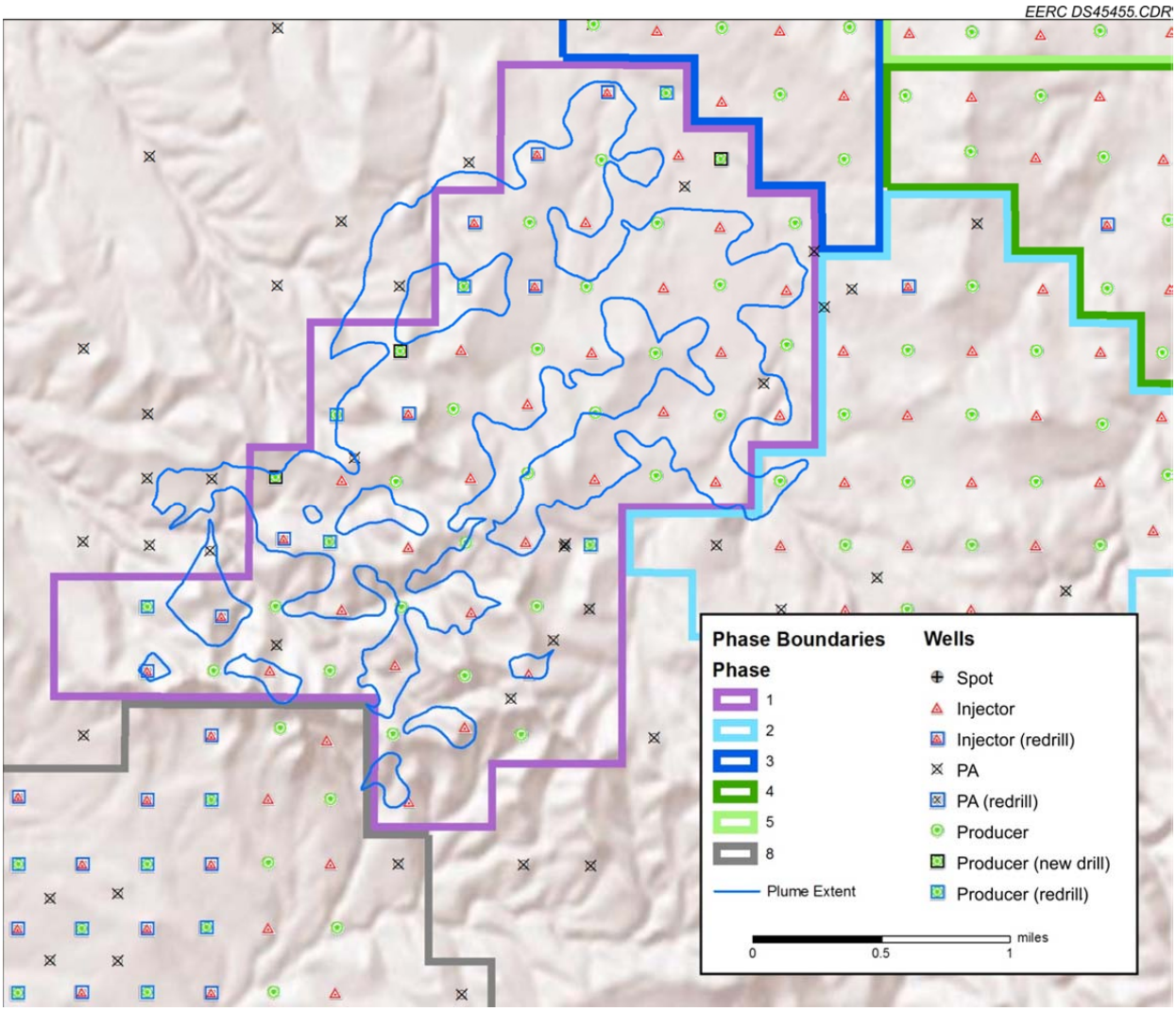

Figure 26. Areal extent of the CO_2 plume at the end of the injection period (Case 10).

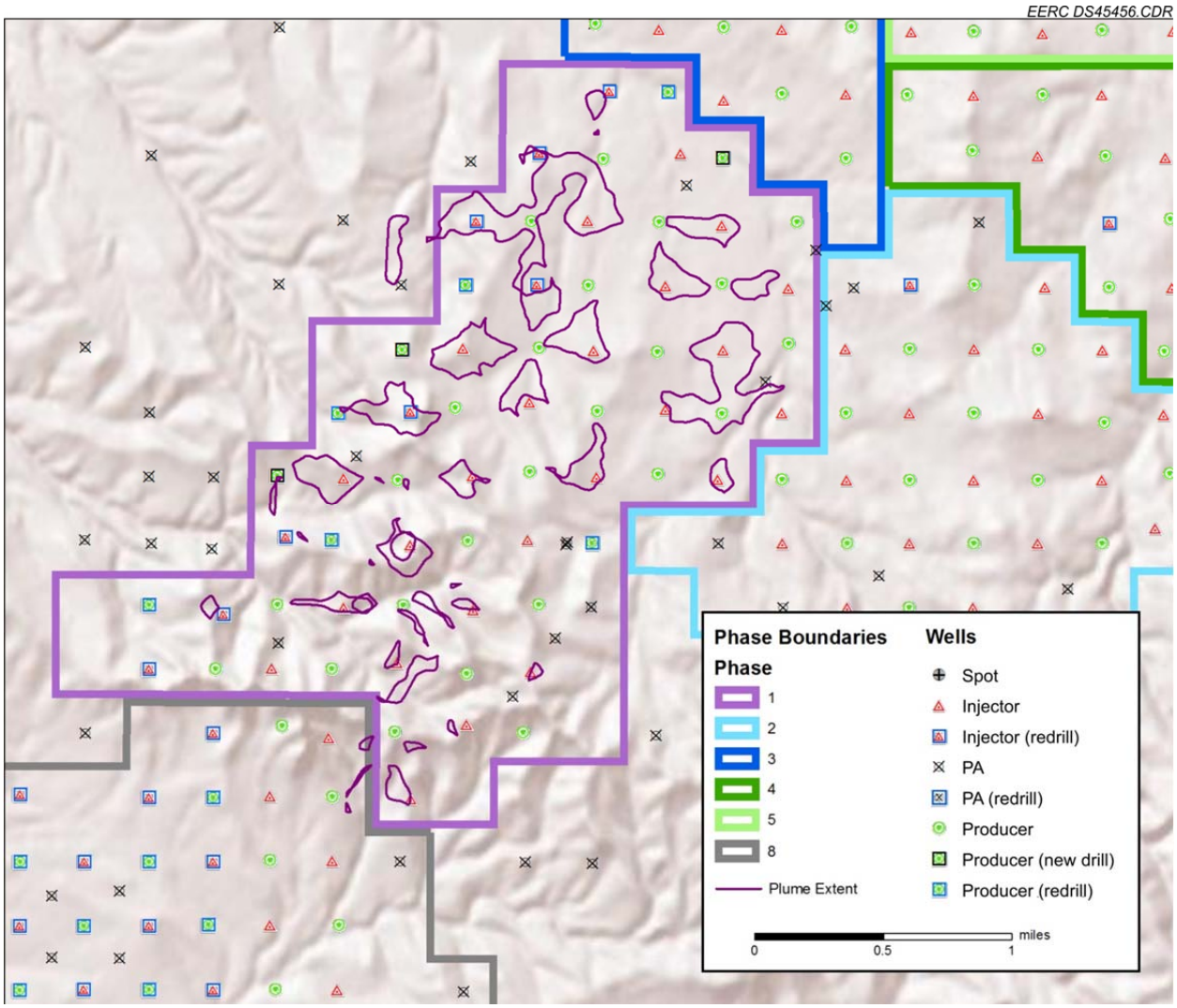

Figure 27. Areal extent of the CO_2 plume at the end of the injection period (Case 11).

Case 12: 2 HCPV WAG Process

Compared to Case 11, the duration of CO_2 injection was doubled for Case 12, and the volume of injected CO_2 was also doubled (Figures C-45 and C-46). The average reservoir pressure is shown in Figure C-47. Figure C-48 shows the daily and cumulative gas rates of Case 12. The gas-to-oil ratio of Case 12 is also shown in Figure C-49. The daily and cumulative water rate of Case 12 is shown in Figure C-50. The prediction result of water cut is shown in Figure C-51. Because of the water injection in the WAG process, the water cut of Case 12 is much higher than the water cut of Cases 9 and 10.

The gas per unit area is shown in Figure C-68. The areal extent of the CO_2 plume at the end of the injection period is shown in Figure 28. An example of CO_2 mole fraction variation over time is shown in Figure C-69. The gas saturation in K Layer 24 (BC20) is shown in Figure C-70. The cross-sectional view of gas saturation is shown in Figure C-71. The average reservoir pressure of Layer 24 is shown in Figure C-72. In this case, a total of 3.00 million tons CO_2 was stored in the reservoir at the end of the injection period. The CO_2 breakthrough times were similar to those in Case 11.

Summary of CO_2 Breakthrough Times

A summary of CO_2 breakthrough times observed in various predictive simulation cases is provided in Table 5.

Limitations

The dynamic reservoir model discussed above has certain limitations, such as nonavailability of reservoir pressure data for the entire history-matching period. Because of lack of time, detailed facies modeling could not be performed while constructing the static geologic model. Thus, a single set of oil/water and gas/oil permeability curves was used for different rock types (low-, moderate-, or high-permeability rocks). Detailed facies modeling and subsequent assignment of representative oil/water and gas/oil relative permeability curves to different rock types would definitely help to improve the accuracy of simulation results.

In this round of dynamic simulations, a manual (iterative) history-matching process was used, which prevented evaluation of the effects of certain other parameters on simulation results. A detailed dynamic simulation workflow developed by the EERC would be utilized in future simulations for more comprehensive validation of the fieldwide reservoir model that is being constructed.

During the process of history matching, it was found that some of the wells were watered out and had early water breakthrough, while other wells produced very little water compared to the production history. This phenomenon could be due to the very high permeability in some areas. In the meantime, the use of one set of relative permeability curves may also be a factor. The estimated CO_2 capacity values for different cases also appear to be on the lower side, as no relative permeability hysteresis and CO_2 solubility in the aqueous phase were considered.

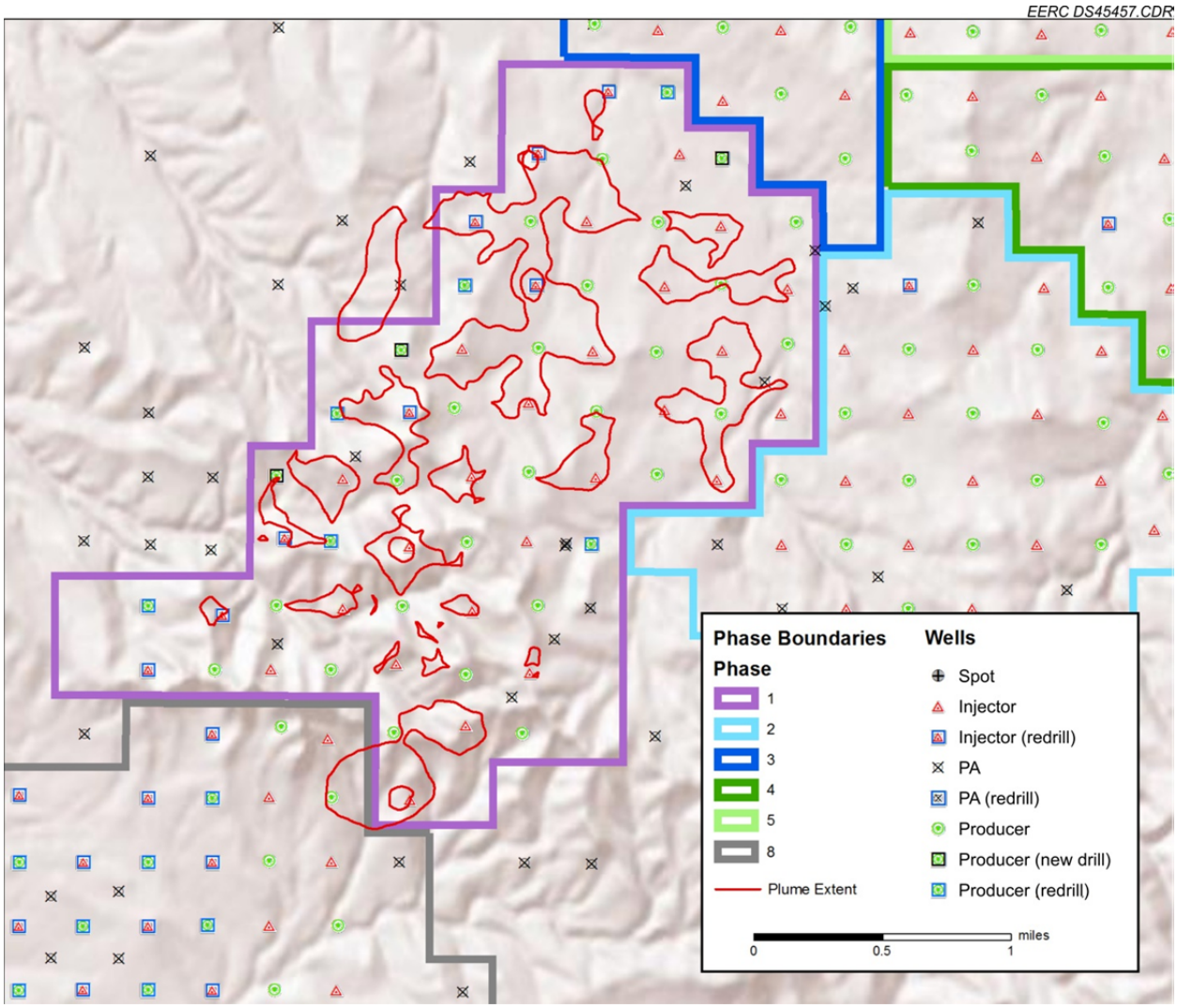

Figure 28. Areal extent of the CO_2 plume at the end of the injection period (Case 12).

Table 5. CO_2 Breakthrough Times (Various Predictive Simulation Cases)

Case	Model	Injection Type	Injection Volume	CO_2 Breakthrough Times: Earliest at Production Well	CO_2 Breakthrough Times: Latest at Production Well	CO_2 Breakthrough Times: Monitoring Well (0506 OW)
Case 1	Quarter five-spot	Continuous CO_2 injection	1 HCPV	2.7 years	–	6 months
Case 2	Quarter five-spot	Continuous CO_2 injection	2 HCPV	2.7 years	–	6 months
Case 3	Quarter five-spot	CO_2 WAG	1 HCPV	3.6 years	–	1.7 years
Case 4	Quarter five-spot	CO_2 WAG	2 HCPV	3.6 years	–	1.7 years
Case 5	Five-spot	Continuous CO_2 injection	1 HCPV	2.7 years	–	6 months
Case 6	Five-spot	Continuous CO_2 injection	2 HCPV	2.7 years	–	6 months
Case 7	Five-spot	CO_2 WAG	1 HCPV	3.7 years	–	7 months
Case 8	Five-spot	CO_2 WAG	2 HCPV	3.7 years	–	7 months
Case 9	Full Phase 1	Continuous CO_2 injection	1 HCPV	6 months	9.2 years	5.5 years
Case 10	Full Phase 1	Continuous CO_2 injection	2 HCPV	6 months	9.2 years	5.5 years
Case 11	Full Phase 1	CO_2 WAG	1 HCPV	3 months	5 years	6 years
Case 12	Full Phase 1	CO_2 WAG	2 HCPV	3 months	5 years	6 years

MVA UPDATE

Monitoring Well (0506 OW)

In December 2011, a new monitoring well (0506 OW) was drilled into the middle of the Phase 1 area in the Bell Creek oil field (Figure 29). The well was designed to be a center point for the MVA strategies deployed for the Phase 1 area. An extensive suite of data was acquired during drilling, and a permanent downhole monitoring system was installed during casing and completion of the well to provide real-time temperature and pressure data from the reservoir and overlying strata. Both a 4-in. core (109 feet) and rotary sidewall cores (47 plugs) were recovered from the well and are currently undergoing standard and special core analysis work. An advanced suite of modern well logs was acquired during eight separate logging runs.

In addition to enabling the collection of new information that will be vital for reducing uncertainties in the injection simulation results, the monitoring well will allow for the implementation of a broad array of monitoring techniques and technologies. These technologies will provide data points to check the validity of the simulation results and provide updated time-lapse data that can be used to update simulation parameters, thereby ensuring agreement between predictions and the physical reservoir response. The monitor well will also be the center of geophysical activities deployed before, during, and after injection begins.

Geophysical Data

Deployment of a base-case 3-D seismic survey is planned during summer 2012. A number of piggybacked geophysical surveys may be acquired to increase resolution of the overall geophysical data set. These reservoir-scale surveys also help predict CO_2 densities and saturations to predict overall sweep efficiency and CO_2 concentration. Additional 3-D surveys may also be run to get a time-lapse 4-D interpretation of CO_2 spatial distribution over time during the injection and postinjection processes.

FIELDWIDE 3-D GEOLOGIC MODELING

To better understand the entire reservoir, a 200-mi^2 study area centered on the Bell Creek oil field has been appointed for the creation of a new fieldwide 3-D geologic model (Version 2 model). The model boundaries are shown in Figure 4. Inside this study area are 748 wells with geophysical logs, and 94 wells with preserved 2.5- to 4-in. cores. In addition, a wealth of geologic, geomechanical, and reservoir properties have been acquired from the recently drilled monitoring well. A suite of 11 geophysical logs has been used to correlate with the historical log suite for use in normalization, stratigraphic, and petrophysical workflows.

Stratigraphic Framework

The Muddy Formation in the Bell Creek oil field area consists of five distinct lithofacies, which were assigned structure and variability according to observed wireline logs, core and

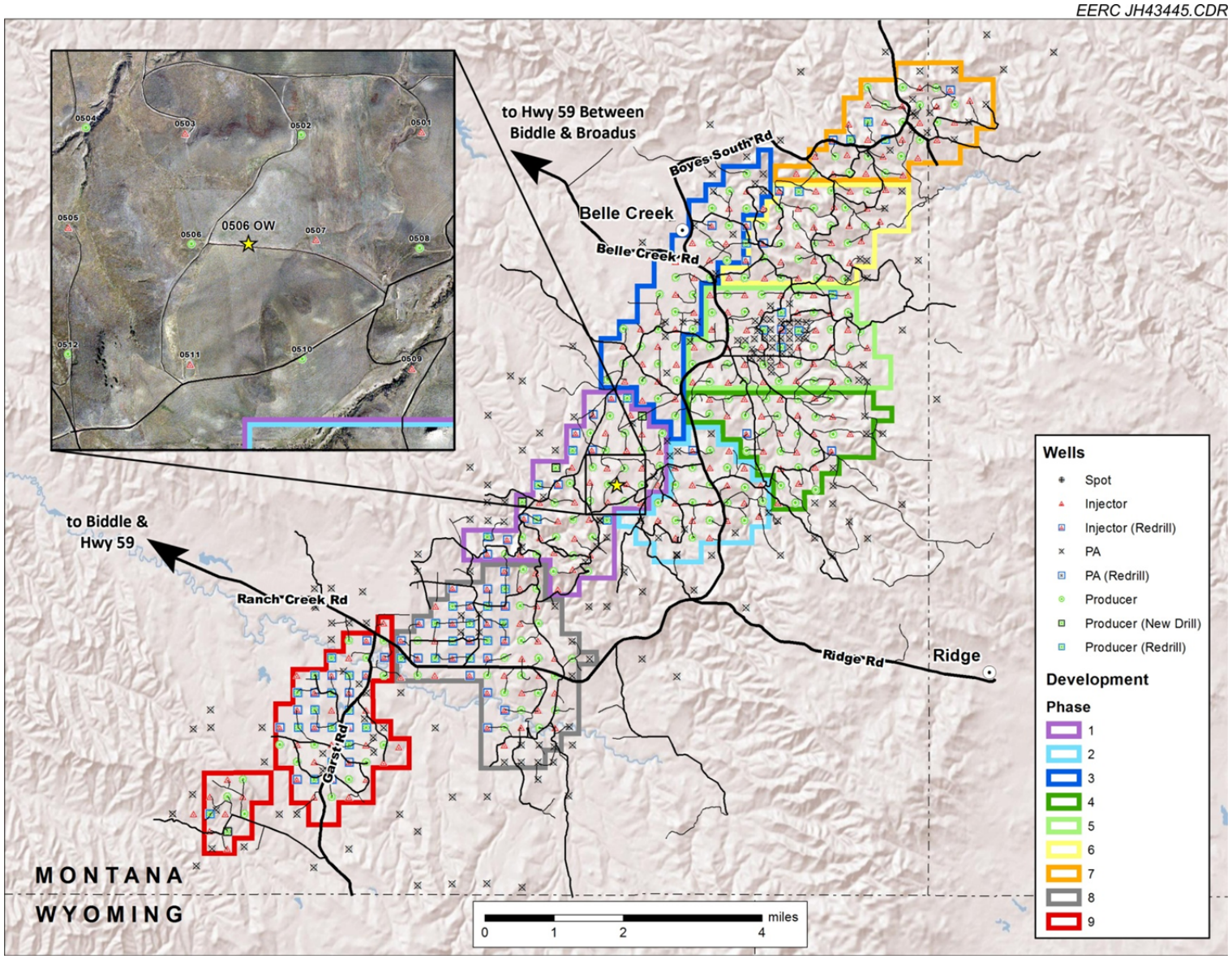

Figure 29. Map illustrating the monitoring well location in relation to the Bell Creek oil field.

outcrop descriptions, and available reservoir properties. In ascending order, these depositional sequences are designated as Skull Creek shale, Rozet siltstone, Bell Creek sandstone, Coastal Plain siltstone, and Springen Ranch and Shell Creek shales (Figure 30). The Rozet facies was originally labeled as shale due to its gamma-ray log behavior, but after several opportunities to describe this facies in both core and outcrop it seems to be a transition zone between the Skull Creek shale and the Bell Creek sandstone, thus primarily consisting of siltstone, with some interbedded shale toward the base and sandstone toward the top (Figure 31).

For the fieldwide geologic model, these five defined lithofacies were picked as the structural tops on the wireline logs and brought into the stratigraphic and petrophysical interpretation workflows. The model stratigraphy was picked across 748 wells including 4400 individual tops. Structural surfaces were interpolated using top depths in a detrending and geostatistical workflow. P10, P50, and P90 realizations were created for the Bell Creek sandstone structural top, and the P10 was then subtracted from the P90 to show uncertainty ranges (Figure 32).

Since the uncertainty range was minimal within the field, the P50 surface was used going forward. All other remaining structural surfaces were interpolated using the P50 Bell Creek sandstone as a trend surface. A generic surface was created for both the top of the cap rock above the reservoir and the base of the cap rock below the reservoir. This was done to limit unnecessary cap rock layers and reduce overall cell count in the reservoir model. Both cap rock packages will

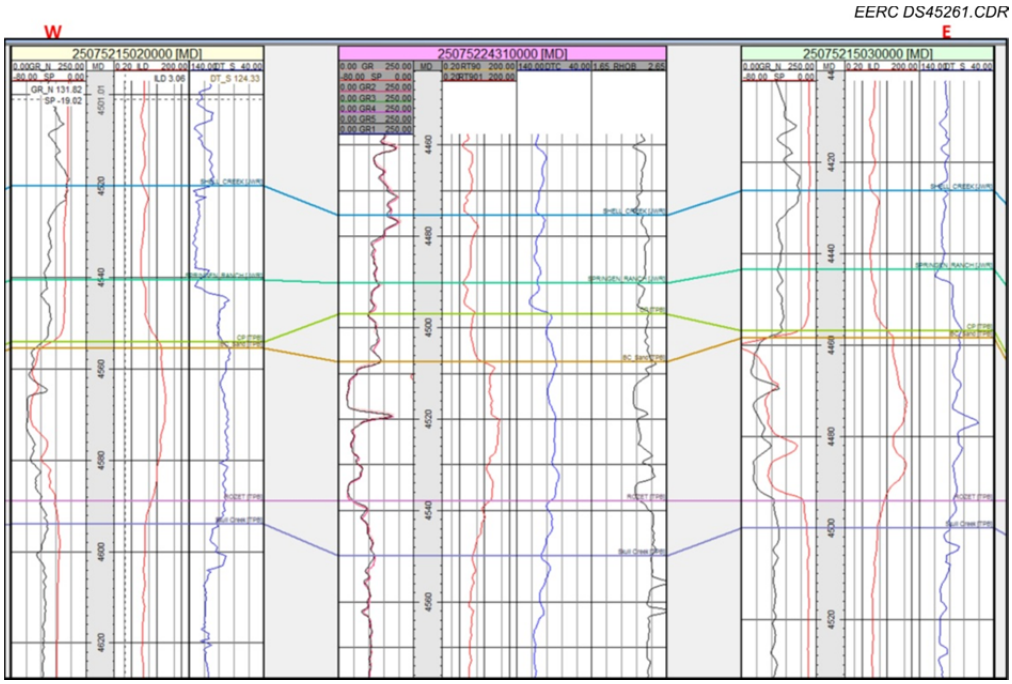

Figure 30. West-to-east cross section through wells nearest to and including the observation well. Six tops are shown in descending order: Shell Creek, Springen Ranch, Coastal Plain, Bell Creek sand, Rozet, and Skull Creek.

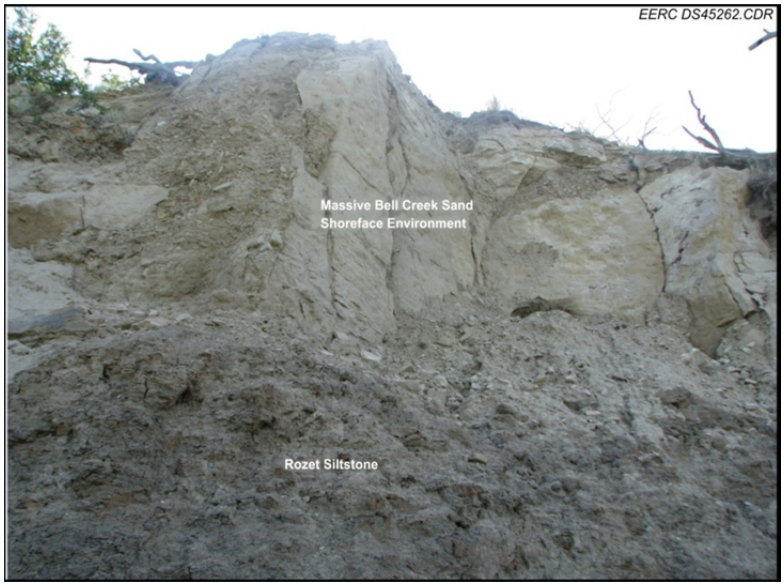

Figure 31. Outcrop photo of the Bell Creek sand conformably lying on top of the Rozet siltstone. Photo taken near New Haven, Wyoming.

be modeled in their entirety for the 3-D geomechanical model. Isopachs were generated between the surfaces and examined for inconsistencies and surface crossover.

Structural Model

The 3-D structural model was created using the seven interpolated structural top surfaces, the extent of the study area, and a cell size of 100 ft × 100 ft. These seven surfaces now represent the six zones within the model: Top Cap Rock, Springen Ranch, Coastal Plain, Bell Creek Sandstone, Rozet, and Bottom Cap Rock. These six zones have been further subdivided into finer layers to help capture the heterogeneity within the lithofacies (Table 6). Thus 41 layers exist in the model, with varying thickness from zone to zone.

Petrophysical Interpretation

The petrophysical workflow includes several steps involving multiple iterations to best capture the reservoir properties and heterogeneity. A drill stem test (DST) review from historical well files was completed to obtain both bottomhole temperature and pressure readings during initial reservoir conditions. These data will be used to compute gradients that will be populated into the model and discretely assigned based on measured depth. All wireline logs and available core analysis data were brought into Techlog to compute the following properties, which will be upscaled into the 3-D structural model:

- Total porosity
- Shale volume
- Effective porosity
- Net-to-gross ratio

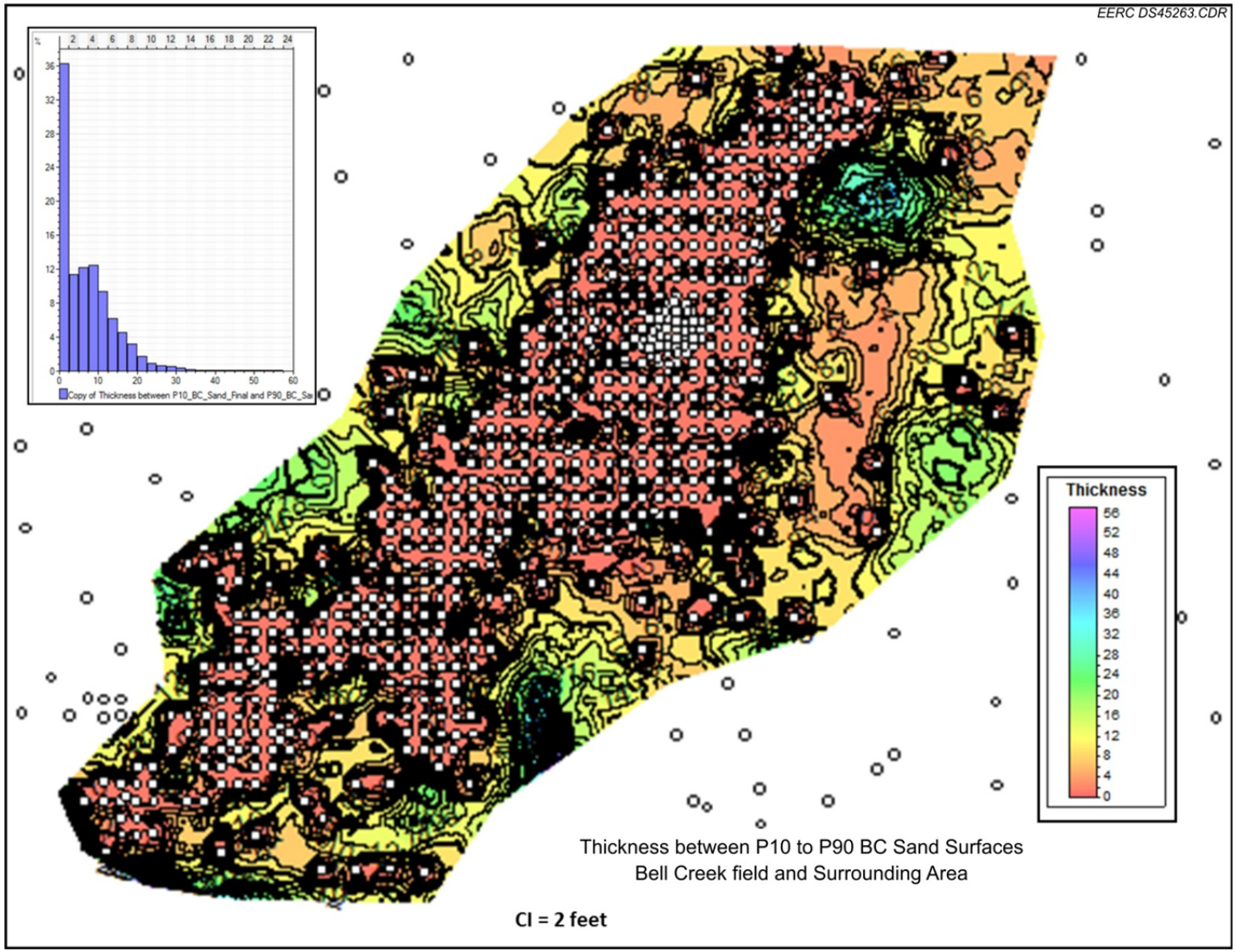

Figure 32. Map of the Bell Creek oil field and flanking edges when the P10 structural surface is subtracted from the P90. Note that the P50 difference would be approximately half of what is shown. Circles denote well control used during surface interpolation.

Table 6. Layers and Associated Thicknesses of Stratigraphy in the Fieldwide Geologic Model

Bell Creek 2012 Fieldwide Model Gridding, 100 ft × 100 ft Grid Dimension				
Zone	Number of Layers	Layer Numbers	Thickness Range, ft	Average Thickness, ft
Cap Rock	5	1–5	3–13	7.79
Coastal Plain	7	6–12	0.12–4.83	0.97
BC Sand	21	13–33	0–3.1	1.01
Rozet	3	34–36	0.38–5.12	1.99
Skull Creek	5	37–41	8.0	8.0

- Absolute permeability
- Water saturation
- Formation pressure
- Formation temperature

After the petrophysical properties have been upscaled, they will be geostatistically populated to create 3-D property models. Each property will have multiple realizations that will ultimately produce a base case model to be used in the uncertainty and sensitivity analysis workflow. This workflow will output P10, P50, and P90 realizations to be used in numerical tuning and history matching, before predictive simulations commence.

GEOMECHANICAL MODELING

To assess the potential for CO_2 leakage during and after injection, a 3-D geomechanical model will be constructed to predict the potential for fault reactivations and fracturing caused by the CO_2 injection and EOR process. The objective of geomechanical modeling is to understand the rock mechanical behavior, including in situ stress and fracture envelopes. The geomechanical model will simulate the long-term variations on the geomechanical parameters to ensure the effective injection and storage of CO_2 for the Bell Creek oil field. Optimization of drilling operations and completion designs are an additional benefit to the Bell Creek CO_2 EOR project.

As the foundation of the geomechanical modeling, mechanical earth modeling (MEM) is a numerical representation of the state of stress and rock mechanical properties as a function of the depth for a specific stratigraphic section in a field or basin. It can be applied to predict and monitor the potential CO_2 leakage paths. From a geomechanical standpoint, a suitable site for CO_2 storage must have sufficient injectivity while maintaining cap rock integrity. With the constructed stress state and rock mechanical properties in MEM, it is convenient to decide whether the cap rock is susceptible to hydraulic fracture propagation, and whether the formation itself can be resistant to fault slippage. A suitable MEM can also predict if the cap rock is capable of resisting the buoyancy-driven flow of CO_2, so that the fluid can be stored over appreciable time scales without leaking.

A one-dimensional mechanical earth model (1-D MEM) has been constructed to assess the state of stress and rock properties with available log data and core data from the monitoring well 0506 OW. The Bell Creek 1-D MEM was constructed with the available data from Well 0506 OW, calibrated with core testing results and validated with the drilling-induced breakouts and fractures. The construction process for the 1-D MEM included data collection and auditing, description of the stratigraphic facies, integration of the bulk density to get the overburden stress, prediction of pore pressure and horizontal stresses, and estimation of the rock mechanical properties such as Young's modulus and Poisson's ratio. The available data from Well 0506 OW include wireline logs (GR [gamma ray], SP [spontaneous potential], Sonic, RHOB [bulk density], XRMI [extended range micro-imager], etc.), drilling data (mud weight and cuttings), core analysis data, and geophysical data. The 1-D MEM is constructed with Schlumberger's Techlog and Petrel and will be incorporated into the structural model for the Bell Creek field. This structural model acts as a framework for both the 3-D geomechanical and geological models. Figure 33 shows the constructed rock mechanical properties and state of stresses for Well 0506 OW. The rock mechanical properties are validated by correlating the dynamic elastic moduli from acoustic velocities at triaxial stress conditions with the triaxial compressive test results. All of the rock mechanical properties and stress states are subjected to improvement with additional data and testing results.

Knowledge and data gained during construction of the 1-D MEM will later be integrated into a robust 3-D MEM simulation model. This model extent will cover the entire Bell Creek oil field and outside the field to the northwest and southeast. The 3-D MEM will include all formations from the reservoir up to the surface and to the bottom of the cap rock below the reservoir. The model will be used for the predictive geomechanical simulation during and after the injection process.

FUTURE WORK

Fieldwide 3-D Geologic Model

Once the petrophysical interpretation is complete, interpreted log data will be upscaled into the structural model to create a property model. Multiple realizations will be produced for each property to define a base case. The base case will be inputted into an uncertainty and sensitivity analysis workflow, which will output P10, P50, and P90 values for use in history matching and predictive simulation.

It is anticipated that there will be another updated 3-D geologic model (Version 3 overall) once all core data analysis has been completed and seismic data have been acquired and interpreted. This model will follow similar but more robust workflows including advanced interpretations as knowledge of this unique reservoir continues to grow.

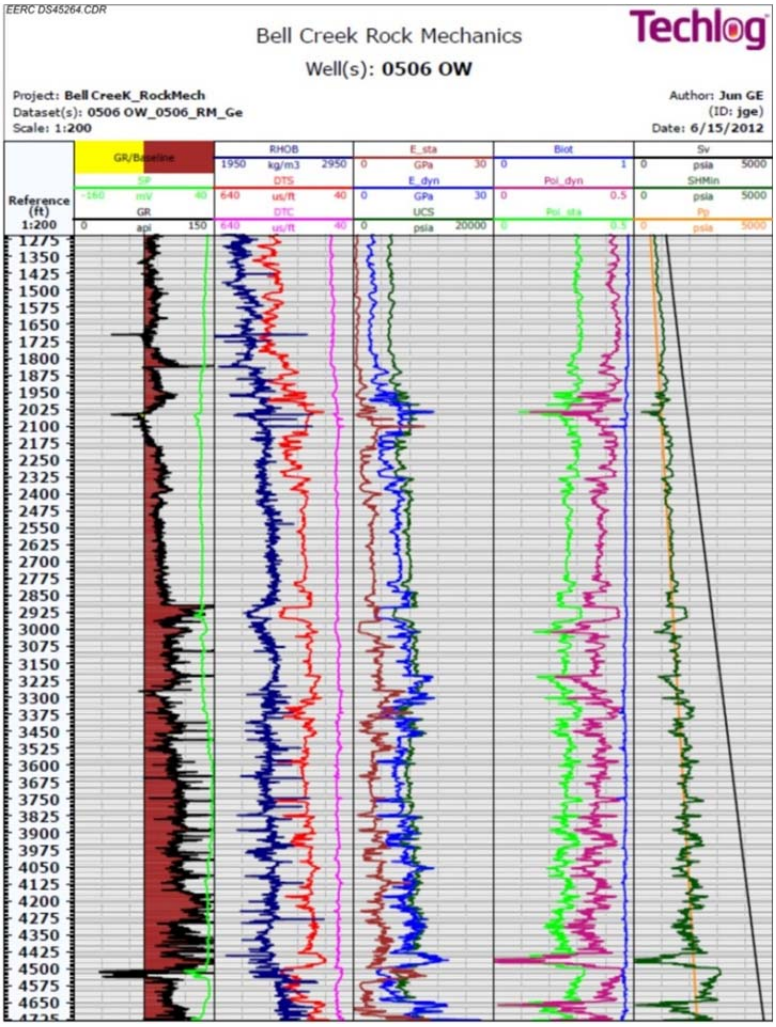

Figure 33. Bell Creek 1-D MEM of 0506 OW, with wireline logs, rock mechanical properties, and in situ stresses shown.

Reservoir Simulation

Upon completion of the uncertainty and sensitivity analysis, numerical tuning and history matching will commence by following a dynamic modeling workflow developed at the EERC using the base case, P10, P50, and P90 realizations and historical production and injection data. These workflows will help validate and minimize uncertainty before running predictive fluid flow simulations. Prior to the start of injection, several fluid flow simulations describing various scenarios will be run to predict CO_2 EOR sweep efficiency, CO_2 breakthrough timing, MVA geophysical deployment periods, and CO_2 storage volumetrics. Future work also includes modeling of relative permeability hysteresis and CO_2 solubility in the aqueous phase for better estimates of CO_2 breakthrough times and storage capacity.

3-D Geomechanical Model

Building of the 3-D geomechnical model has just begun. The model shares an identical structural framework with the fieldwide geologic model for the reservoir interval. The geomechanical model will also have several additional structural surfaces picked from the reservoir up to the surface and to the bottom of the cap rock below the reservoir. This model will be used for the predictive geomechanical simulation during and after the injection process.

SUMMARY

A 3-D static geologic model of the Phase 1 area (Version 1 model) was built to provide a geologic framework for performing dynamic simulations. The detailed geologic modeling has resulted in new interpretations regarding the total porosity, shale volume, effective porosity, permeability, reservoir thickness, and water saturation. The constructed geologic model was validated through history matching and was used with various predictive simulation scenarios.

Key results of current simulation work include the following:

- A seven-component PR-EOS model was developed and tuned based on the available experimental PVT data. The simulated results of standard PVT tests are in good agreement with the laboratory measurements. PVT simulations indicate that miscibility between CO_2 and initial Bell Creek recombined live crude oil will be attained with CO_2 gas at approximately 2800 psia.

- Qualitative investigation of the effect of GOR on MMP indicates that GOR could significantly affect MMP between injected CO_2 and crude oil in the depleted Bell Creek oil field, and current MMP could be closer to 2100 psia.

- To ensure the robustness of the developed EOS model, 1-D compositional simulation of the experimental slim-tube tests was performed. The MMP estimated from slim-tube simulation is lower than the MMP determined from the slim-tube experiment.

- A good agreement between the field history and simulation results (oil rate, water cut, and GOR) for the Phase 1 area model was observed.

- The estimated CO_2 storage capacity at 2 HCPV of continuous CO_2 injection is 5.3 million tons. In the case of 2 HCPV WAG (1:1) injection, CO_2 storage capacity is 3.00 million tons. In all the predictive simulation scenarios, the CO_2 plume is not expected to cross the Phase I area boundary. However, some of the CO_2 injected at down-structure wells appears to move into the adjacent downdip aquifer region.

- Reservoir simulation results suggest that alternately injecting slugs of CO_2 and water during the CO_2 injection program would be more effective than continuously injecting a single CO_2 slug. In the case of continuous CO_2 injection, the earliest CO_2 breakthrough at production wells appears to be in 6 months after the commencement of CO_2 injection.

After 5.5 years of injection, injected CO_2 is expected to reach the newly drilled monitoring well. Overall, WAG injection slows down gas breakthrough and yields a better sweep efficiency, although the earliest CO_2 breakthrough at production wells occurs in 3 months. In the WAG process, injected CO_2 is expected to reach the monitoring well after 6 years of injection.

Ongoing and future work consists of the following:

- A new fieldwide 3-D geologic model (Version 2) is being constructed. Once the petrophysical interpretation is complete, interpreted log data will be upscaled into the structural model to create a property model. The log and core data acquired from the newly drilled monitoring well and lidar survey are expected to greatly improve this new model.

- Upon completion of the uncertainty and sensitivity analysis, numerical tuning and history matching will be performed for the Version 2 model. The base case, P10, P50, and P90 realizations and historic production and injection data will be used for history matching and future predictive simulations. The dynamic modeling workflow developed at the EERC will be used to perform this simulation work.

- Prior to the start of injection, several fluid flow simulations describing various scenarios will be run to predict CO_2 EOR sweep efficiency; evaluate multiple likely CO_2 EOR and storage schemes; predict the migration pathway, plume size, and reservoir storage efficiency of the injected CO_2; predict CO_2 breakthrough timing; establish MVA geophysical deployment periods and CO_2 storage volumetrics; and determine the long-term fate of injected CO_2 in the simultaneous CO_2 EOR and CO_2 storage operations.

- A 3-D geomechanical model is being constructed to identify, anticipate, and evaluate the potential risk for out-of-zone fluid migration caused by a possible breach of reservoir integrity. This model will be used for the predictive geomechanical simulation during and after the injection process in order to guide the monitoring program.

REFERENCES

Computer Modelling Group Ltd., 2011, CMG's GEM user's guide: Calgary, Alberta, Computer Modelling Group, 1246 p.

Encore Acquisition Company, 2009, Bell Creek CO_2 project: internal report, July 2009, 8 p.

Molnar, P.S., and Porter, M.L., 1990, Geologic reservoir study of the Bell Creek Field, Carter and Powder River Counties, Montana: Exxon USA proprietary report, Midland, Texas, 127 p.

Vuke, S.M., 1984, Depositional environments of the Early Cretaceous Western Interior Seaway in southwestern Montana and the northern United States, in Stott, D.F., and Glass, D.J., eds.,

The Mesozoic of Middle North America: Canadian Society of Petroleum Geologists, Memoir 9, p. 127–144.

Weimer, R.J., Emme, J.J., Farmer, C.L., Anna, L.O., Davis, T.L., and Kidney, R.L., 1982, Tectonic influence on sedimentation, Early Cretaceous, east flank Powder River Basin, Wyoming and South Dakota: Colorado School of Mines Quarterly, v. 77, no. 4.

Wulf, G.R., 1962, Lower Cretaceous Albian rocks in northern Great Plains: American Association of Petroleum Geologists Bulletin, v. 46, no. 8, p. 1372–1415.

Young, R.G., 1970, Lower Cretaceous of Wyoming and the southern Rockies: Mountain Geologist, v. 7, p. 105–121.

APPENDIX A

PHASE 1 3-D GEOLOGIC MODELING

PHASE 1 3-D GEOLOGIC MODELING

A 3-D geologic model was developed to define the spatial extent of the sands and the spatial distributions of reservoir rock and fluid properties.

3-D Grid

Figure A-1 shows the geographic locations of three horizontal and two vertical cross sections within the model area (cross-sectional lines are plotted in black). Cross Section Lines A–A', B–B', C–C', and F–F' trend west to east across the project area, and Lines D–D', E–E', and G–G' trend north to south. These sections were constructed on the basis of the geologic map and well data.

Population of the Grid with Petrophysical Properties

Volume of shale (VSH) expressed as a decimal fraction or percentage: Figure A-2 shows the VSH for the coastal plain (CP) and Bell Creek (BC) zones. The VSH map demonstrates a high abundance of shale in the CP sequence, with smaller isolated shale bodies in the BC sands. The cross-sectional view of VSH for Cross Section G–G' is shown in Figure A-3.

Porosity and permeability (low, mid-, high case): Figure A-4 shows the distributions of porosity for the CP and BC zones. The cross-sectional view of porosity for Cross Section G-G' is shown in Figure A-5.

The distribution of permeability for the CP and BC zones is shown in Figure A-6. The cross-sectional view of permeability for Cross Section G-G' is shown in Figure A-7.

Water saturation (S_w) (low, mid-, high case): The distribution of S_w and the depth of oil–water contact (OWC) are illustrated in Figure A-8. The OWC for low, mid-, and high cases is −830, −835, and −840 ft, respectively. The cross-sectional view of permeability for Cross Section G–G' is shown in Figure A-9.

Net-to-gross ratio (NTG): Figure A-10 shows the midcase NTG distribution map for the CP and BC zones. The cross-sectional view of NTG for Cross Section G–G' is shown in Figure A-11.

Formation pressure: Drill stem test (DST) data were utilized to construct a formation pressure gradient map for the Muddy sandstone. Formation pressure in the geologic model for the CP, BC10, BC20, and BC30 zones was assigned as the product of a cell's measured depth and the pressure gradient, while the formation pressure for the Springen Ranch and the Rozet zones is equal to the cell's measured depth times 0.433 psi/ft (normal pressure gradient). Figure A-12 shows the formation pressure distribution in the 3-D model.

Formation temperature: A formation temperature gradient map for the Phase 1 project area was constructed using DST data from a number of wells in the project area. The formation temperature in the geologic model is the cell's measured depth times the temperature gradient. The formation temperature distribution in the 3-D model is shown in Figure A-13.

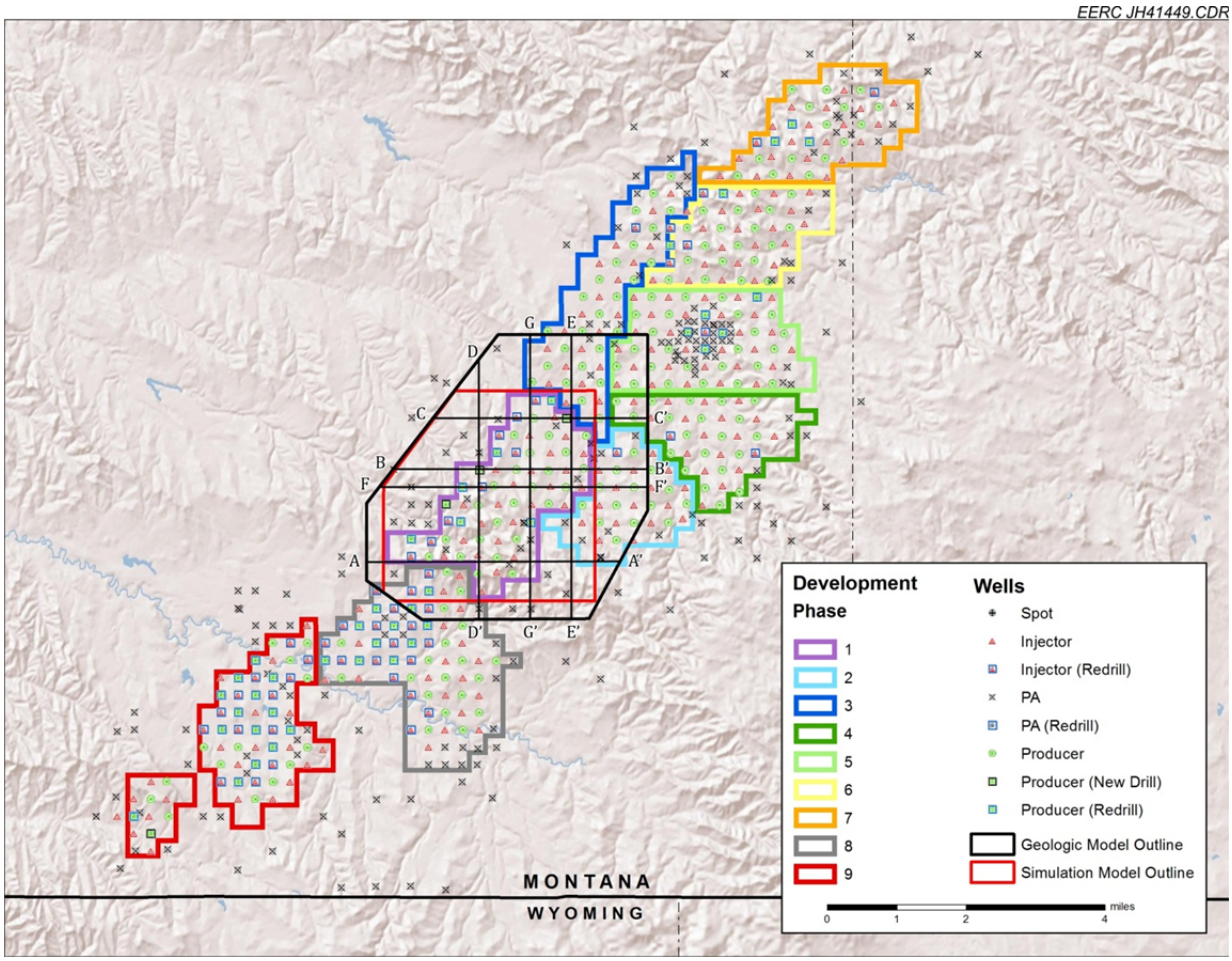

Figure A-1. Locations of cross sections generated for model reporting (PA means plugged and abandoned).

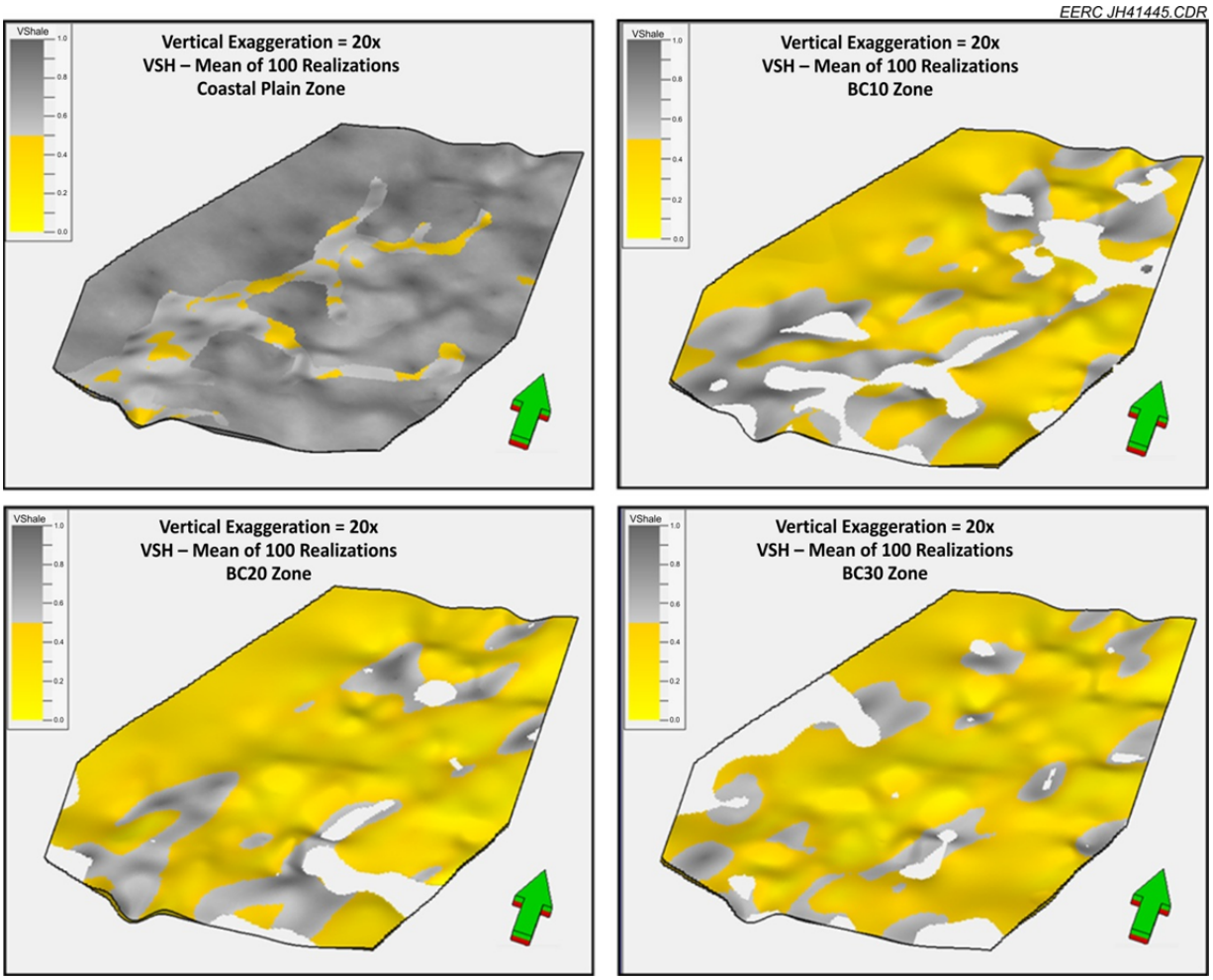

Figure A-2. VSH of CP and BC zones.

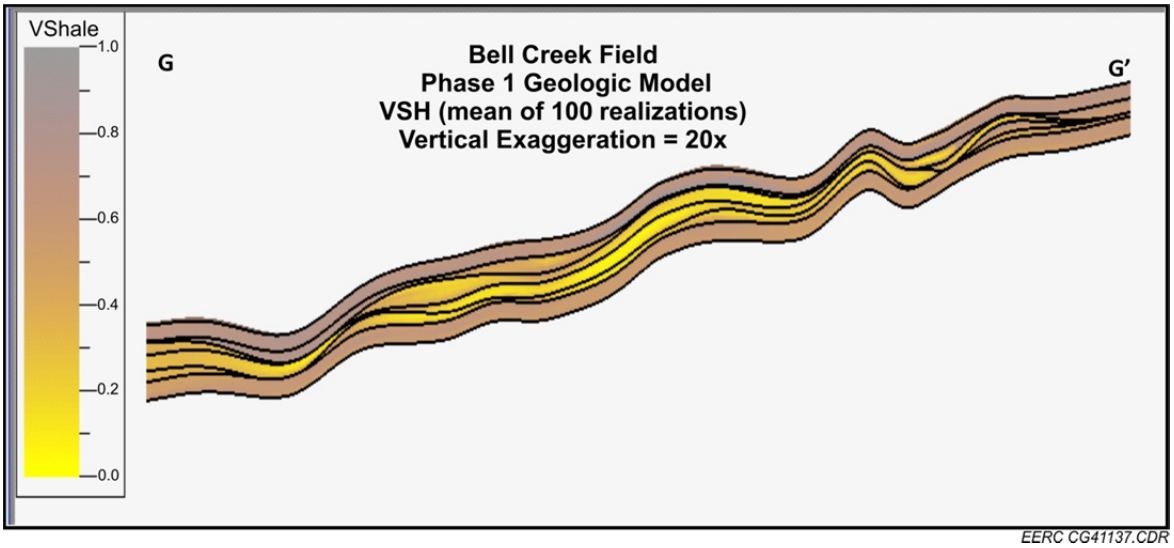

Figure A-3. VSH along Cross Section G–G'.

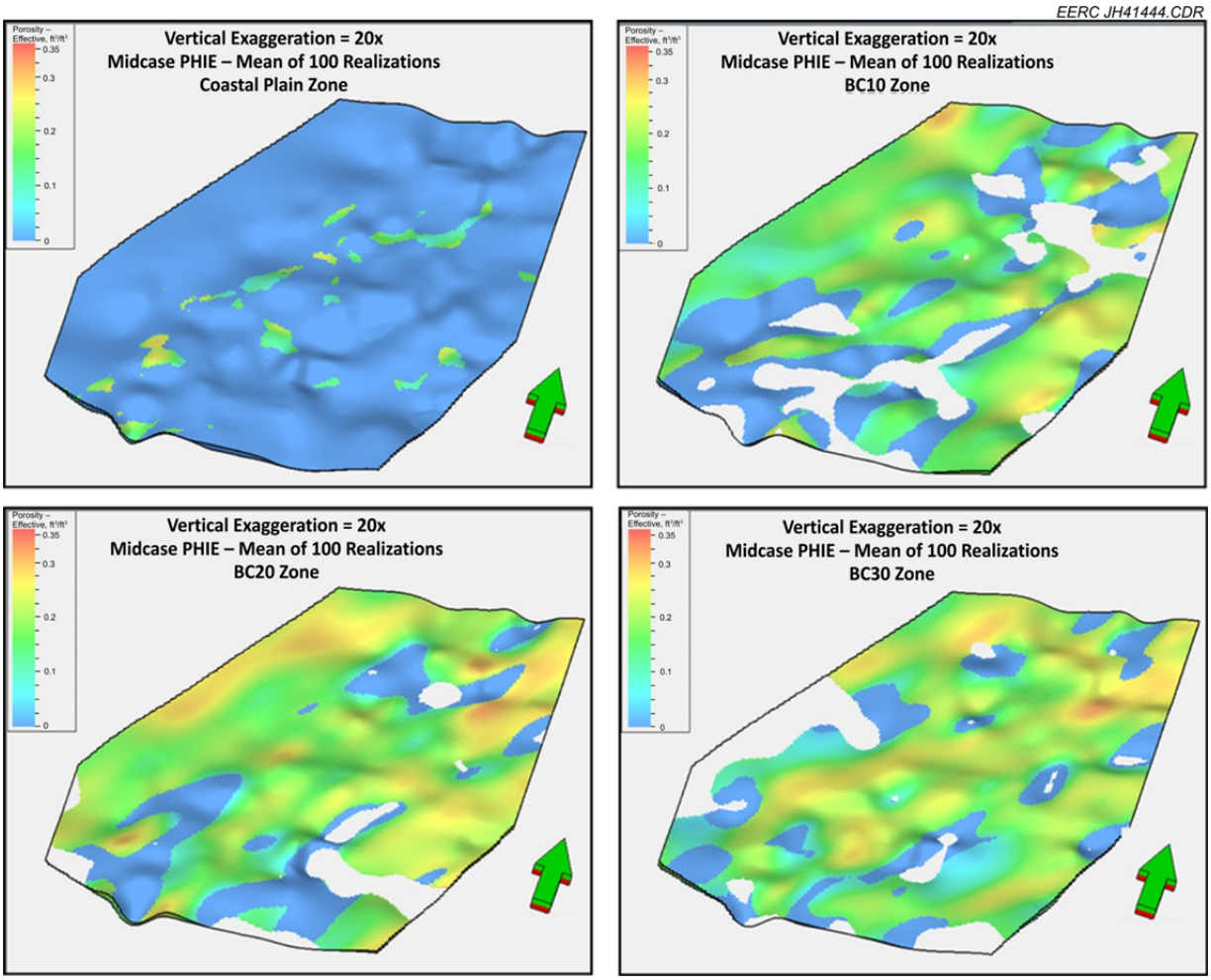

Figure A-4. Porosity (PHIE) of CP and BC zones (midcase).

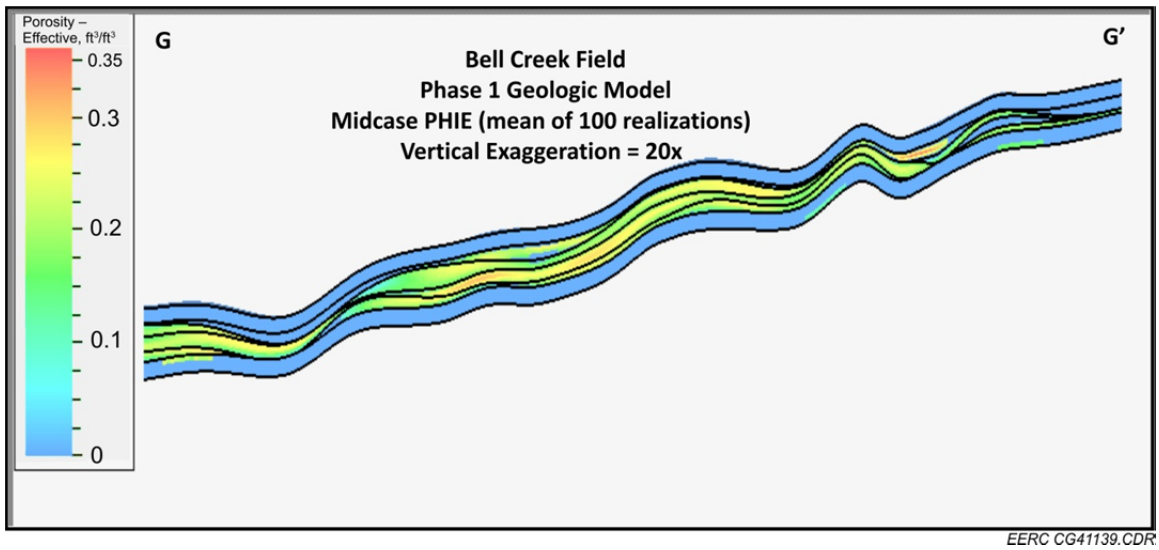

Figure A-5. Distribution of porosity along Cross Section G–G'.

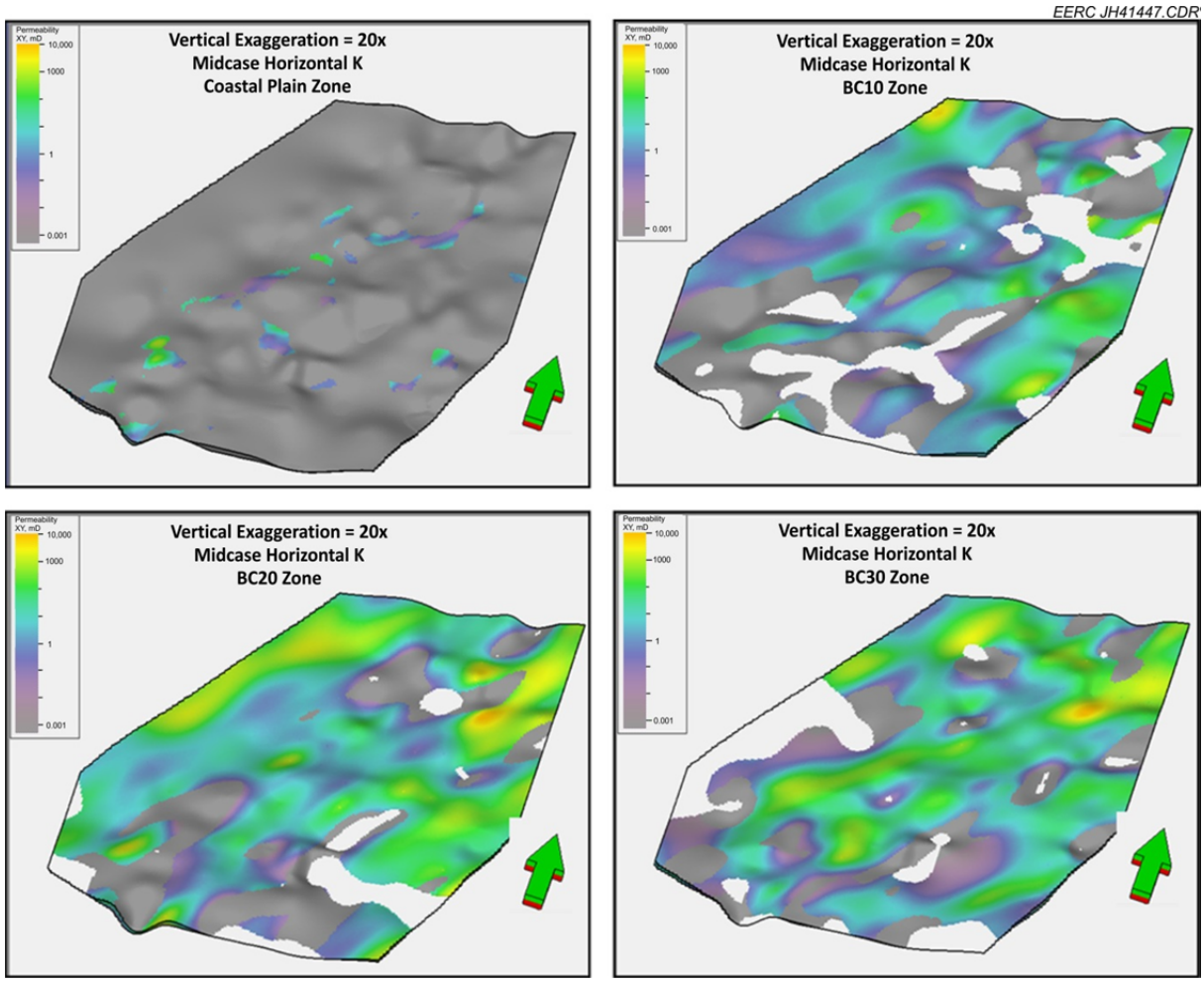

Figure A-6. Horizontal permeability (Kxy) of CP and BC zones (midcase).

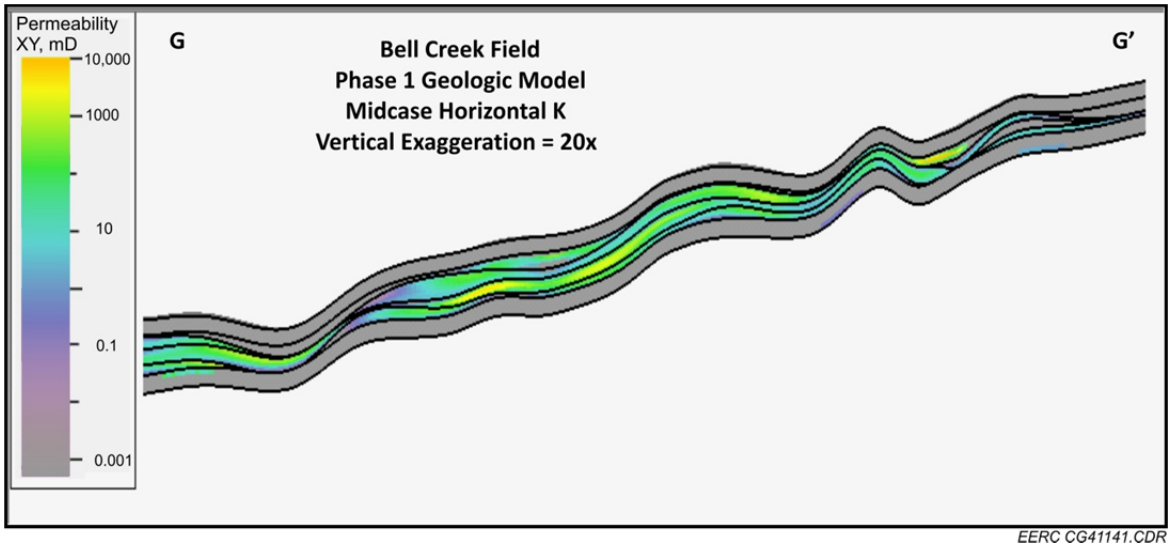

Figure A-7. Distribution of permeability along Cross Section G–G'.

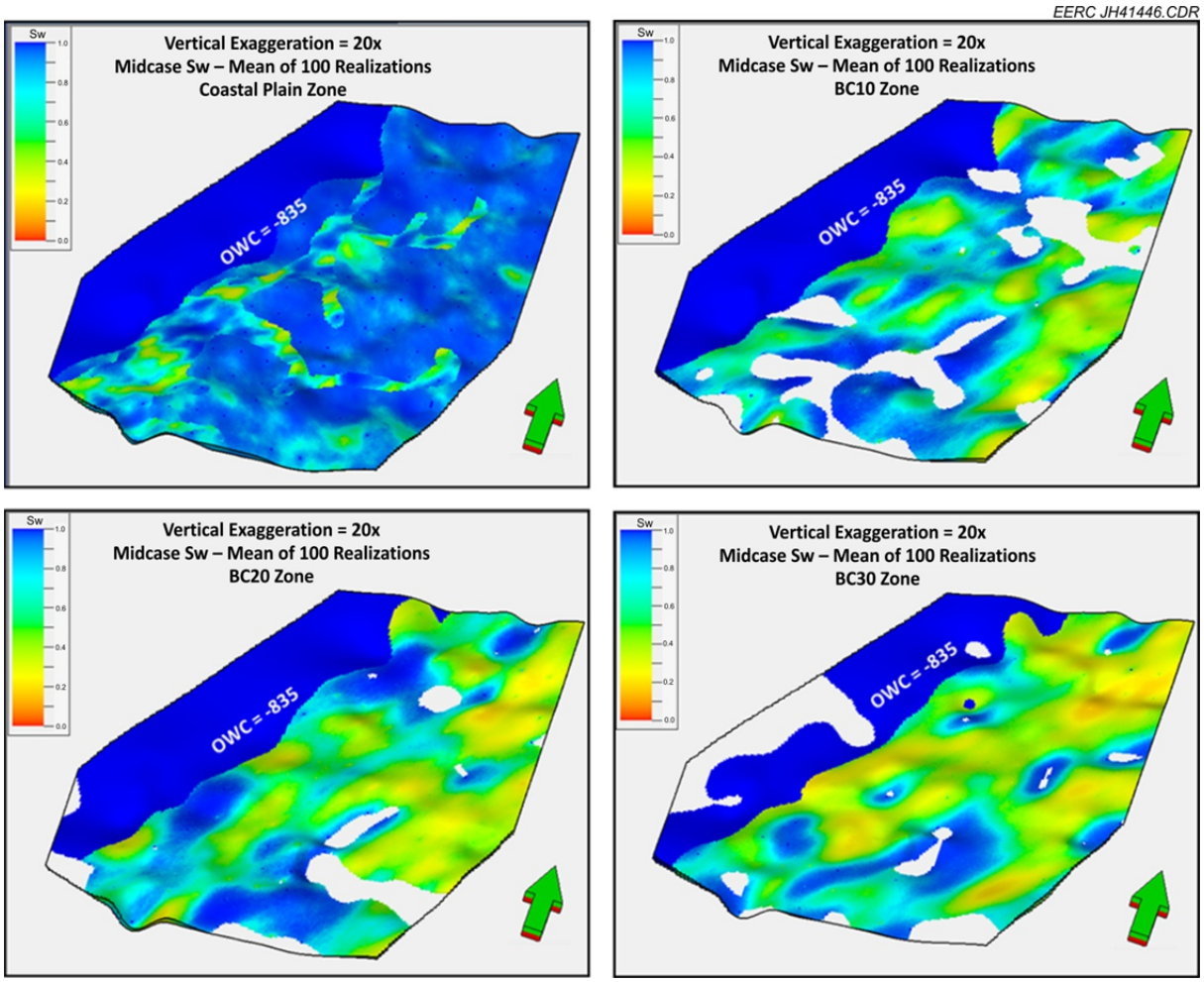

Figure A-8. Water saturation (Sw) of CP and BC zones (midcase).

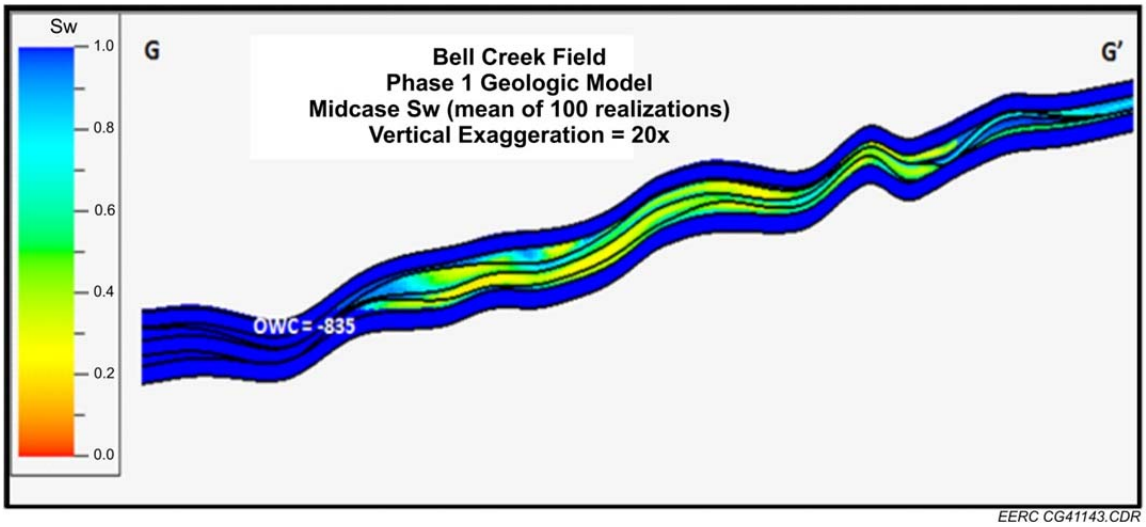

Figure A-9. Distribution of water saturation along Cross Section G–G'.

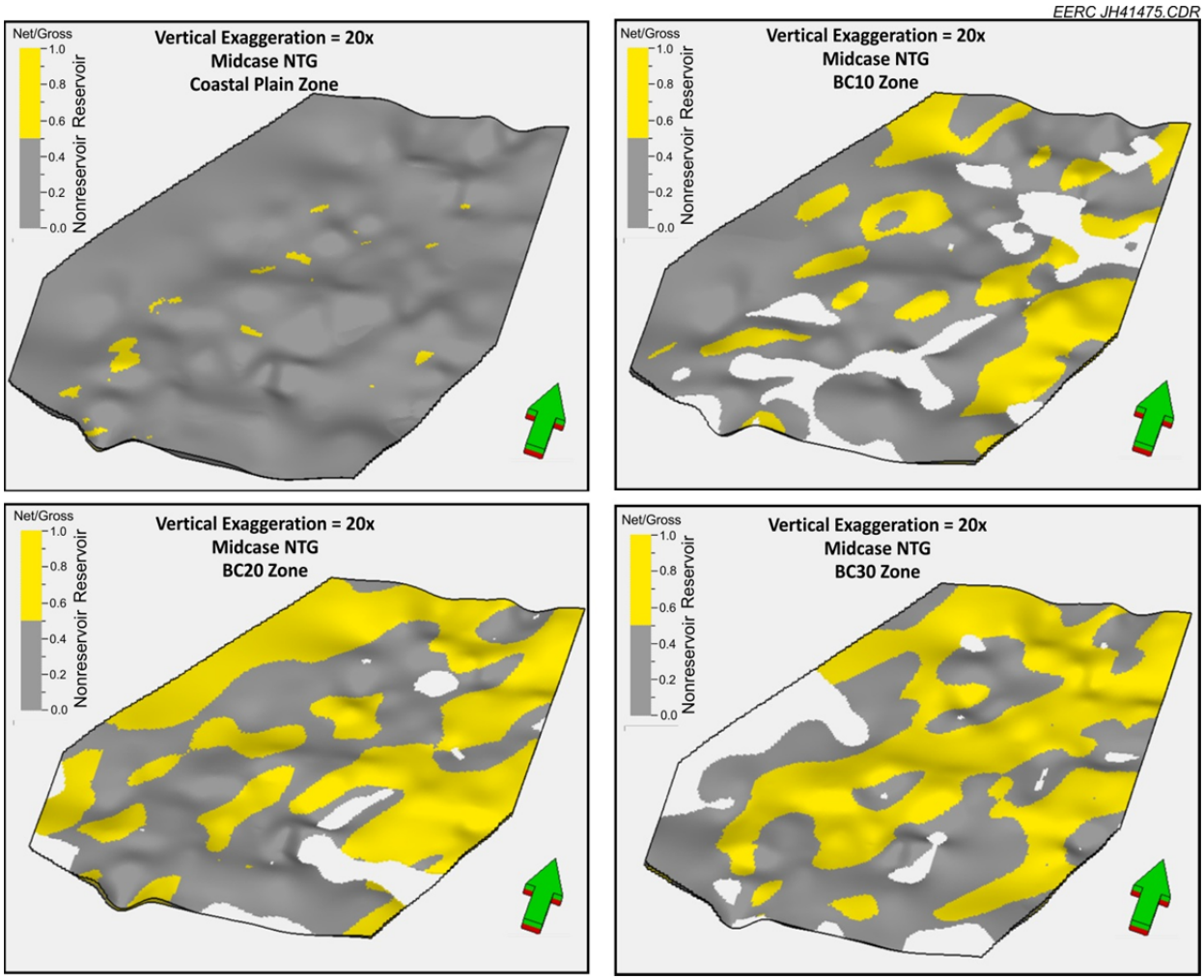

Figure A-10. Net to gross (NTG) of CP and BC zones (midcase).

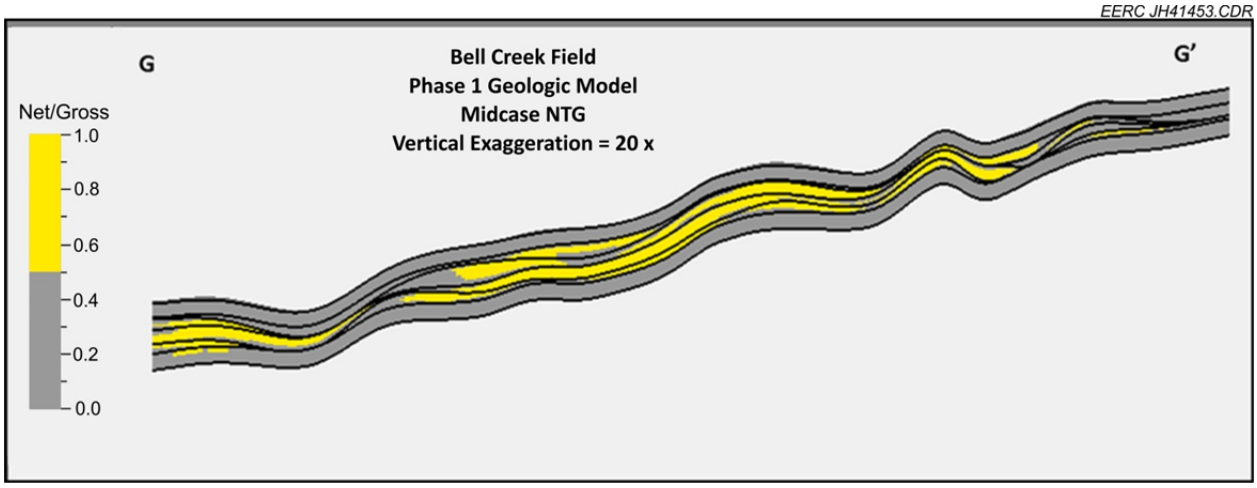

Figure A-11. Distribution of NTG along Cross Section G–G'.

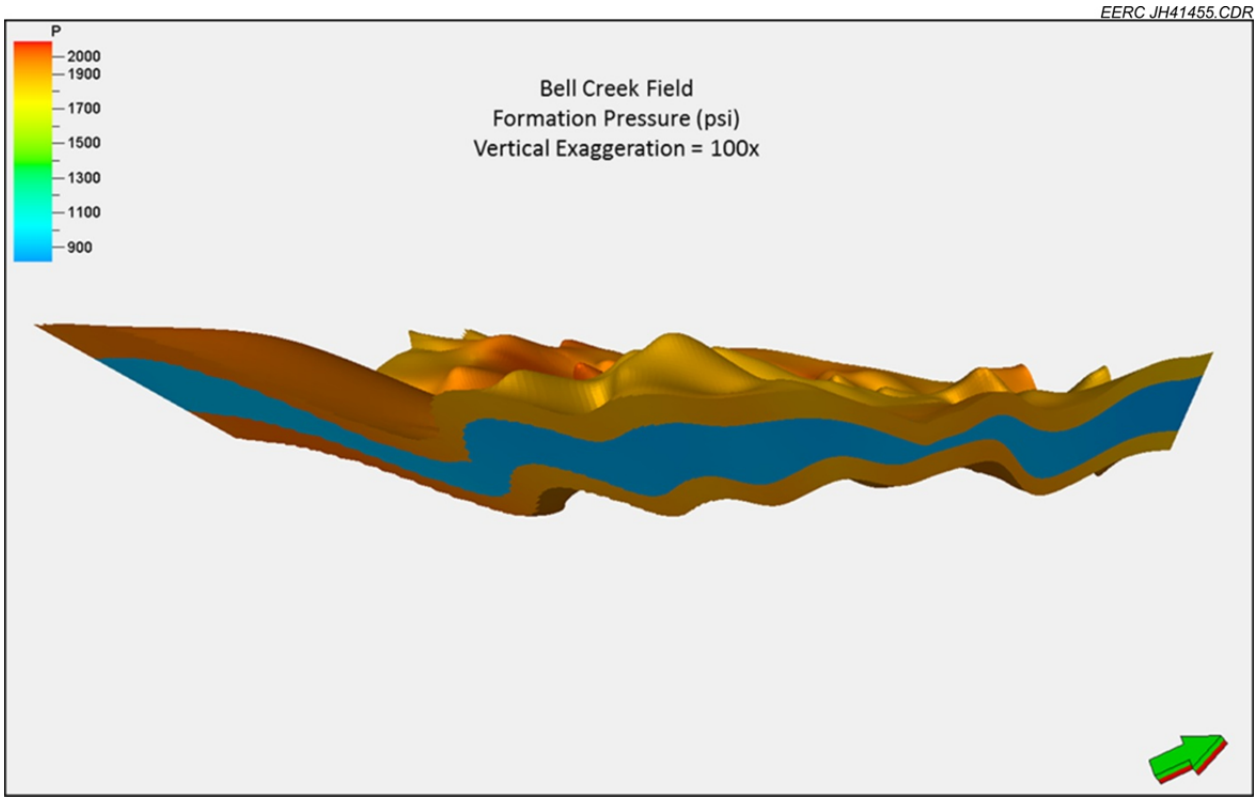

Figure A-12. Formation pressure of geologic model.

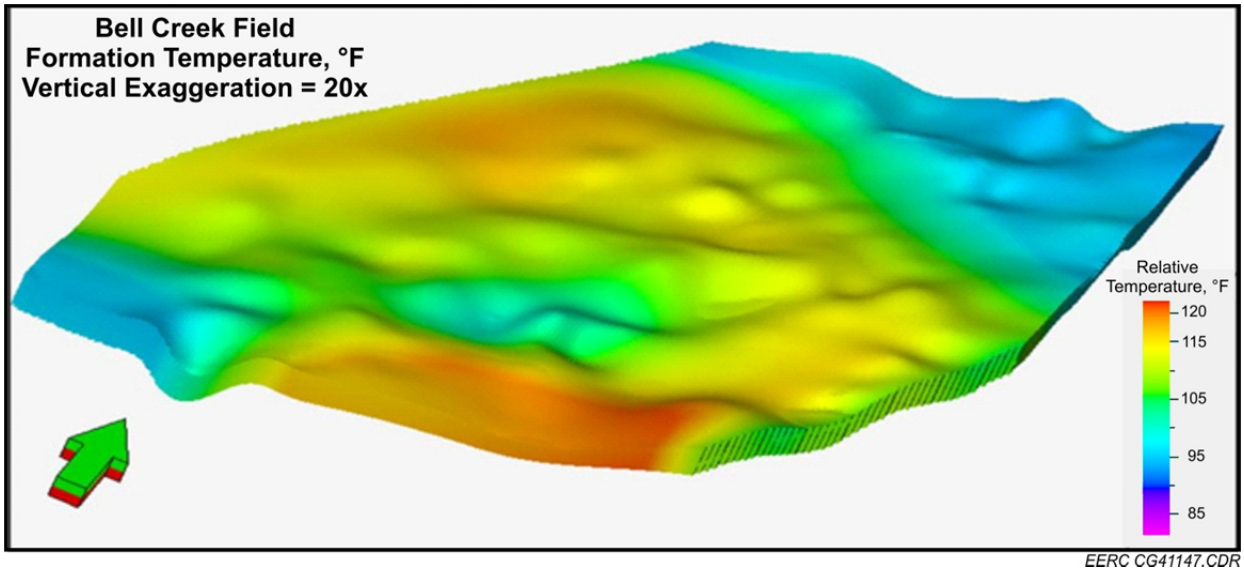

Figure A-13. Formation temperature of geologic model.

APPENDIX B

PVT AND SLIM-TUBE EXPERIMENT MODELING

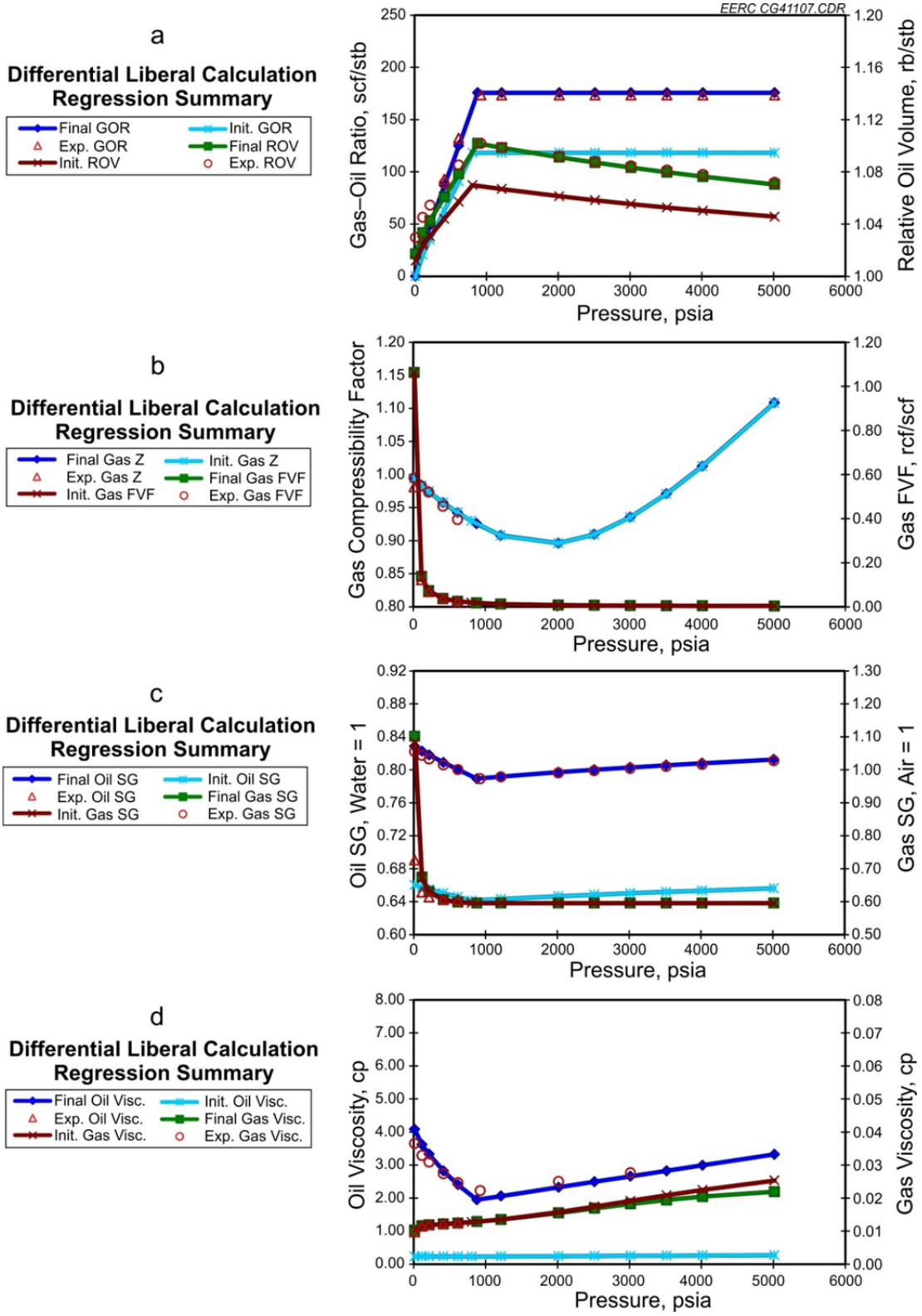

Figure B-1. a) Regression results of GOR and ROV for the DL test (C_{6+}, Well 0511), b) regression results of gas Z and FVF for the DL test (C_{6+}, Well 0511), c) regression results of oil and gas SG for the DL test (C_{6+}, Well 0511), and d) regression results of the oil and gas viscosity for the DL test (C_{6+}, Well 0511).

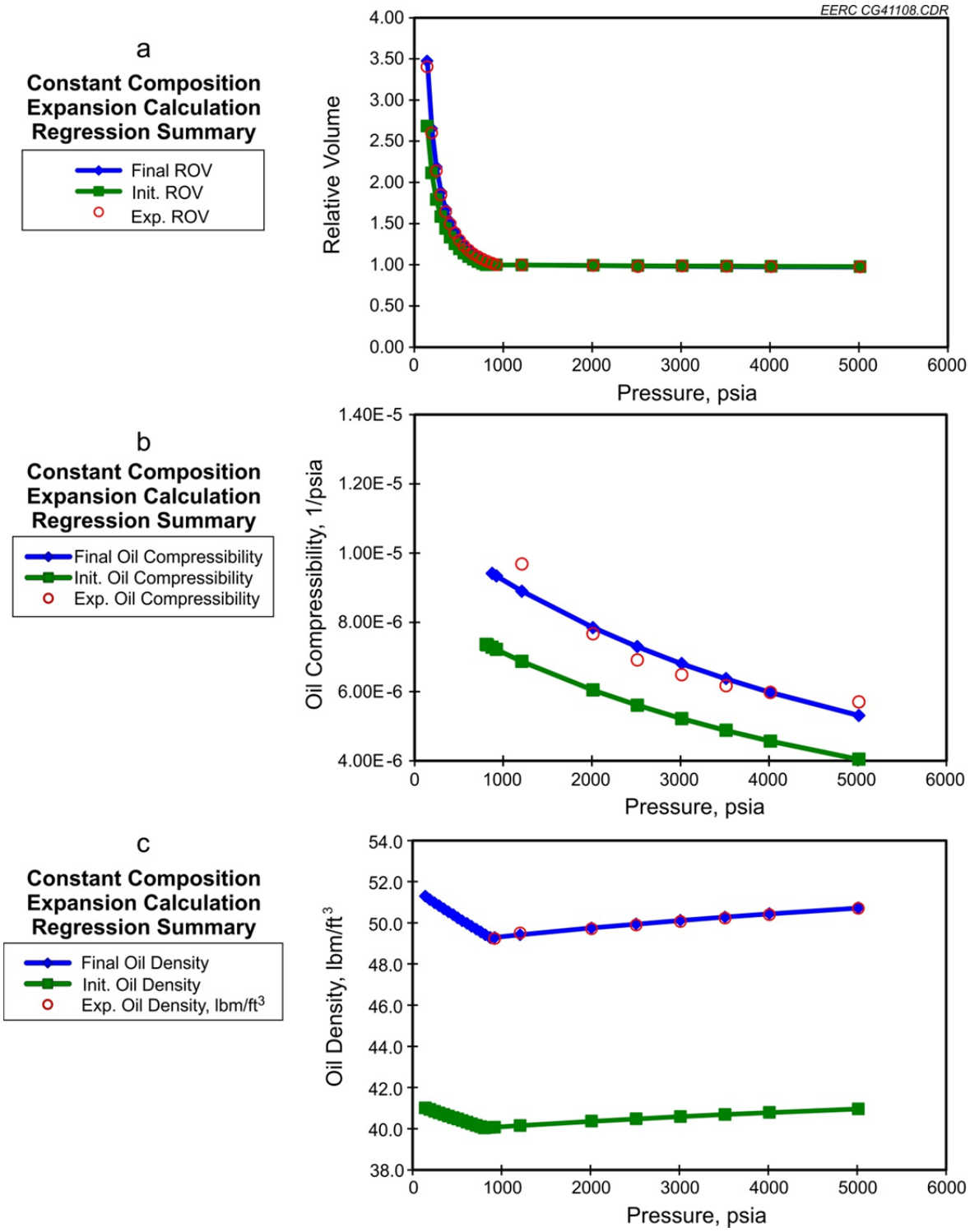

Figure B-2. a) Regression results of ROV for the CCE test (C_{6+}, Well 0511), b) regression results of oil compressibility for the CCE test (C_{6+}, Well 0511), and c) regression results of oil density for the CCE test (C_{6+}, Well 0511).

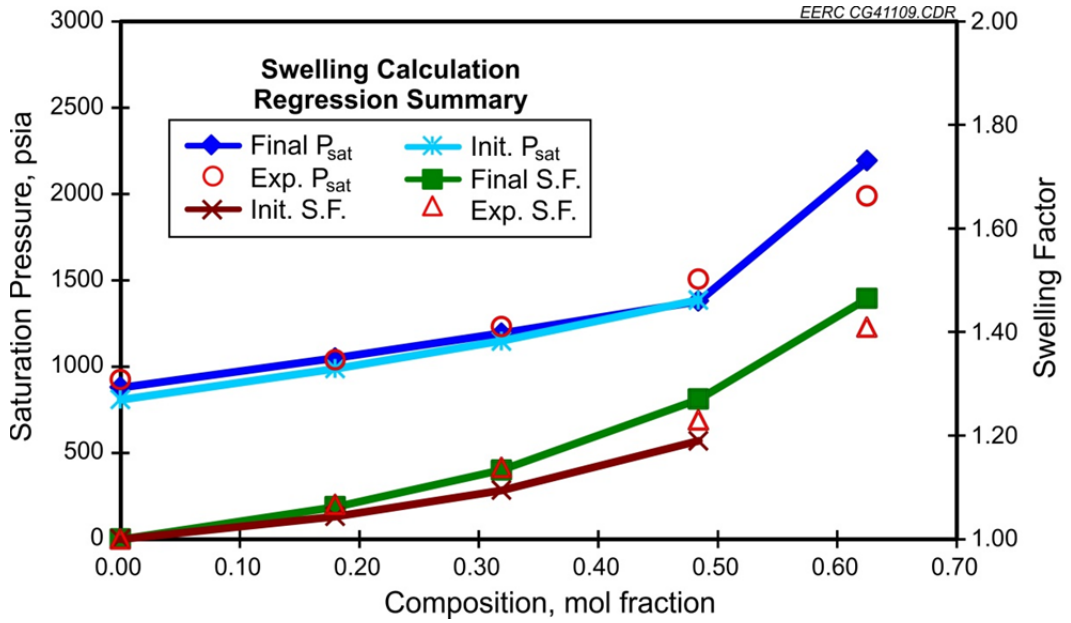

Figure B-3. Saturation pressure (P_{sat}) and swelling factor (S.F.) comparison (C_{6+}, Well 0511).

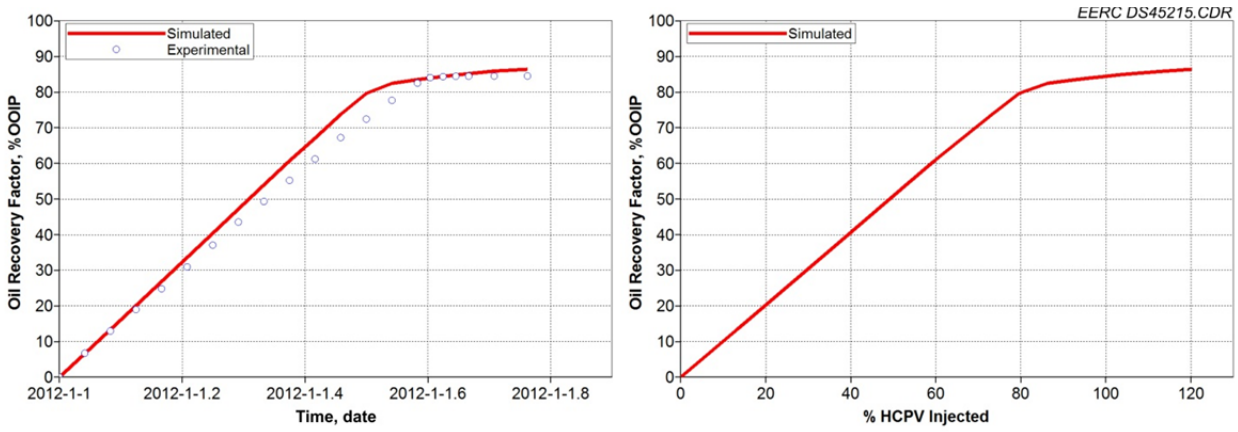

Figure B-4. Recovery of slim tube at 1215 psi.

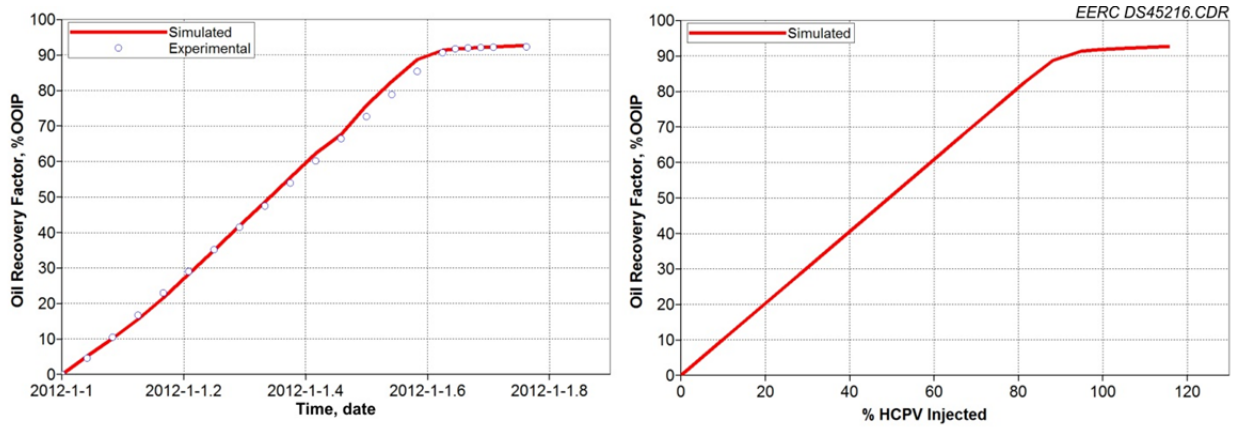

Figure B-5. Recovery of slim tube at 3015 psi.

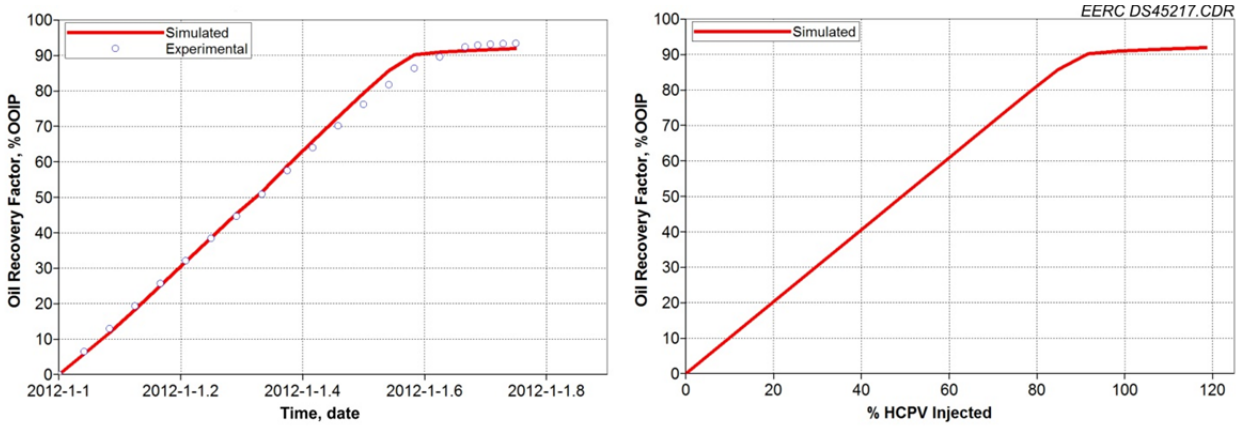

Figure B-6. Recovery of slim tube at 3515 psi.

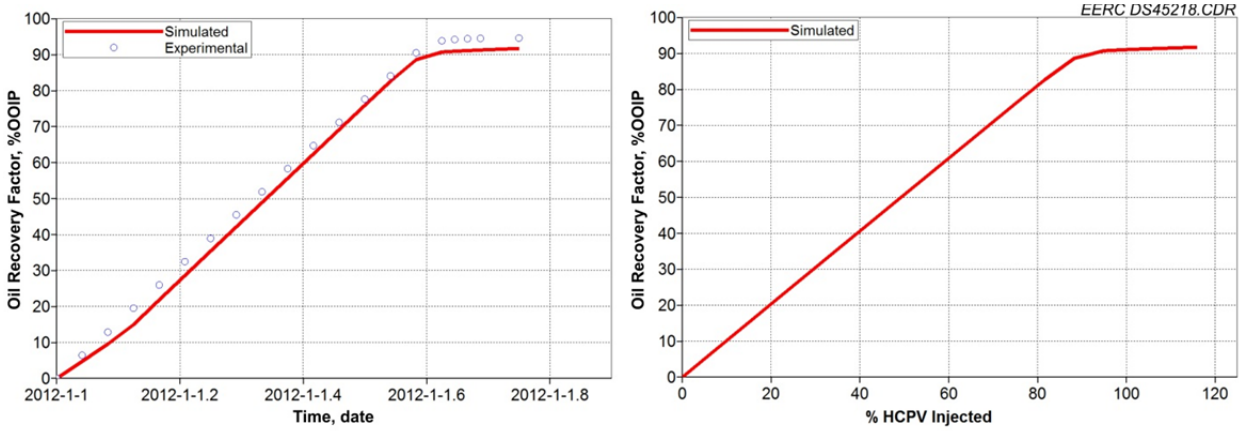

Figure B-7. Recovery of slim tube at 4515 psi.

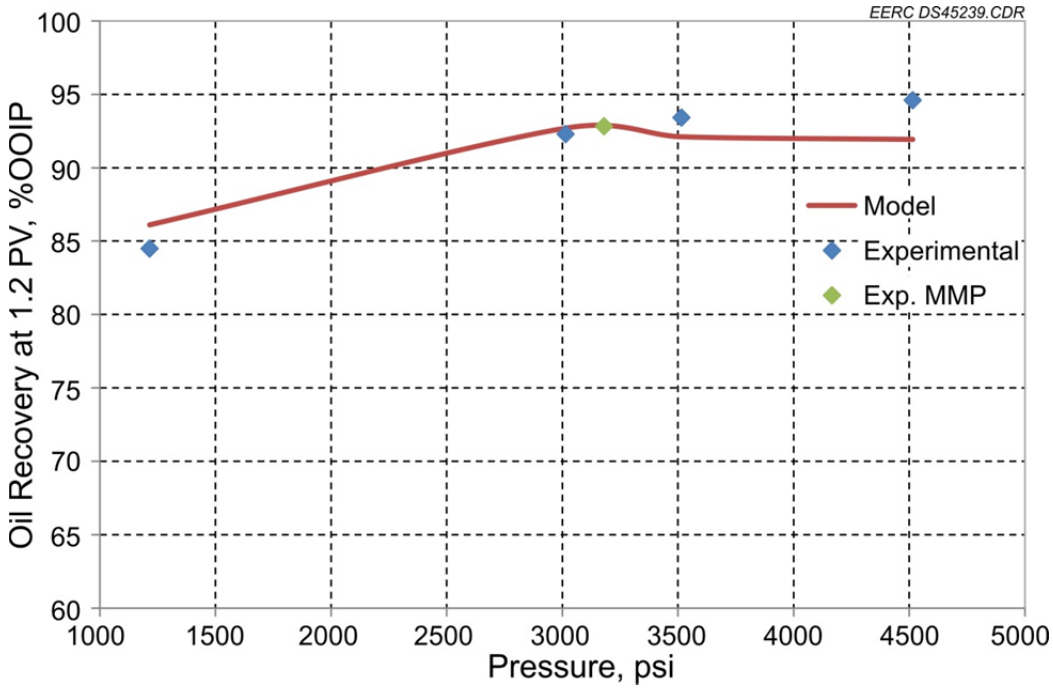

Figure B-8. Comparison of simulated MMP and experimental MMP at 108°F with CO_2.

APPENDIX C

RESERVOIR SIMULATION

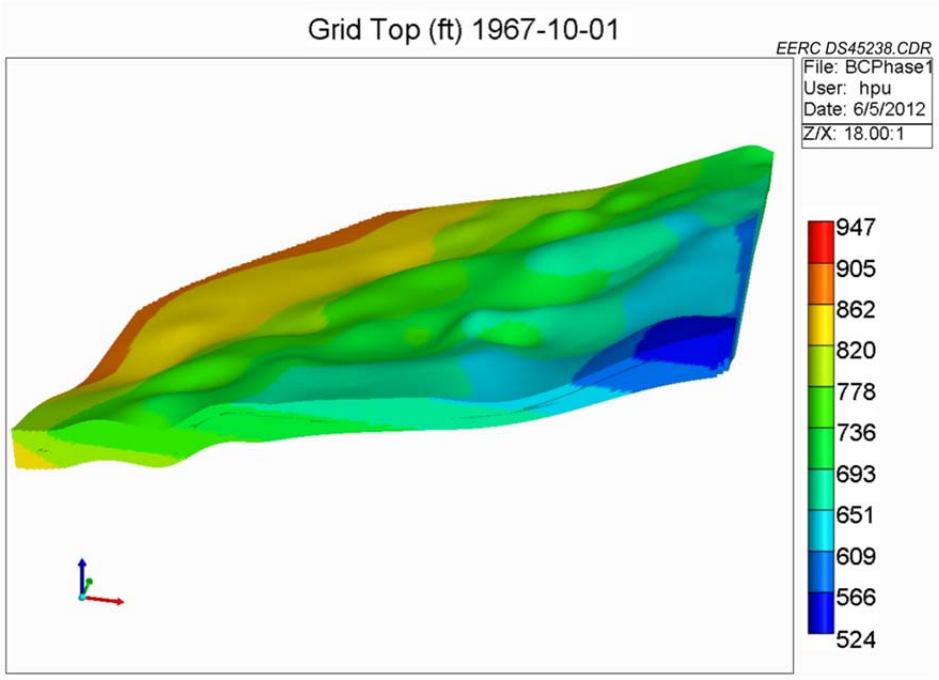

Figure C-1. 3-D View of simulation model.

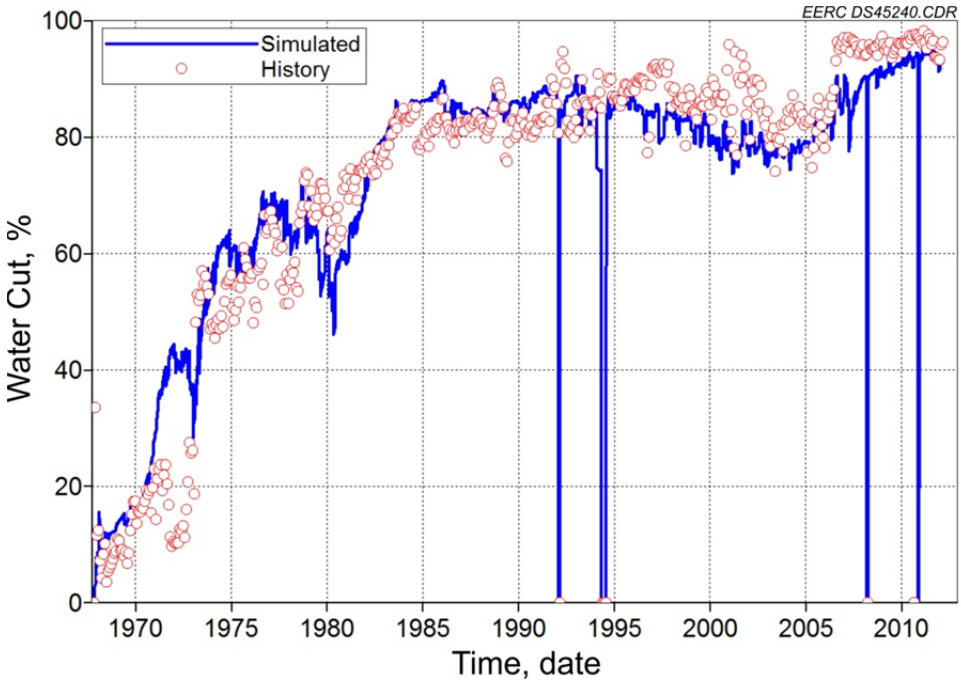

Figure C-2. History-matching result of field water cut.

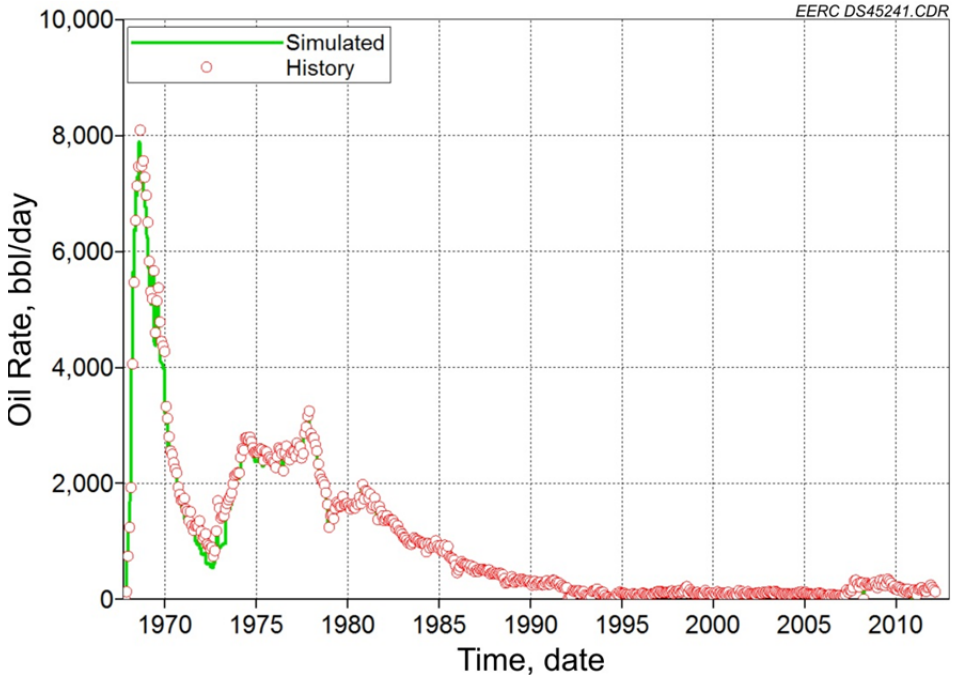

Figure C-3. History-matching result of field oil rate.

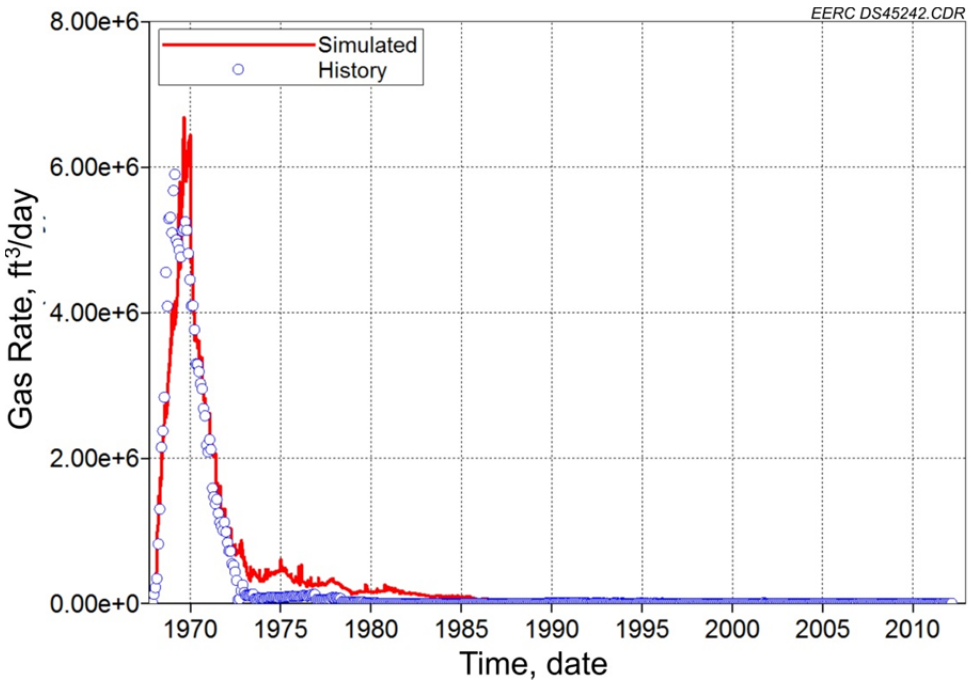

Figure C-4. History-matching result of field gas rate.

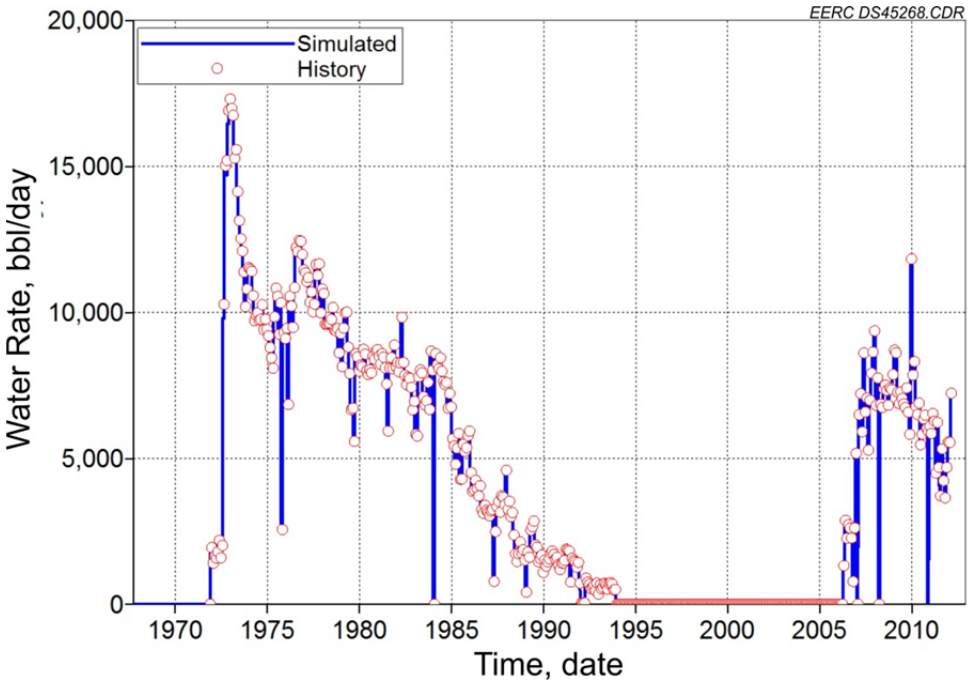

Figure C-5. Field water injection rate.

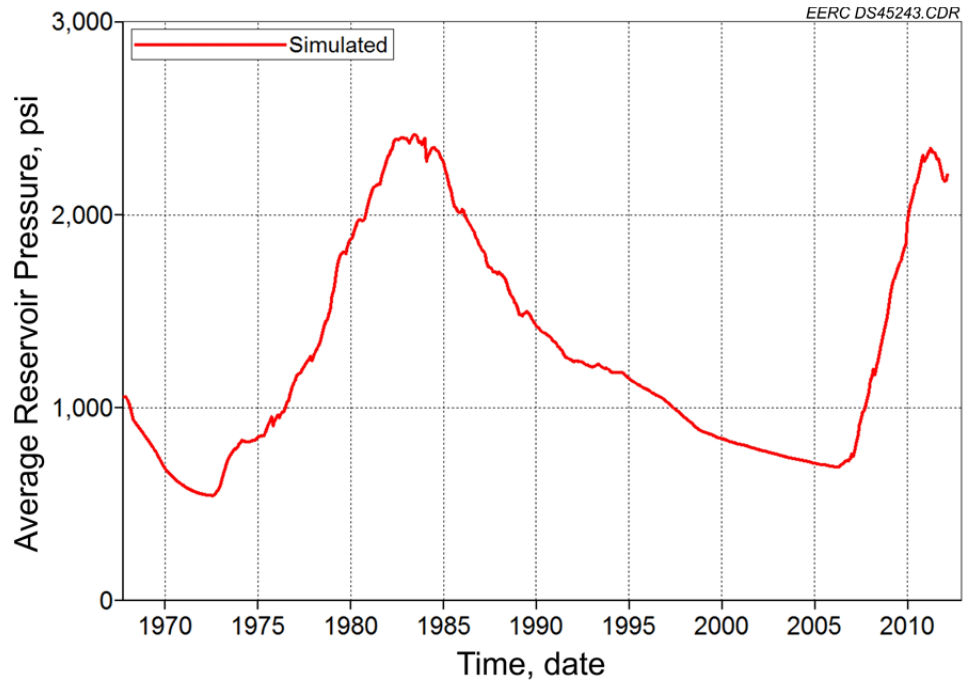

Figure C-6. Average reservoir pressure.

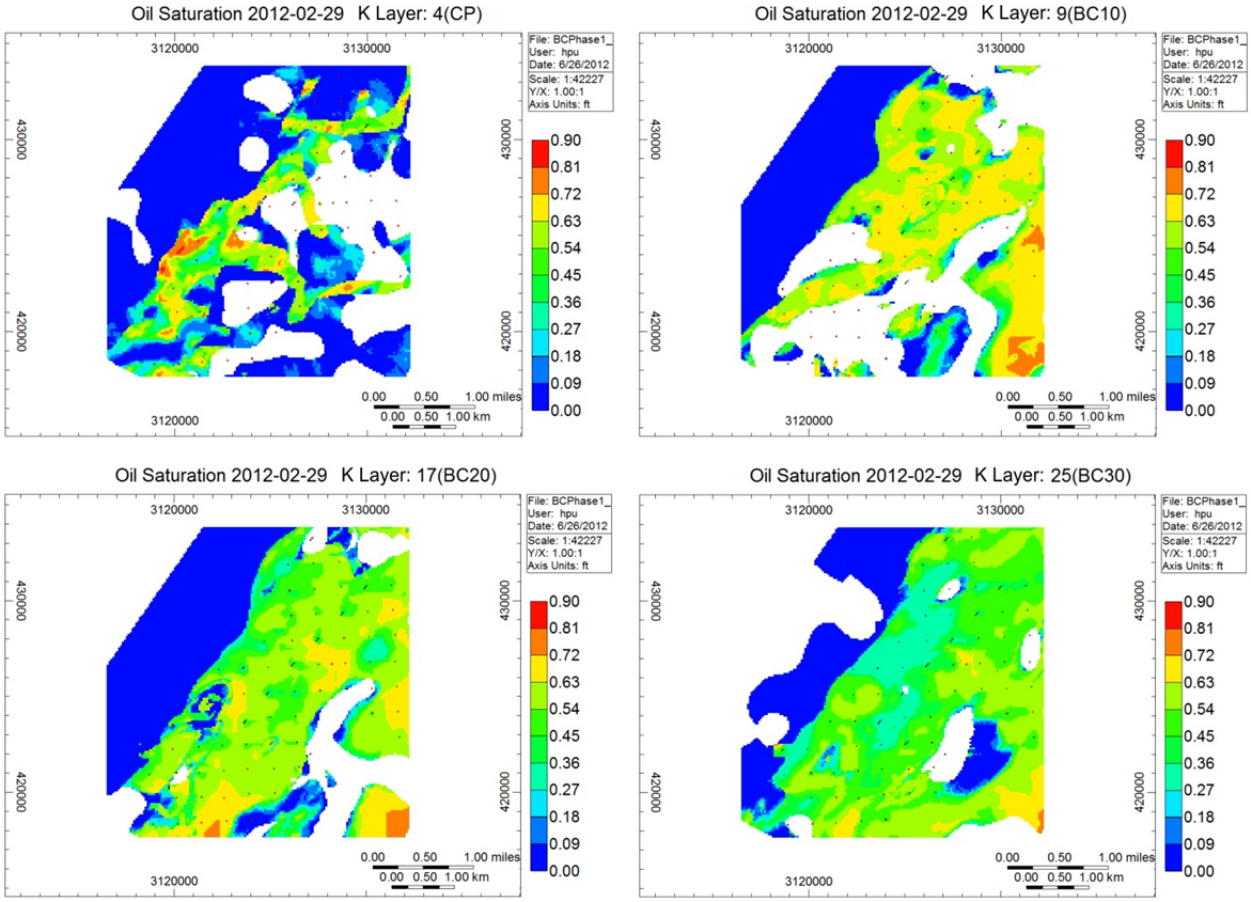

Figure C-7. Oil saturation in 2-D view for top layers of Coastal Plain and BC Sand.

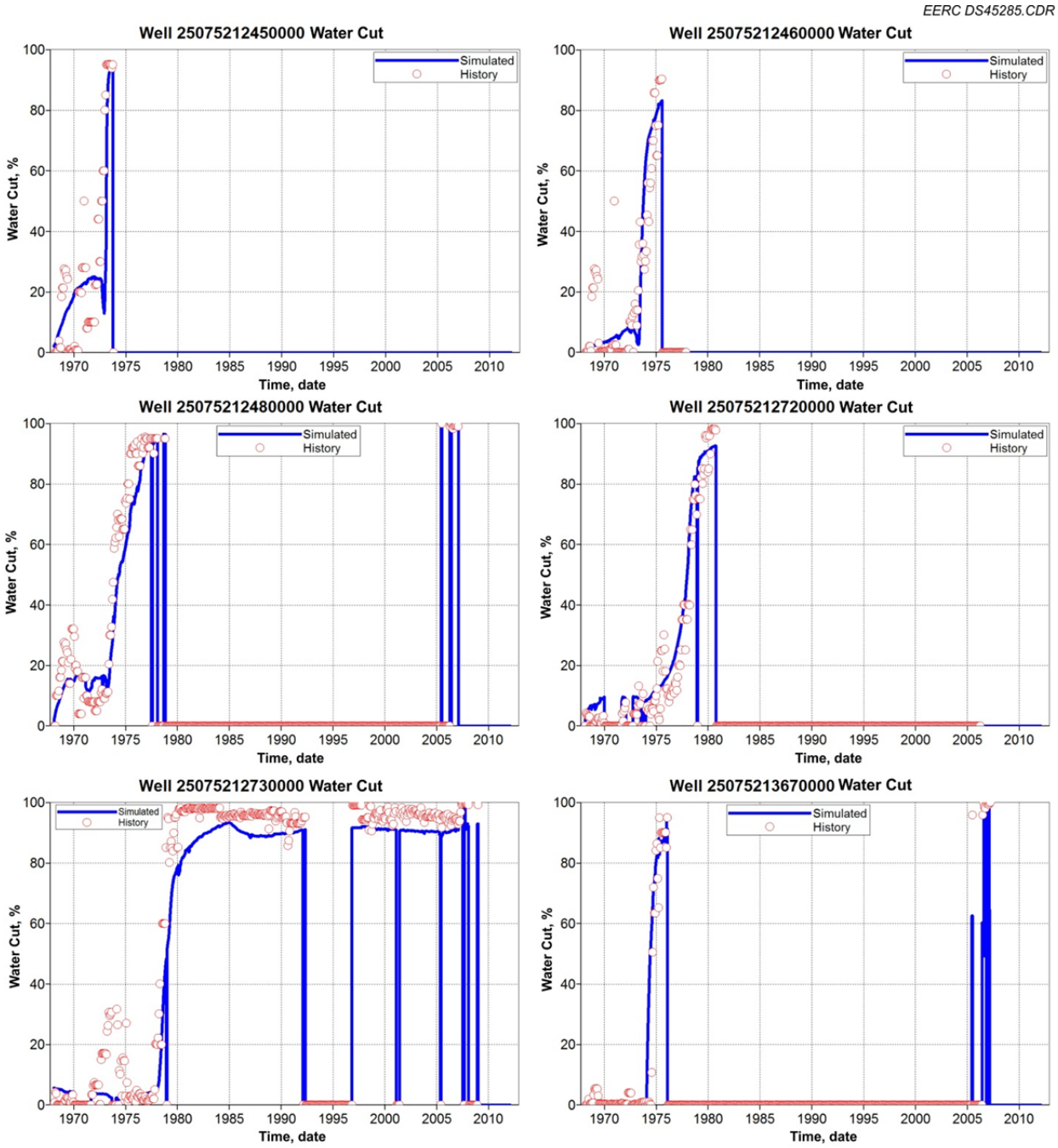

Figure C-8. Individual well history matching of water cut (Part 1).

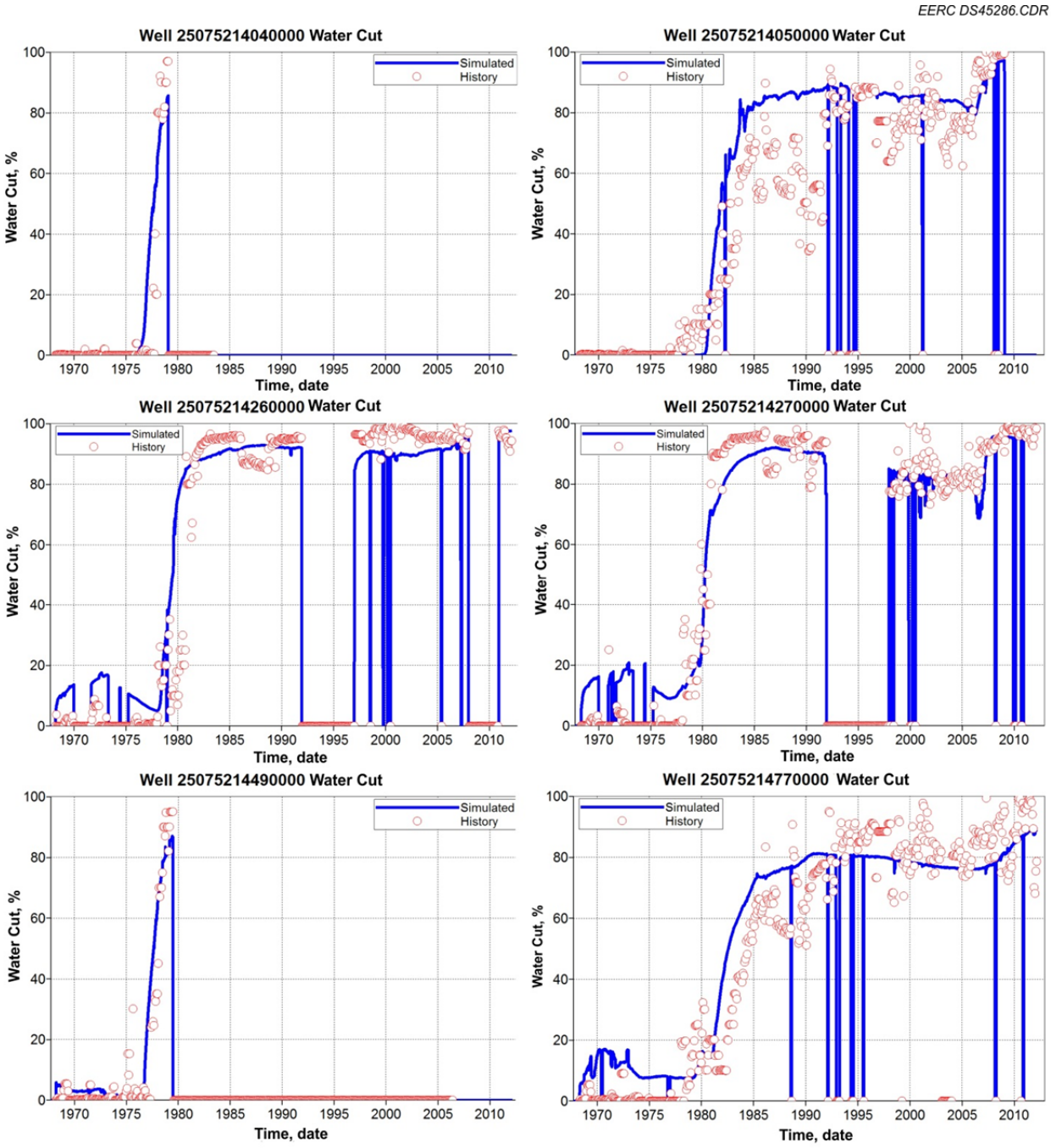

Figure C-9. Individual well history matching of water cut (Part 2).

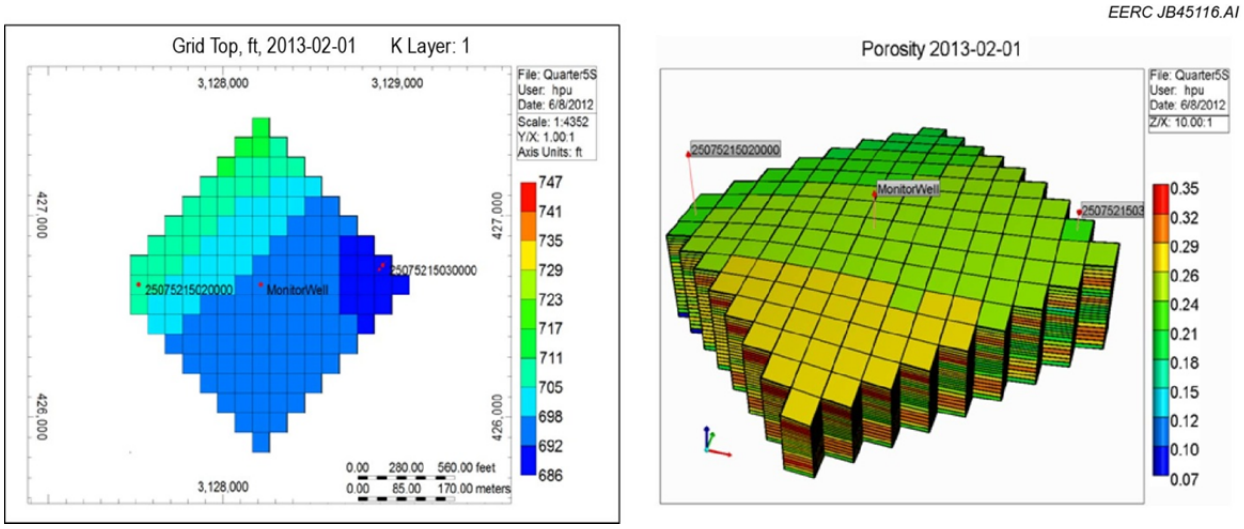

Figure C-10. Quarter five-spot pattern model.

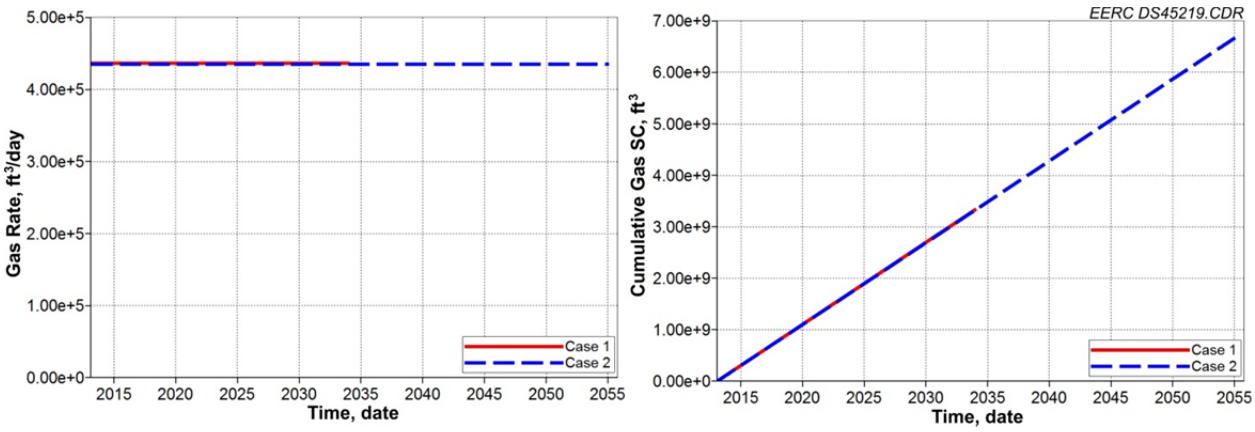

Figure C-11. Standard condition (SC) injection rate and cumulative injection rate of CO_2 for Cases 1 and 2.

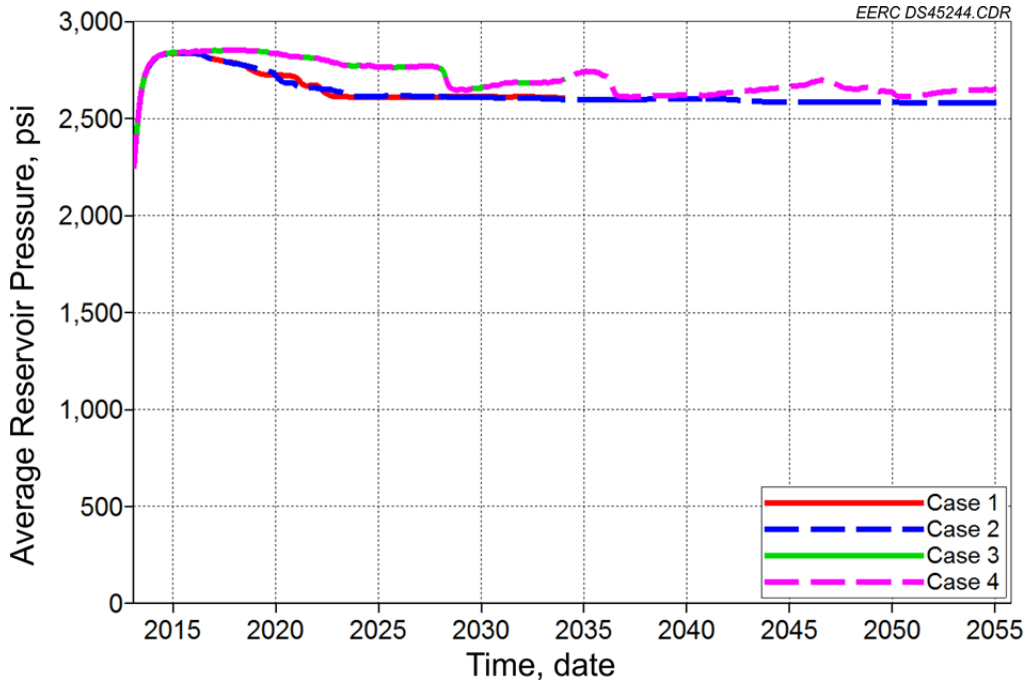

Figure C-12. Average reservoir pressure of Cases 1–4 for quarter five-spot pattern model.

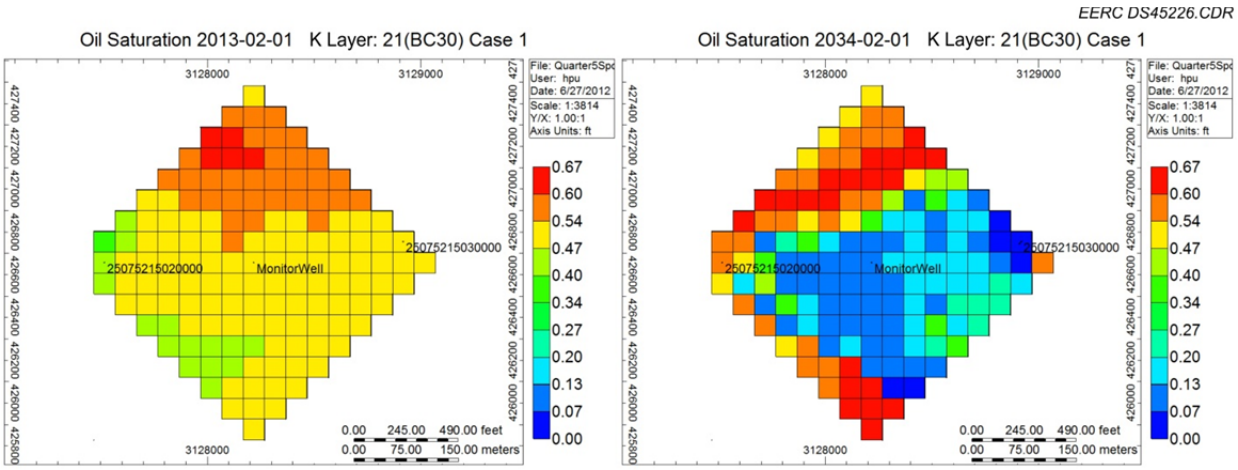

Figure C-13. Comparison of oil saturation before and after CO_2 flooding (Case 1: 1 HCPV).

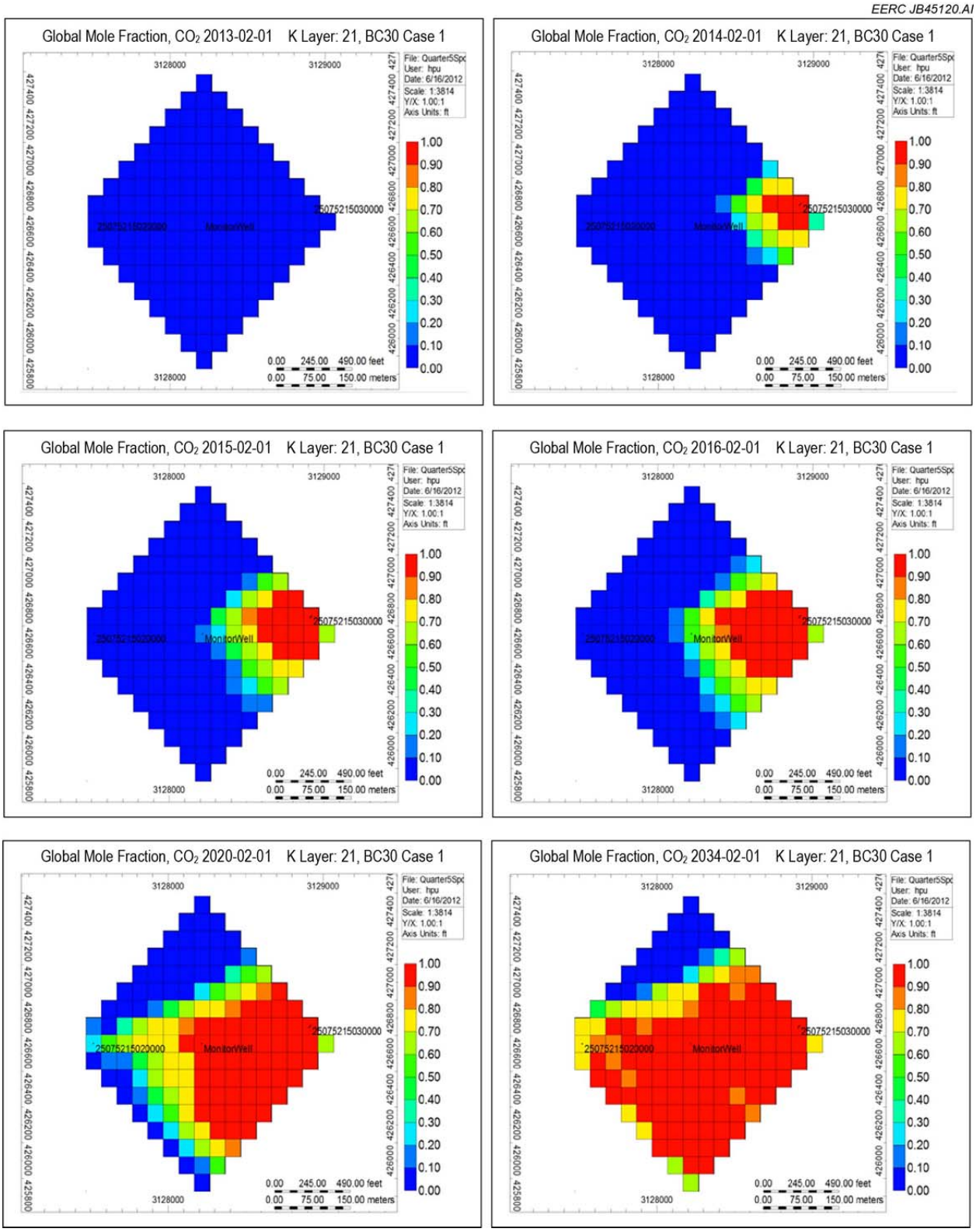

Figure C-14. Maps of global mole fraction of CO_2 in Layer 21 during CO_2 injection (Case 1: 1 HCPV).

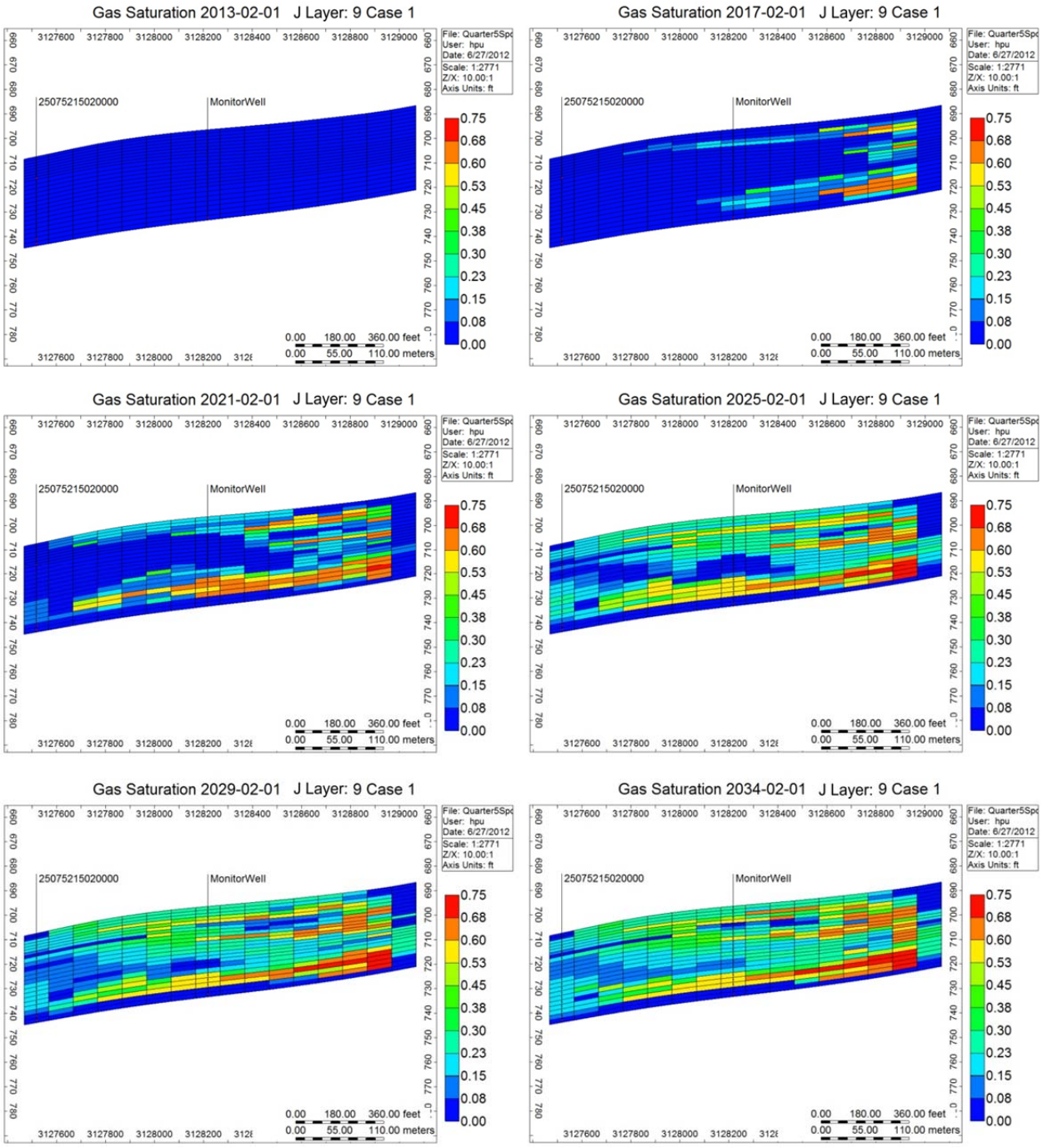

Figure C-15. Cross-sectional view of CO_2 saturation during CO_2 injection (Case 1: 1 HCPV).

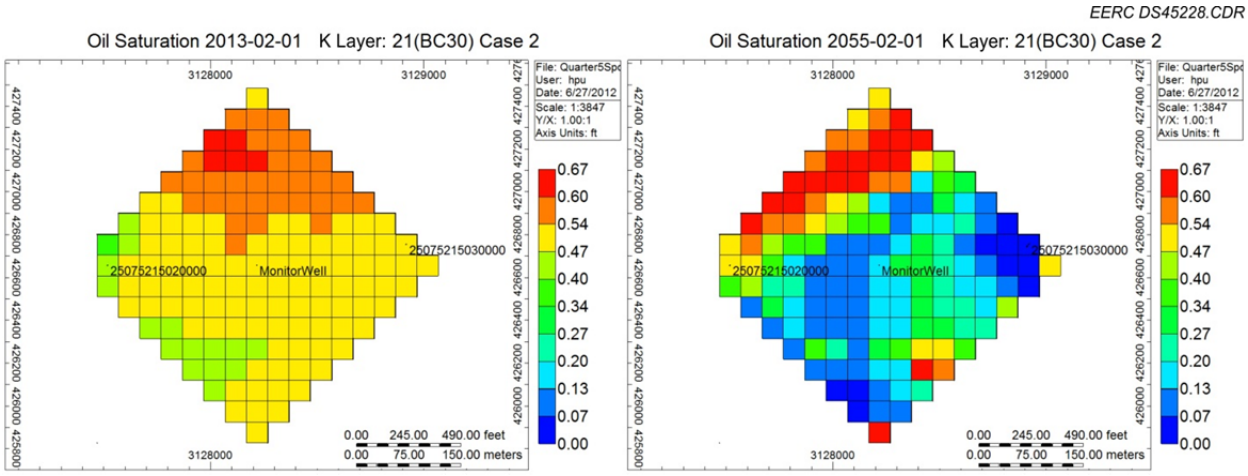

Figure C-16. Comparison of oil saturation before and after CO_2 flooding (Case 2: 2 HCPV).

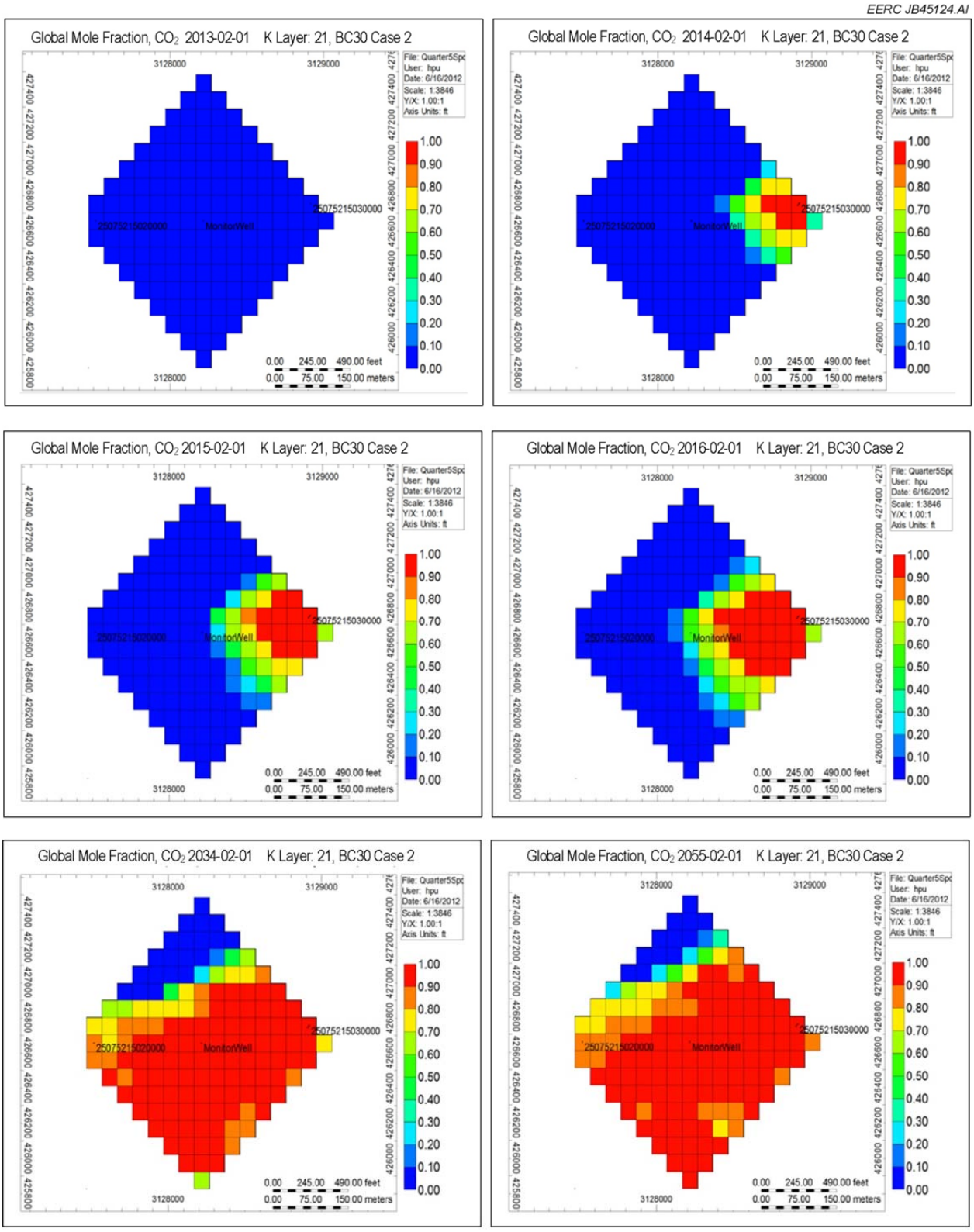

Figure C-17. Maps of global mole fraction of CO_2 in K Layer 21 during CO_2 injection (Case 2: 2 HCPV).

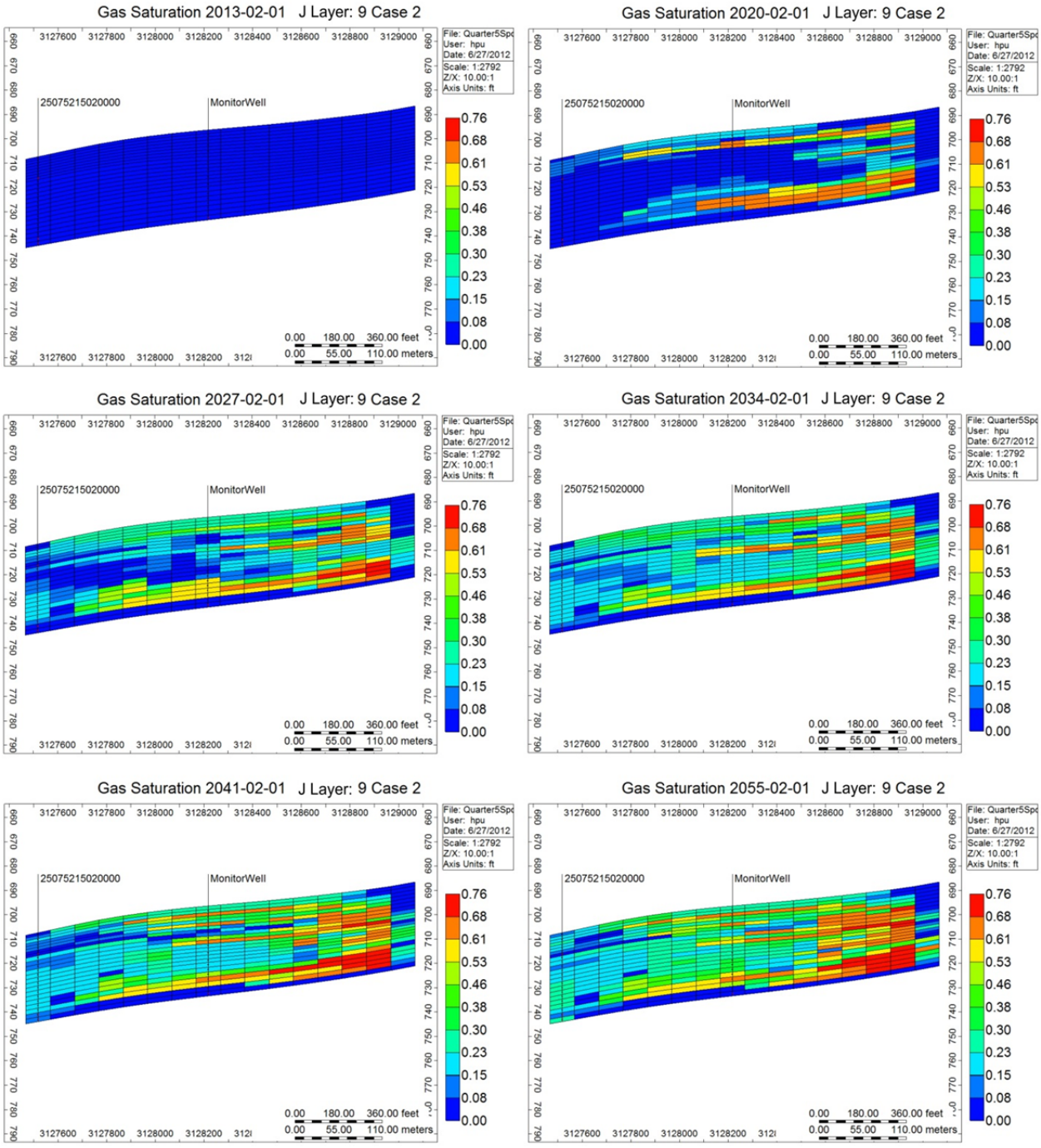

Figure C-18. Cross-sectional view of CO_2 saturation during CO_2 injection (Case 2: 2 HCPV).

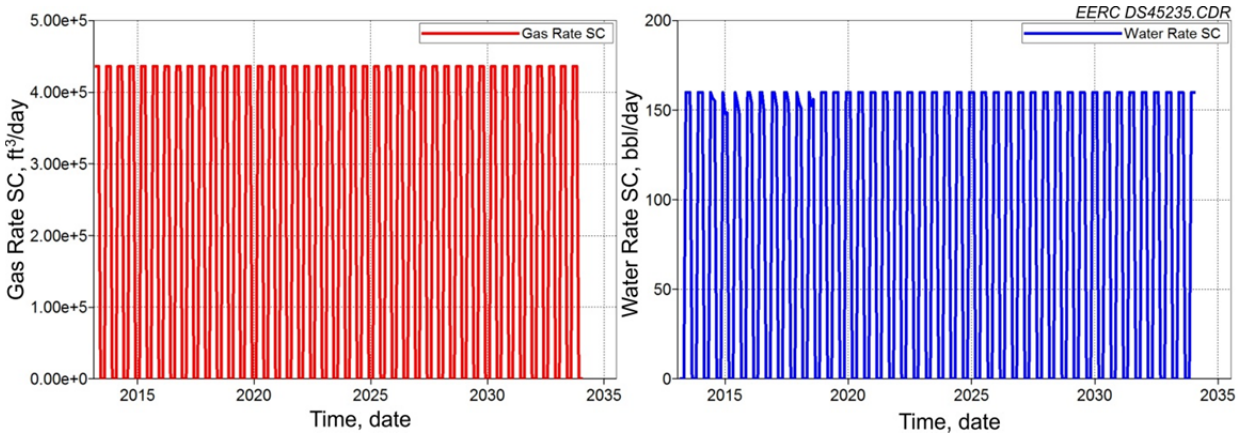

Figure C-19. Injection rate of CO_2 and water for Case 3.

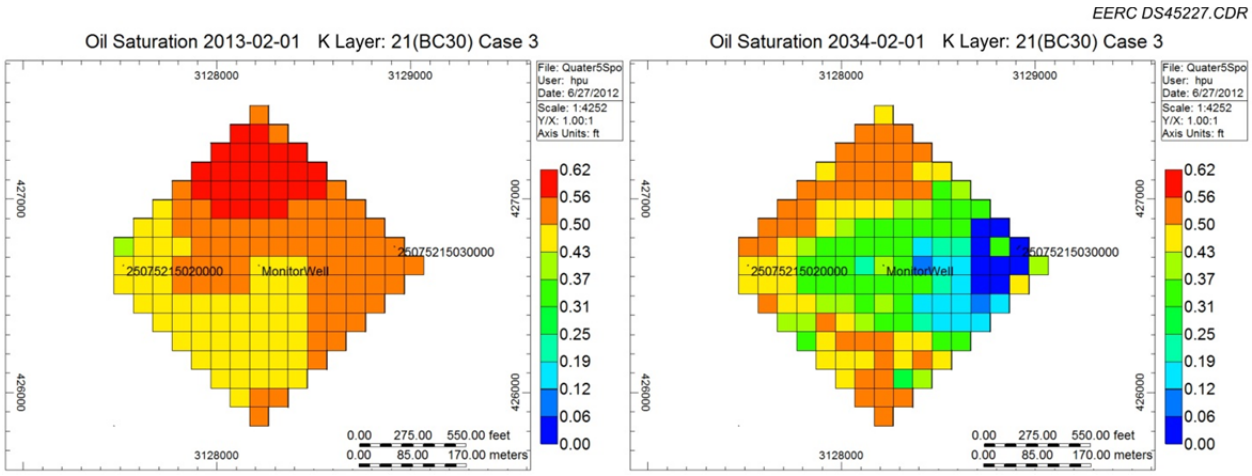

Figure C-20. Comparison of oil saturation before and after CO_2 flooding (Case 3: 1 HCPV WAG).

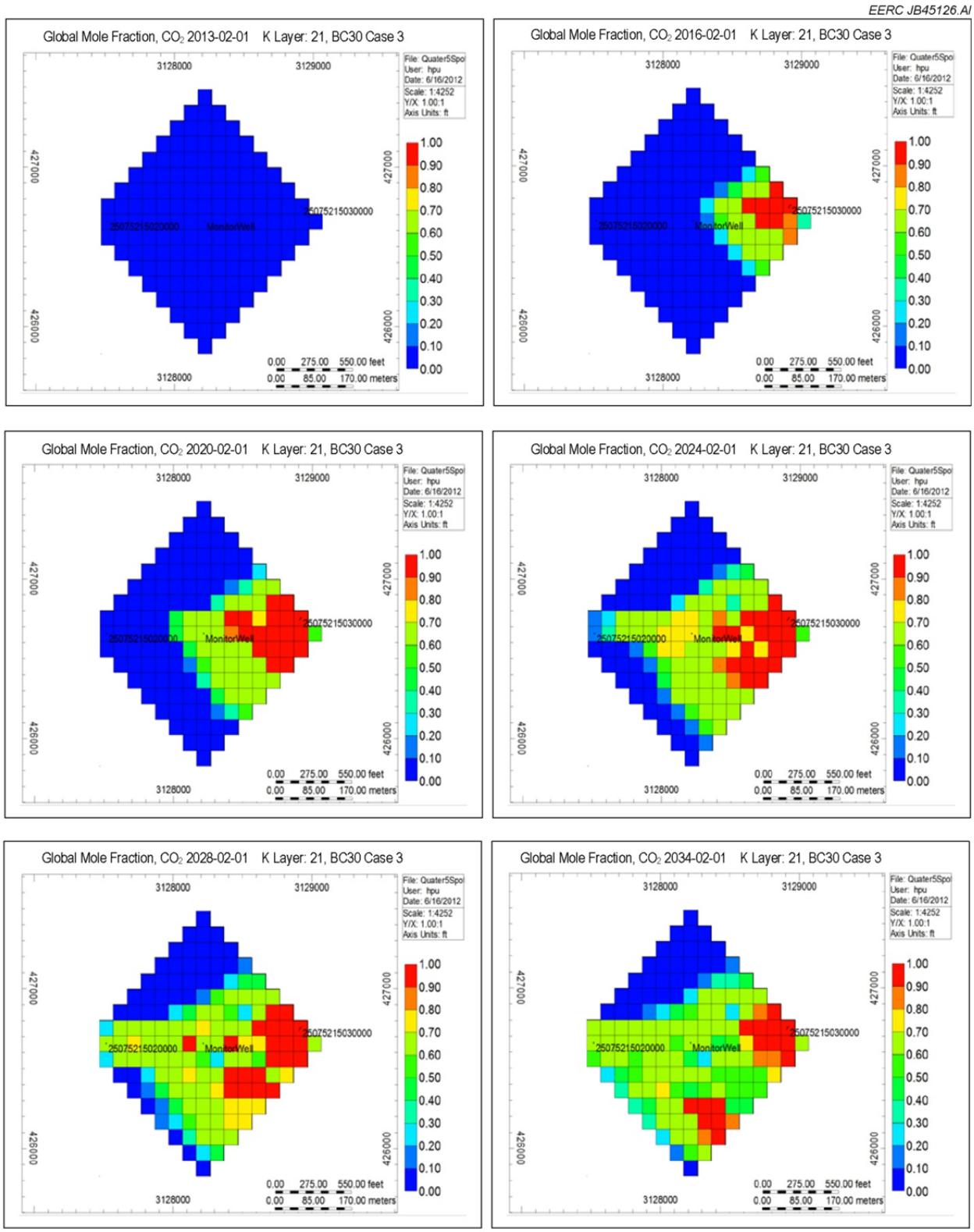

Figure C-21. Maps of global mole fraction of CO_2 in K Layer 21 during CO_2 injection (Case 3: 1 HCPV WAG).

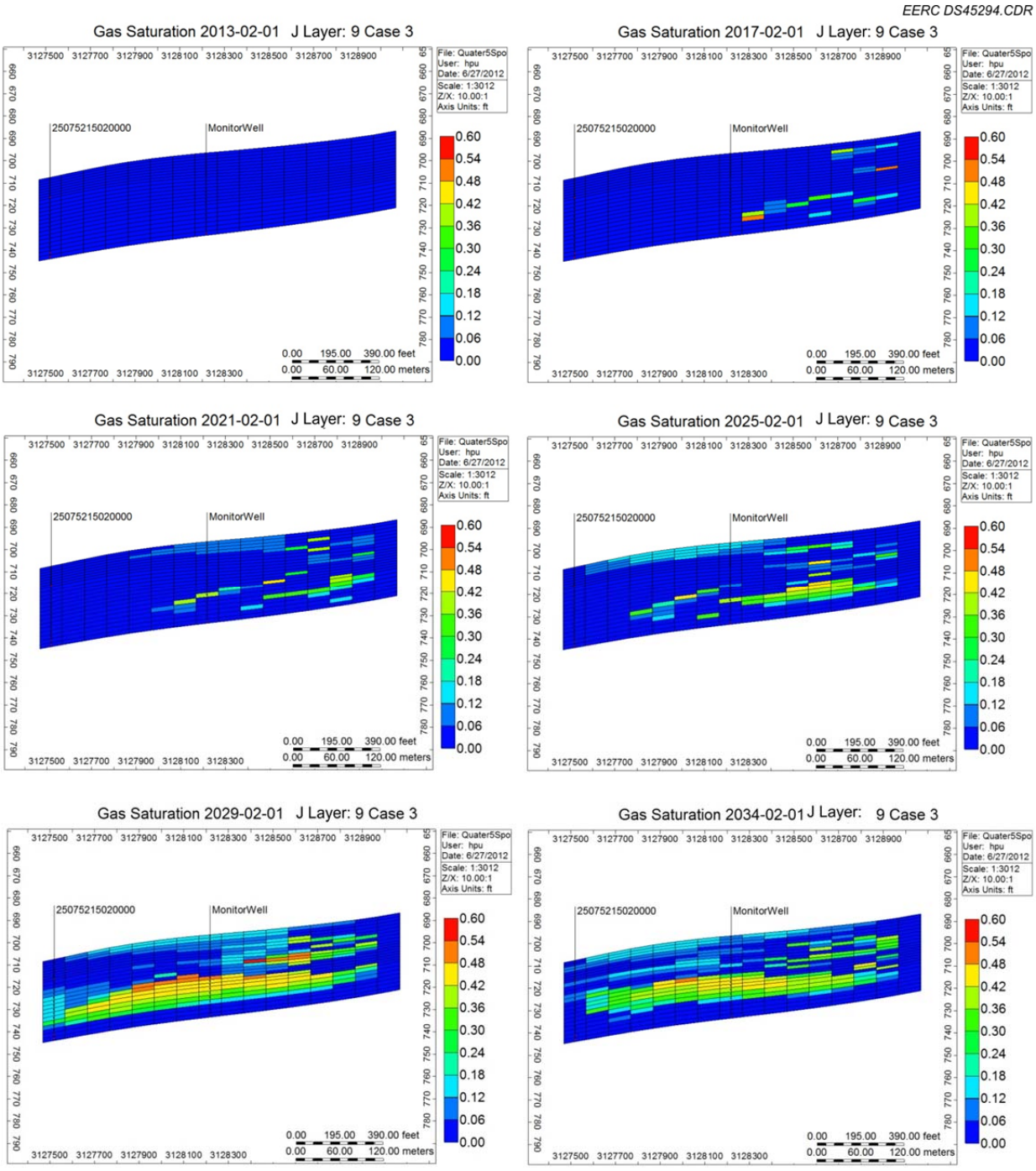

Figure C-22. Cross-sectional view of CO_2 saturation during CO_2 injection (Case 3: 1 HCPV).

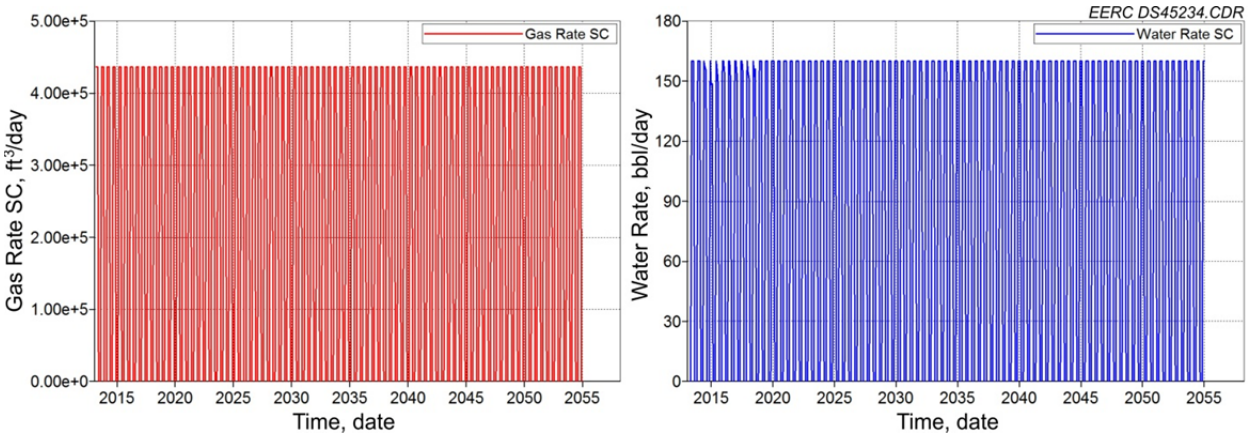

Figure C-23. Injection rate of CO_2 and water for Case 4.

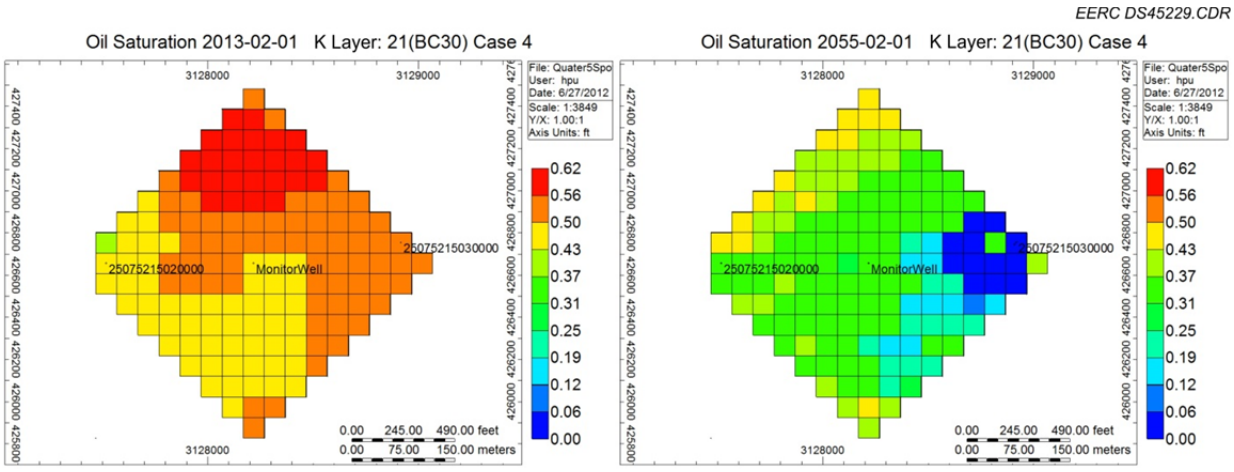

Figure C-24. Comparison of oil saturation before and after CO_2 flooding (Case 4: 2 HCPV WAG).

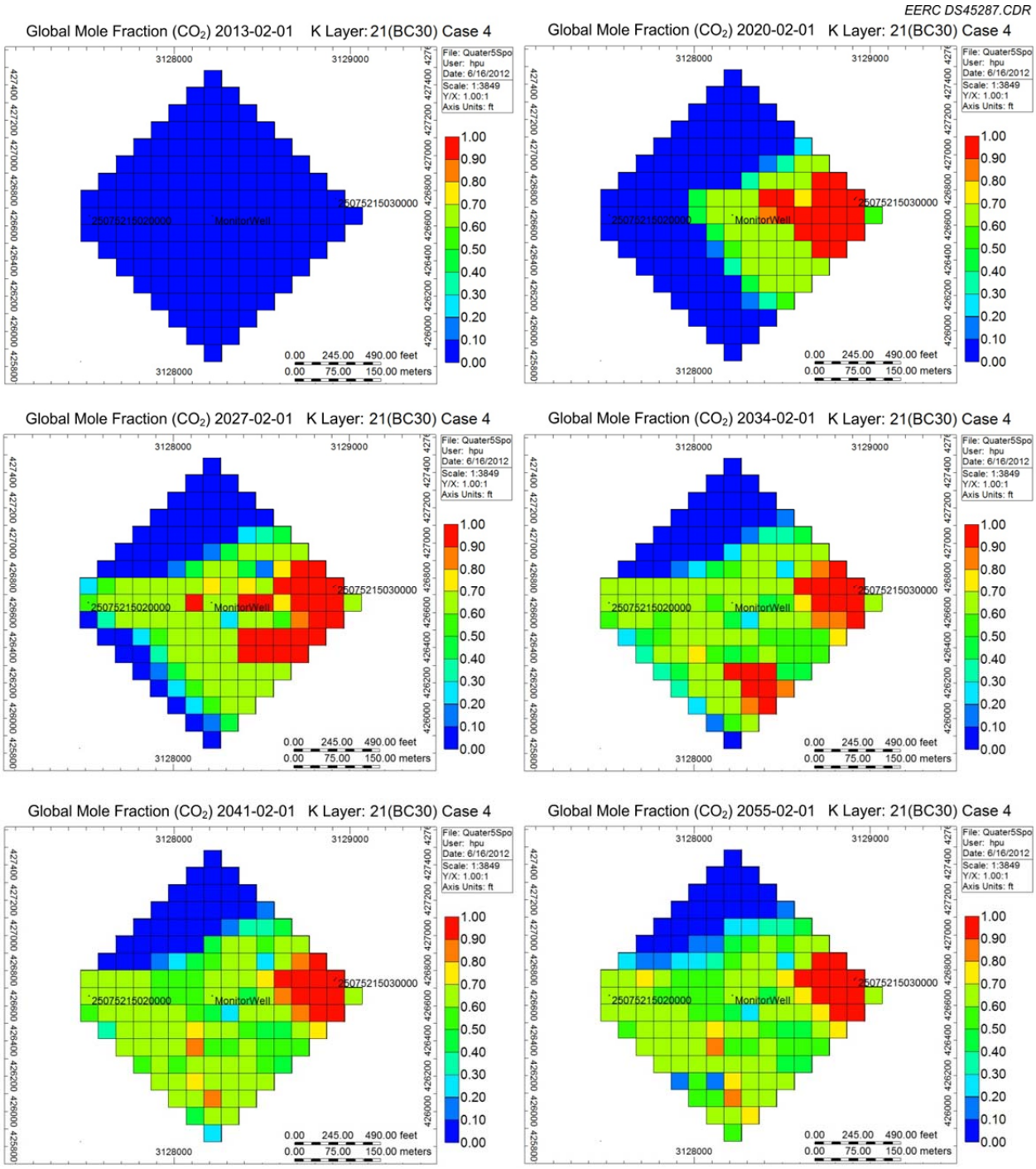

Figure C-25. Maps of global mole fraction of CO_2 in K Layer 21 during CO_2 injection (Case 4: 2 HCPV WAG).

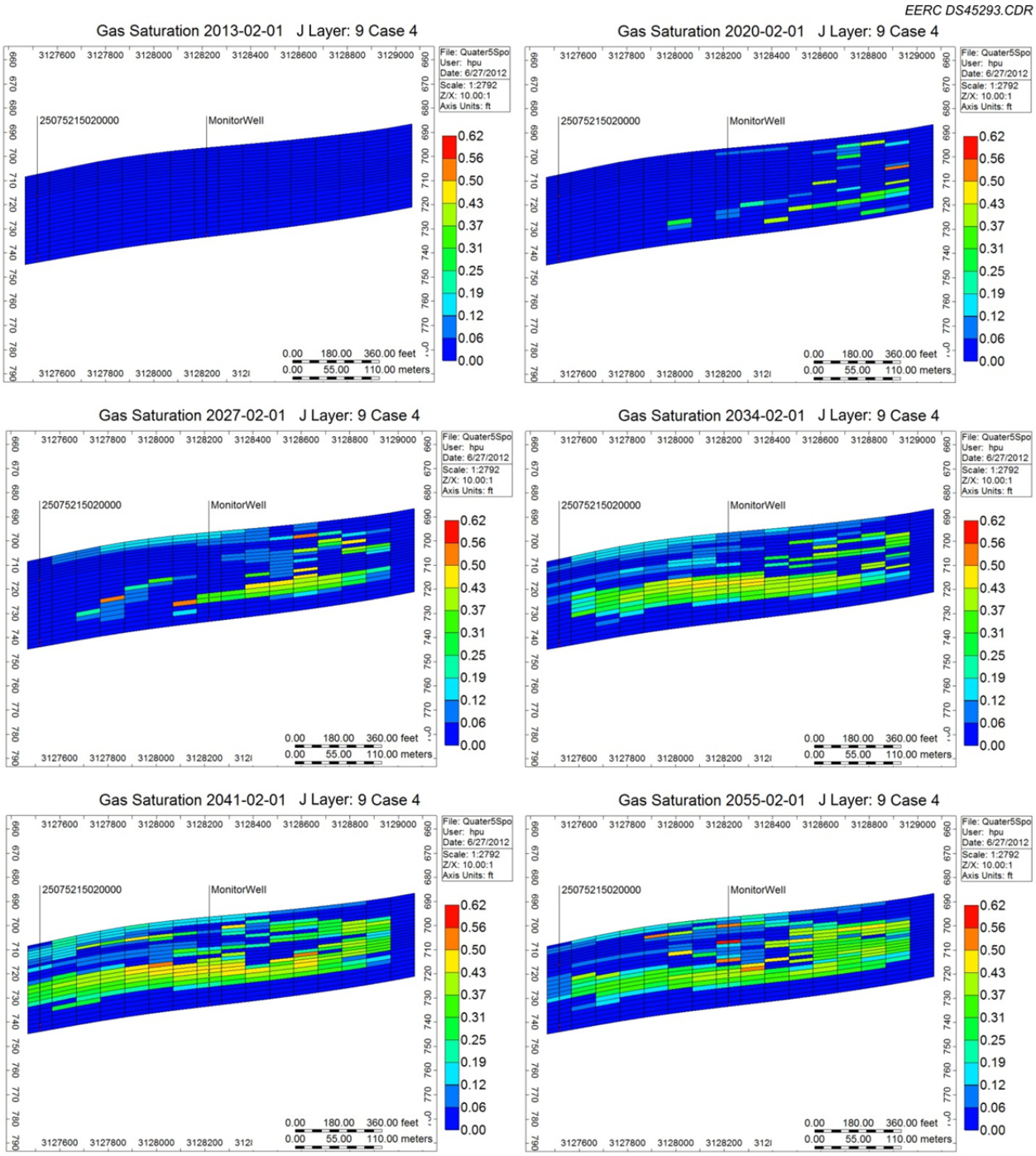

Figure C-26. Cross-sectional view of CO_2 saturation during CO_2 injection (Case 4: 2 HCPV WAG).

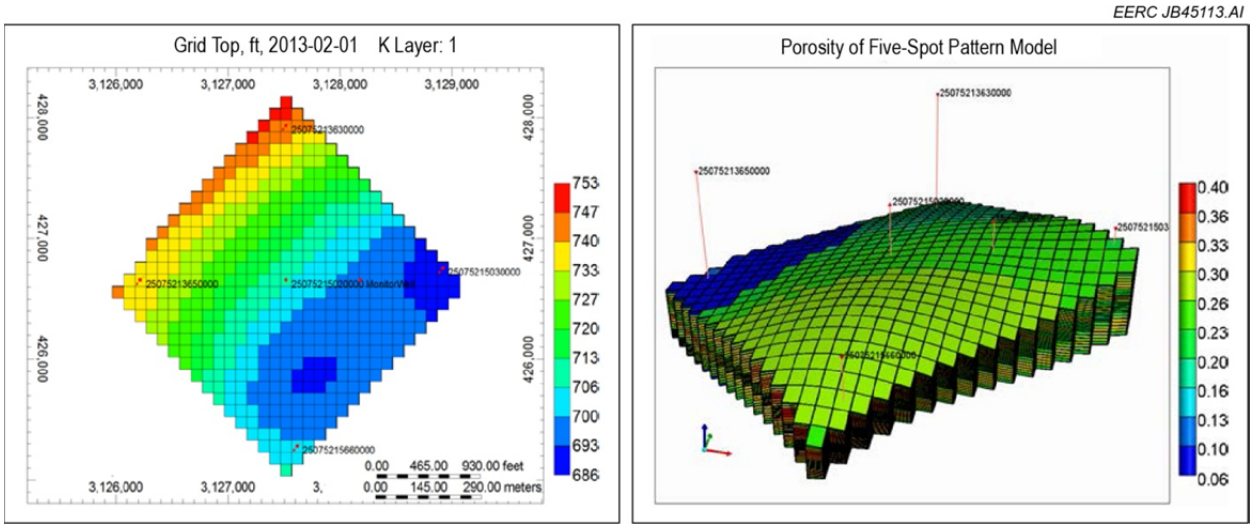

Figure C-27. Five-spot pattern model.

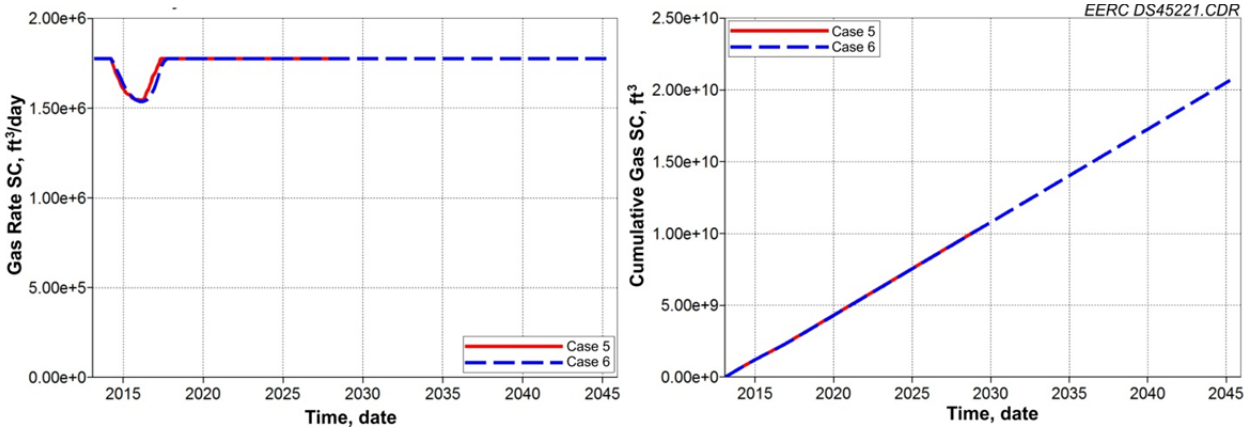

Figure C-28. Injection rate and cumulative injection rate of CO_2 for Cases 5 and 6.

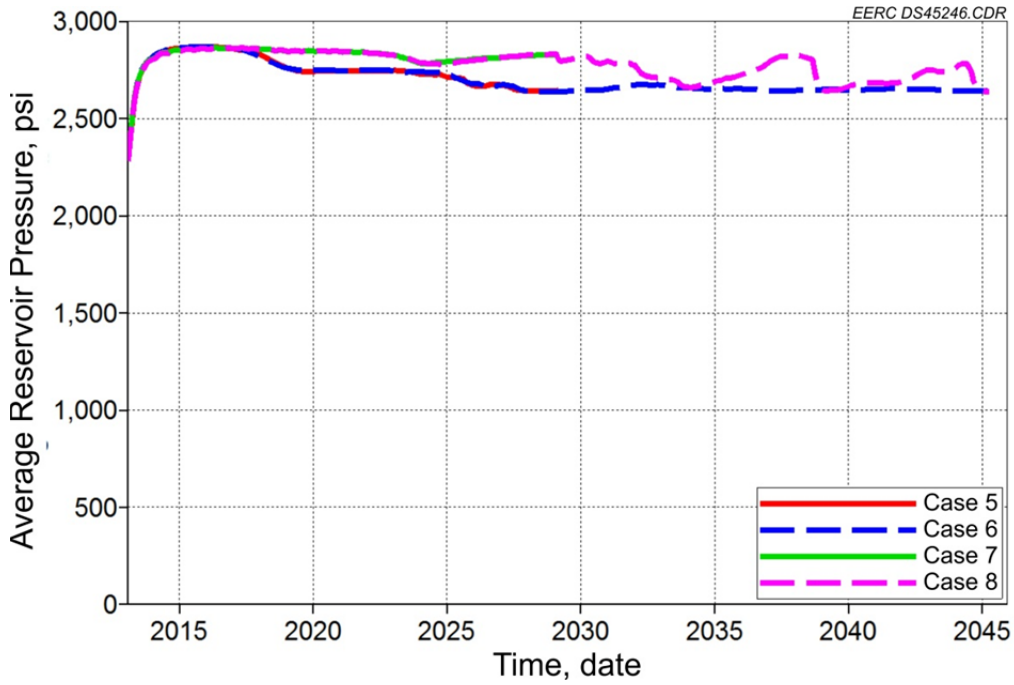

Figure C-29. Average reservoir pressure of Cases 5–8 for five-spot pattern model.

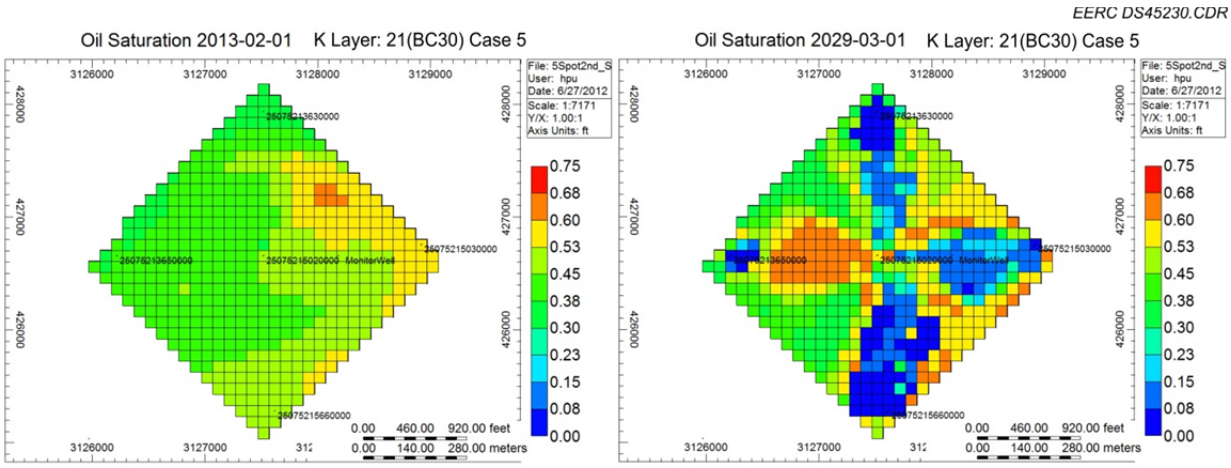

Figure C-30. Comparison of oil saturation before and after CO_2 flooding (Case 5).

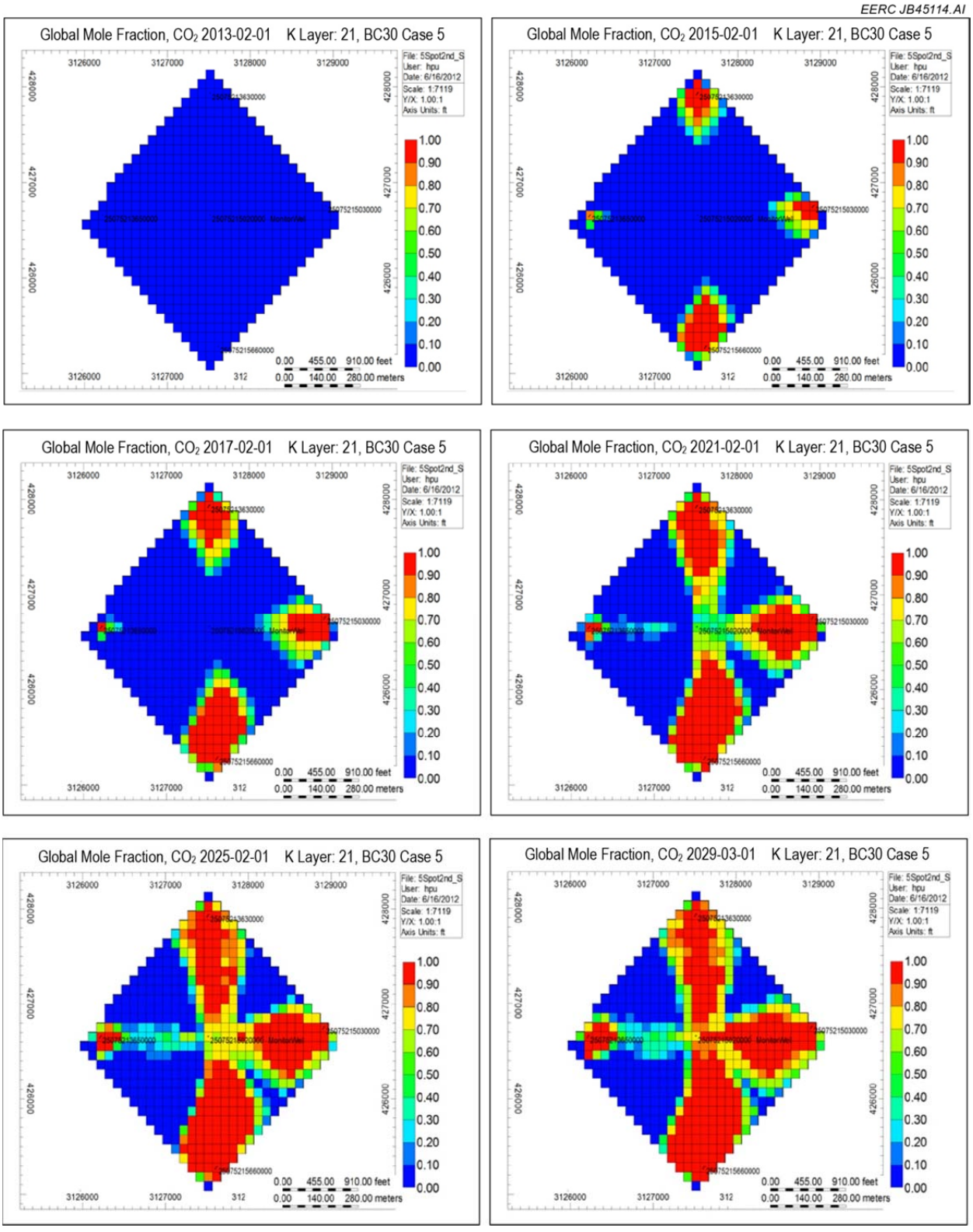

Figure C-31. Maps of global mole fraction of CO_2 in K Layer 21 during CO_2 injection (Case 5).

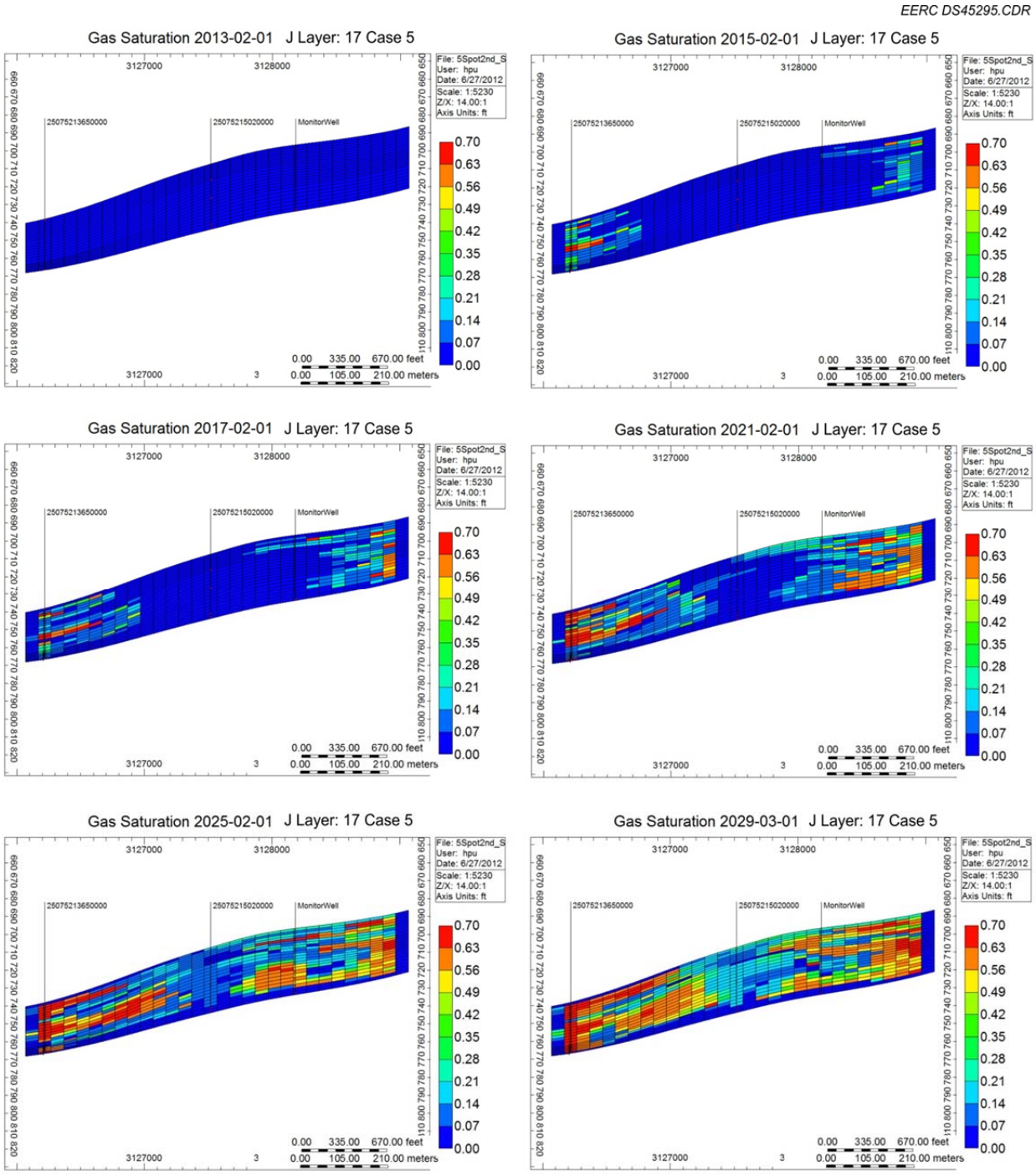

Figure C-32. Cross-sectional view of CO_2 saturation during CO_2 injection (Case 5: 1 HCPV).

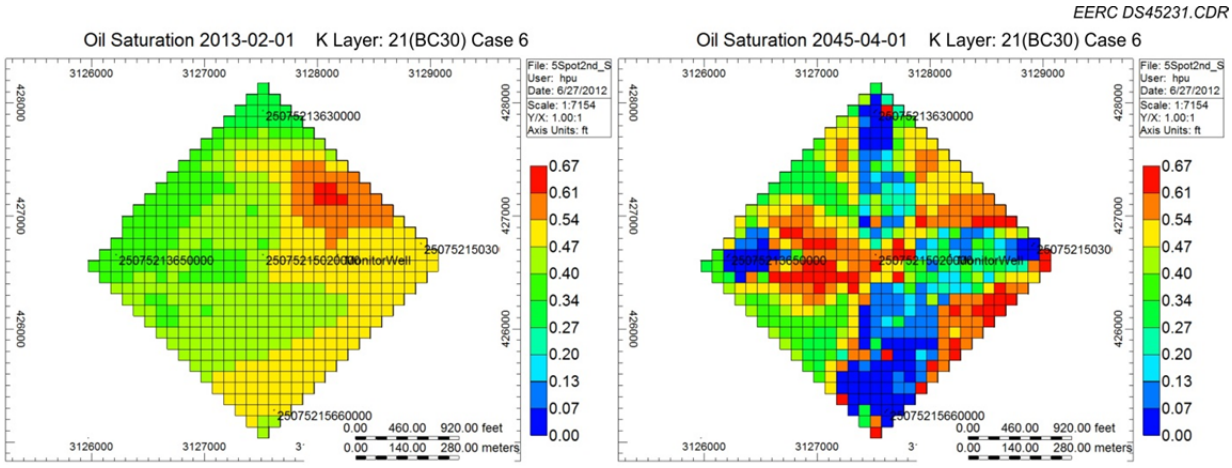

Figure C-33. Comparison of oil saturation before and after CO_2 flooding (Case 6).

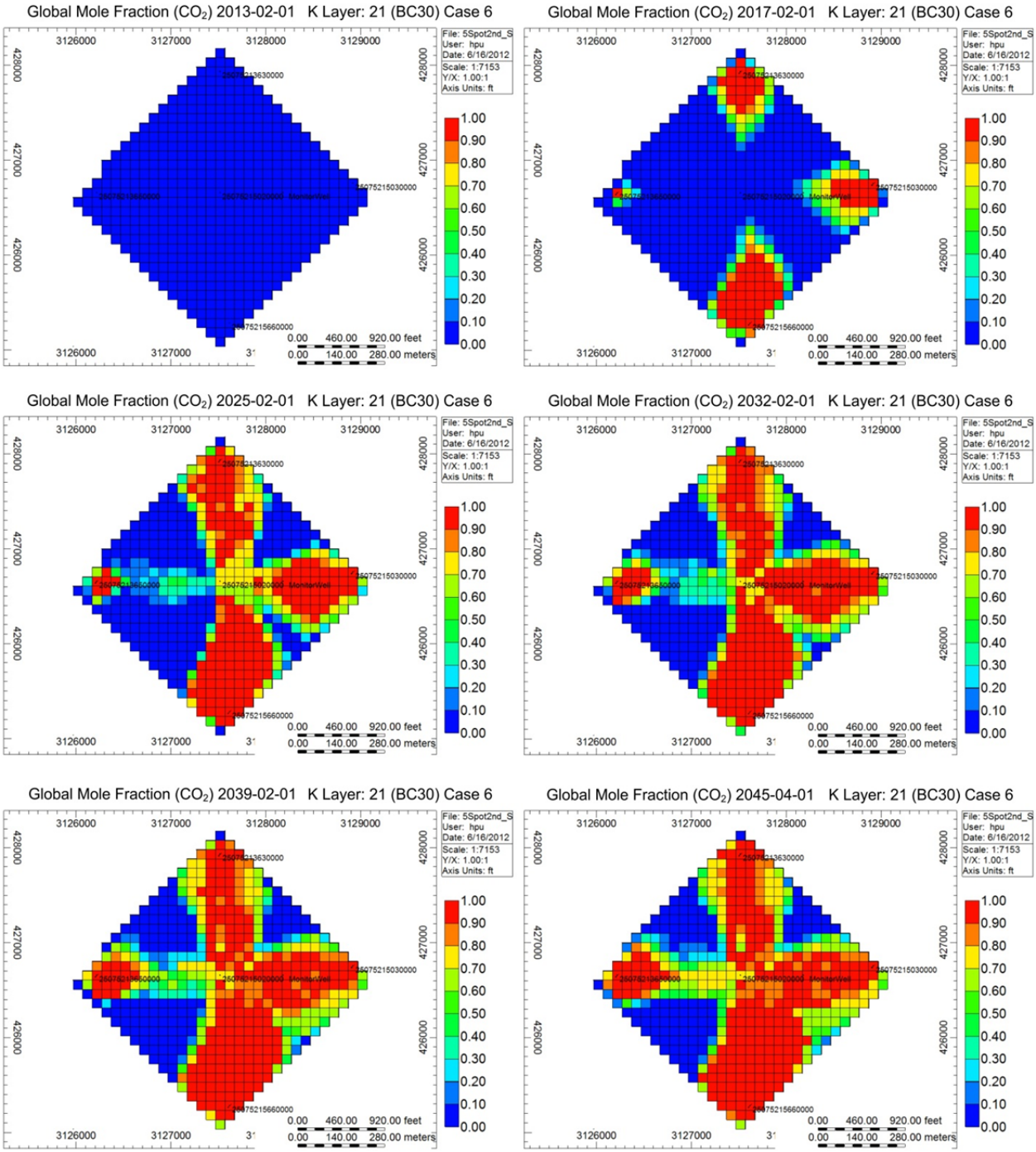

Figure C-34. Maps of global mole fraction of CO_2 in K Layer 21 during CO_2 injection (Case 6).

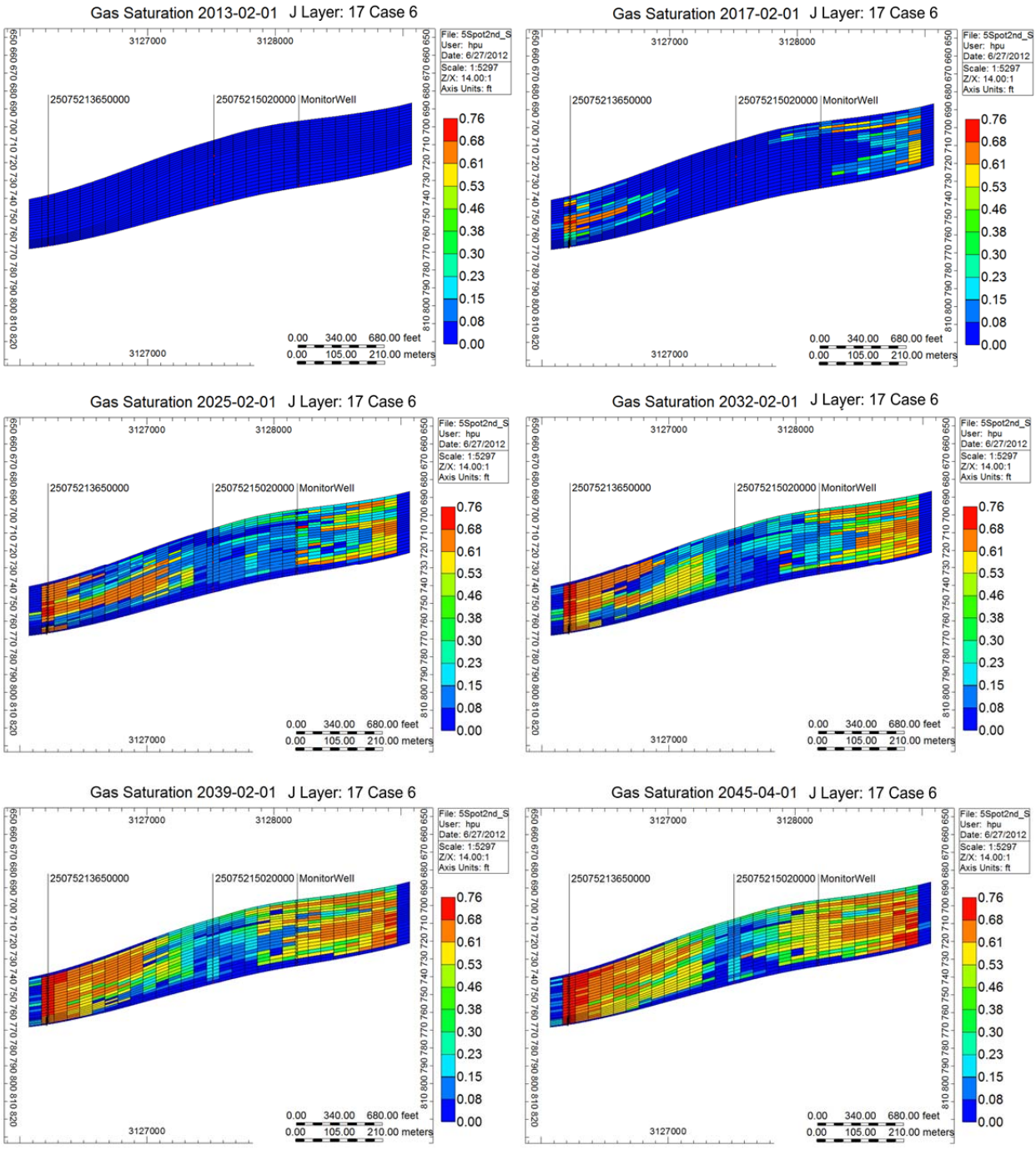

Figure C-35. Cross-sectional view of CO_2 saturation during CO_2 injection (Case 6: 2 HCPV).

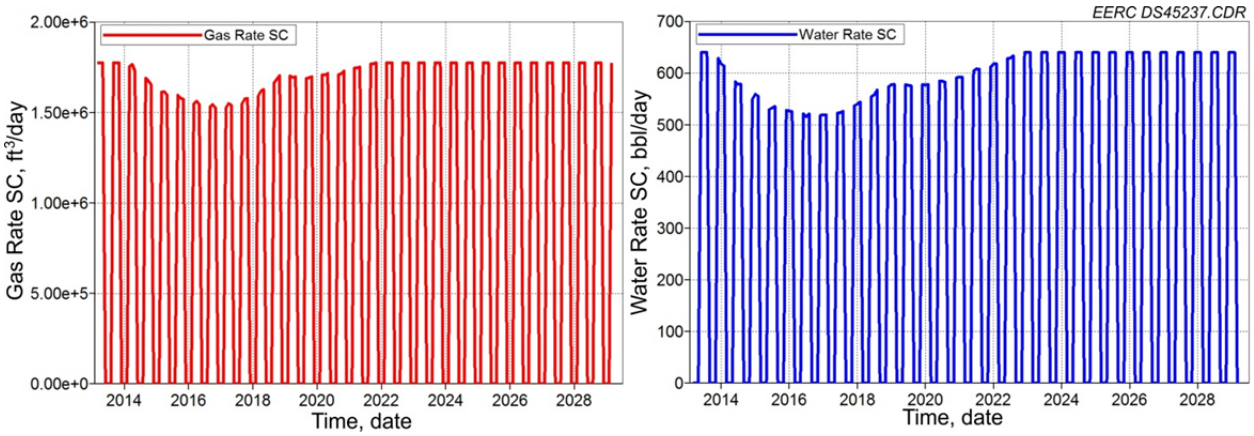

Figure C-36. Injection rate of CO_2 and water for Case 7.

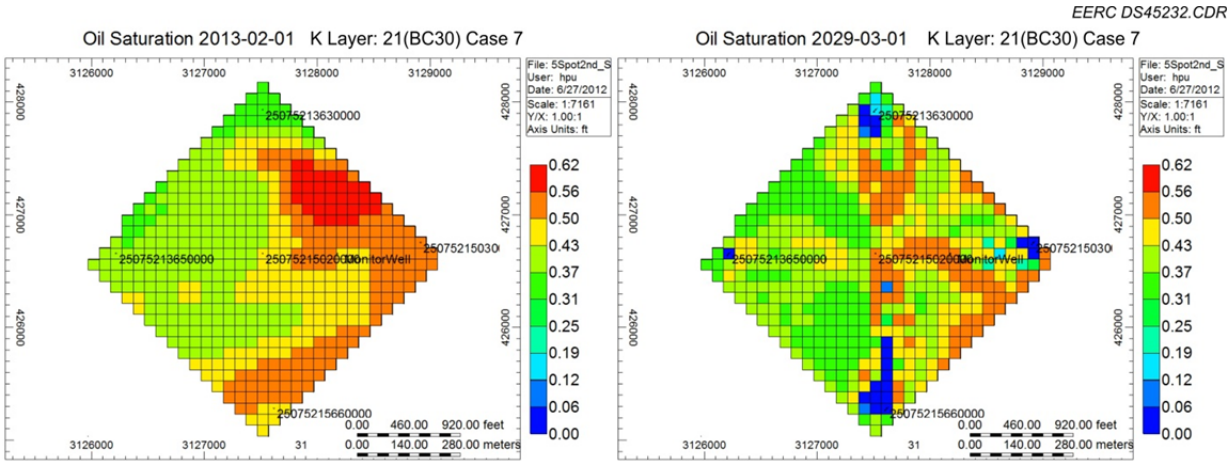

Figure C-37. Comparison of oil saturation before and after CO_2 flooding (Case 7).

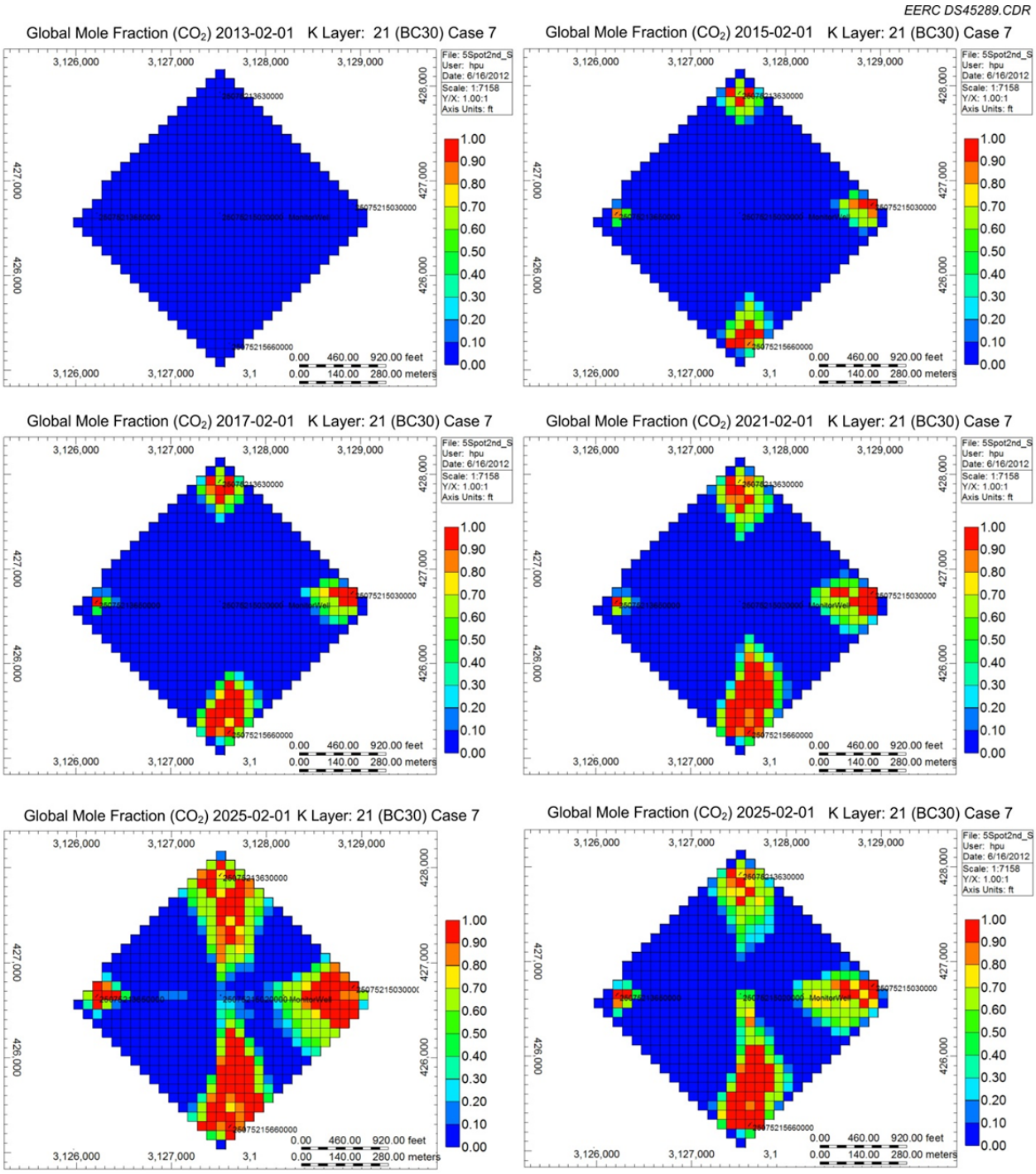

Figure C-38. Maps of global mole fraction of CO_2 in K Layer 21 during CO_2 injection (Case 7).

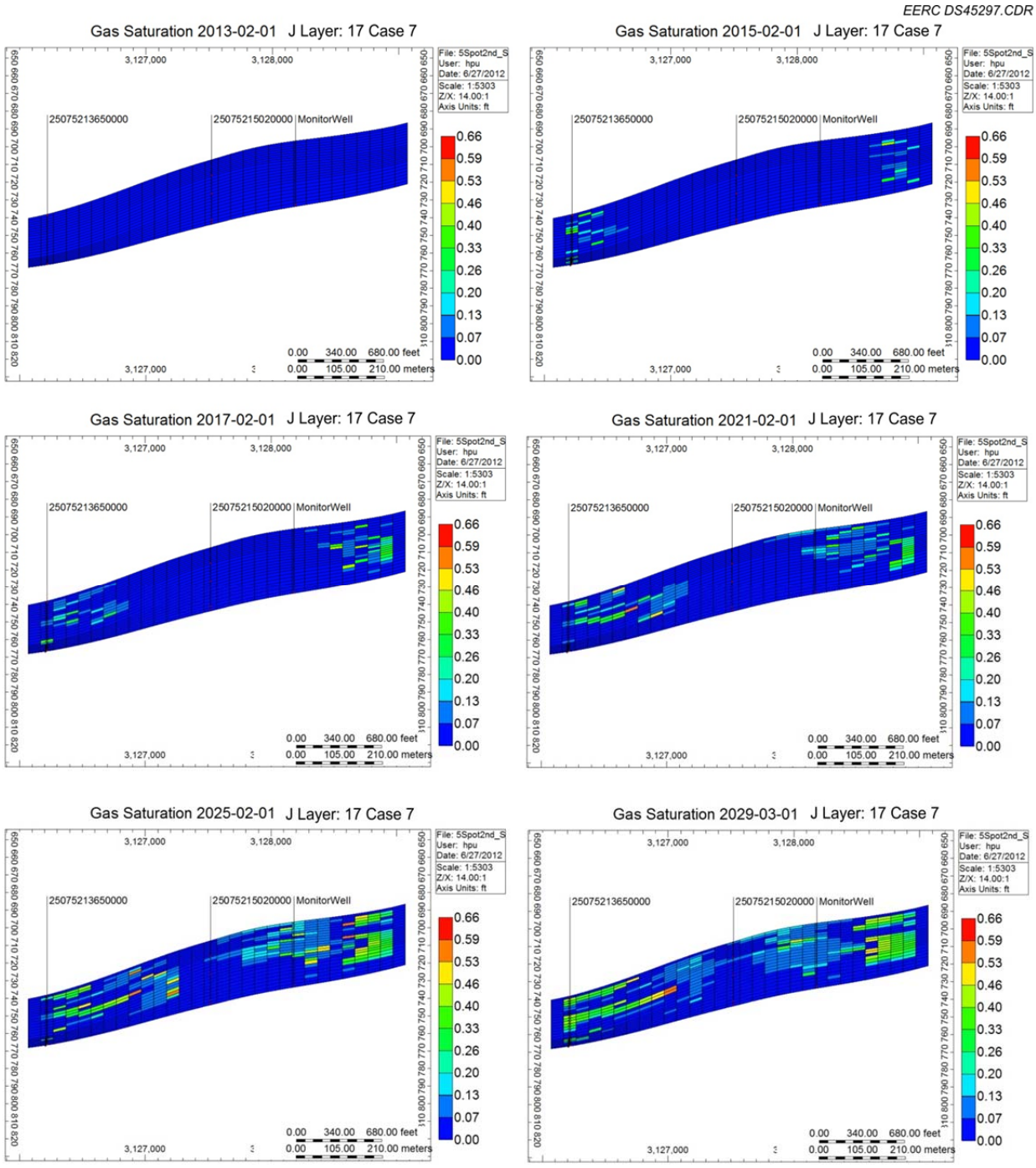

Figure C-39. Cross-sectional view of CO_2 saturation during CO_2 injection (Case 7: 1 HCPV WAG).

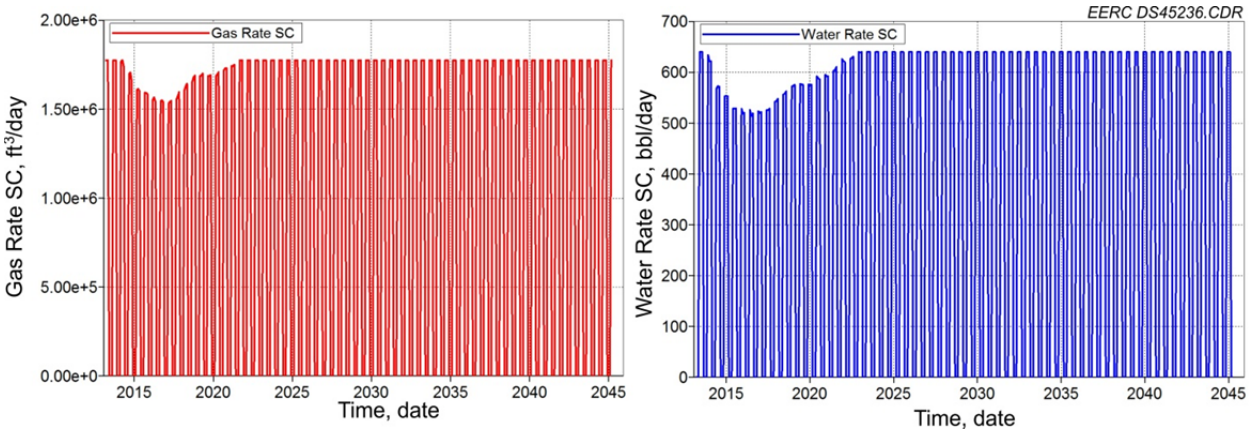

Figure C-40. Injection rate of CO_2 and water for Case 8.

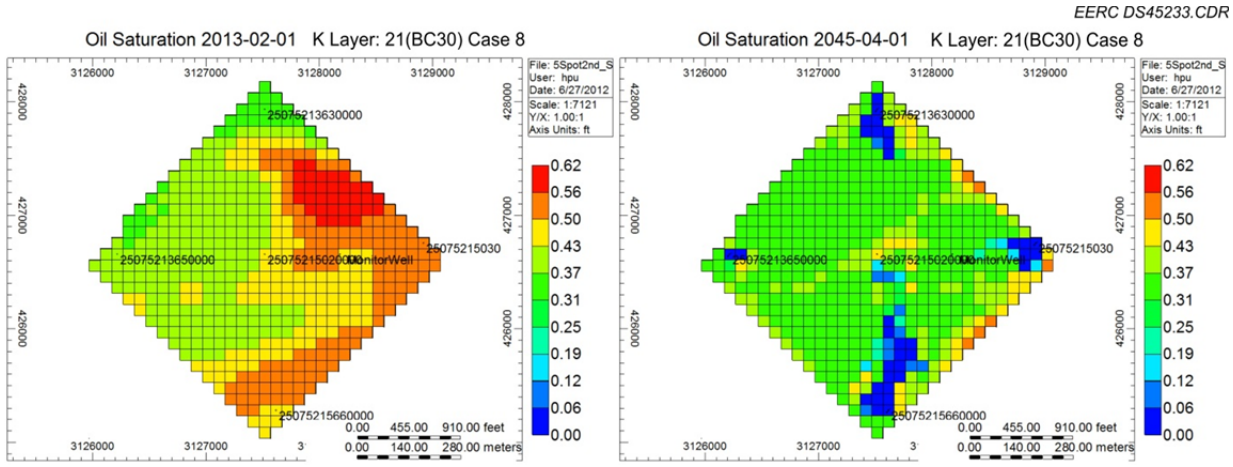

Figure C-41. Comparison of oil saturation before and after CO_2 flooding (Case 8).

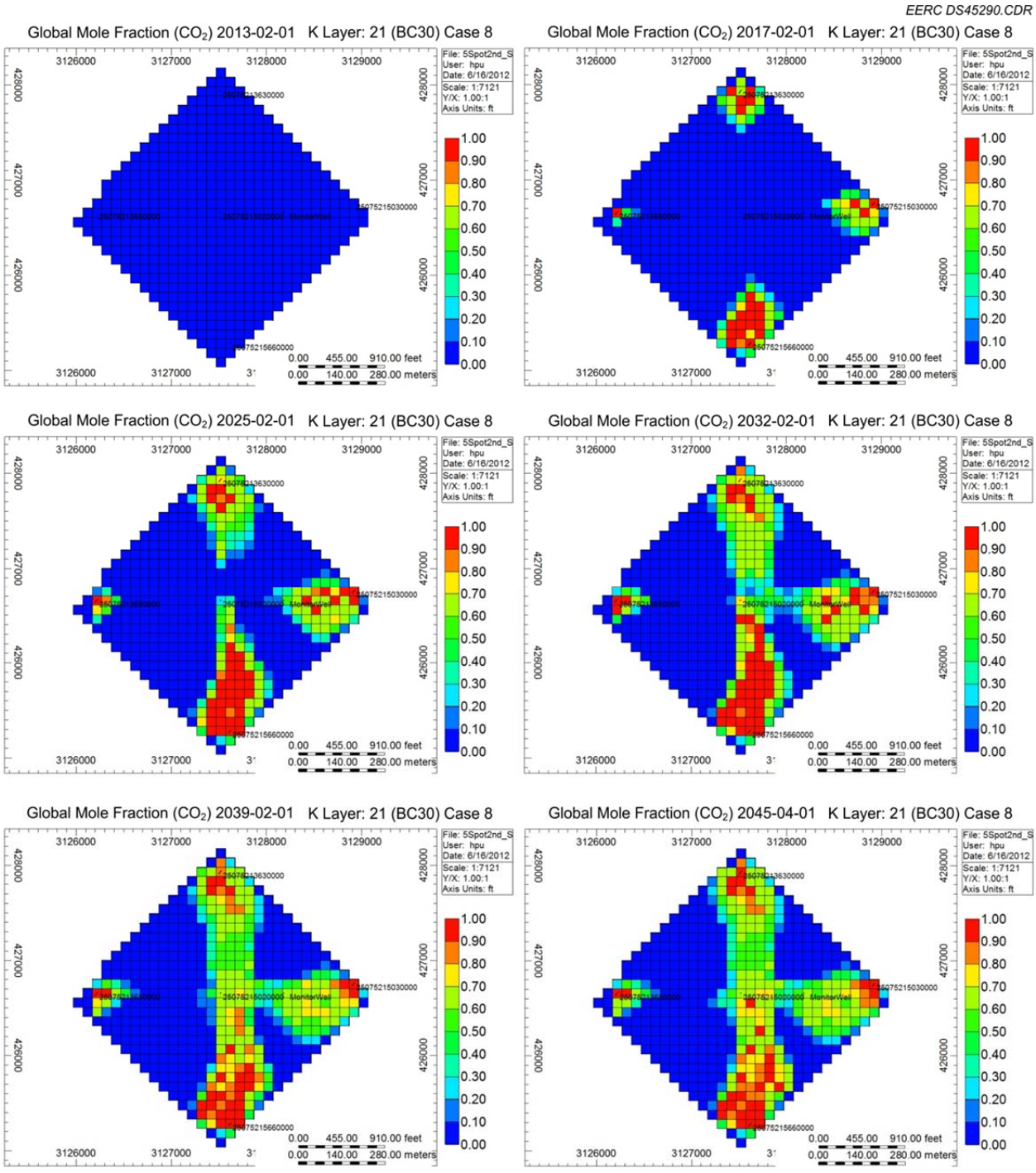

Figure C-42. Maps of global mole fraction of CO_2 in K Layer 21 during CO_2 injection (Case 8).

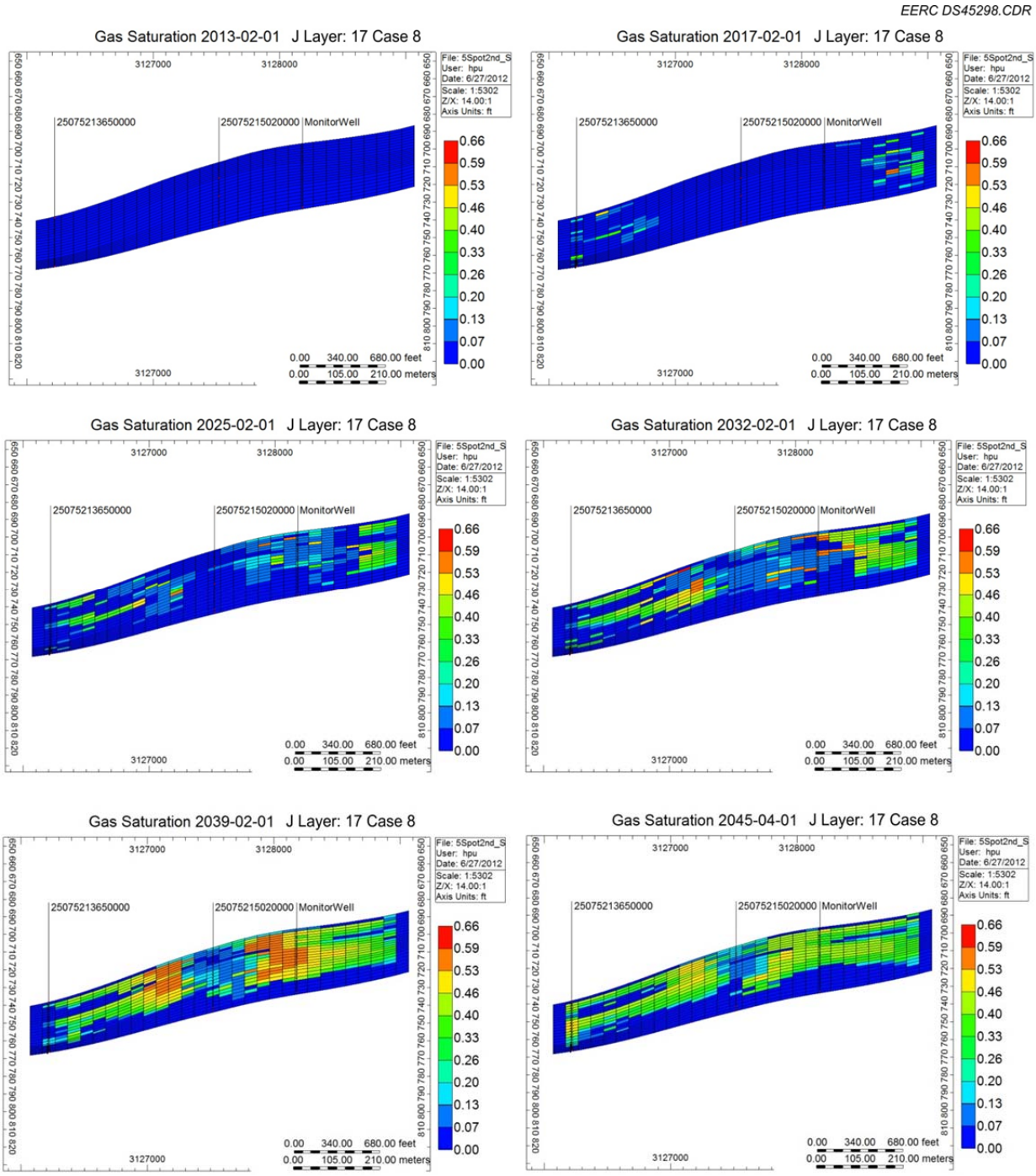

Figure C-43. Cross-sectional view of CO_2 saturation during CO_2 injection (Case 8: 2 HCPV WAG).

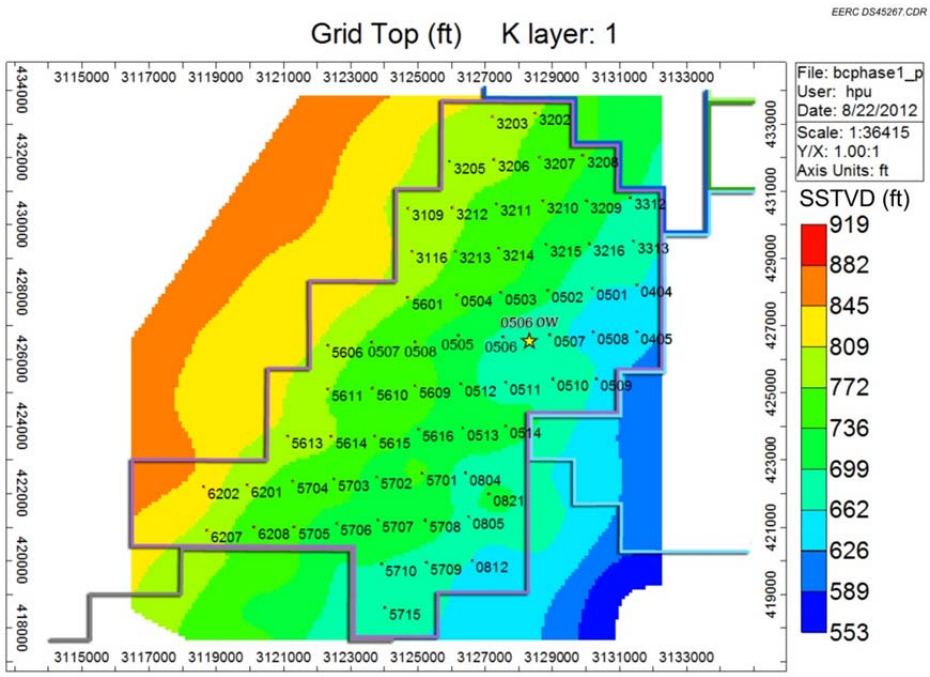

Figure C-44. 2-D view of full Phase 1 model.

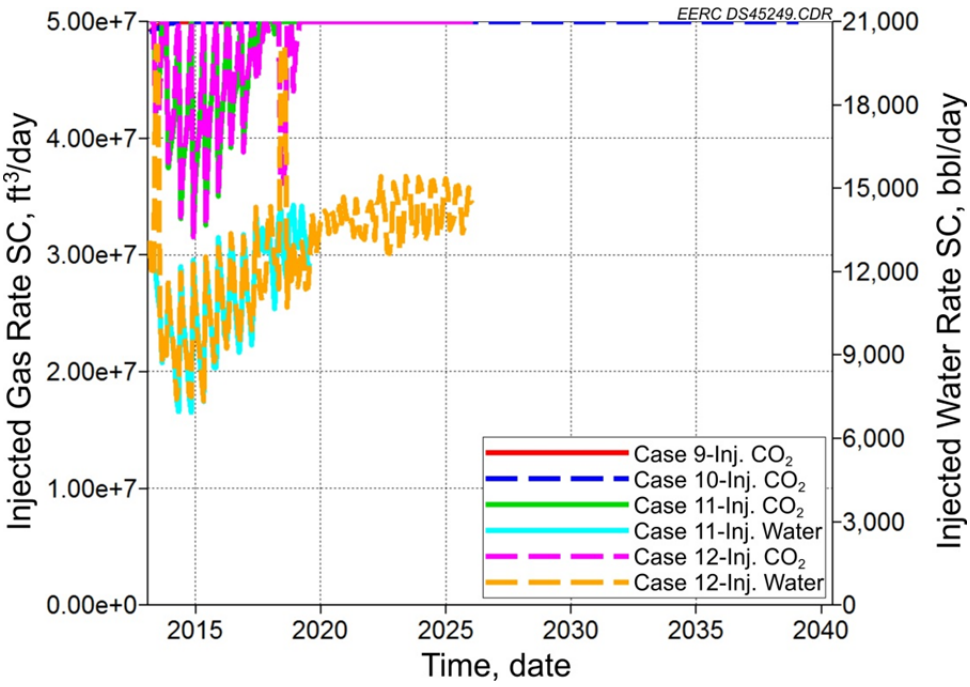

Figure C-45. Daily injected CO_2 and water for Cases 9–12.

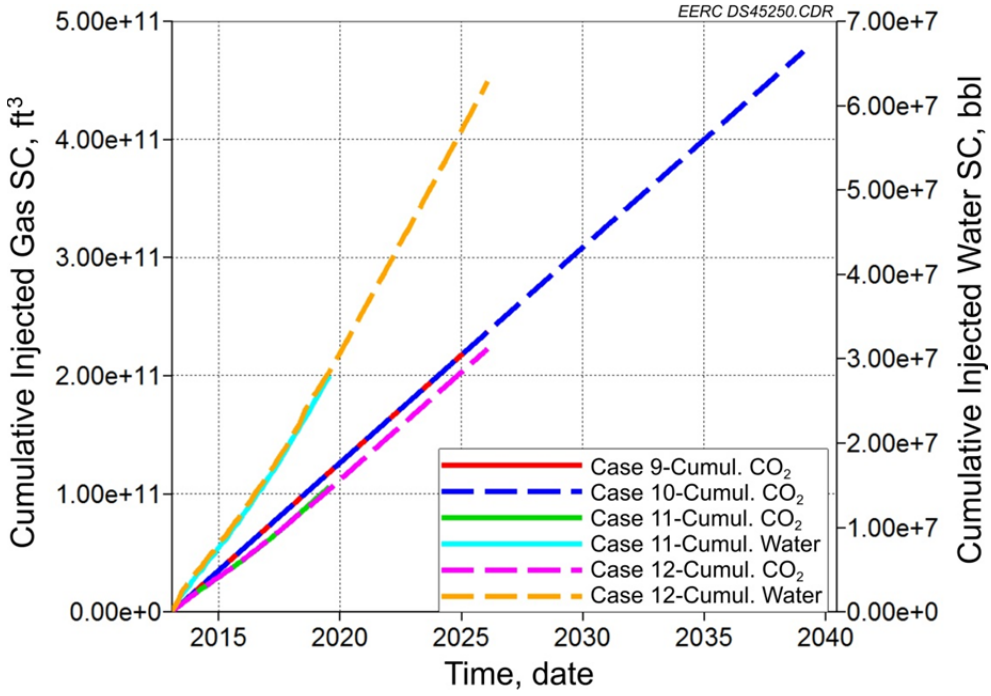

Figure C-46. Cumulative injected CO_2 and water for Cases 9–12.

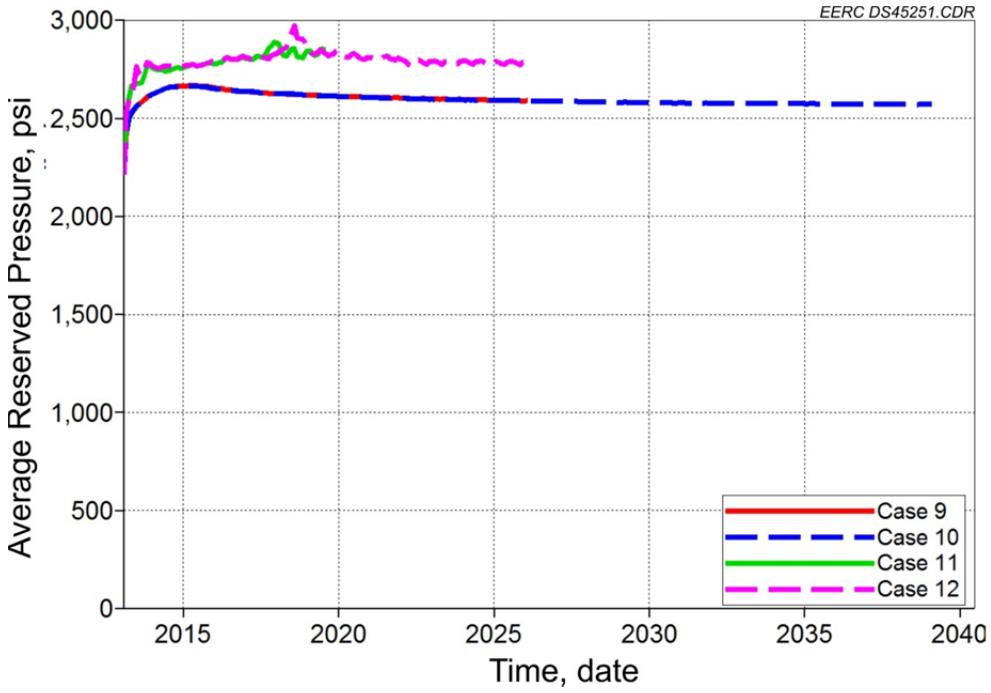

Figure C-47. Average reservoir pressure of Cases 9–12 for Phase 1 model.

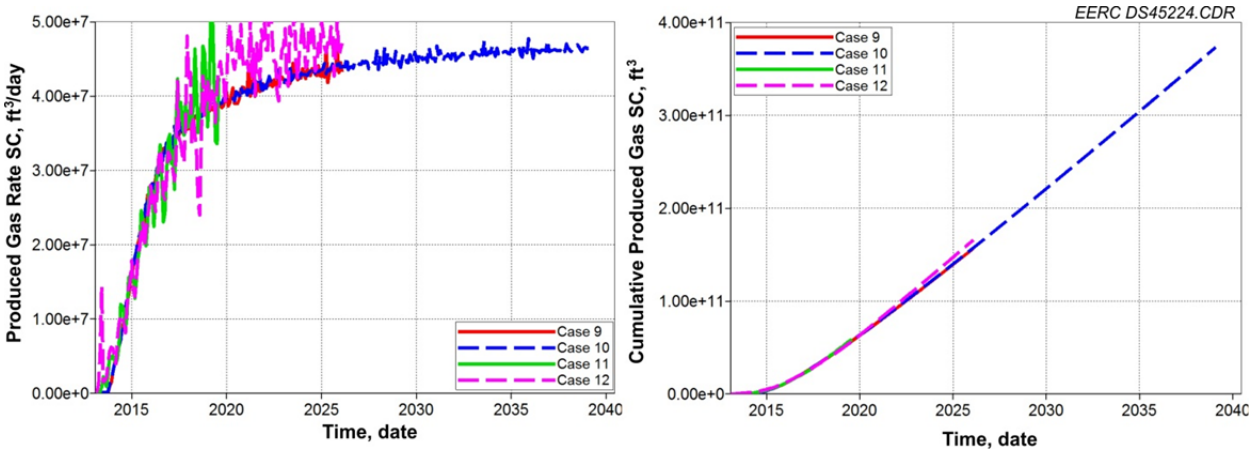

Figure C-48. Daily gas and cumulative gas rate of Cases 9–12 for Phase 1 model.

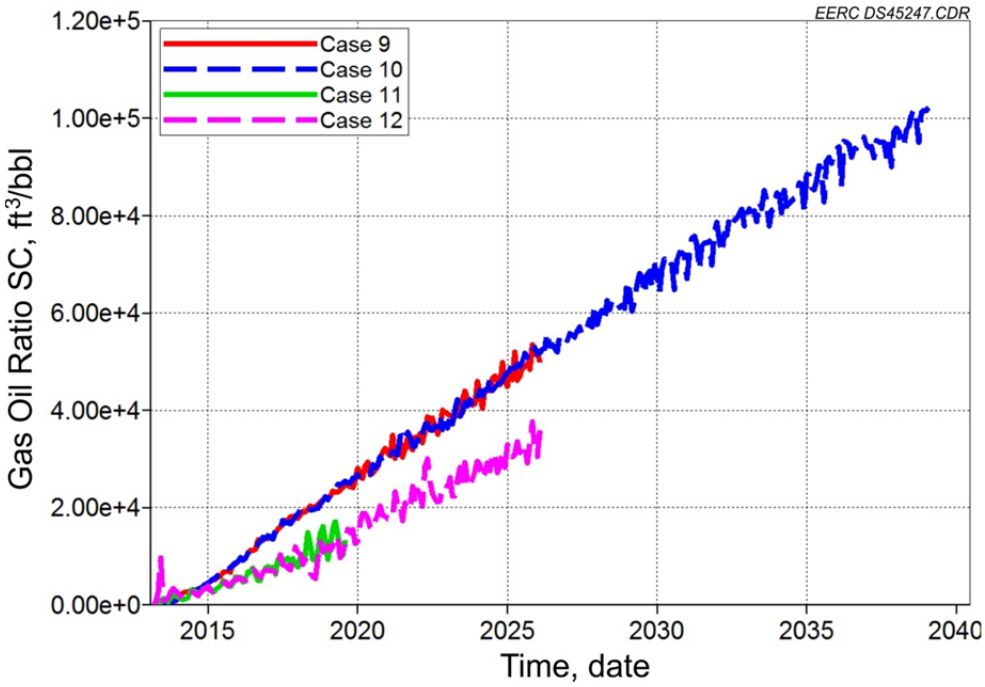

Figure C-49. Gas oil ratio of Cases 9–12 for Phase 1 model.

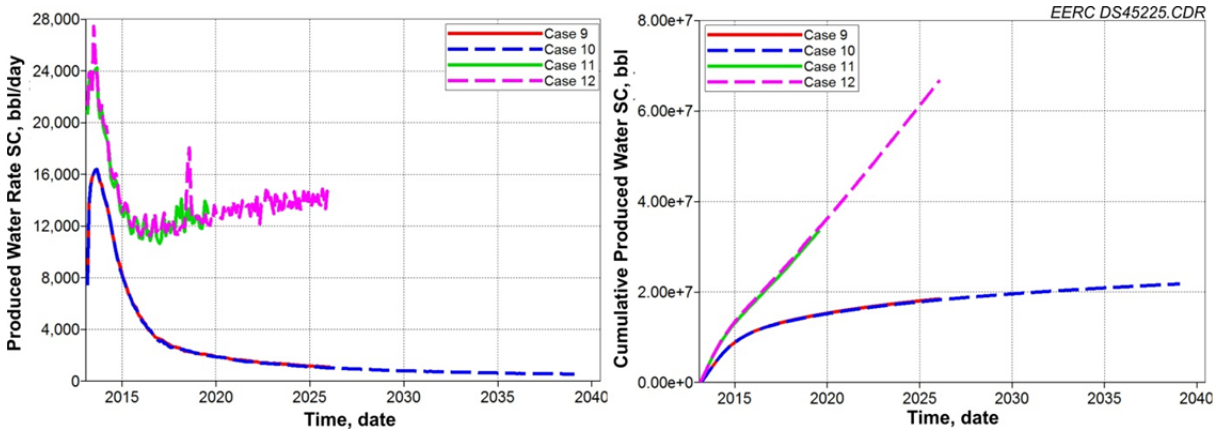

Figure C-50. Daily water and cumulative water rate of Cases 9–12 for Phase 1 model.

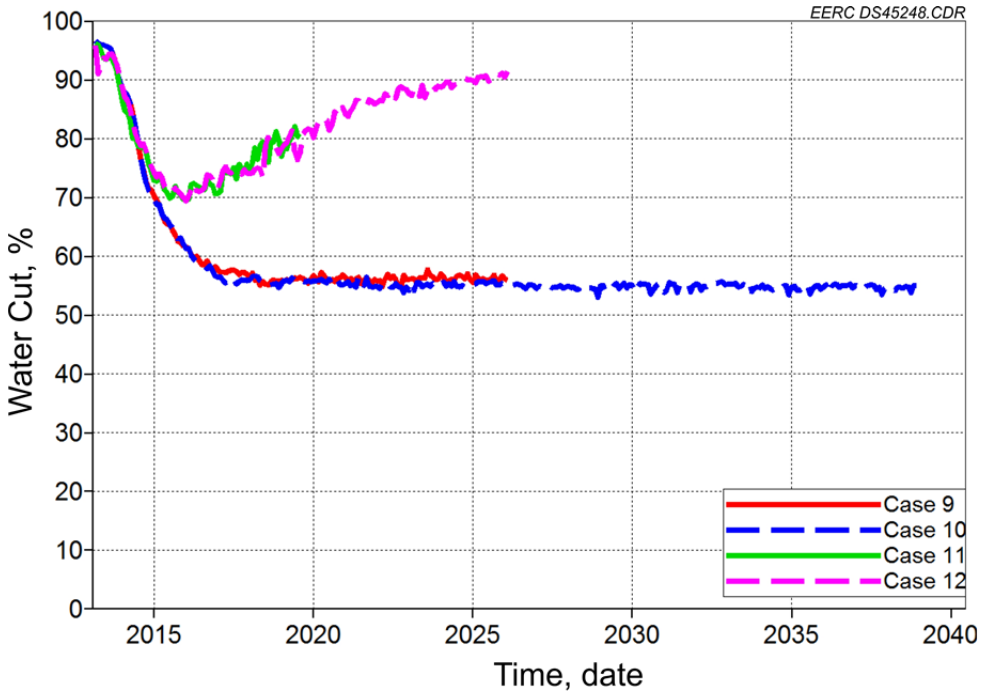

Figure C-51. Water cut of Cases 9–12 for Phase 1 model.

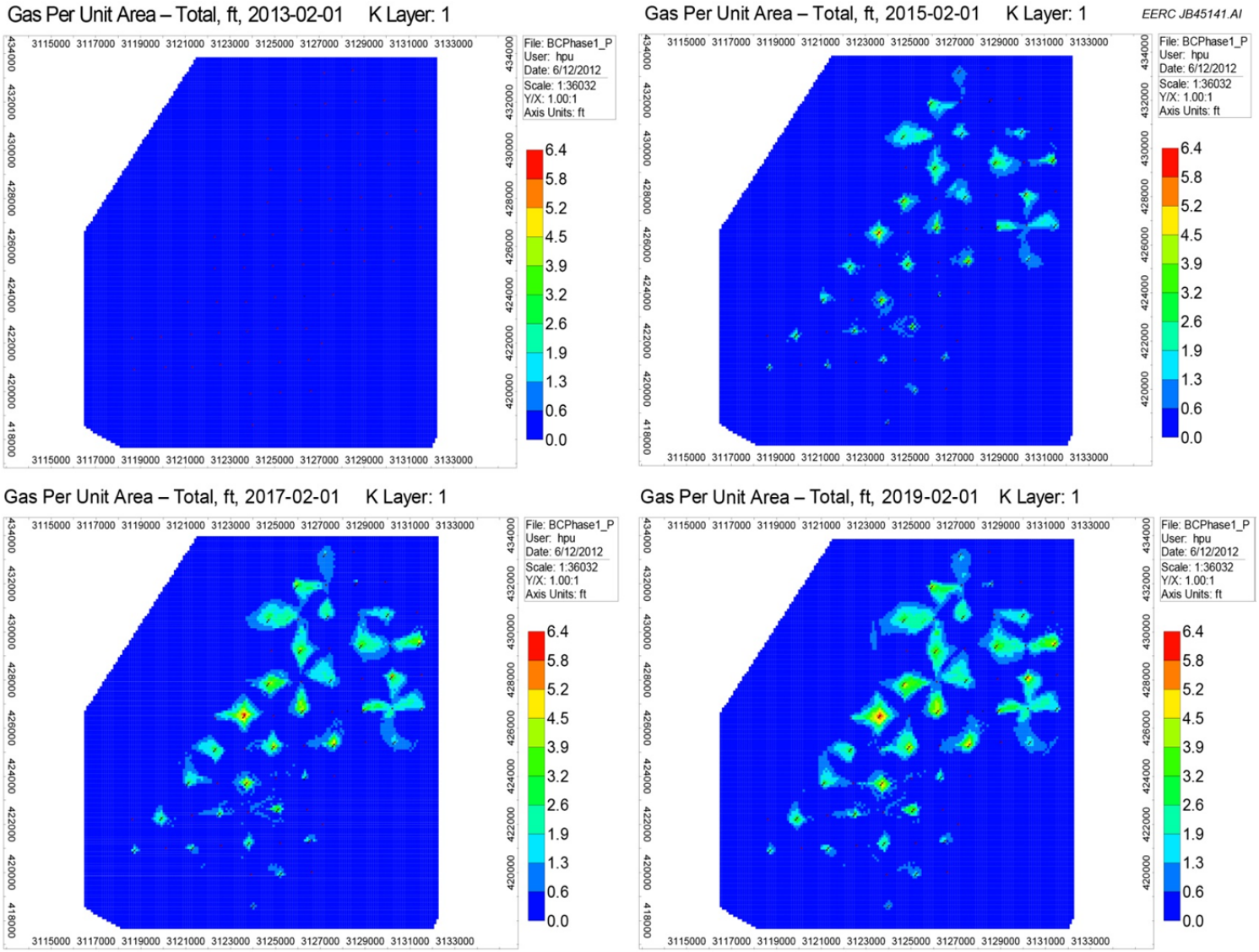

Figure C-52. Changes of gas per unit area of Case 9 over time (Part 1).

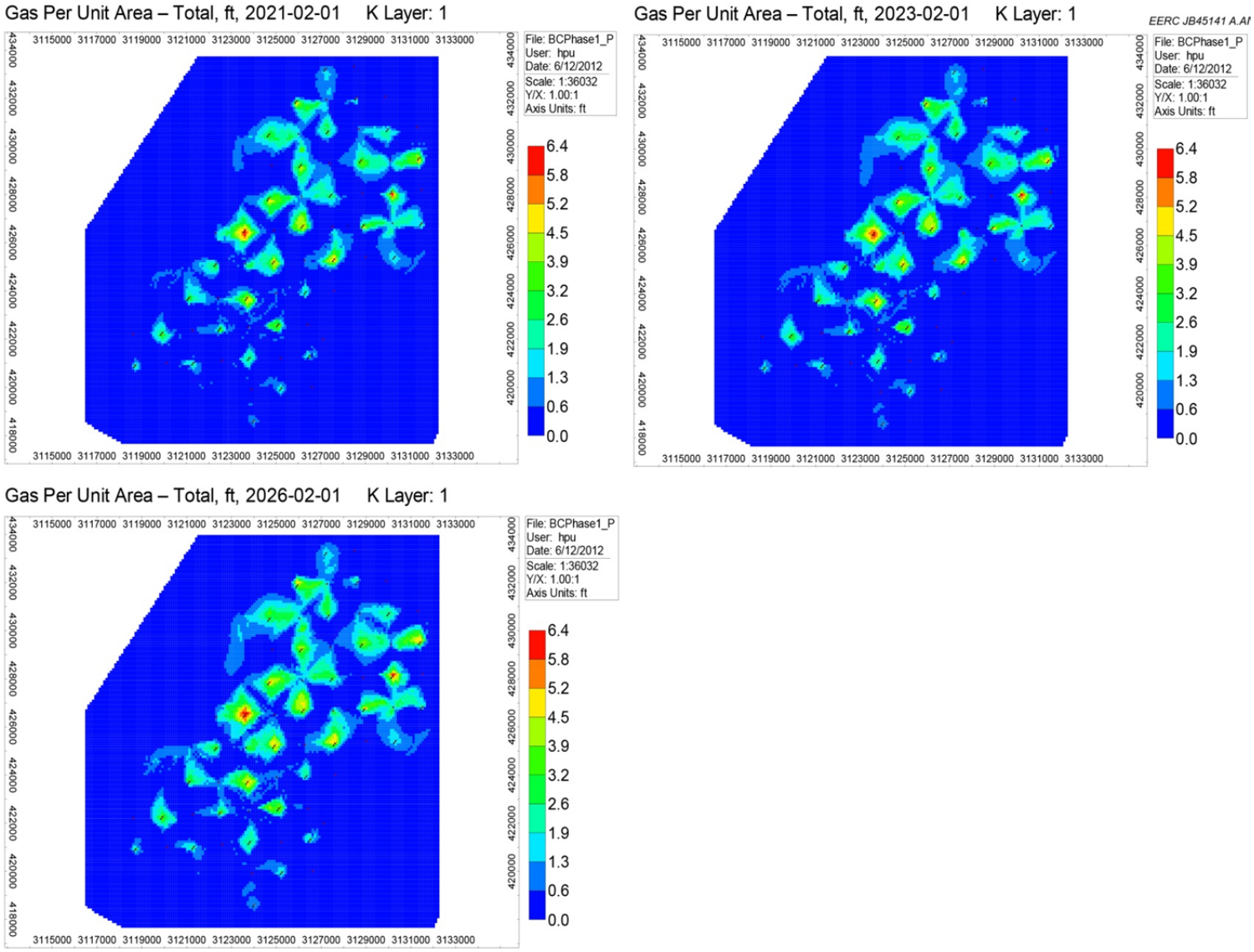

Figure C-52. Changes of gas per unit area of Case 9 over time (Part 2).

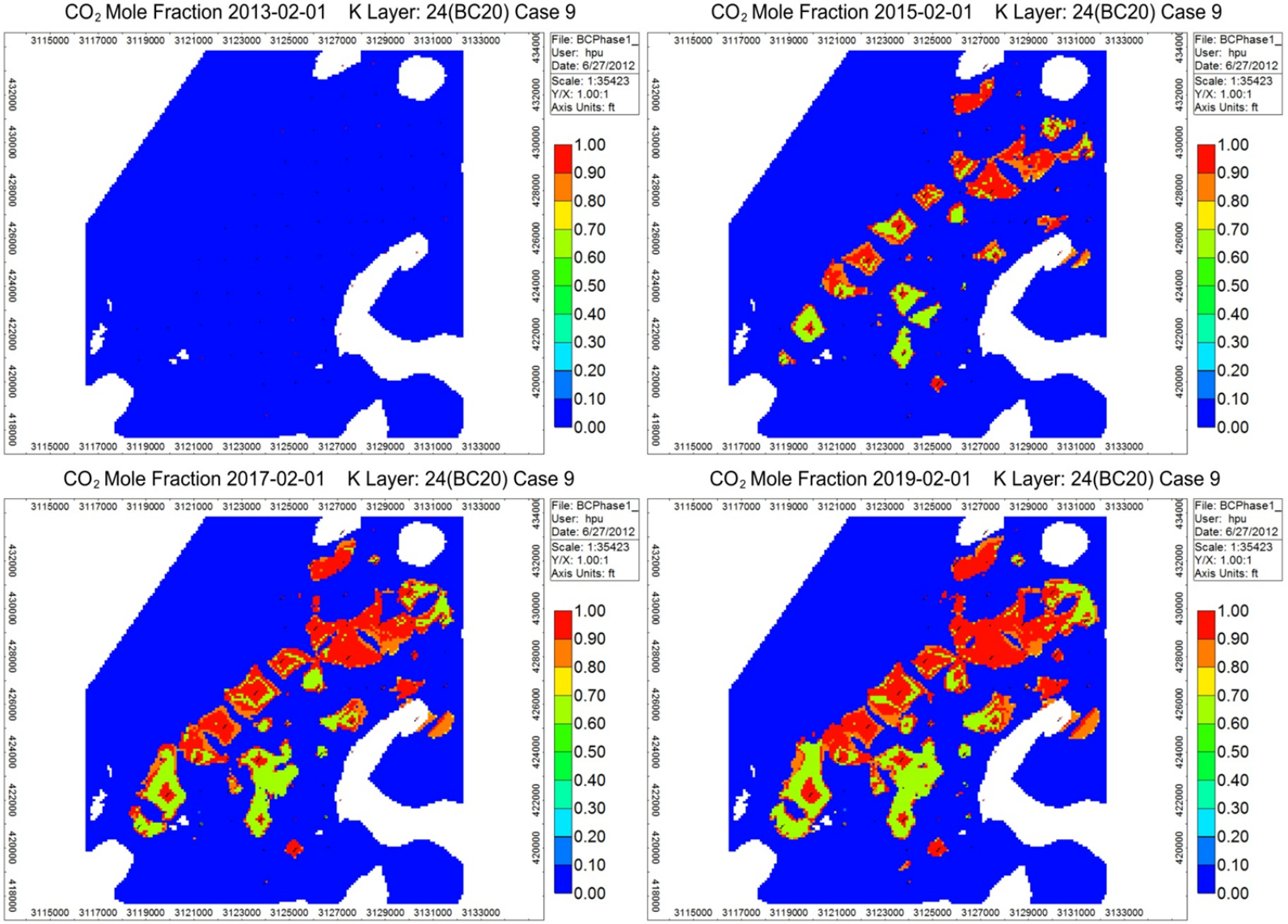

Figure C-53. Changes of CO_2 mole fraction in K Layer 24 (BC20) over time (Case 9) (Part 1).

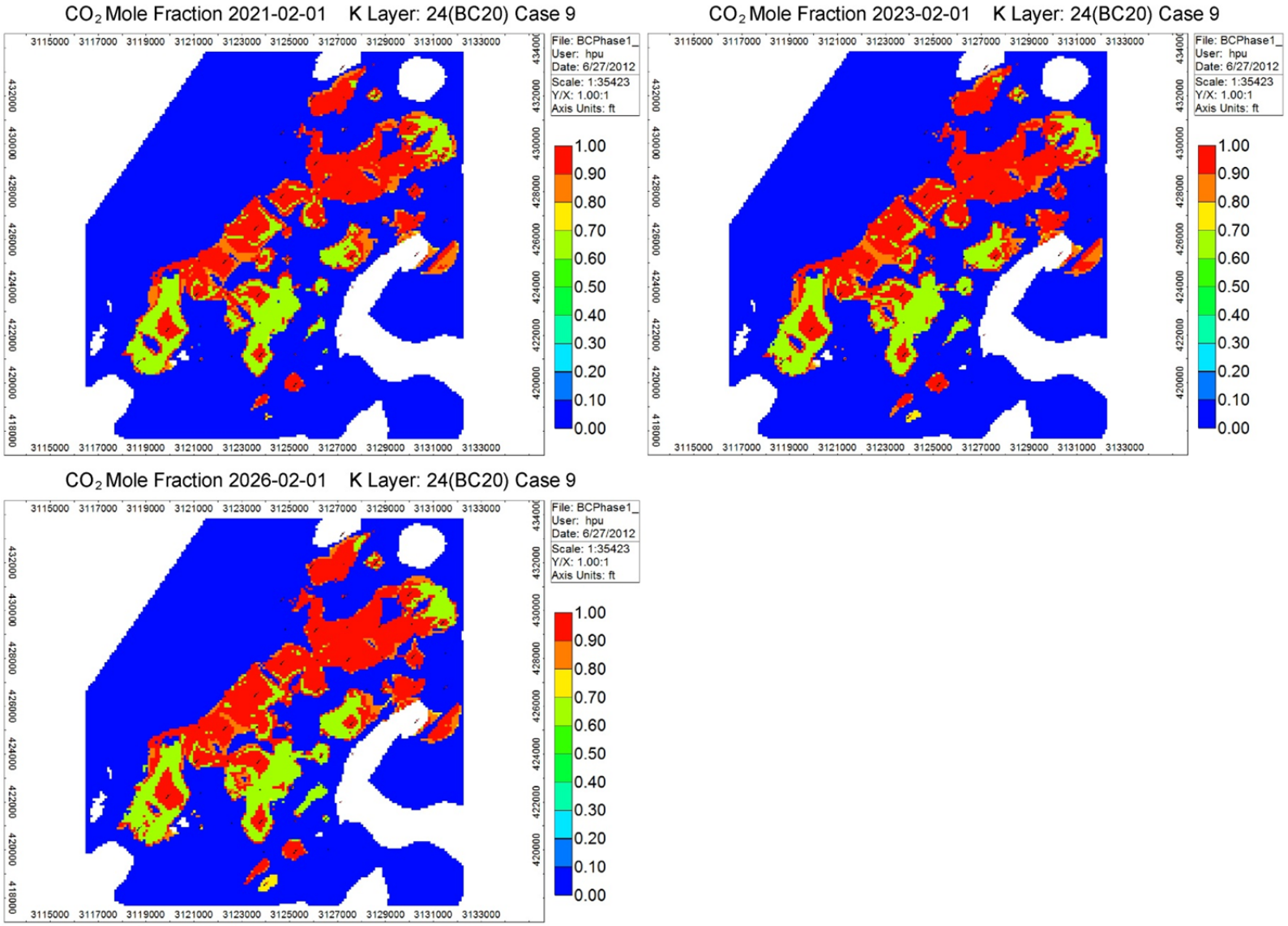

Figure C-53. Changes of CO_2 mole fraction in K Layer 24 (BC20) over time (Case 9) (Part 2).

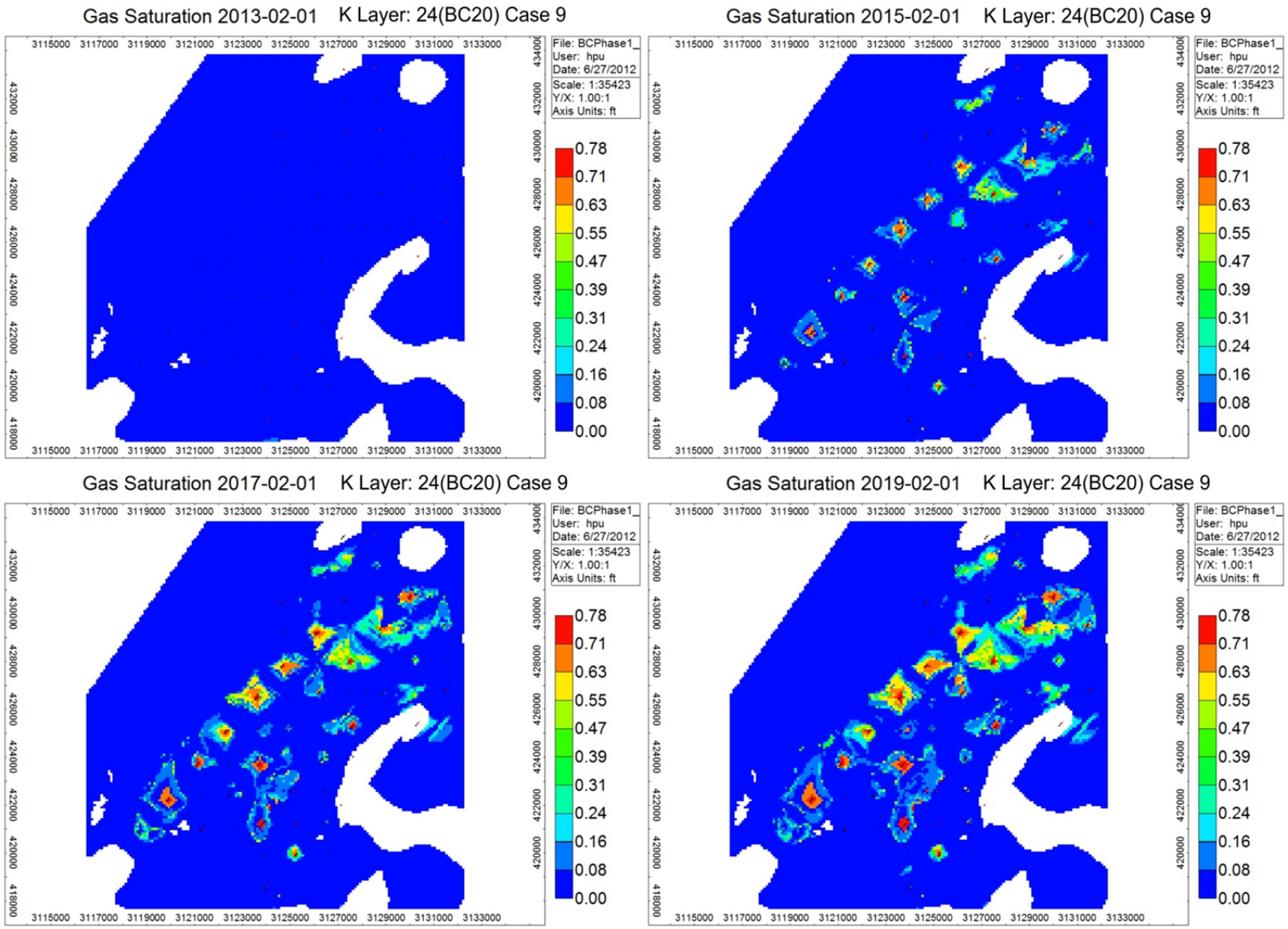

Figure C-54. Changes of gas saturation in K Layer 24 (BC20) over time (Case 9) (Part 1).

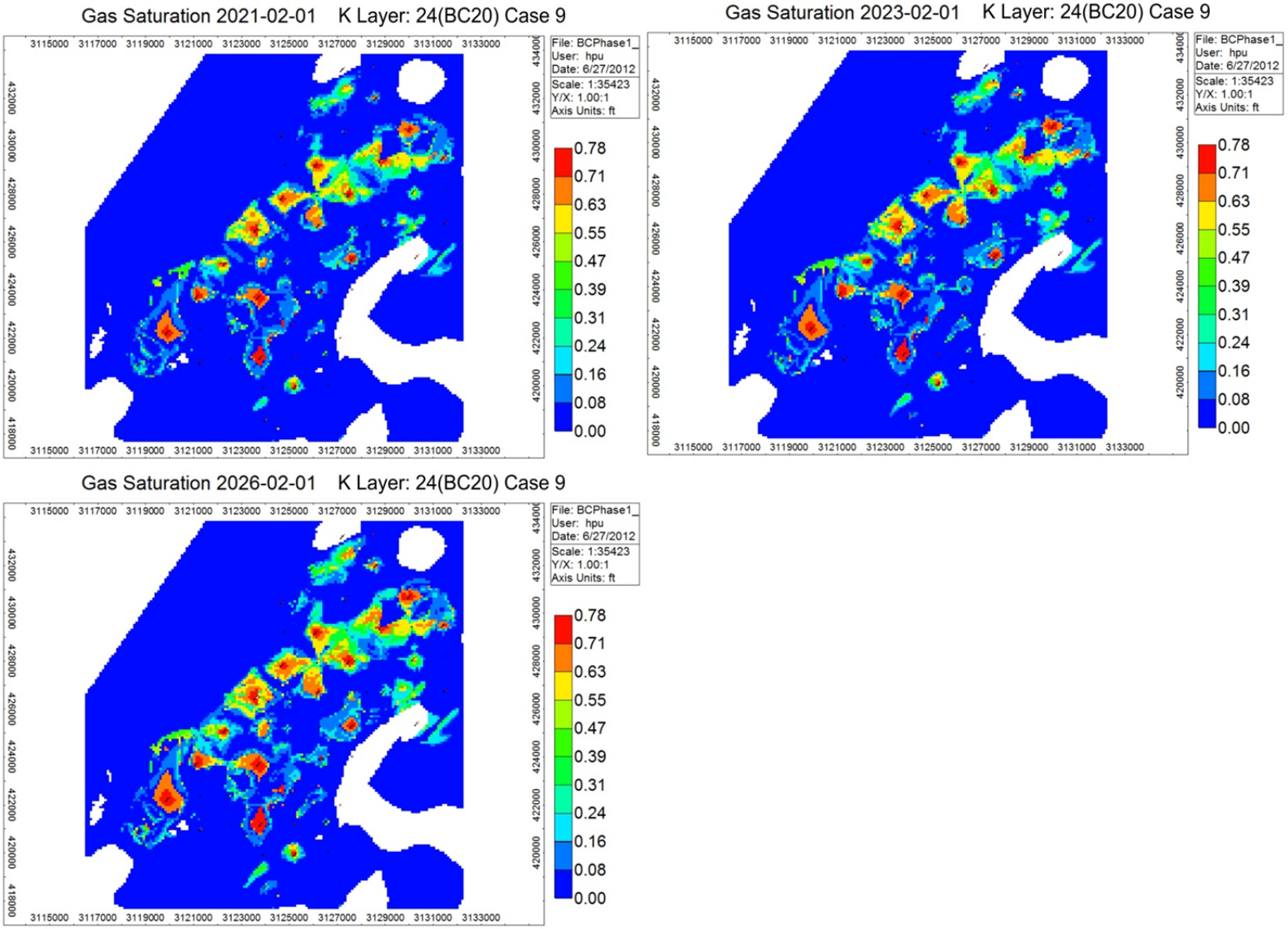

Figure C-54. Changes of gas saturation in K Layer 24 (BC20) over time (Case 9) (Part 2).

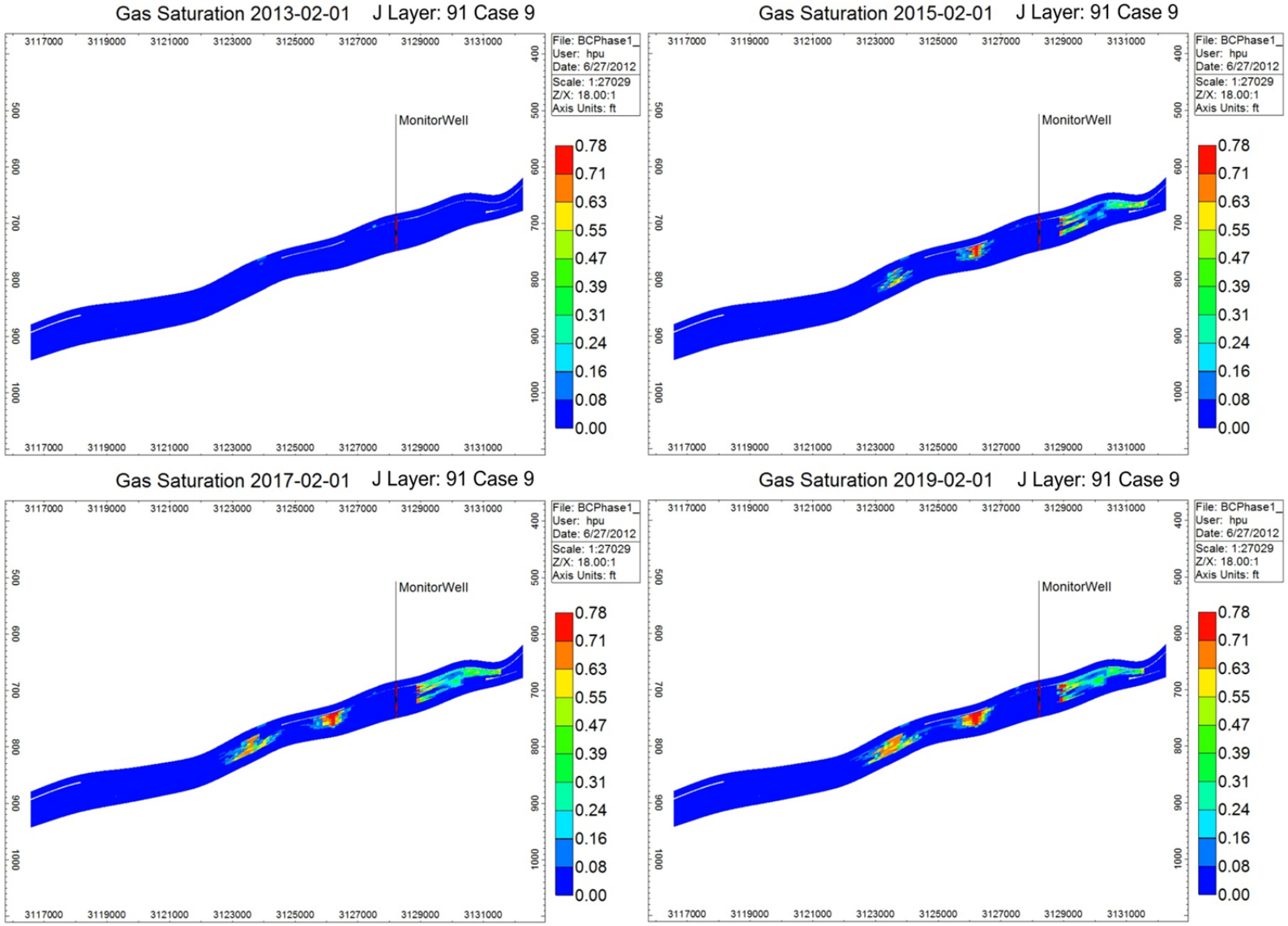

Figure C-55. Cross-sectional view of gas saturation (Case 9) (Part 1).

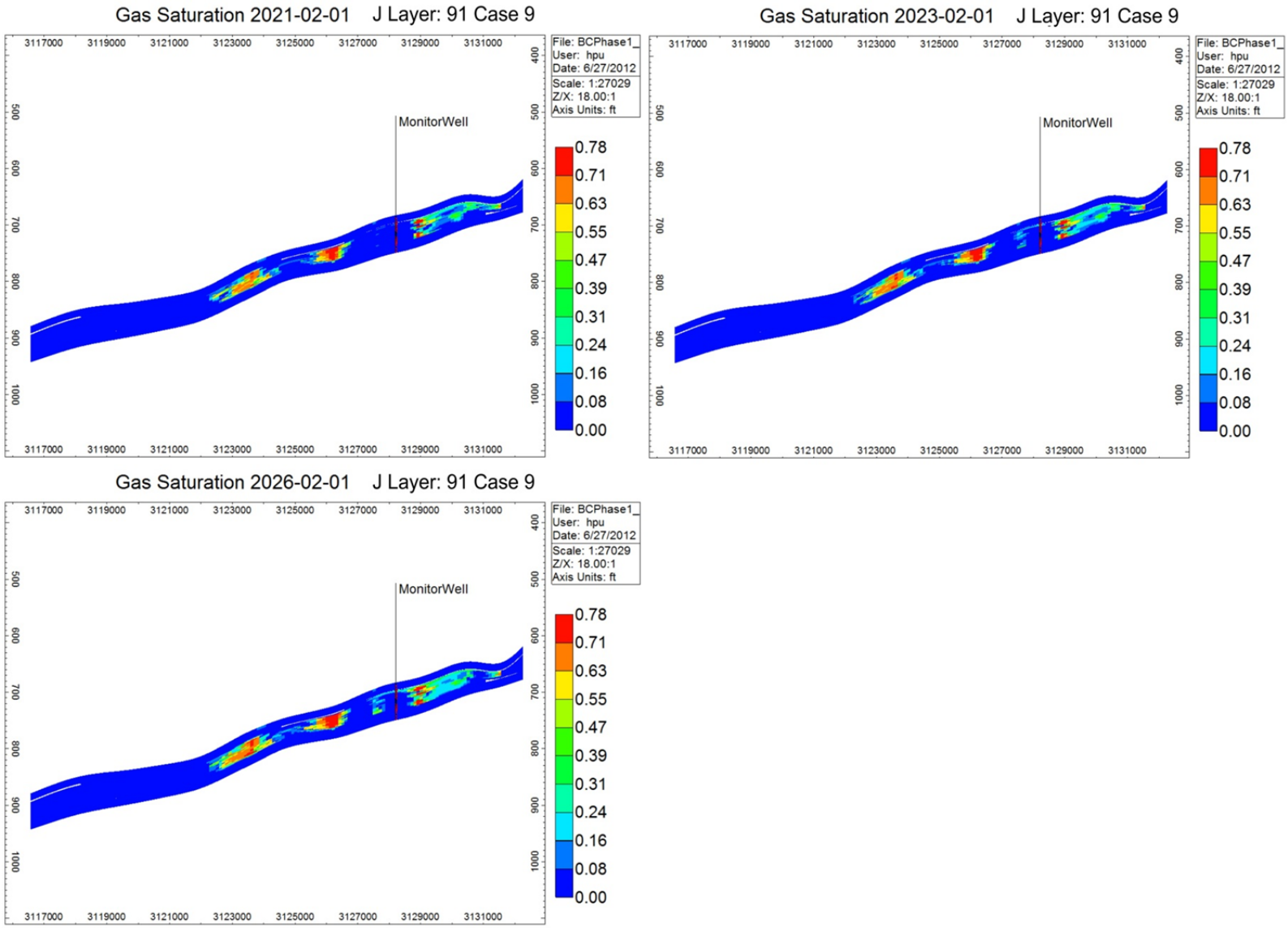

Figure C-55. Cross-sectional view of gas saturation (Case 9) (Part 2).

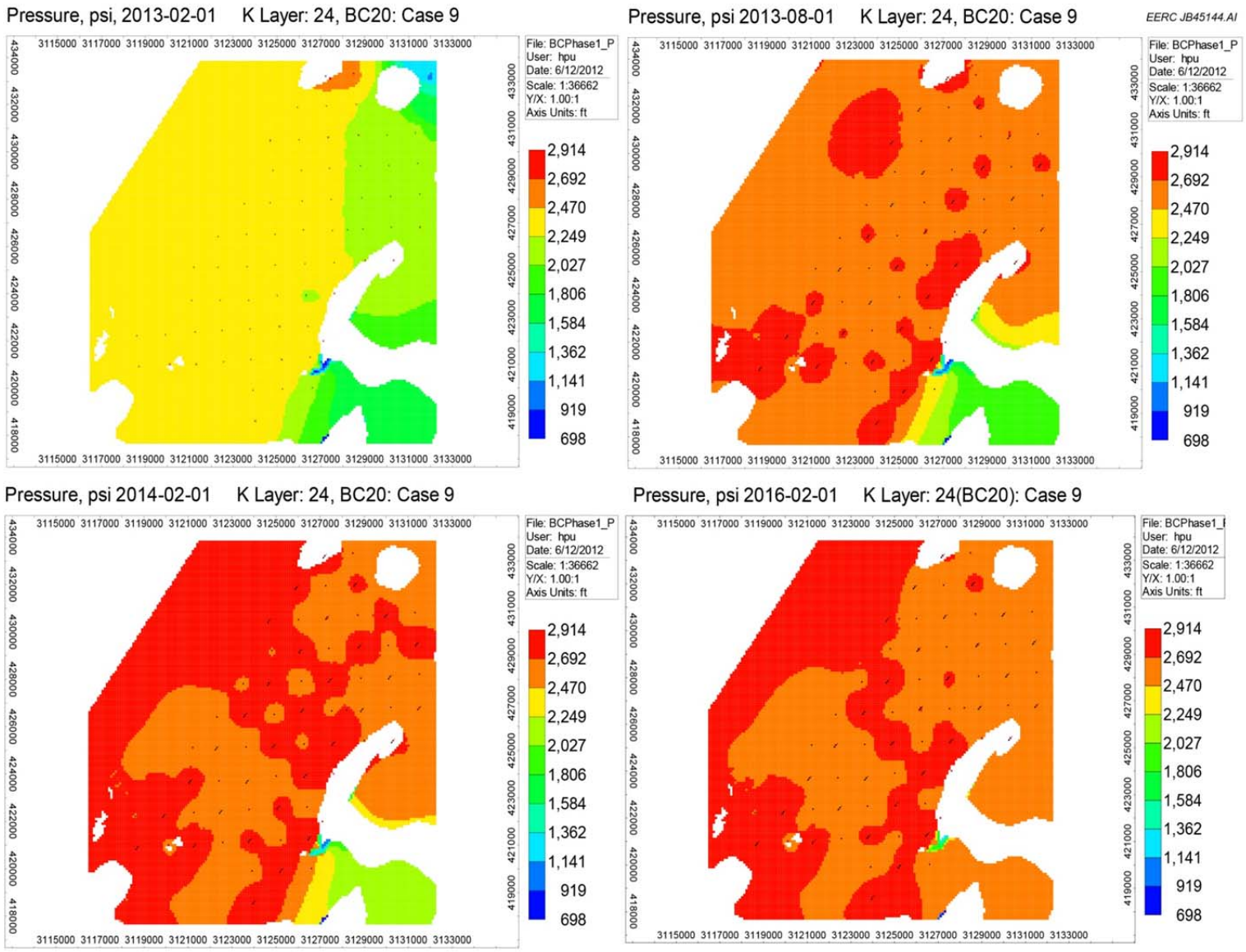

Figure C-56. Areal view of average reservoir pressure (Case 9) (Part 1).

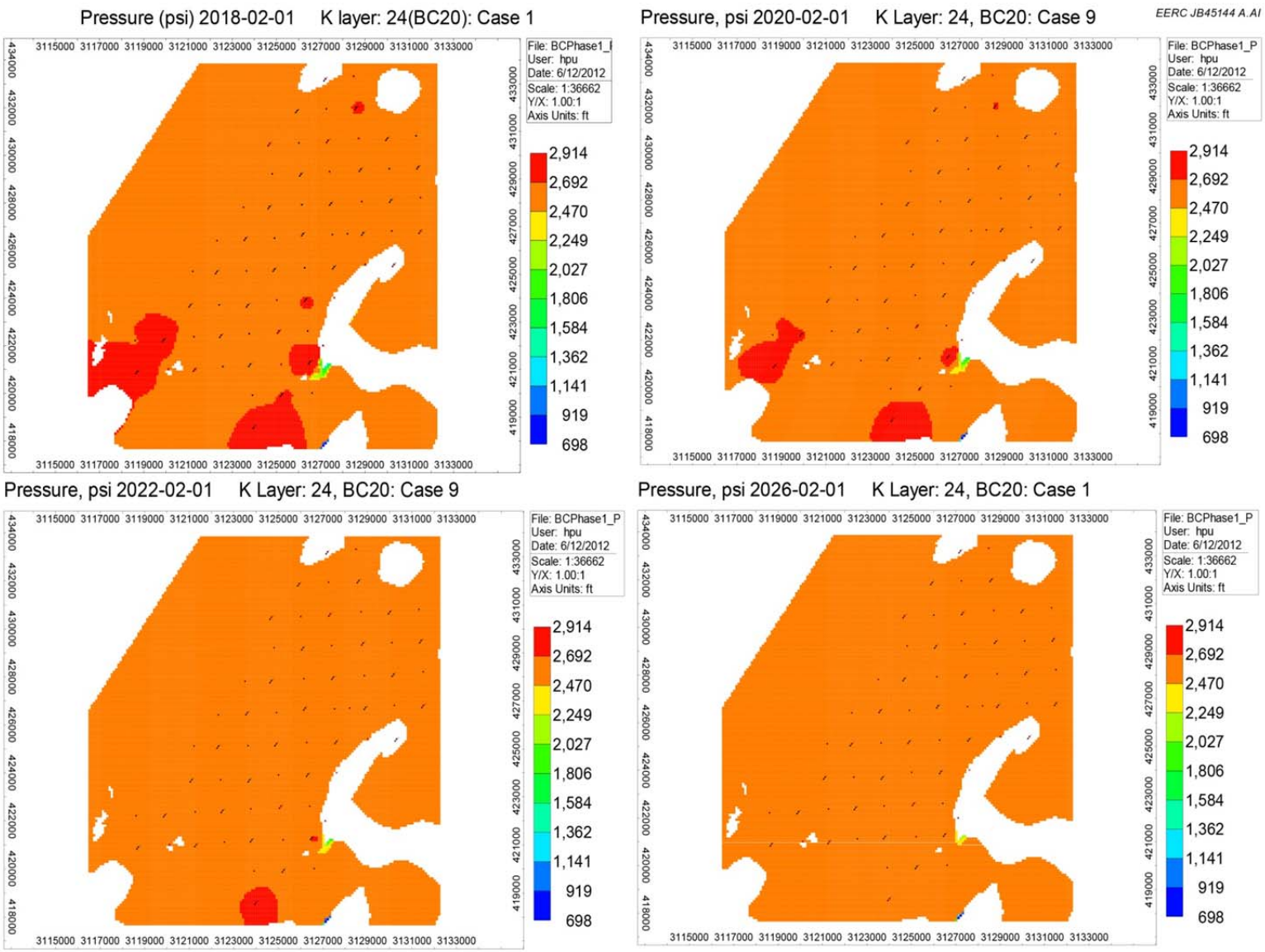

Figure C-56. Areal view of average reservoir pressure (Case 9) (Part 2).

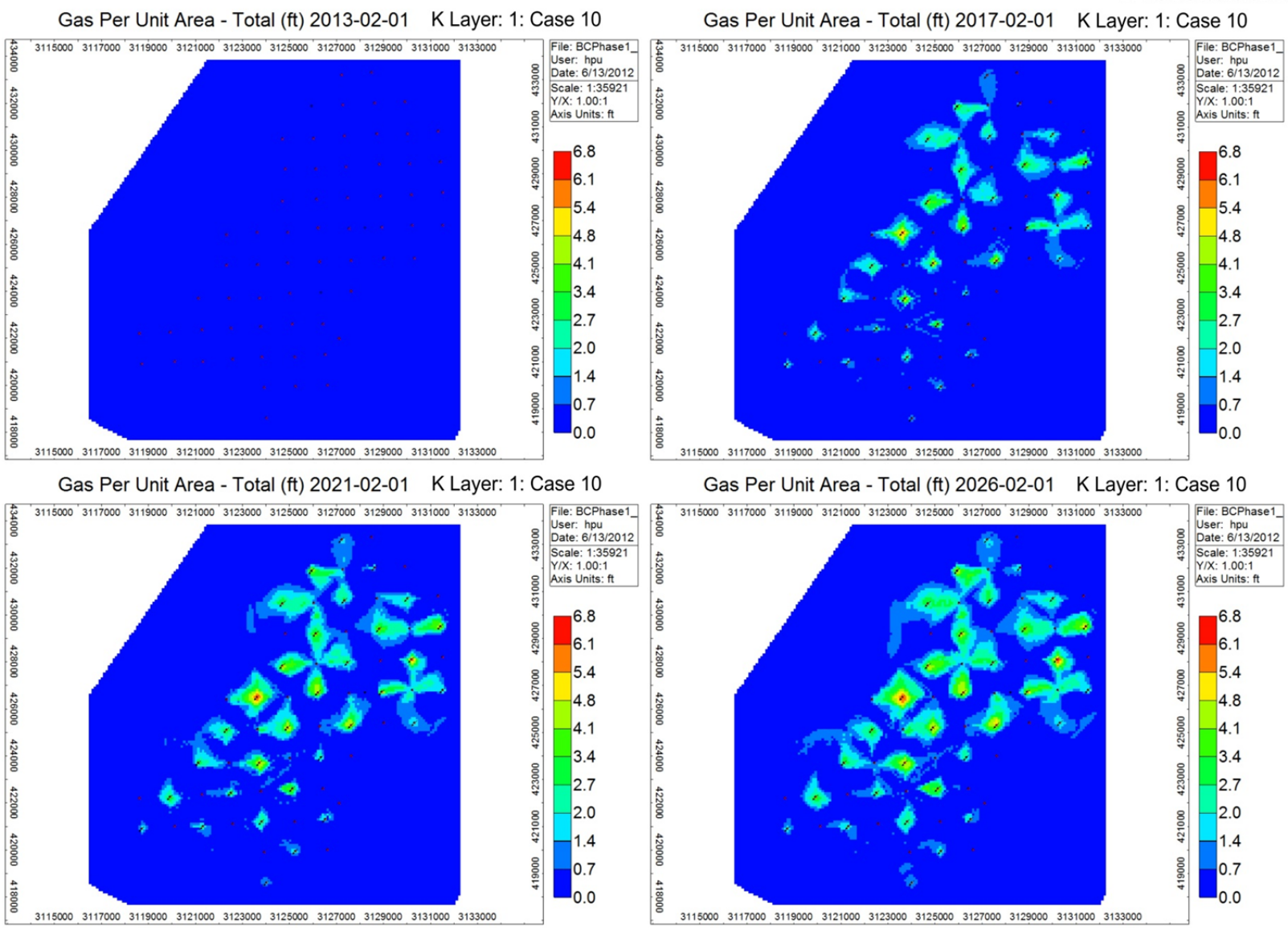

Figure C-57. Changes of gas per unit area of Case 10 over time (Part 1).

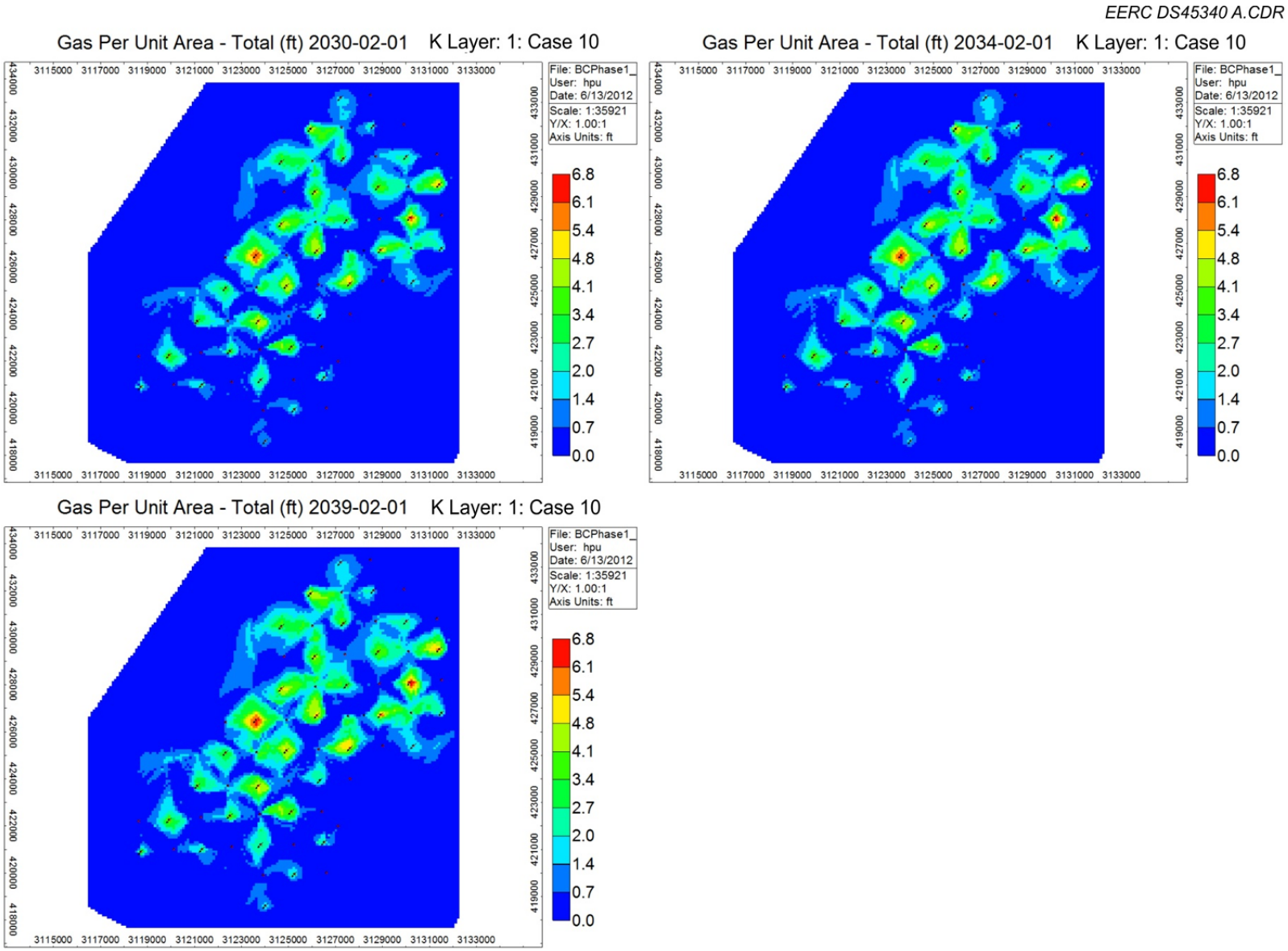

Figure C-57. Changes of gas per unit area of Case 10 over time (Part 2).

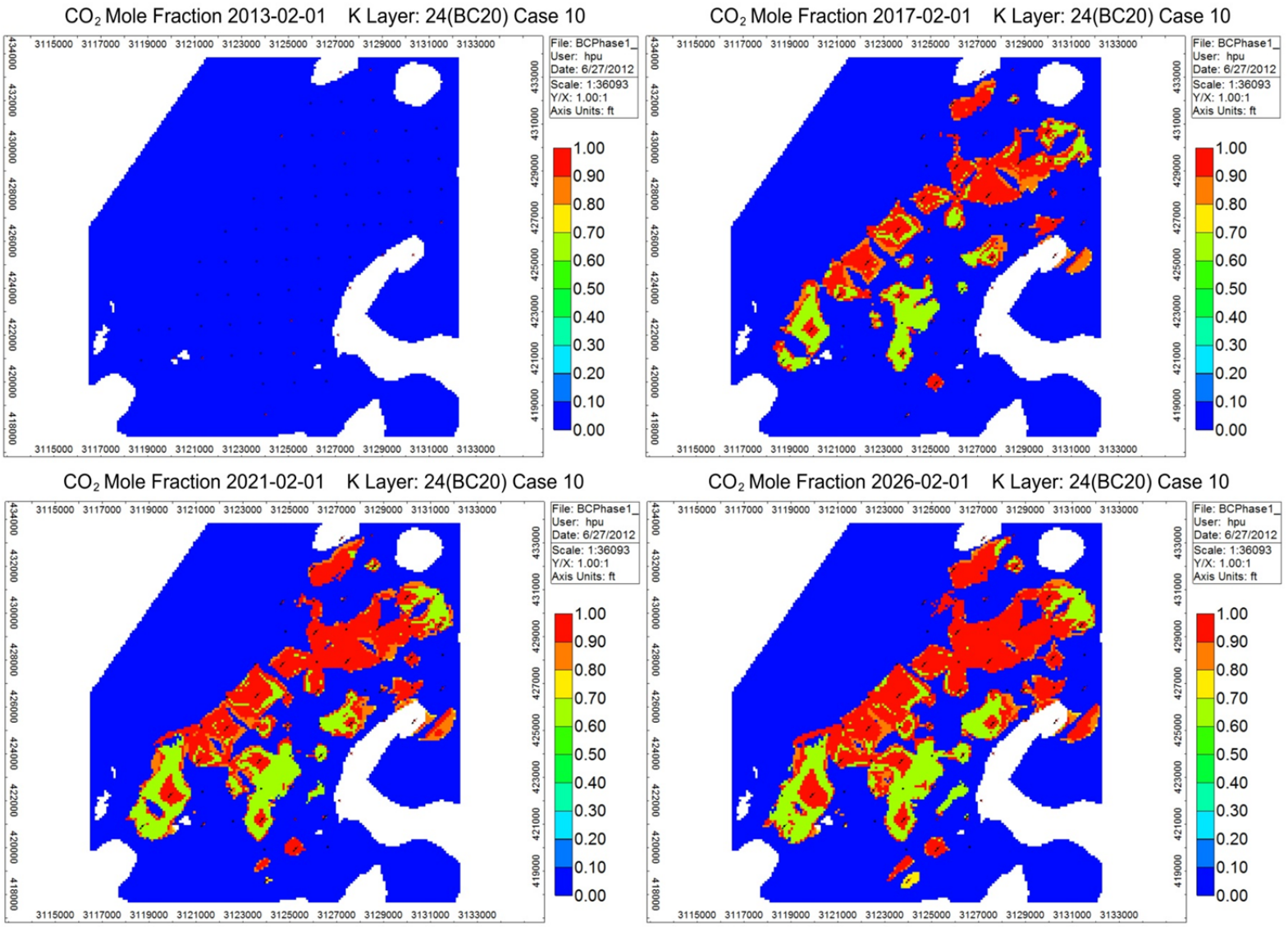

Figure C-58. Changes of CO_2 mole fraction over time (Case 10) (Part 1).

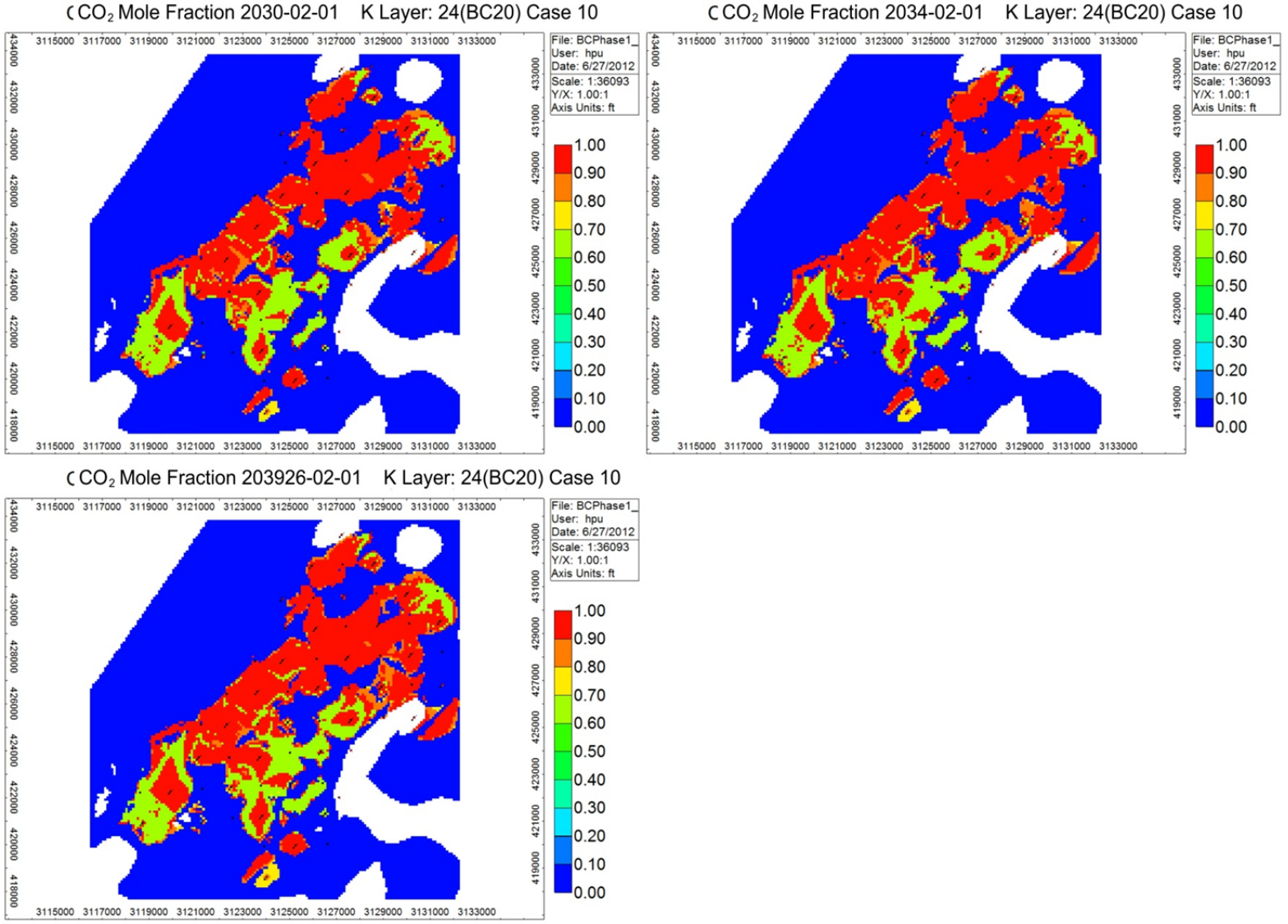

Figure C-59. Changes of CO_2 mole fraction over time (Case 10) (Part 2).

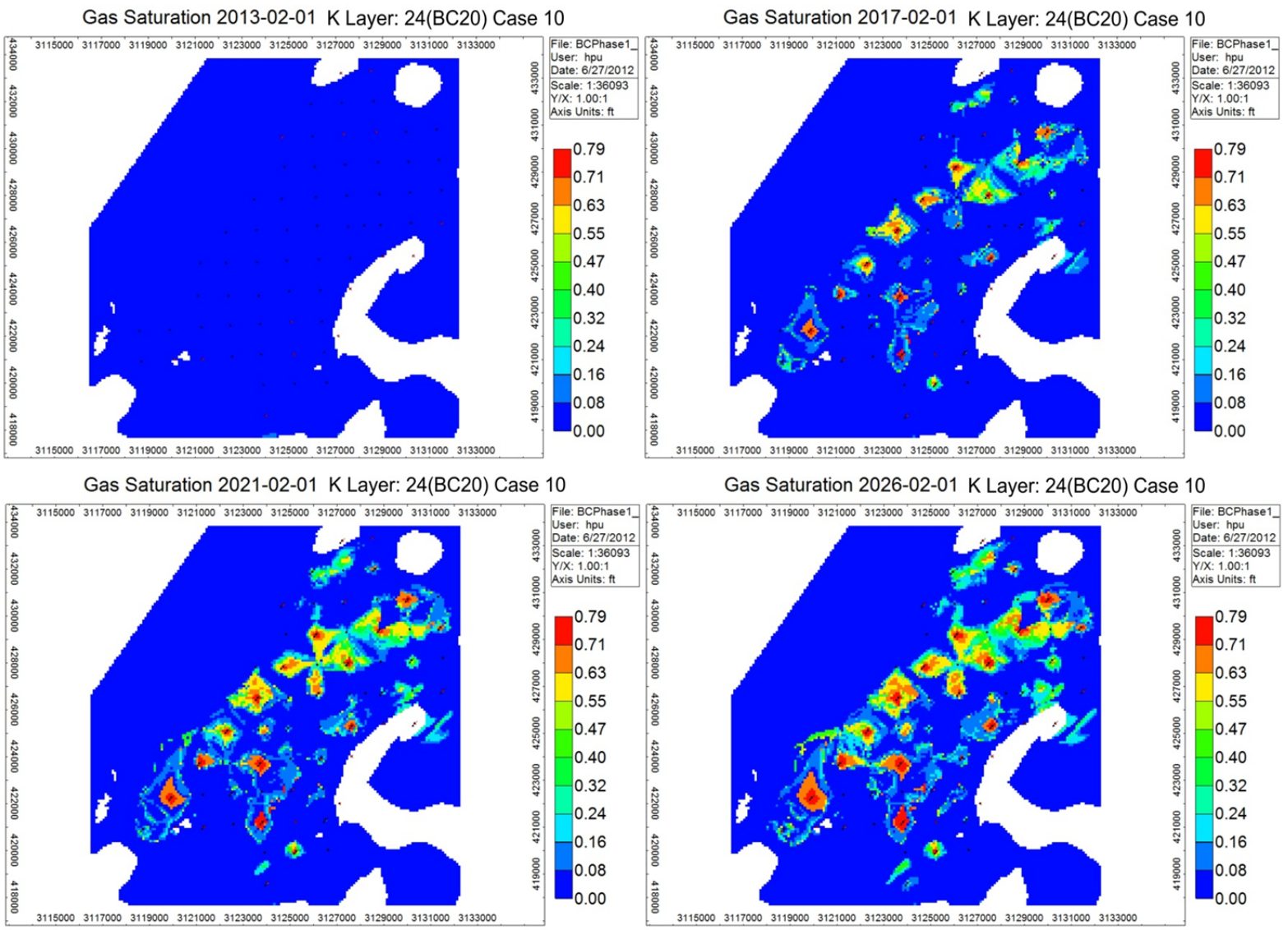

Figure C-60. Changes of gas saturation in K Layer 24 (BC20) over time (Case 10) (Part 1).

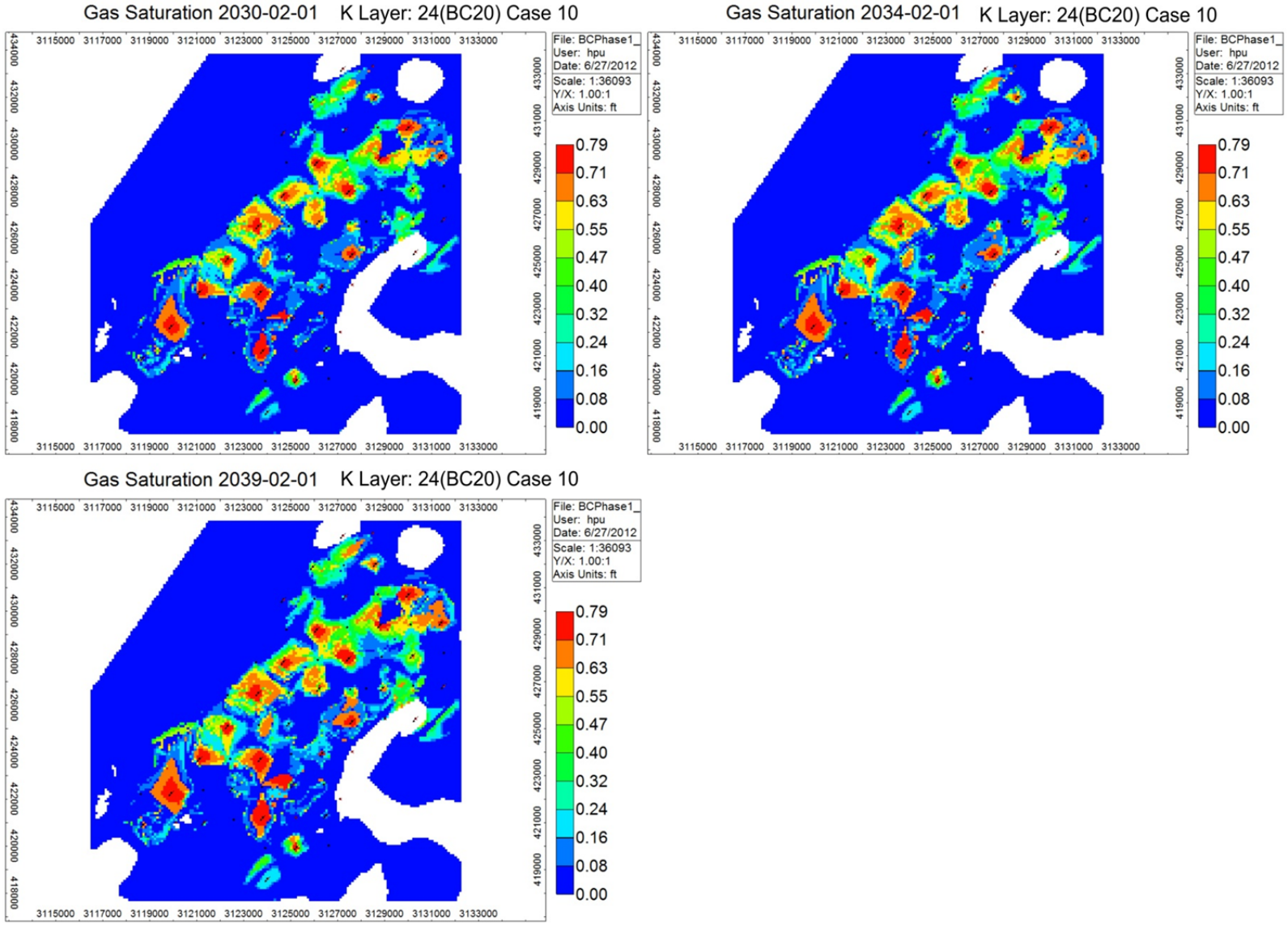

Figure C-60. Changes of gas saturation in K Layer 24 (BC20) over time (Case 10) (Part 2).

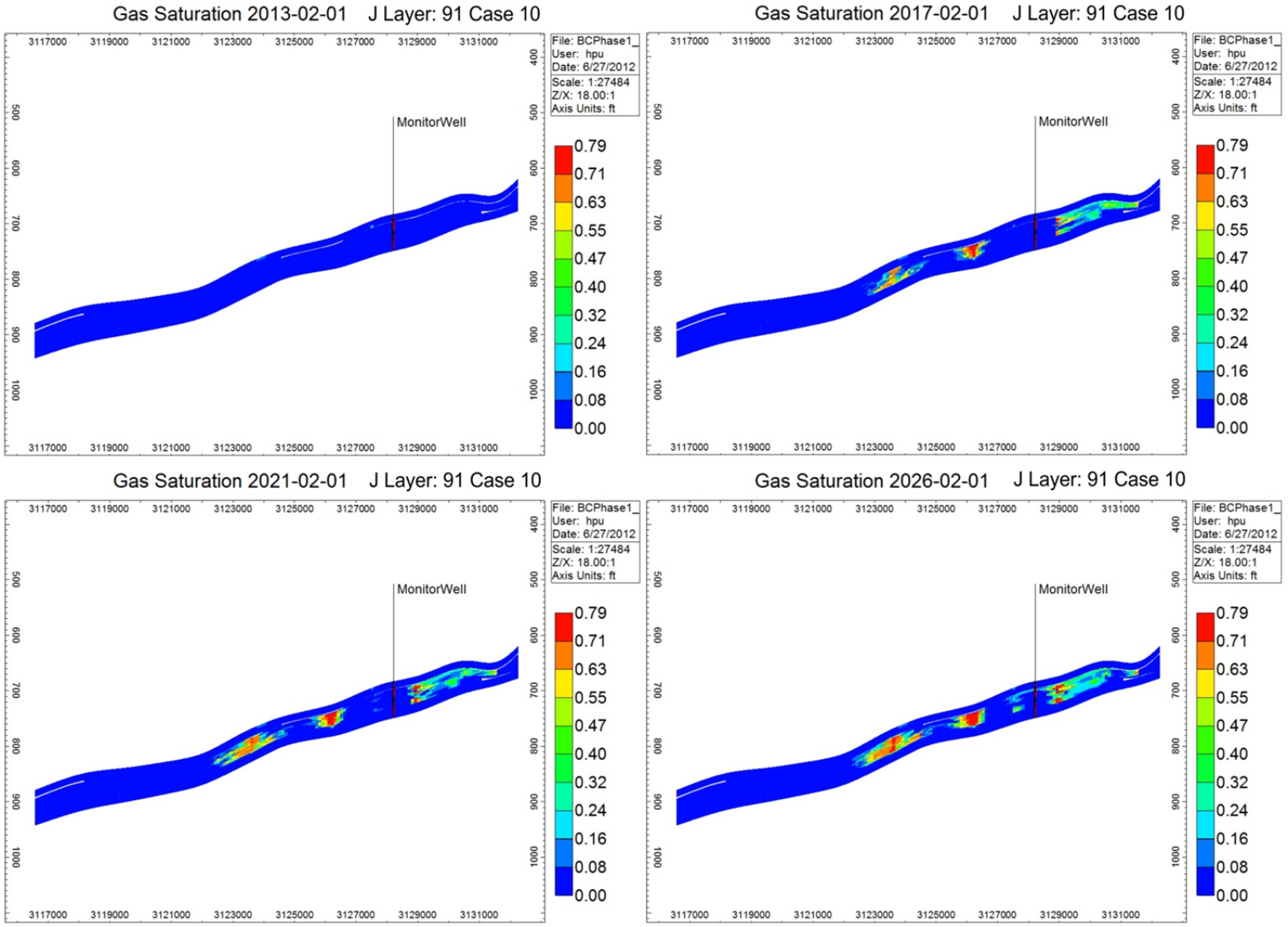

Figure C-61. Cross-sectional view of gas saturation (Case 10) (Part 1).

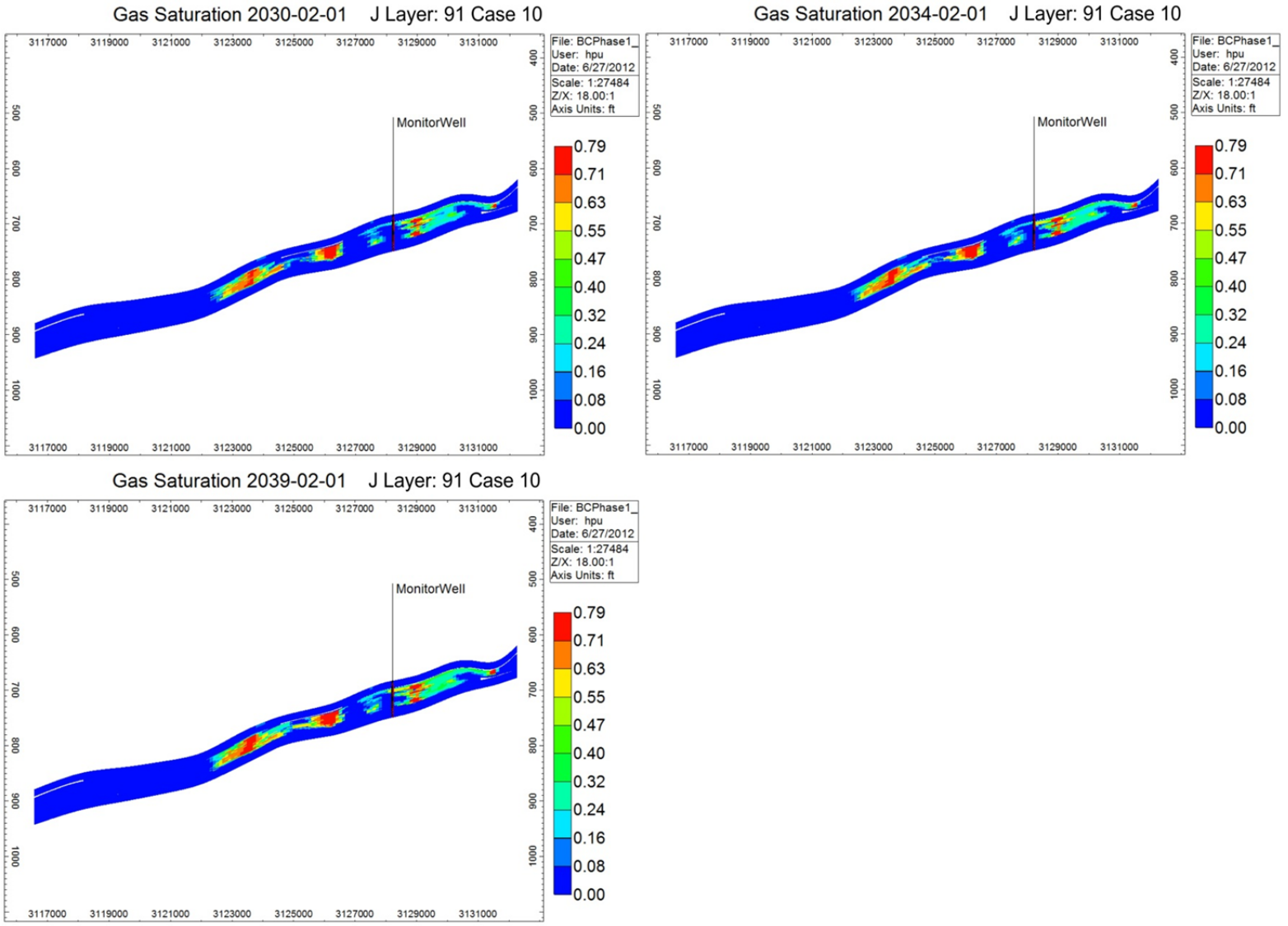

Figure C-61. Cross-sectional view of gas saturation (Case 10) (Part 2).

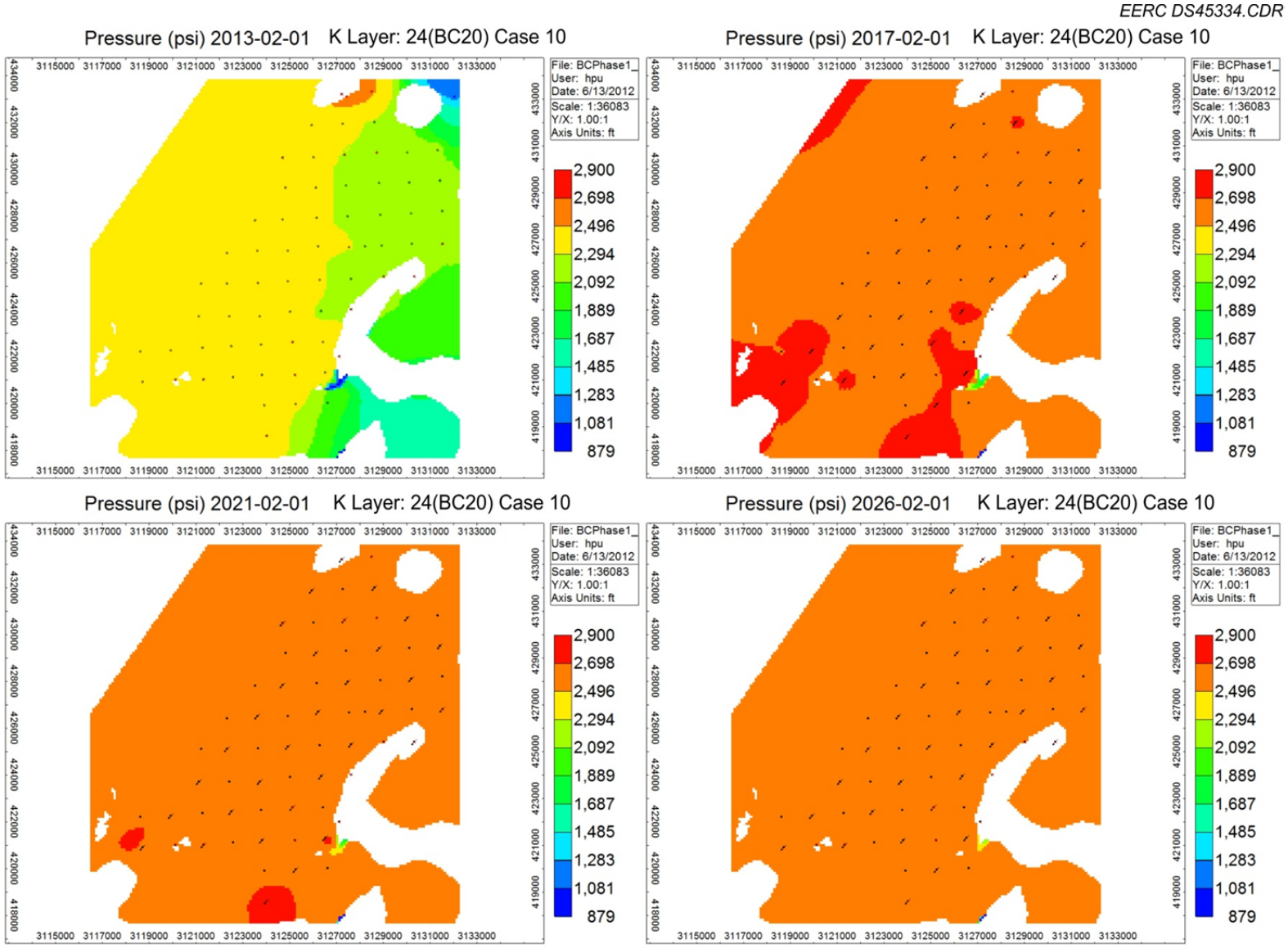

Figure C-62. Areal view of pressure (Case 10) (Part 1).

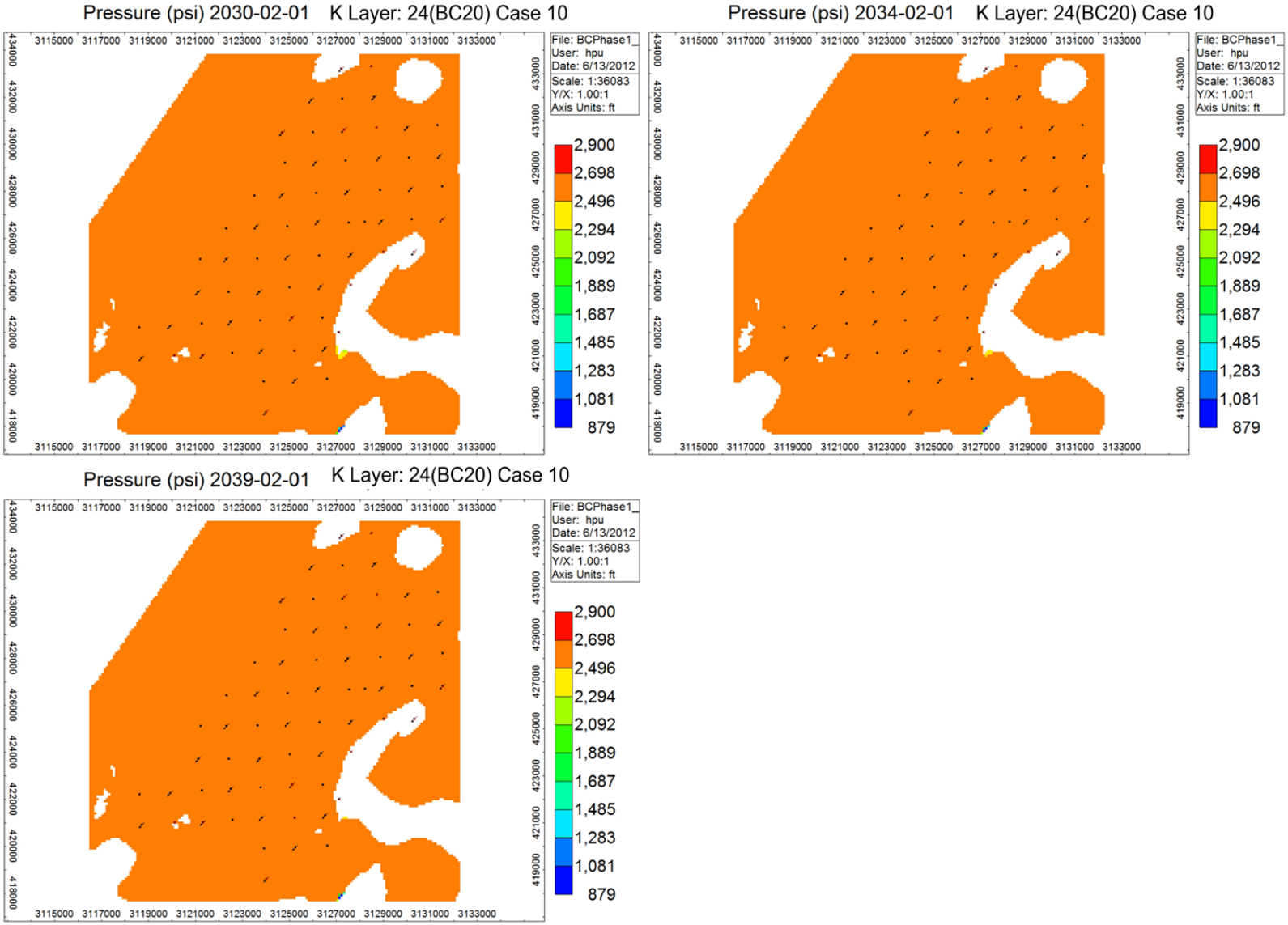

Figure C-62. Areal view of pressure (Case 10) (Part 2).

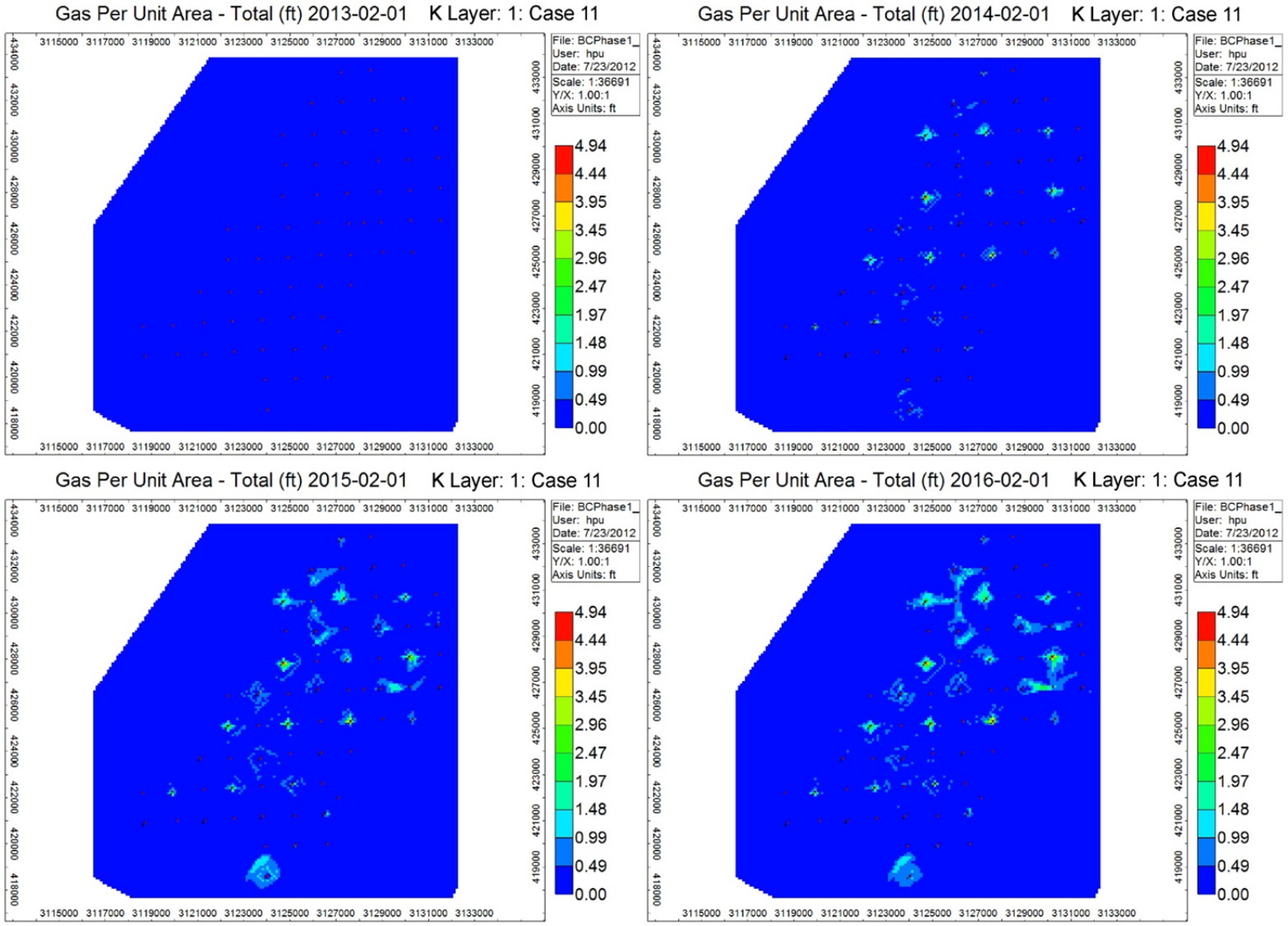

Figure C-63. Changes of gas per unit area over time (Case 11) (Part 1).

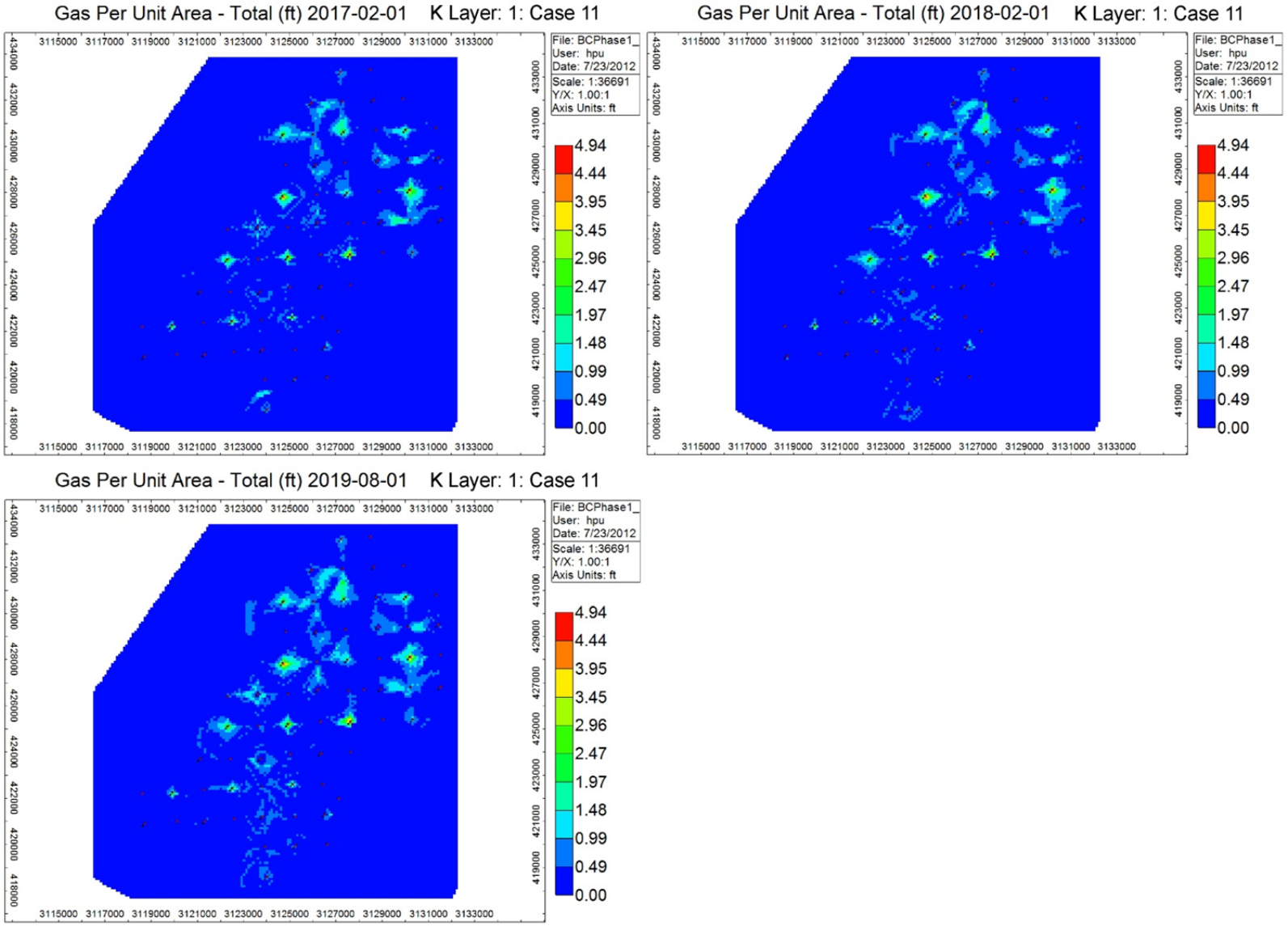

Figure C-63. Changes of gas per unit area over time (Case 11) (Part 2).

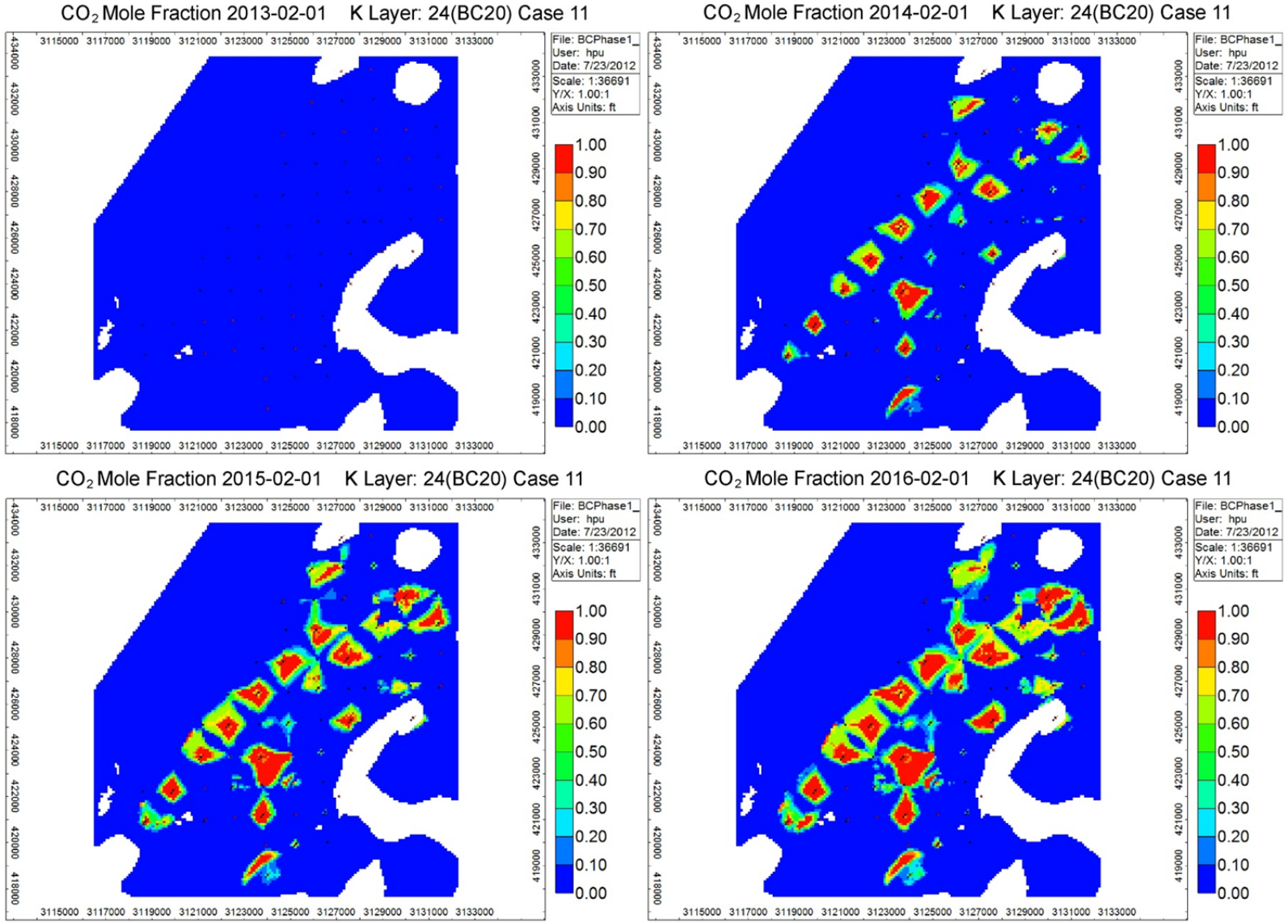

Figure C-64. Changes of CO_2 mole fraction of Case 11 over time (Part 1).

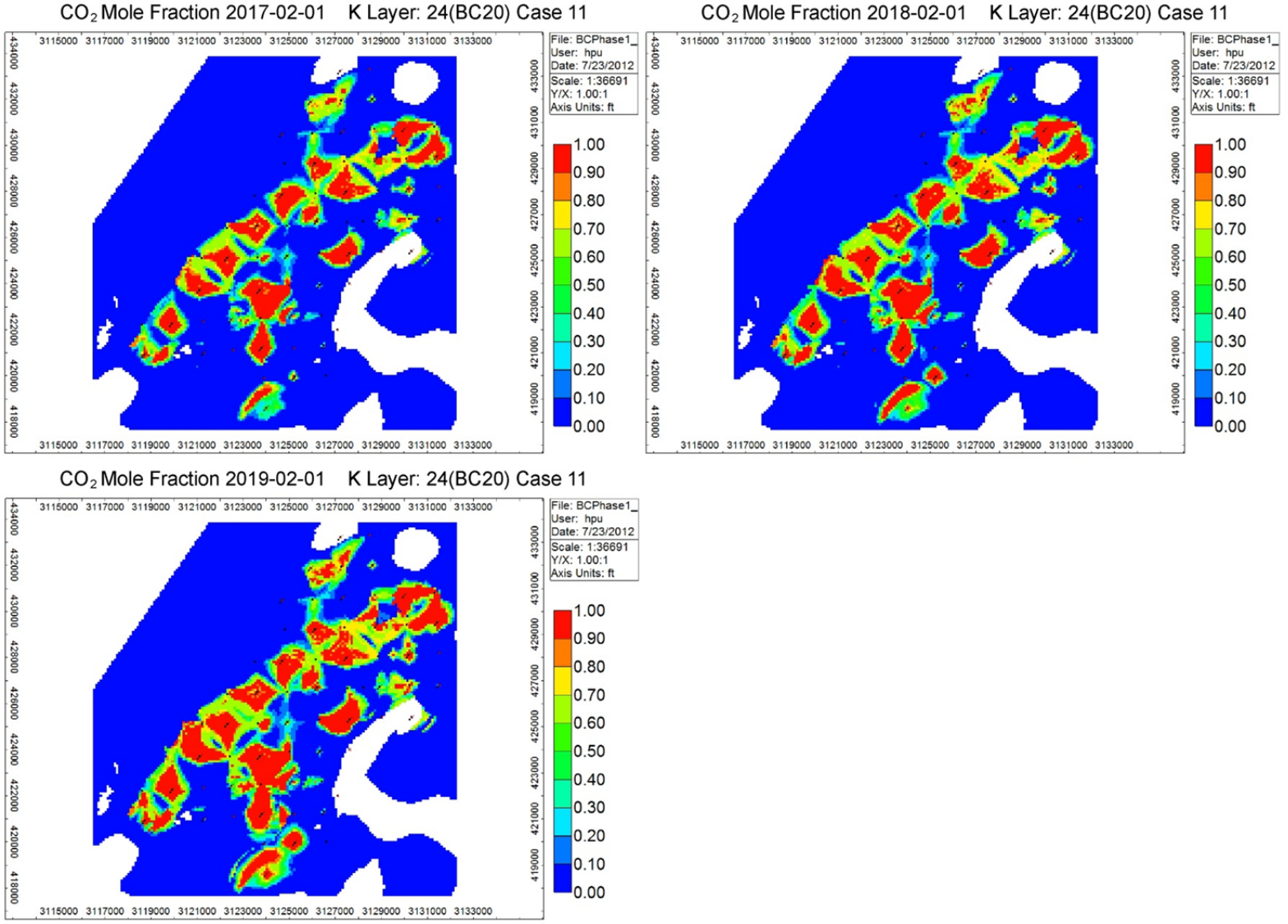

Figure C-64. Changes of CO_2 mole fraction of Case 11 over time (Part 2).

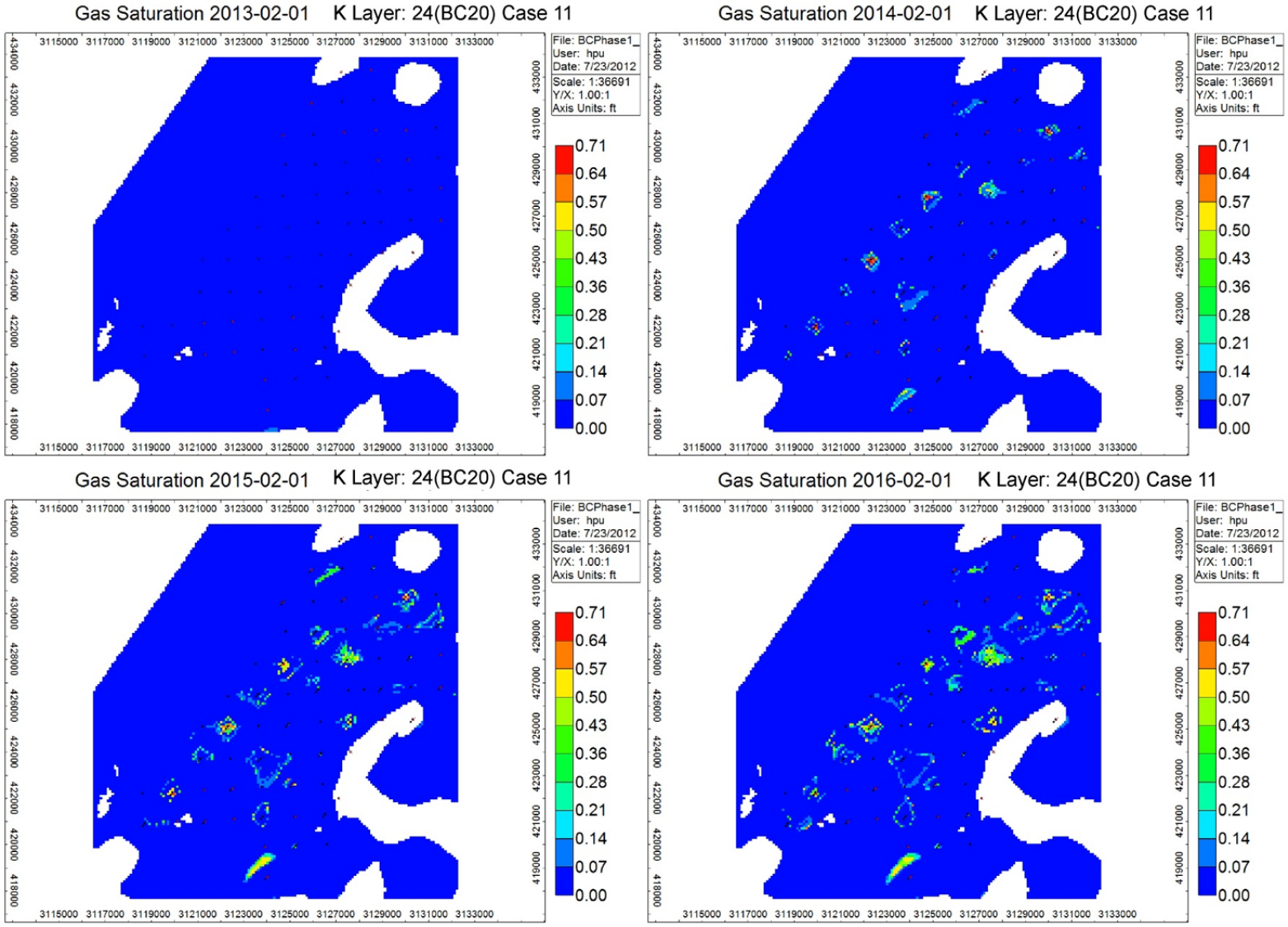

Figure C-65. Changes of gas saturation in K Layer 24 (BC20) over time (Case 11) (Part 1).

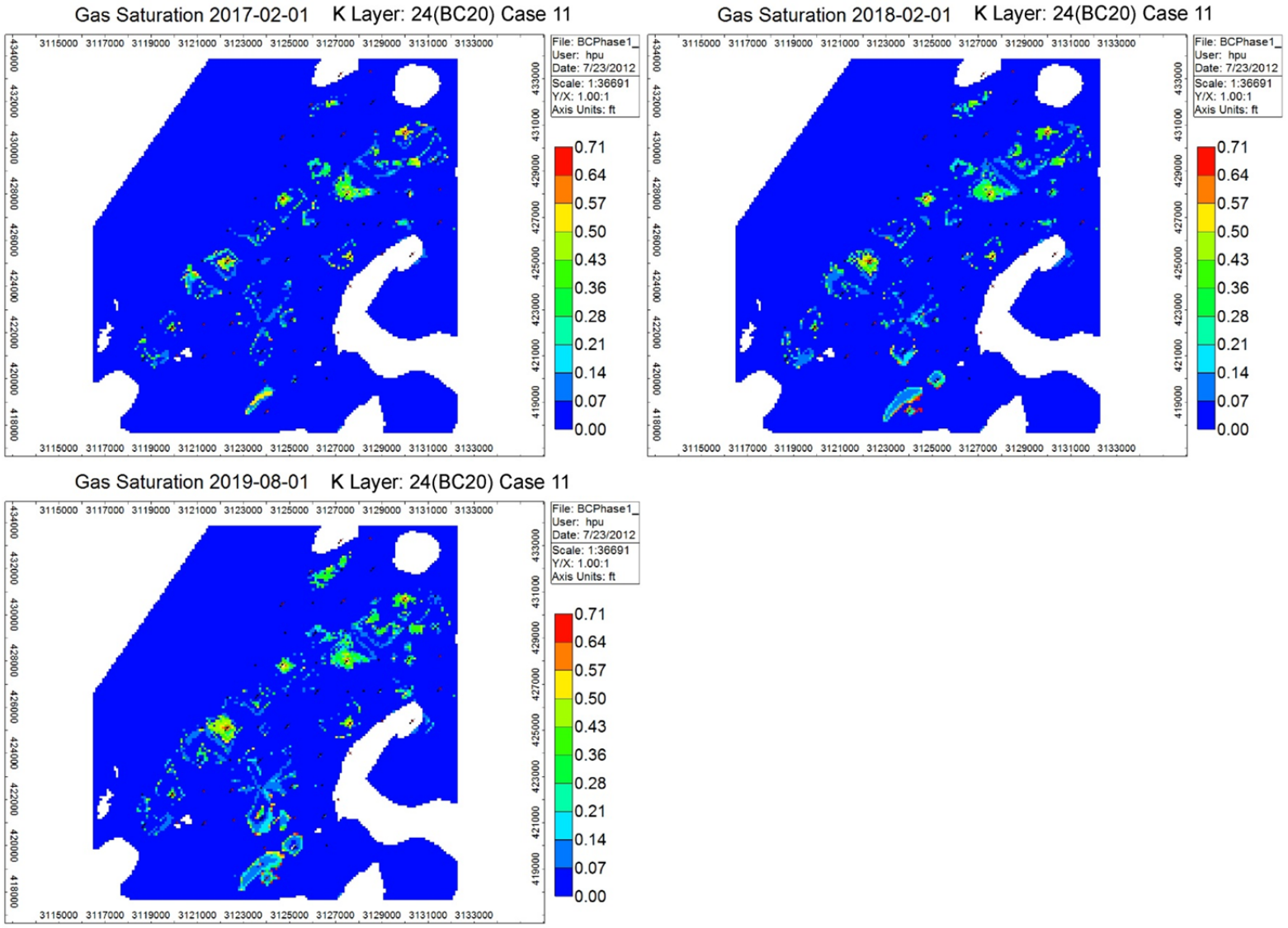

Figure C-65. Changes of gas saturation in K Layer 24 (BC20) over time (Case 11) (Part 2).

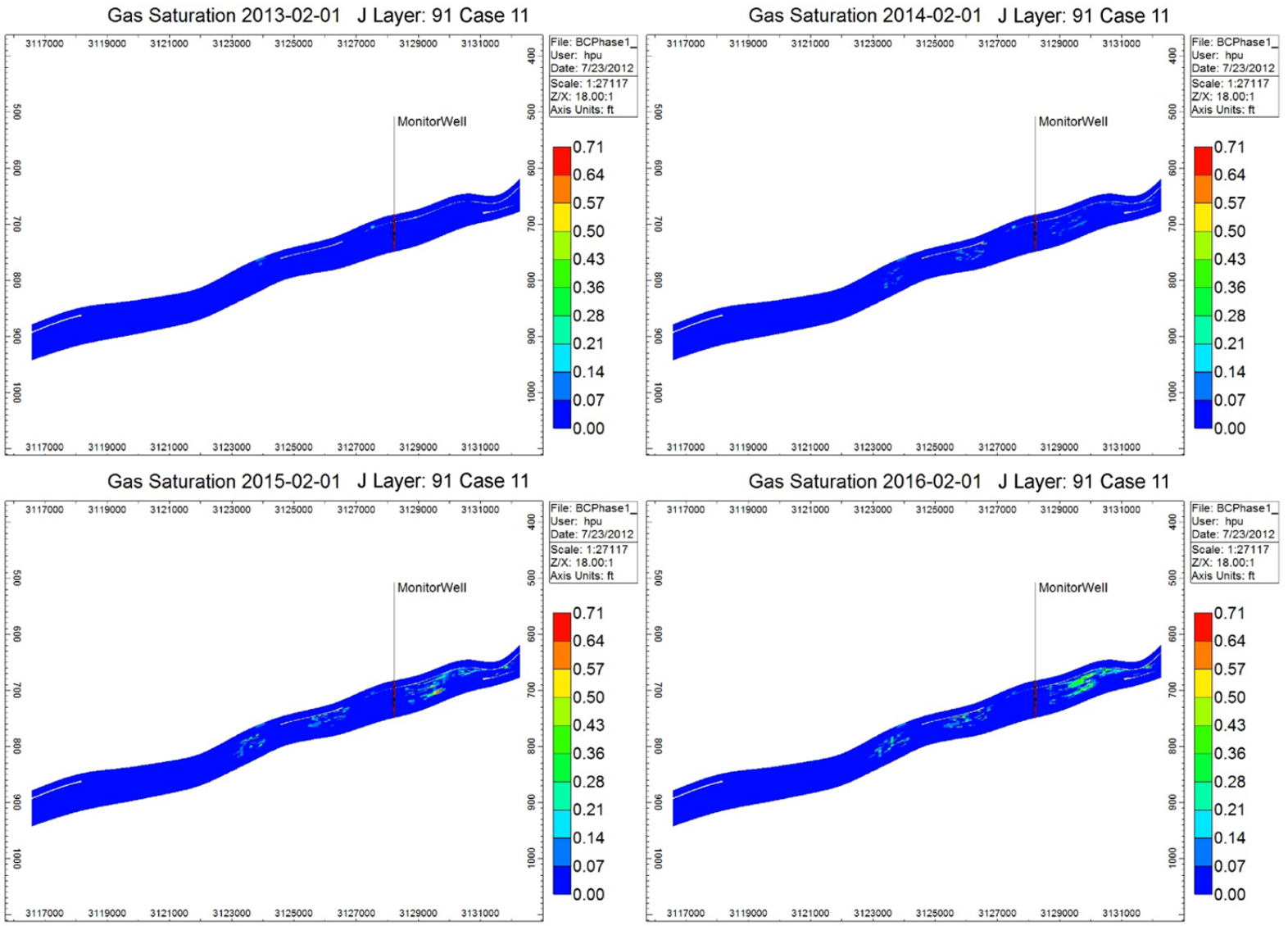

Figure C-66. Cross-sectional view of gas saturation (Case 11) (Part 1).

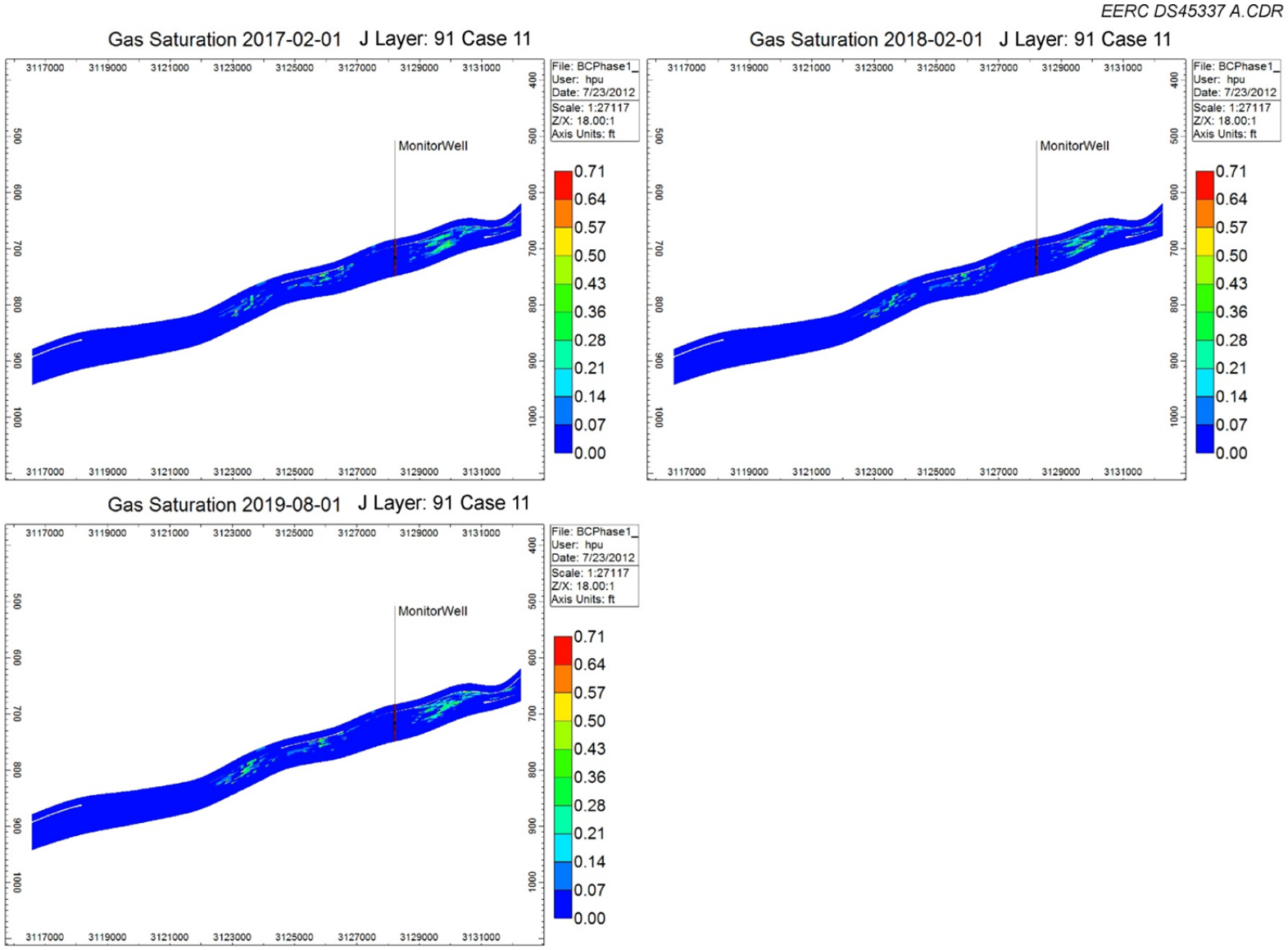

Figure C-66. Cross-sectional view of gas saturation (Case 11) (Part 2).

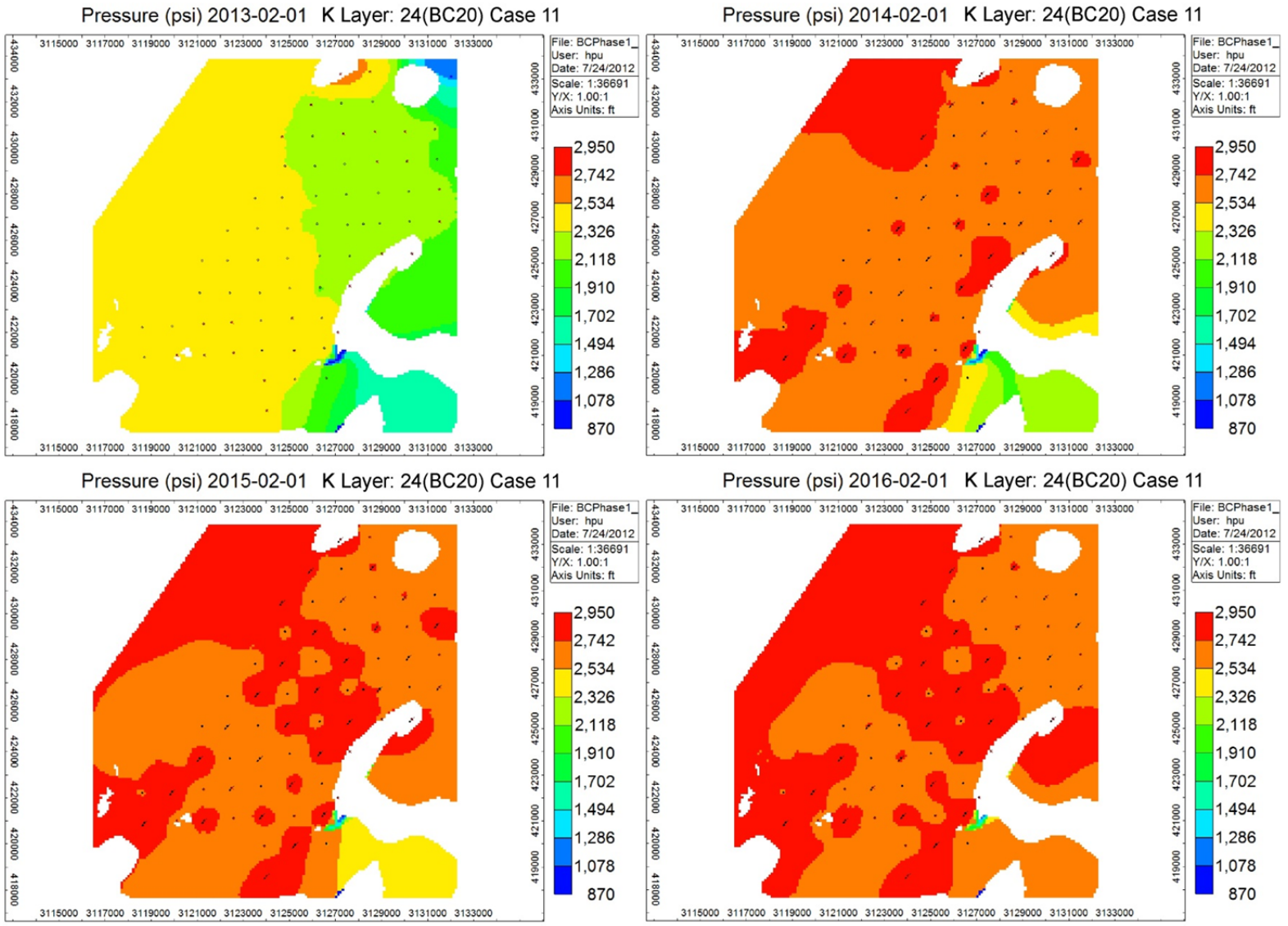

Figure C-67. Areal view of pressure (Case 11) (Part 1).

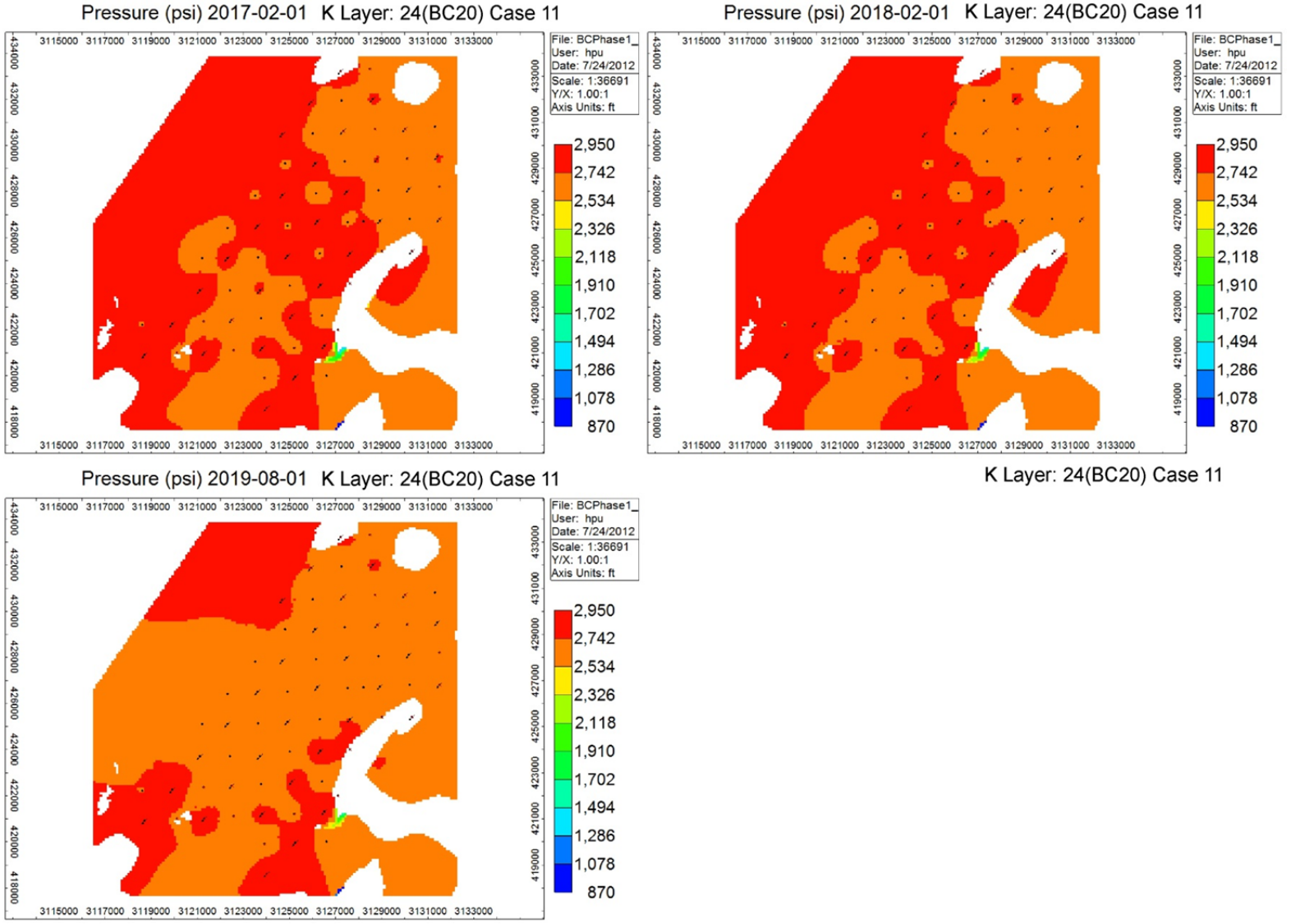

Figure C-67. Areal view of pressure (Case 11) (Part 2).

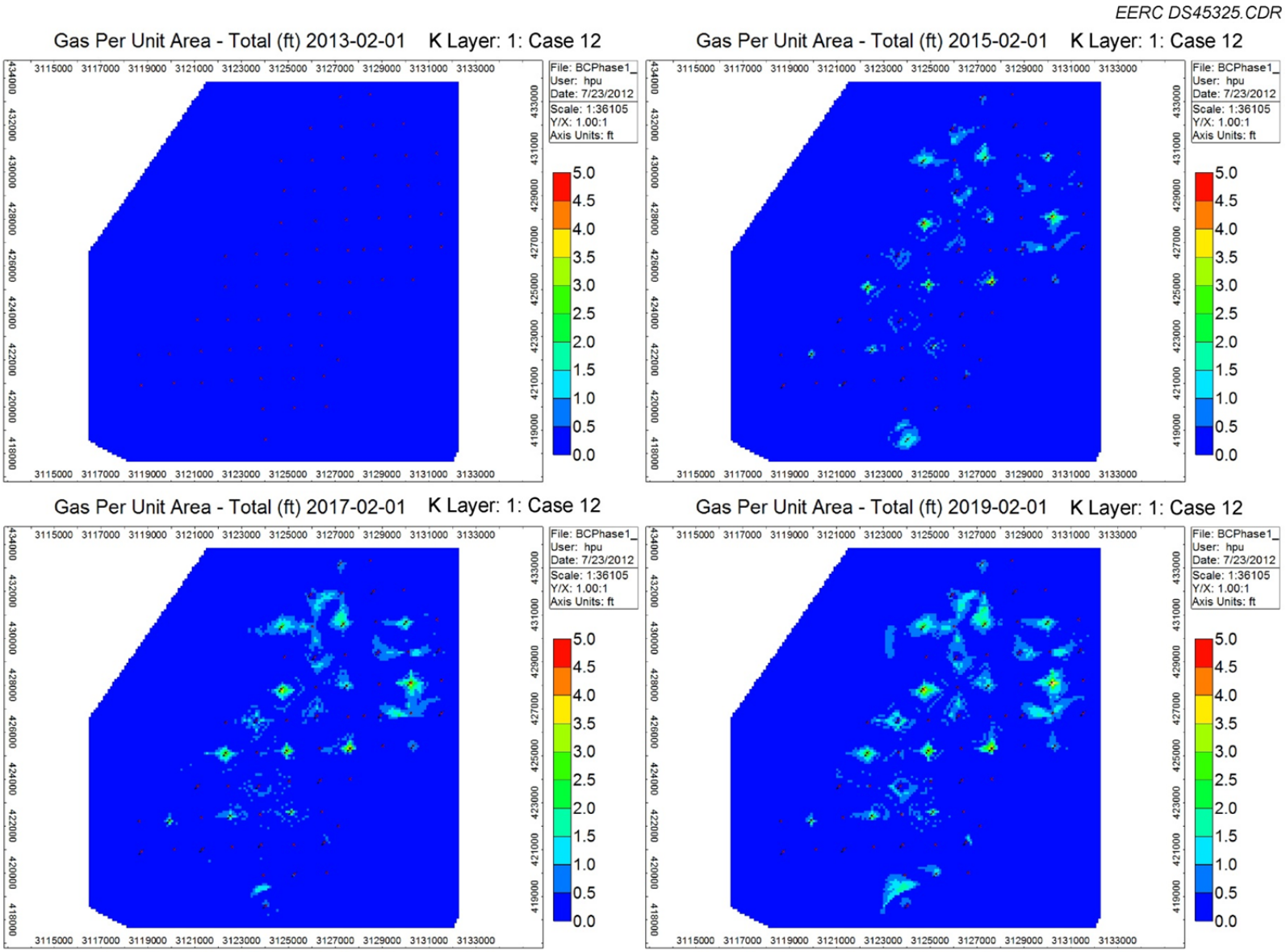

Figure C-68. Changes of gas per unit area of Case 12 over time (Part 1).

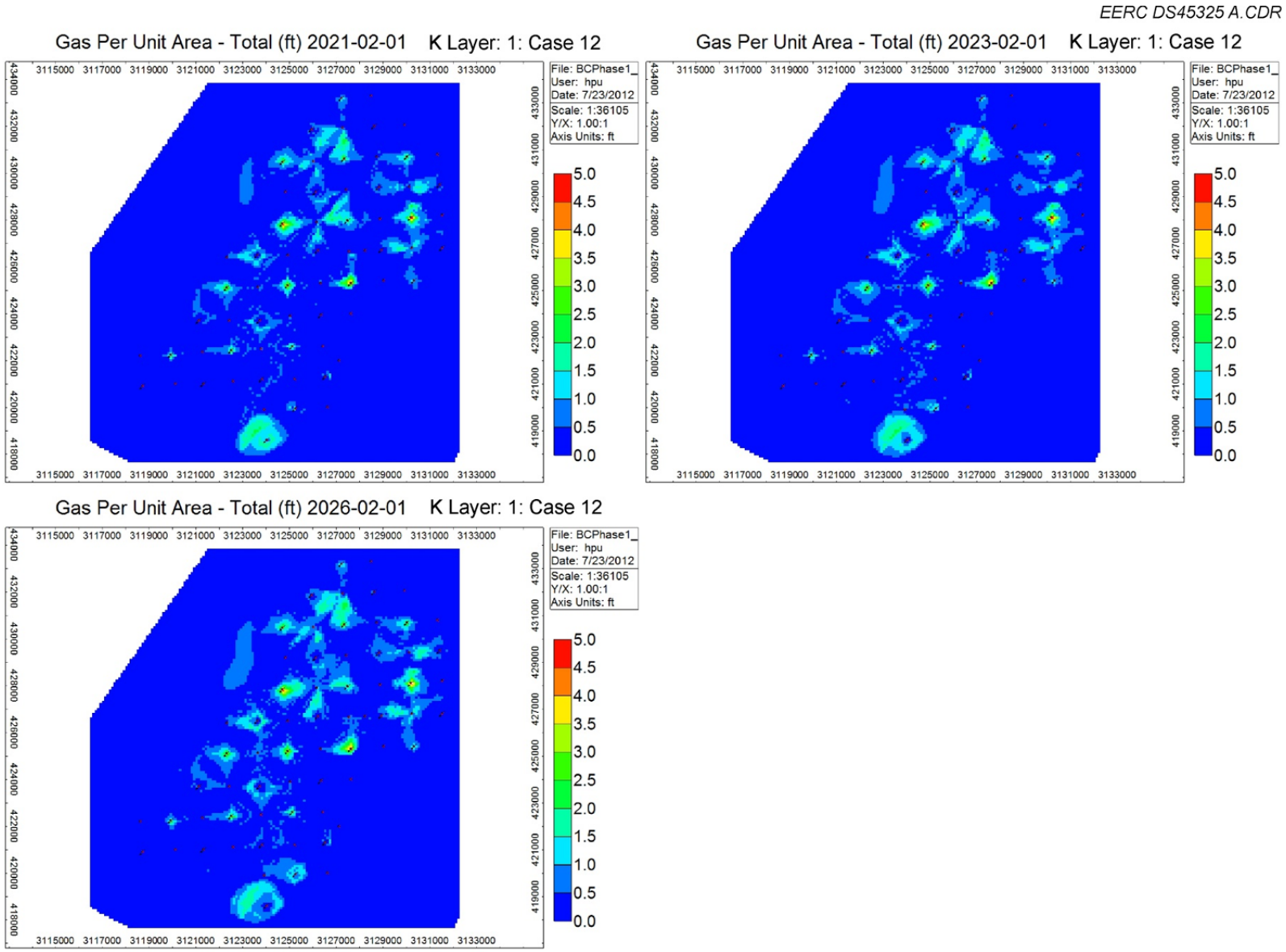

Figure C-68. Changes of gas per unit area of Case 12 over time (Part 2).

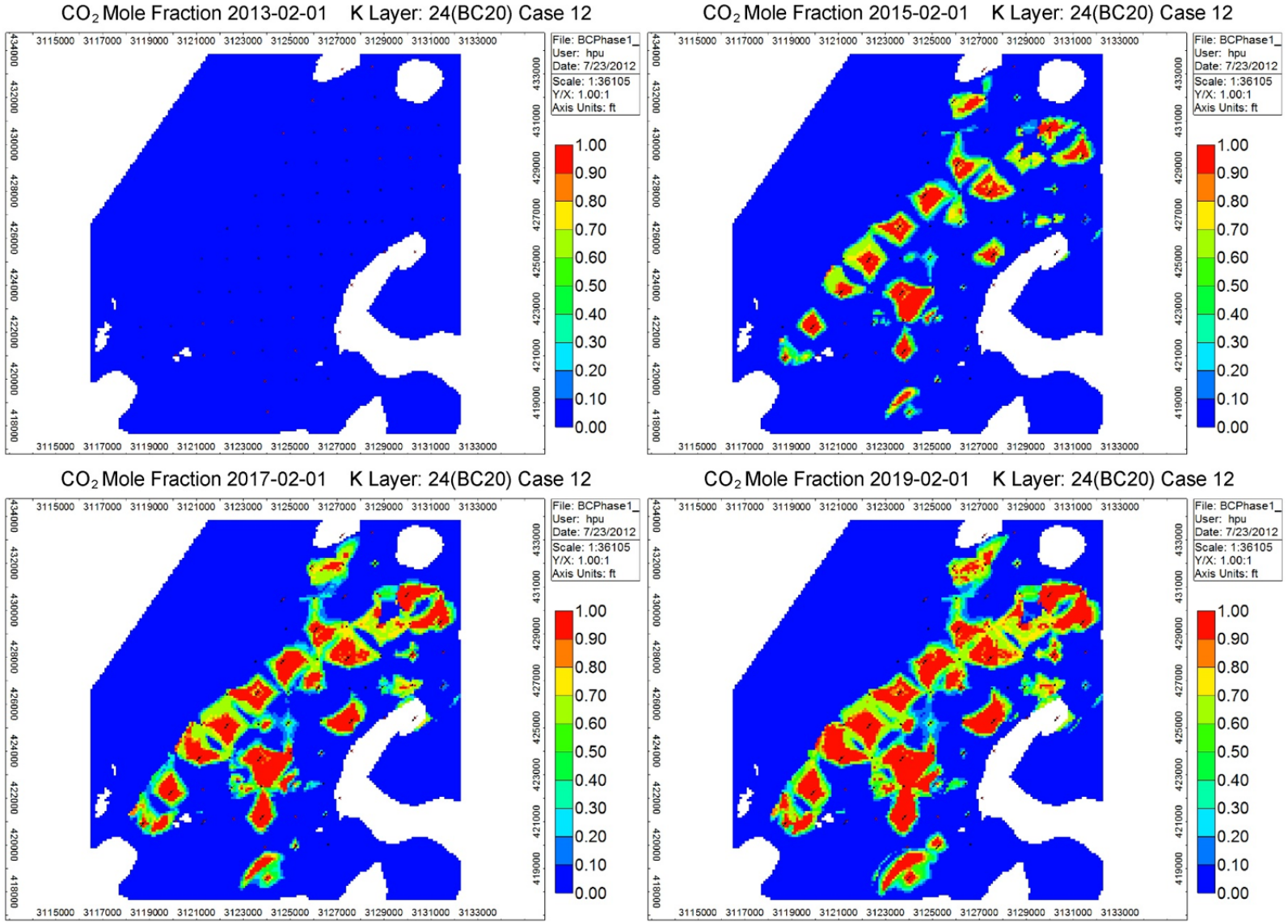

Figure C-69. Changes of CO_2 mole fraction over time (Case 12) (Part 1).

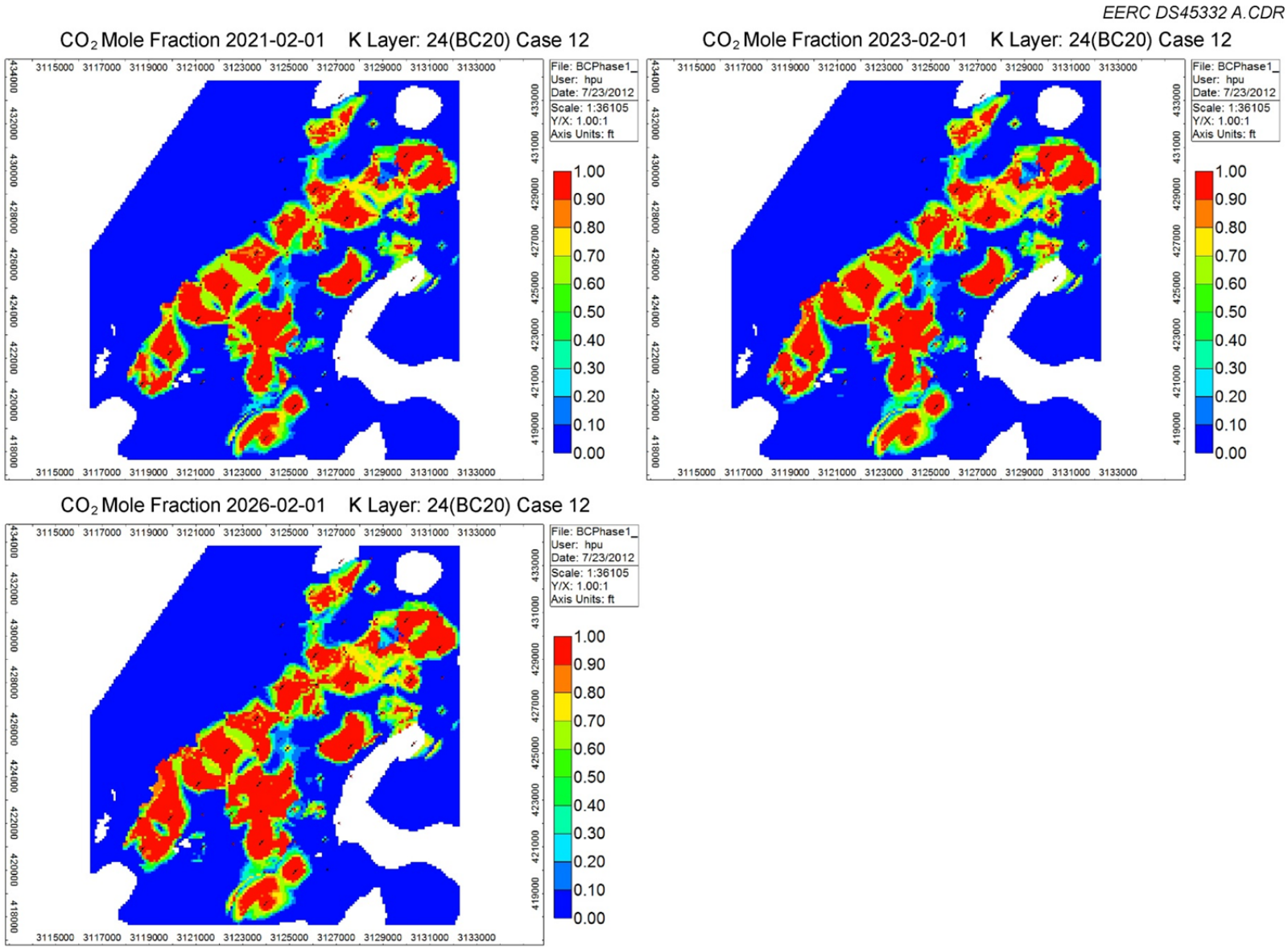

Figure C-69. Changes of CO_2 mole fraction over time (Case 12) (Part 2).

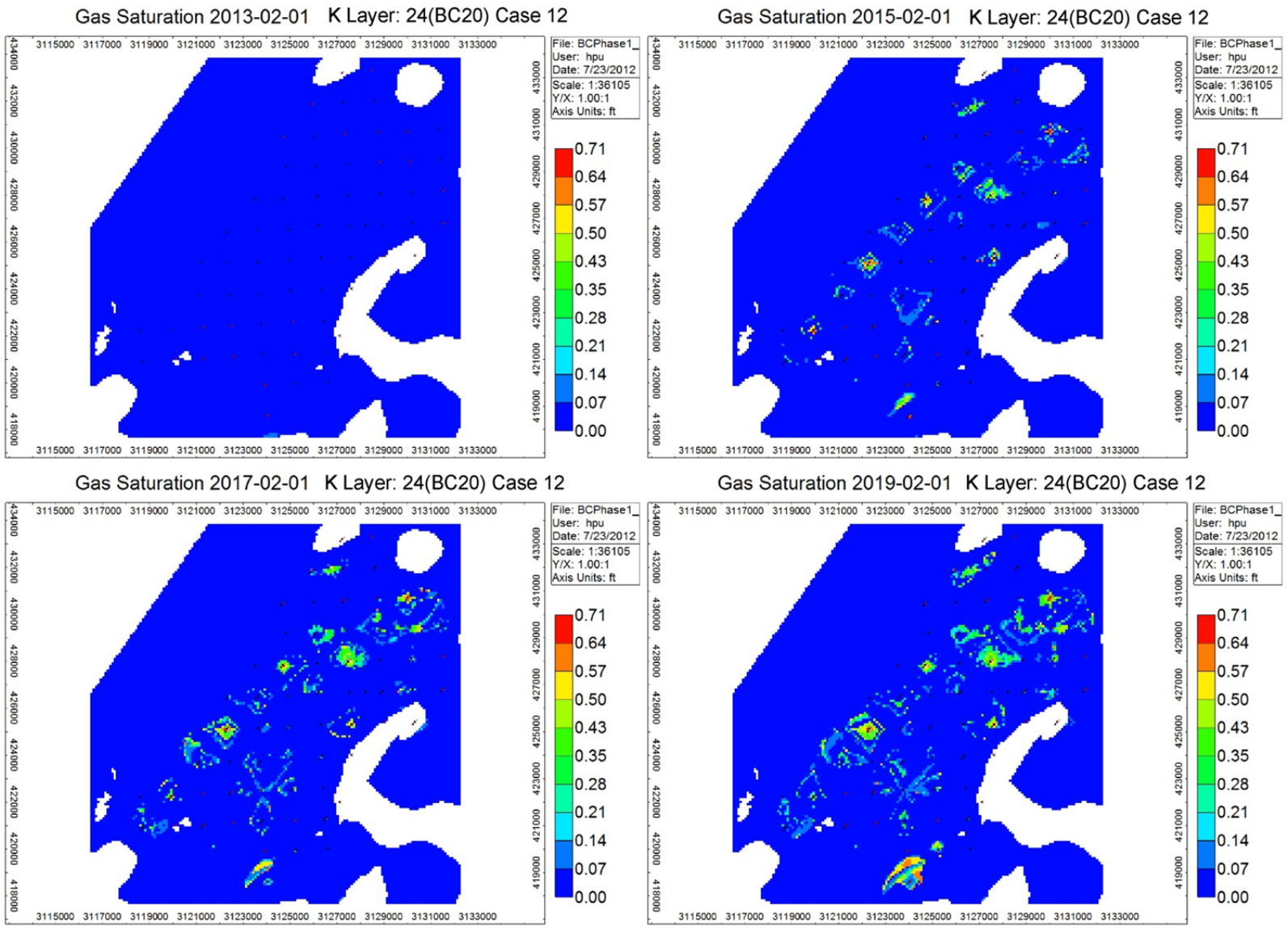

Figure C-70. Changes of gas saturation in K Layer 24 (BC20) over time (Case 12) (Part 1).

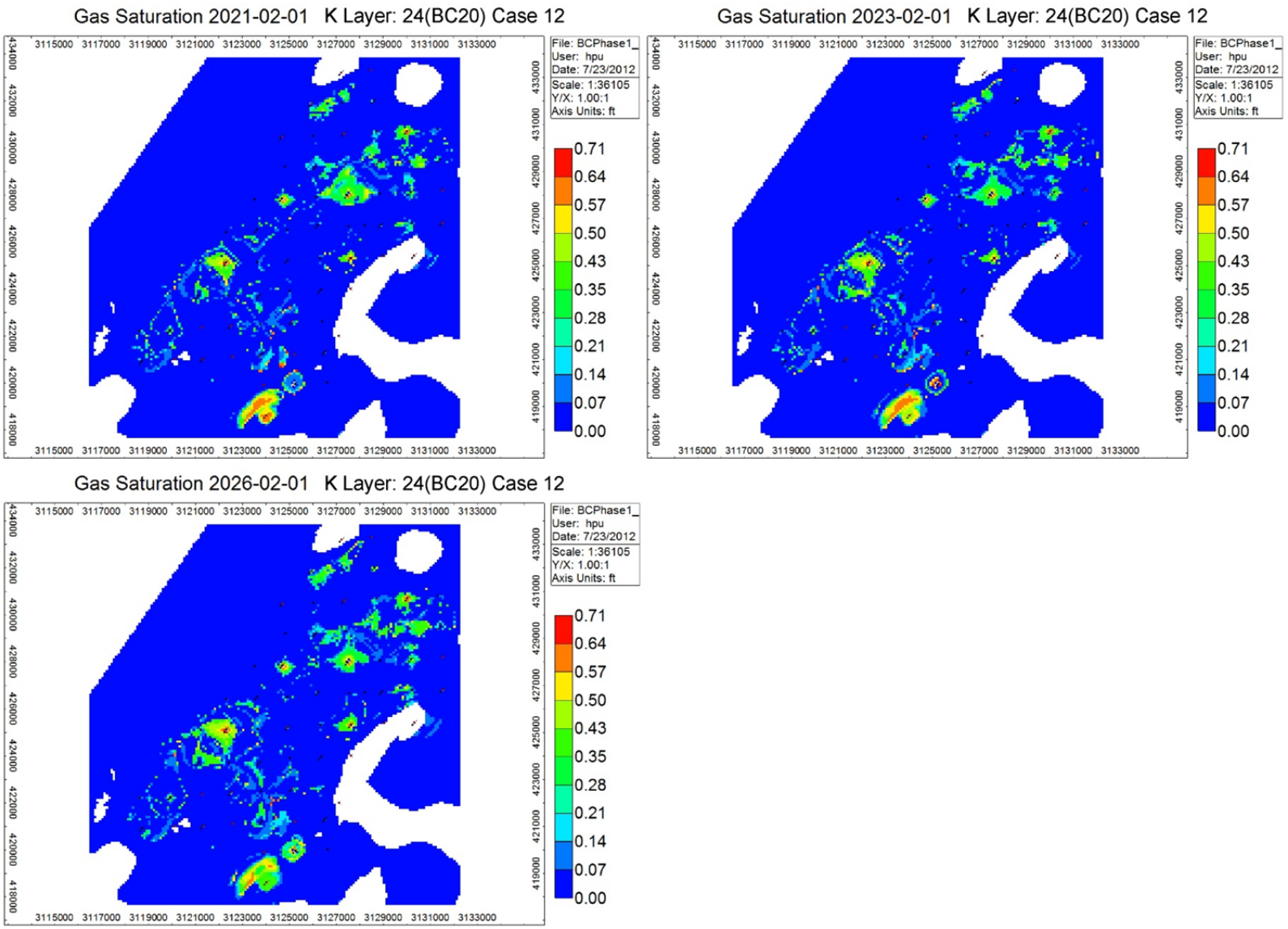

Figure C-70. Changes of gas saturation in K Layer 24 (BC20) over time (Case 12) (Part 2).

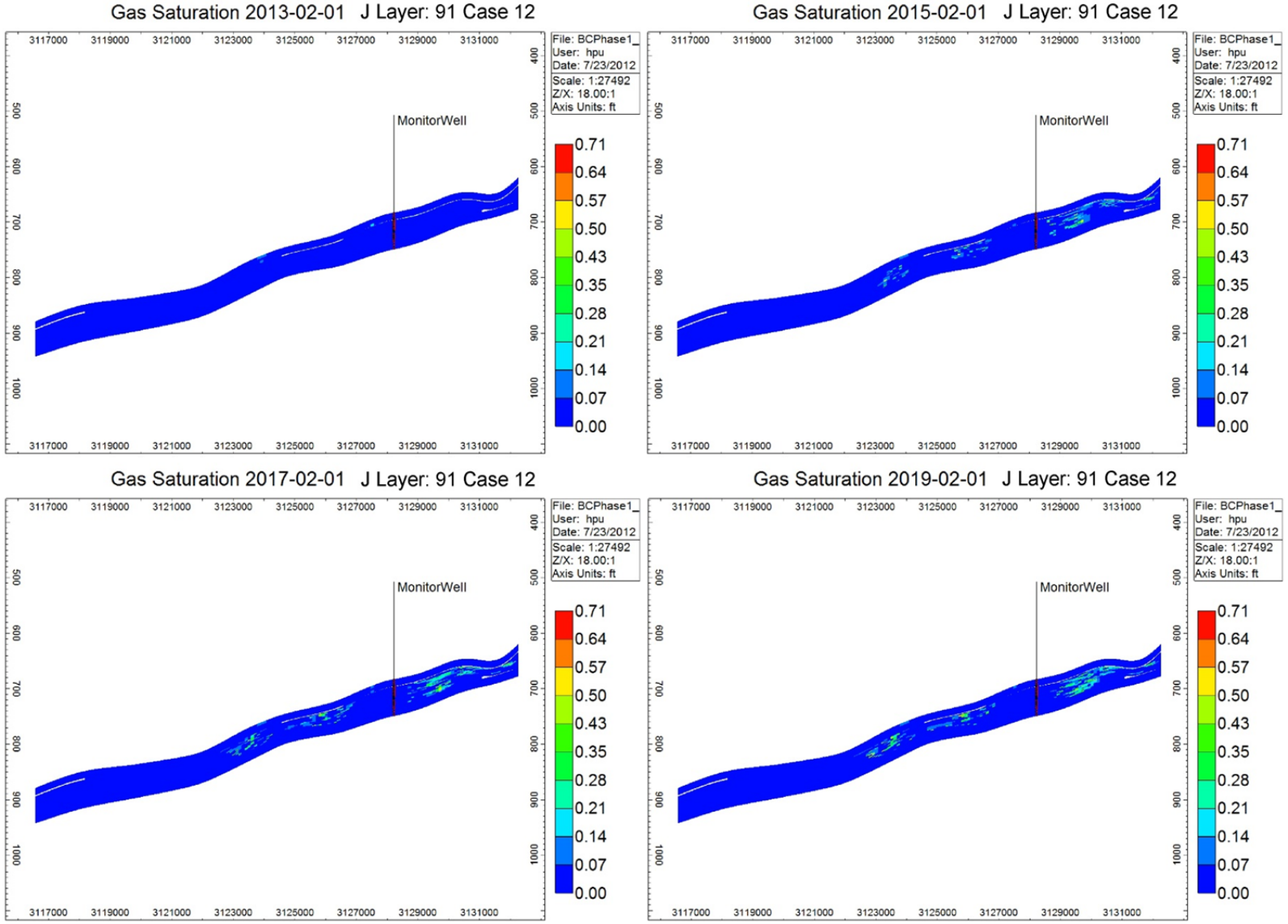

Figure C-71. Cross-sectional view of gas saturation (Case 12) (Part 1).

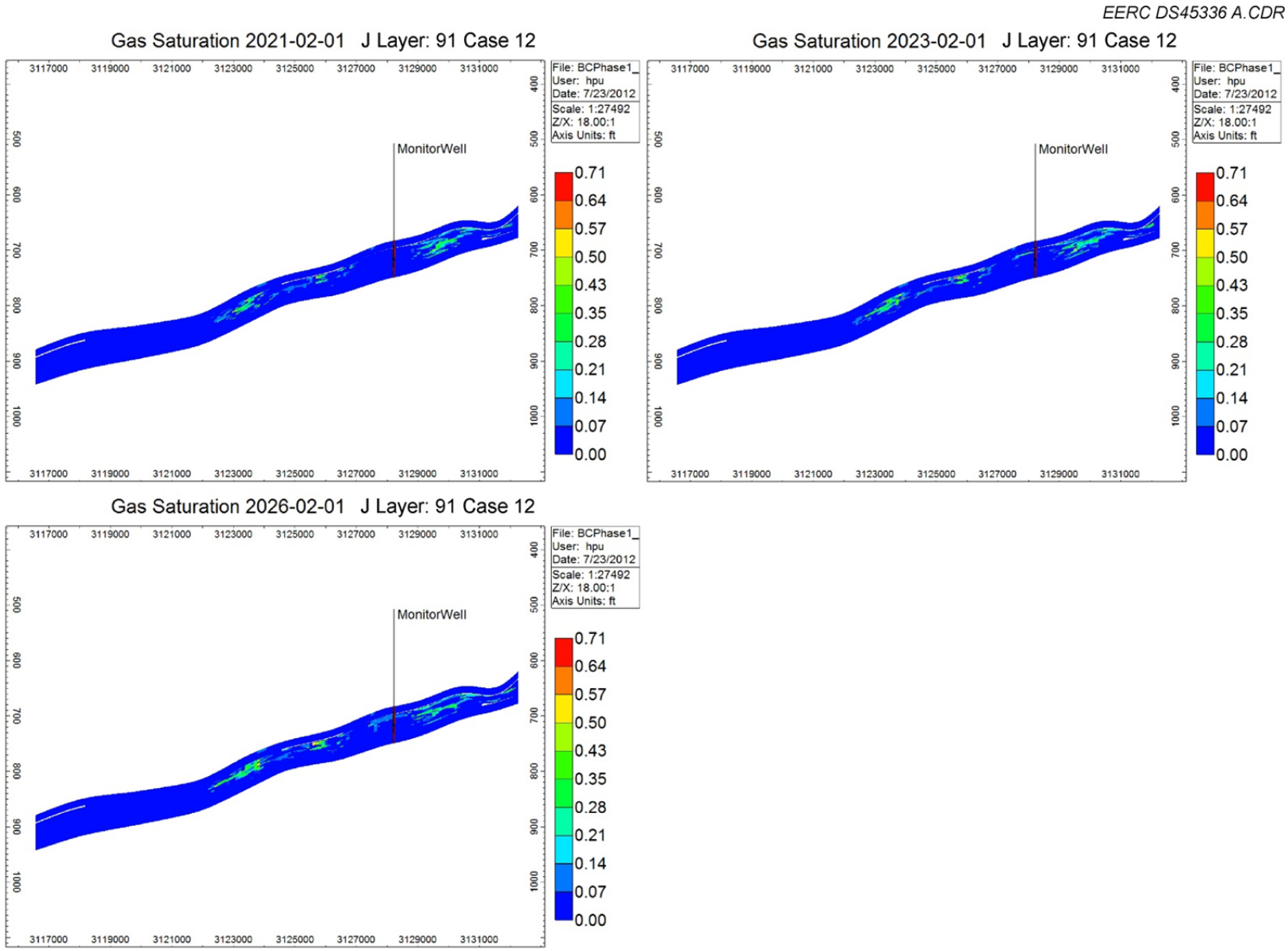

Figure C-71. Cross-sectional view of gas saturation (Case 12) (Part 2).

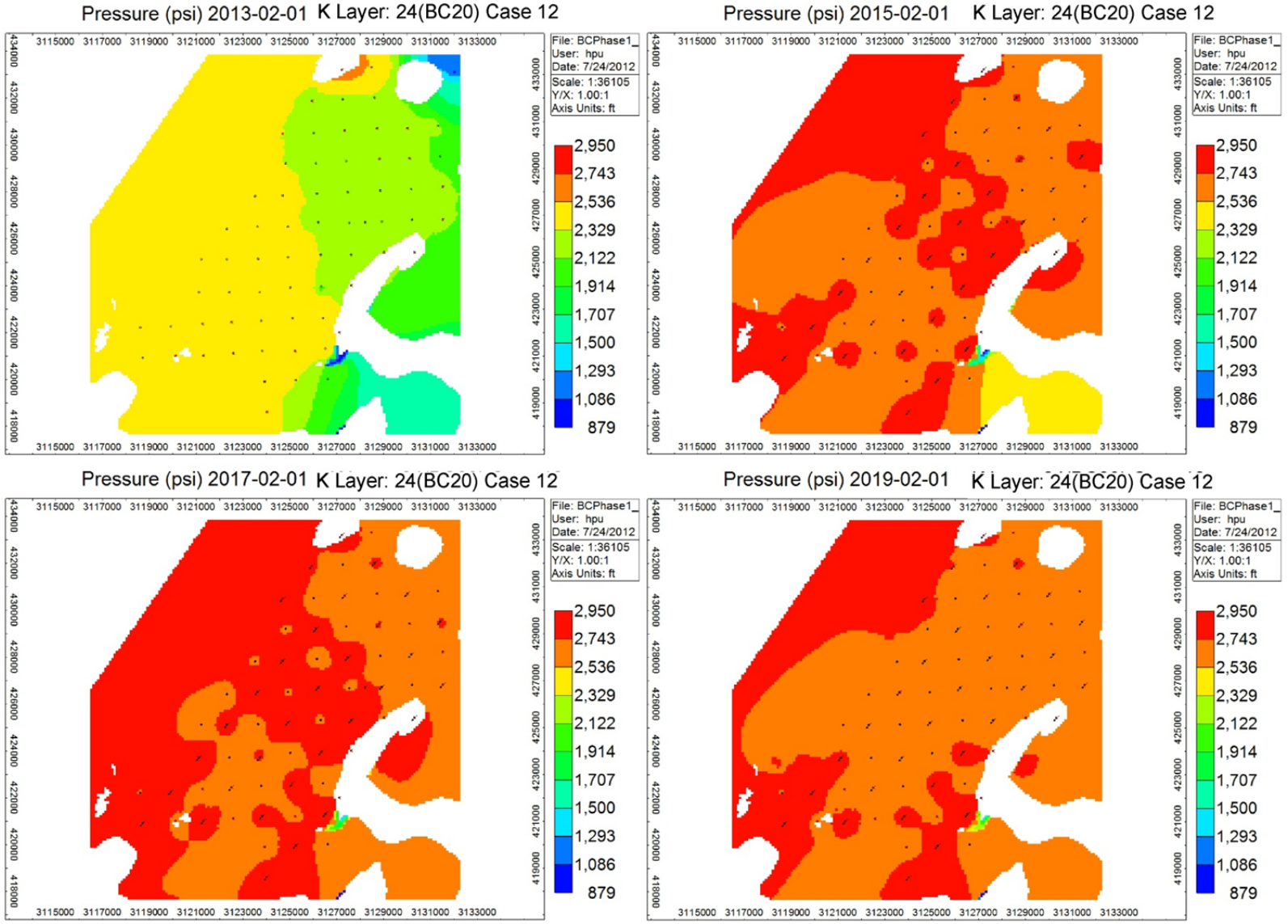

Figure C-72. Areal view of pressure (Case 12) (Part 1).

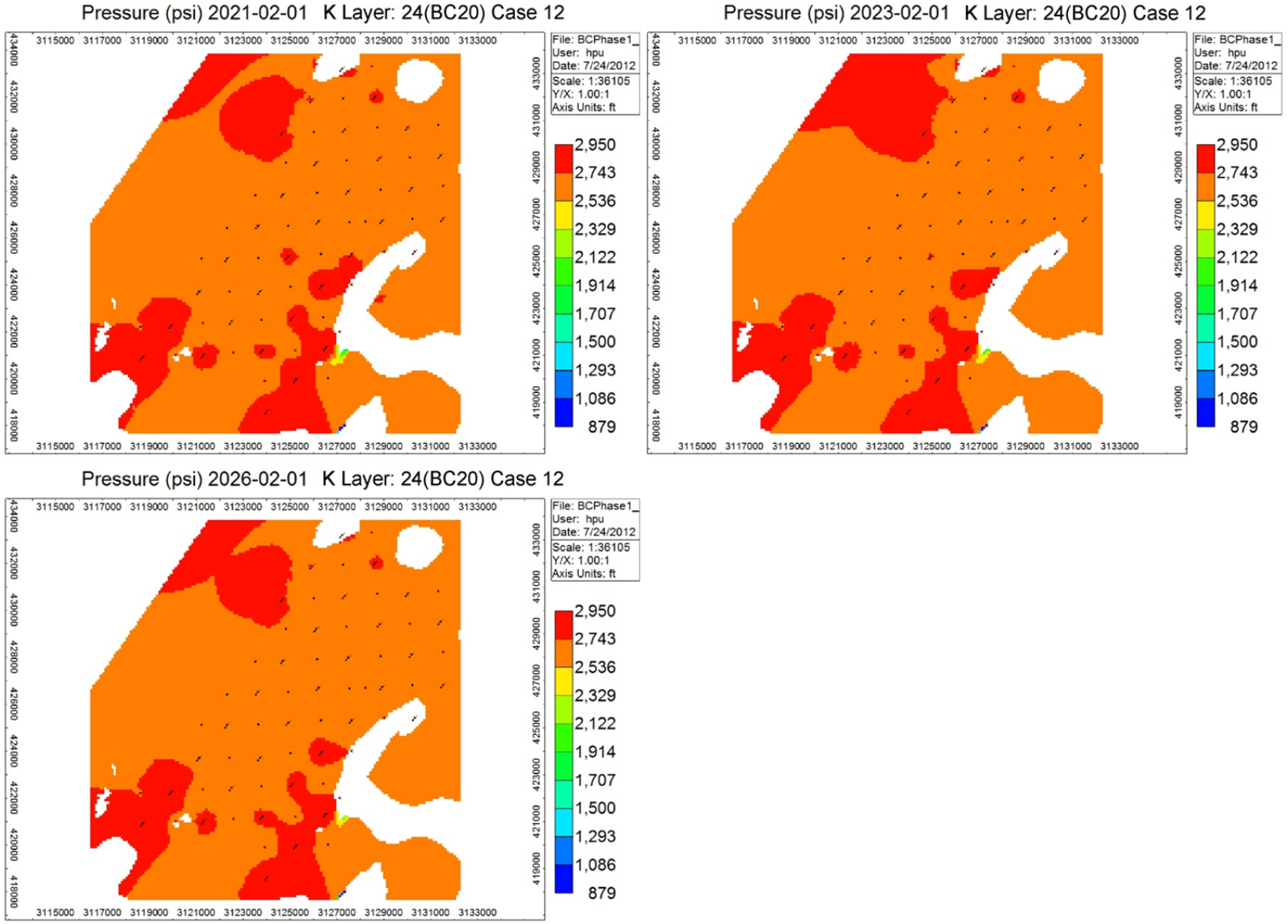

Figure C-73. Areal view of pressure (Case 12) (Part 2).